Abstract

LYVE-1 and Hyaluronan – A Molecular Velcro

William Lawrance, Lady Margaret Hall

Submitted for the degree of DPhil, Michaelmas Term, 2013

The lymphatic system comprises a network of vessels whose primary functions are the maintenance of extracellular fluid balance and the transport of antigen-presenting cells from the periphery to the lymph nodes, thus facilitating immunological surveillance of the tissues and activation of adaptive immunity. In malignant disease, the lymphatics are both a route for dissemination and a reservoir for metastatic cancers such as cutaneous melanoma and breast carcinoma, where lymph node involvement is an early indicator of prognosis. Yet, despite such obvious importance in disease, the fundamental biology of the lymphatics is poorly understood and critical mechanisms such as those underlying trafficking of dendritic and tumour cells have been largely overlooked.

The focus of this thesis is lymphatic vessel endothelial hyaluronan receptor LYVE-1, and the regulation of its binding to the extracellular matrix glycosaminoglycan, hyaluronan (HA). Found selectively on the surface of lymphatic vessels, but sharing many of the features of the leukocyte homing receptor CD44, LYVE-1 appears a likely candidate for regulation of lymphatic trafficking during the stage at which cells migrate into the vessel. However, the precise function of LYVE-1 in recent years has remained enigmatic, not least because the native receptor is subject to post-translational modification with sialic acid, with the effect that HA binding is inhibited in lymphatic endothelium. The results of this thesis demonstrate that sialylation of LYVE-1 is not a short term regulatory modification, but rather a longer term mechanism that imposes a requirement for higher order receptor complex formation or HA crosslinking to achieve stable binding. This implies that native LYVE-1 is an active HA binding protein even when sialylated, with implications for our understanding of the role played by the receptor in HA uptake and metabolism, and transmigration of lymphatic endothelium by migratory leukocytes. Like CD44, HA binding to LYVE-1 is dependent on multivalent interactions between receptor and ligand, and may be enhanced by processes that increase the avidity of the interaction. Here for the first time it is shown that the native LYVE-1 molecule on lymphatic endothelium may be activated to bind HA following clustering of the receptor, or presentation of HA in a cross-linked form, such as that resulting from incubation with the HA binding protein TSG-6.

Acknowledgments

Firstly I would like to thank Professor David Jackson for giving me the opportunity to undertake this DPhil in his laboratory, and for his support and encouragement during its course. I would also like to thank all of the members of the Jackson laboratory, past and present, for their guidance, laughter and enthusiasm during my studies. I am particularly indebted to Dr Suneale Banerji, who refused to let me fail, taught me the most 'efficient' way to conduct an experiment, and generally stole all of my stuff. I arrived in Oxford innocent, 'web-toed' and clutching my mother's telephone number; I leave with my ~~dignity~~ intact, and my sense of humour forever corrupted. For this I hold the rest of the lab responsible.

The Weatherall Institute of Molecular Medicine is as friendly and supportive a learning environment as one could wish for, and I was fortunate to make a number of good friends there, particularly among the members of cake club, to whom I apologise for my lack of baking prowess. I would particularly like to thank Professor Vincenzo Cerundolo for funding following submission of this thesis, and to Alistair Waugh and his team for keeping HIU running so smoothly. Outside of Oxford, I am very grateful to Professor Ralf Richter for the invitation to spend time in his lab in San Sebastian, in order to perform the QCM-D experiments in this thesis.

My fondest memories of Oxford revolve around Lady Margaret Hall, and the extraordinarily kind, funny and generous members of its Middle Common Room. It is testament to the character of many wonderful individuals that the MCR was, and remains a much-loved home to so many of its members. To name all of these individuals would be

impossible, but a few people stand out; Megan Edwards, Holly Morse, Charlie, Emily and Lucy Popp-Finch, Andrew Joseph, Sean O'Reilly, Io Pinnerup, Astrid Van den Bossche, Bhaveet Radia, Rachael Millar, Elena Müller, Helen Batchelor, Leandro Abade, James Sinclair, Tracy Jennings, Timothy Clark, John Turing, Danielle Basson and Julia Shanks; you made my time in Oxford, and I feel enormously privileged to have known you all. Amongst the wider LMH community, I am very grateful to Bart Ashton and Richard Sommers for their valued assistance during my time as MCR President. Finally, I must thank the various coaches and many former team-mates at LMHBC, who made a gloriously unsuccessful rowing career so enjoyable!

At home in Lowestoft are a group of people who know me better than most, and without their love and support I would have struggled to complete this thesis. They include a group of guys who I have known since primary school, and who I count as life-long friends; Simon Howlett, John Gowen, Joe Pennington, Craig Peek and Ricky Cook. Many late nights of study were fuelled by baked goods provided by my grandmother, Barbara Lawrance, who passed away during the final year of my DPhil and would have loved to see it completed, and probably read it cover-to-cover too. Finally there are my sisters, Megan and Grace, of whom I am immensely proud, and my parents Martin and Jane, who worked so hard for us siblings to have the opportunities that we have enjoyed; this one's for you.

Contents

Chapter 1. GENERAL INTRODUCTION 19

1.1 The Lymphatic System 20

1.1.1 General anatomy of the lymphatic system 20

1.1.2 Embryonic development of the lymphatics 24

1.1.3 Physiological functions of the lymphatics 29

1.1.4 Involvement of lymphatics in disease pathology 38

1.2 Hyaluronan 43

1.2.1 Hyaluronan structure and solution properties 43

1.2.2 Hyaluronan synthesis 45

1.2.3 Hyaluronan turnover and degradation 47

1.2.4 Hyaluronan function 49

1.2.5 Hyaluronan and cancer 51

1.3 Hyaluronan binding proteins 55

1.3.1 Type A hyaluronan binding domains 56

1.3.2 Type B hyaluronan binding domains 59

1.3.3 Type C hyaluronan binding domains 62

1.4 LYVE-1 69

1.4.1 Tissue specific expression of LYVE-1 69

1.4.2 Structure of the LYVE-1 protein 71

1.4.3 Regulation of hyaluronan binding 76

1.4.4 Potential interactions of LYVE-1 with ligands other than HA 78

1.4.5 Potential physiological functions of LYVE-1 80

1.5 Aims of this thesis 84

Chapter 2. MATERIALS AND METHODS 86

2.1 Materials and Reagents 87

2.1.1 Chemicals and buffers 87

2.1.2 Reagents for molecular biology 87

2.1.3 Reagents for cell culture 88
2.1.4 Antibodies 88
2.1.5 Labelling of hyaluronan 89
2.2 Bacterial Culture 91
2.2.1 Bacterial Strains 91
2.2.2 Bacterial media and culture conditions 91
2.2.3 Transformation of competent cells 91
2.2.4 Preparation of glycerol stocks 92
2.3 Molecular Biology 93
2.3.1 Plasmids and constructs 93
2.3.2 Purification of plasmid DNA from bacterial cultures 93
2.3.3 PCR (Polymerase Chain Reaction) 94
2.3.4 Agarose gel electrophoresis 95
2.3.5 Digestion of DNA with restriction endonucleases 96
2.3.6 Purification of DNA fragments 96
2.3.7 Ligation of DNA fragments 96
2.4 Cell culture and generation of cell lines 97
2.4.1 Cell lines 97
2.4.2 Isolation of primary Human Dermal Lymphatic Endothelial Cells (HDLEC) 97
2.4.3 Cell culture conditions 98
2.4.4 Cryopreseveration 99
2.4.5 Recovery of frozen cells 99
2.4.6 Transient transfection of HEK 293T fibroblasts 99
2.4.7 Lentiviral Vector Production and Infection of cell lines 100
2.4.8 Fluorescence-activated cell sorting 100
2.5 Recombinant protein and monoclonal antibodies 102
2.5.1 Expression of LYVE-1-Fc fusion proteins by transiently-transfected HEK 293T fibroblasts 102
2.5.2 Expression and purification of recombinant histidine-tagged LYVE-1 extracellular domain from Chinese Hamster Ovary (CHO) cells 103
2.5.3 Hybridoma cell culture and affinity purification of monoclonal antibodies 104
2.6 Protein biochemistry 105

2.6.1 Preparation of protein from whole-cell lysates 105
2.6.2 LDS Polyacrylamide gel electrophoresis (LDS-PAGE) 105
2.6.3 Western blotting 106
2.7 Experimental protocols 107
2.7.1 Generation of mouse LYVE1 site-directed mutants 107
2.7.2 Transient transfection of HEK 293T cells with mouse LYVE-1 mutants 107
2.7.3 Assessment of antibody and hyaluronan binding to LYVE-1 transfectants 108
2.7.4 Generation of an *in silico* structural model of mouse LYVE-1 109
2.7.5 Assay for blocking of hyaluronan-binding to mLYVE-1 by anti-mLYVE-1 monoclonal antibodies (ELISA) 110
2.7.6 Assay for binding of anti-mLYVE-1 monoclonal antibodies to mLYVE-1 Δ165 and Δ232 Fc (ELISA) 110
2.7.7 Assays for constitutive HA binding by LYVE-1 transfected cells and the influence of LYVE-1 mAbs on HA binding 111
2.7.8 Cross-blocking assay for mLYVE-1 monoclonal antibodies 112
2.7.9 Influence of LYVE-1 expression level on HA binding in transfected cells 113
2.7.10 Super-transfection of primary HDLEC with LYVE-1 113
2.7.11 LYVE-1 distribution and HA binding in adherent wildtype and LYVE-1 super-transfected HDLEC. 113
2.7.12 Influence of LYVE-1 mAbs on HA binding by primary HDLEC 114
2.7.13 Generation of Fab fragments of LYVE-1 mAbs and their influence on LYVE-1 ..... distribution and HA binding in HDLEC 115
2.7.14 Influence of anti-hLYVE-1 monoclonal antibodies on HA binding by recombinant hLYVE-1 monomer and dimer 115
2.7.15 Effect of streptavidin crosslinking of biotinylated HA on binding by human LYVE-1 expressing Jurkat cells 116
2.7.16 Assays for TSG-6-mediated enhancement of HA binding by LYVE-1 transfected Jurkat cells 117
2.7.17 Assays for TSG-6-mediated enhancement of bHA binding by HDLEC 117
2.7.18 Influence of TSG-6:HA complexes on HA binding and LYVE-1 distribution in adherent HDLEC monolayers. 118
2.7.19 Modification of HA with heavy chains from inter-α-inhibitor and the influence on HA binding by LYVE-1 transfected Jurkat cells 118

2.7.20 Binding of hyaluronan-coated fluorescent microspheres by HDLEC 119

2.7.21 Quantitation of LYVE-1 monomer:dimer ratio in different fractions of total cellular protein from HDLEC 120

2.7.22 Comparison of hyaluronan binding by recombinant hLYVE-1 samples using ELISA 121

2.7.23 Quartz Crystal Microbalance with Dissipation monitoring (QCM-D) 121

Chapter 3. CHARACTERIZATION OF LYVE-1-SPECIFIC MONOCLONAL ANTIBODIES WITH FUNCTION BLOCKING PROPERTIES 124

3.1 Introduction 125

3.2 Aims 129

3.3 Results 130

3.3.1 Selection of target residues for site-directed mutagenesis of mouse LYVE-1 130

3.3.2 Site-directed mutagenesis of mouse LYVE-1 and assay development 133

3.3.3 Characterisation of the hyaluronan binding site in mouse LYVE-1 134

3.3.4 Influence of mouse LYVE-1-specific monoclonal antibodies on hyaluronan binding by LYVE-1 138

3.3.5 Prediction of shared epitopes using a cross-blocking assay 142

3.3.6 Mapping the epitopes of function-blocking anti-mLYVE-1 monoclonal antibodies using site-directed mutagenesis. 145

3.4 Discussion 155

Chapter 4. REGULATION OF HYALURONAN BINDING IN LYMPHATIC ENDOTHELIAL CELLS BY LYVE-1 SURFACE DENSITY 159

4.1 Introduction 160

4.2 Aims 164

4.3 Results 165

4.3.1 The relationship between LYVE-1 expression and hyaluronan binding 165

4.3.2 Triggering hyaluronan binding by lymphatic endothelial cells using monoclonal antibodies directed against human LYVE-1 173

4.3.3 Influence of LYVE-1 mAbs on HA binding by adherent HDLEC monolayers 180

4.3.4 Antibody-mediated potentiation of HA binding to LYVE-1 transfected cells 182

4.3.5 Effect of LYVE-1 antibodies on hyaluronan binding by mouse LYVE-1 transfected Jurkat cells 187

4.3.6 Mechanism of antibody-mediated potentiation of hyaluronan binding by LYVE-1 189

4.3.7 Enhancement of HA binding to LYVE-1 by monoclonal antibodies – dependence on antibody bivalency 190

4.3.8 Influence of Fab fragments on LYVE-1 distribution in adherent HDLEC monolayers ... 196

4.3.9 Influence of LYVE-1 antibodies and Fab fragments on HA binding by recombinant LYVE-1 199

4.3.10 Formation of artificial LYVE-1 dimers by potentiating antibodies 203

4.4 Discussion 206

Chapter 5. MODIFYING THE VALENCY OF THE LIGAND – ENHANCED BINDING OF CROSS-LINKED HYALURONAN 210

5.1 Introduction 211

5.2 Aims 215

5.3 Results 217

5.3.1 Cross-linking of biotinylated hyaluronan using streptavidin enhances binding by LYVE-1 transfected cells 217

5.3.2 Cross-linking of hyaluronan with the inflammation-associated protein TSG-6 activates binding by LYVE-1 219

5.3.3 Influence of TSG-6:HA complexes on LYVE-1 surface distribution 227

5.3.4 Modification of hyaluronan with heavy-chains from on inter-α-inhibitor and the influence on binding by LYVE-1 230

5.3.5 Binding of hyaluronan-coated fluorescent microspheres to LYVE-1 in primary lymphatic endothelial cells 237

5.4 Discussion 242

Chapter 6. ANALYSIS OF LYVE-1-HYALURONAN INTERACTIONS USING CELLULAR ASSAYS AND THE QUARTZ CRYSTAL MICROBALANCE 246

6.1 Introduction 247

6.1.1 Function of LYVE-1 homodimers 247

6.1.2 Mechanism of inhibition of hyaluronan binding by sialic acid 248

6.1.3 Use of QCM-D for the study of hyaluronan binding proteins 250

6.2 Aims 253
6.3 Results 255
6.3.1 Prevalence of LYVE-1 dimers in primary LEC and LYVE-1 transfected cells 255
6.3.2 Significance of LYVE-1 homodimers for hyaluronan binding by LYVE-1 transfected cells 260
6.3.3 Role played by LYVE-1 homodimers in primary lymphatic endothelial cells 265
6.3.4 Rationale for analysis of LYVE-1-hyaluronan interactions in an artificial membrane system 268
6.3.5 Characterization of recombinant LYVE-1 samples for use in QCM-D studies 270
6.3.6 Characterization of Tris-NTA functionalized lipids 273
6.3.7 Analysis of LYVE-1-Hylauronan Interactions using an Artificial Membrane System monitored by QCM-D 277
6.3.8 Comparison of hyaluronan binding by recombinant LYVE-1 monomer and dimer 281
6.3.9 Influence of LYVE-1 mAb on HA binding by recombinant LYVE-1 monitored by QCM-D 286
6.4 Discussion 288

Chapter 7. GENERAL DISCUSSION 292
7.1 Summary 293
7.2 Biological implications 303
7.3 Future Work 308

List of Figures

Figure 1.1. **Architecture of the lymphatic vasculature** 23

Figure 1.2. **Primary steps in mammalian lymphatic vascular development** 26

Figure 1.3. **Organisation of the lymph node and trafficking of immune cells via the lymphatic vessels** 32

Figure 1.4. **Structure of hyaluronan** 44

Figure 1.5. **False colour electron micrograph and schematic of an Aggrecan-decorated HA chain from cartilage** 49

Figure 1.6. **Localization of hyaluronan and potential roles in a malignant invasive tumour arising from simple epithelia** 54

Figure 1.7. **The Link superfamily of hyaluronan binding proteins** 56

Figure 1.8. **Solution structure of the Link module from TSG-6 in the presence (green) and absence (orange) of a hyaluronan octasaccharide** 57

Figure 1.9. **The consensus Link domain of TSG-6 and the extended Link domain of CD44** 61

Figure 1.10. **Homology models of cartilage link protein (HAPLN1) with an HA dodecamer** 64

Figure 1.11. **The domain structure of aggrecan and link protein and sites of interaction with HA** ... 66

Figure 1.12. **Functionally specialized junctions between endothelial cells of lymphatic vessels** 70

Figure 1.13. **Schematic of LYVE-1 monomer and dimer bound to an HA chain** 72

Figure 1.14. **Multiple sequence alignment of LYVE-1 and CD44 from human and mouse** 73

Figure 1.15. **Structure-based model of the extended Link domain and HA-binding surface in LYVE-1** 75

Figure 1.16. **LYVE-1 function-blocking mAbs inhibit entry of dendritic cells to afferent lymphatic vessels of the skin** 82

Figure 3.1. **Binding of anti-mLYVE-1 monoclonal antibodies (mAbs) to recombinant Fc fusion proteins of mouse LYVE-1** 131

Figure 3.2. **Selection of target residues for site-directed mutagenesis using structure-based modelling of the mouse LYVE-1 HABD** 132

Figure 3.3. **Influence of site-directed mutagenesis on hyaluronan binding by mouse LYVE-1 transfected HEK 293T cells** 135

Figure 3.4. **The Hyaluronan binding site of mouse LYVE-1 shows similarities to both human LYVE-1 and human CD44** 137

Figure 3.5. **Influence of anti-mLYVE-1 monoclonal antibodies (mAbs) on hyaluronan binding by recombinant mouse LYVE-1** 140

Figure 3.6. **Influence of anti-mLYVE-1 monoclonal antibodies on hyaluronan binding by mLYVE-1 transfected Jurkat cells** 141

Figure 3.7. **Binding of dye-conjugated anti-mLYVE-1 monoclonal antibodies (mAbs) to mLYVE-1 expressing Jurkat cells** 143

Figure 3.8. **Detection of shared epitopes for mouse LYVE-1-specific monoclonal antibodies (mAbs) by cross-blocking assay** 144

Figure 3.9. **Influence of site-directed mutagenesis of mLYVE-1 on binding by anti-mLYVE-1 monoclonal antibodies (mAbs)** 151

Figure 3.10. **Partial epitopes derived for anti-mLYVE-1 monoclonal antibodies (mAbs) shown in relation to the hyaluronan binding site** 153

Figure 4.1. **Primary lymphatic endothelial cells (LEC) lack the constitutive hyaluronan binding observed for LYVE-1-transfected cell lines** 166

Figure 4.2. **Influence of LYVE-1 expression level on hyaluronan binding by LYVE-1 transfected Jurkat cells** 168

Figure 4.3. **Over-expression of human LYVE-1 in primary lymphatic endothelial cells using lentiviral infection** 170

Figure 4.4. **Hyaluronan binding in adherent wildtype and hLYVE-1-GFP super-transfected HDLEC** 172

Figure 4.5. **Induction of hyaluronan binding by co-incubation of primary lymphatic endothelial cells with appropriate LYVE-1-specific monoclonal antibodies** 174

Figure 4.6. **Influence of anti-human-LYVE-1 monoclonal antibodies on hyaluronan binding by primary HDLEC and the relationship between LYVE-1 expression and antibody-mediated potentiation of HA binding** 177

Figure 4.7. **Quantitation of mAb-mediated potentiation of HA binding to HDLEC resulting from different sequences of mAb/HA incubation**..... 178

Figure 4.8 **Influence of passage on LYVE-1 expression and antibody-mediated potentiation of HA binding**..... 179

Figure 4.9. **Influence of anti-human-LYVE-1 monoclonal antibodies on hyaluronan binding by adherent primary LEC** 181

Figure 4.10. **Influence of anti-human-LYVE-1 monoclonal antibodies on hyaluronan binding by LYVE-1-expressing HEK 293T cells**..... 184

Figure 4.11. **Influence of anti-hLYVE-1 monoclonal antibodies on hyaluronan binding by hLYVE-1-GFP transfected Jurkat cells** 185

Figure 4.12. **Influence of LYVE-1 expression level on antibody-mediated potentiation of HA binding to hLYVE-1 transfected Jurkats** 186

Figure 4.13. **Influence of commercially sourced anti-mouse-LYVE-1 monoclonal antibodies on hyaluronan binding by Jurkat cells expressing mouse LYVE-1** 188

Figure 4.14. **Potential mechanisms of antibody-mediated potentiation of HA binding**..... 189

Figure 4.15. **Generating Fab fragments of anti-human-LYVE-1 monoclonal antibodies 8C and 6A** 191

Figure 4.16. **Influence of 8C and 6A monoclonal antibodies and Fab fragments on hyaluronan binding by human LYVE-1 expressing Jurkat cells**..... 193

Figure 4.17. **Influence of 8C and 6A monoclonal antibodies and Fab fragments on hyaluronan binding by primary human dermal lymphatic endothelial cells**..... 194

Figure 4.18. **Influence of Fab fragments on hyaluronan binding by LYVE-1 expressing cells summarised** 195

Figure 4.19. **Influence of 8C and 8C Fab fragments on LYVE-1 distribution in adherent primary LEC**..... 197

Figure 4.20. **Influence of 8C and 8C Fab fragments on LYVE-1 distribution in hLYVE-1-GFP HDLEC**..... 198

Figure 4.21. **Influence of anti-hLYVE-1 monoclonal antibodies on HA binding by recombinant hLYVE-1 monomer and dimer**..... 201

Figure 4.22. **Influence of anti-hLYVE-1 monoclonal antibodies on HA binding by recombinant hLYVE-1 monomer and dimer**..... 202

Figure 4.23. **Antibody-mediated potentiation of hyaluronan binding to Jurkat cells expressing a mutant LYVE-1 that cannot form disulfide-linked dimers**..... 204

Figure 5.1. **Effect of streptavidin crosslinking of biotinylated HA on binding by human LYVE-1 expressing Jurkat cells** 218

Figure 5.2. **Titration of hyaluronan bound to human LYVE-1 expressing Jurkat cells in the presence or absence of Link TSG-6 or Full Length TSG-6** 221

Figure 5.3. **Comparison of TSG-6:bHA binding by Jurkat transfectants expressing high or low levels of human LYVE-1** 222

Figure 5.4. **Effect of varying TSG-6:HA ratio on hyaluronan binding by Human Dermal Lymphatic Endothelial Cells (HDLEC)** 223

Figure 5.5. **Influence of Link_TSG-6 on hyalurona binding by primary Human Dermal Lymphatic Endothelial Cells (HDLEC)** 225

Figure 5.6. **Influence of Full Length_TSG-6 on hyaluronan binding by primary Human Dermal Lymphatic Endothelial Cells (HDLEC)**..... 226

Figure 5.7. **Influence of pre-incubation of Link_TSG-6 or Full length TSG-6 with hyaluronan on binding by primary HDLEC super-transfected with wildtype human LYVE-1 or GFP-tagged human LYVE-1**..... 227

Figure 5.8. **Influence of pre-incubation of hyaluronan with Link TSG-6 or Full Length TSG-6 on binding by adherent primary Human Dermal Lymphatic Endothelial Cells** 228

Figure 5.9. **Influence of Heavy Chain Hylauronan (HA•HC) and Full Length TSG-6 on hyaluronan binding by LYVE-1 expressing Jurkat cells**..... 232

Figure 5.10 **Influence of Heavy Chain Hylauronan (HA•HC) and Full Length TSG-6 on hyaluronan binding by LYVE-1 expressing Jurkat cells – Comparison of TSG-6 from different sources**..... 234

Figure 5.11. **Western blot of Heavy Chain Hylauronan (HA•HC) formation by recombinant TSG-6 samples**..... 236

Figure 5.12. **Binding of Hyaluronan-coated fluorescent microspheres by adherent monolayers of primary HDLEC**..... 239

Figure 5.13. **Influence of hyaluronan-coated fluorescent microspheres on LYVE-1 distribution in adherent HDLEC monolayers**..... 240

Figure 5.14. **Binding of hyaluronan-coated fluorescent microspheres by LYVE-1-GFP over-expressing adherent HDLEC monolayers** 241

Figure 6.1. **Hypothetical models for the regulation of hyaluronan binding by sialic acid** 249

Figure 6.2. **Schematic of a QCM-D experiment, showing formation of a supported lipid bilayer** ... 251

Figure 6.3. **Western blot of LYVE-1 expressed by different cell types under reducing and non-reducing conditions**..... 256

Figure 6.4 **Quantification of monomer:dimer ratio in primary Lymphatic Endothelial Cells and LYVE-1 expressing cell lines** 257

Figure 6.5. **Quantitation of LYVE-1 monomer:dimer ratio in different fractions of total cellular protein using surface biotinylation and western blot** 259

Figure 6.6. **Effect of ablating dimer formation on hyaluronan binding by LYVE-1 transfected cells** 261

Figure 6.7. **Comparison of hyaluronan binding in Jurkat cells expressing wildtype GFP-tagged LYVE-1 or a non-dimerizing LYVE-1 C201A mutant**..... 263

Figure 6.8. **Hyaluronan binding by primary lymphatic endothelial cells over-expressing GFP-tagged wildtype or C201A hLYVE-1** 266

Figure 6.9. **Western blot of primary lymphatic endothelial cells over-expressing wildtype, GFP-tagged or C201A mutant human LYVE-1**..... 267

Figure 6.10. **Schematic representation of recombinant LYVE1 anchored to an artificial lipid bilayer formed on the surface of a quartz crystal microbalance** 269

Figure 6.11. **Recombinant human LYVE-1 samples used in QCM-D studies, visualised by LDS-PAGE following storage** 271

Figure 6.12. **Comparison of hyaluronan binding by recombinant hLYVE-1 samples using ELISA** 272

Figure 6.13. **Formation of supported lipid bilayers using lipid vesicles with different compositions** 274

Figure 6.14. **Adsorption of His-tagged CD44 HABD onto 5% Tris-NTA functionalized SLBs and subsequent binding of 250 kDa hyaluronan** 276

Figure 6.15. **Analysis of Hyaluronan interactions with recombinant hLYVE-1 monomer in an artificial membrane system monitored by QCM-D** 279

Figure 6.16. **Adsorption behaviour of recombinant hLYVE-1 monomer samples monitored by QCM-D** 280

Figure 6.17. **Comparison of Hyaluronan interactions with untreated or neuraminidase-digested recombinant hLYVE-1 monomer and dimer as saturating density** 283

Figure 6.18. **Adsorption behaviour of recombinant hLYVE-1 monomer samples monitored by QCM-D** 284

Figure 6.19. **Comparison of Hyaluronan interactions with untreated or neuraminidase-digested recombinant hLYVE-1 monomer and dimer as 'low' density** 285

Figure 6.20. **Influence of potentiating and blocking antibodies on HA-binding by monomeric LYVE-1 in the QCM-D system** 287

Figure 7.1 **Regulation of hyaluronan binding to LYVE-1** 298

Figure 7.2 **Influence of site-directed mutagenesis of mLYVE-1 on binding by anti-mLYVE-1 monoclonal antibodies (mAbs)** 312

Abbreviations

APC	Antigen Presenting Cell
bp	Base Pair
bHA	Biotinylated Hyaluronan
bHABP	Biotinylated HA-Binding Probe
cDNA	Complementary DNA
CD	Cluster of differentiation
CHO	Chineese Hamster Ovary Cell
CRSBP	Cell Surface Retention Sequence Binding Protein
C4S	Chondroitin-4-sulphate
C6S	Chondroitin-6-sulphate
DC	Dendritic Cell
DMEM	Dulbecco's Modified Eagle's Medium
DMSO	Dimethyl Sulphoxide
DNA	Deoxyribonucleic Acid
dNTP	Deoxynucleoside triphosphate
DTT	Dithiothrietol
E. coli	Escherichia Coli
EBM-2	Endothelial Basal Medium-2
EGM-2	Endothelial Growth Medium-2
ECM	Extracellular Matrix
EDAC	*N*-(3-Dimethylaminopropyl)-*N'*-ethylcarbodiimide
EDTA	Ethylenediaminetetra-acetic acid
ECM	Extracellular Matrix
ELISA	Enzyme Linked Immunosorbant Assay
ER	Endoplasmic Reticulum
EST	Expressed Sequence Tag
Fab	Fragment Antigen Binding

FACS	Fluorescence Activated Cell Sorting
FBS	Fetal Bovine Serum
FCS	Fetal Calf Serum
FGF	Fibroblast Growth Factor
Fc	Fragment Crystallizable
Fig	Figure
FITC	Fluorescein Isothiocyanate
Fl-HA	Fluorescein-labelled Hyaluronan
FL_TSG-6	Full Length TSG-6
GAG	Glycosaminoglycan
GFP	Green Fluorescent Protein
CSPG	Chondroitin Sulphate Proteoglycan
hr	Hour
HA	Hyaluronan
HAS	HA Synthase
HC	Heavy chain (in IαI)
HC•HA	Heavy chain Hyaluronan
HDLEC	Human Dermal Lymphatic Endothelial Cell
HEV	High Endothelial Venule
HRP	Horse Radish Peroxidase
Hyal	Hyaluronidase
IαI	Inter-alpha-inhibitor
ICAM	Intercellular Adhesion Molecule
Ig	Immunoglobulin
kDa	Kilodalton
LB	Luria Broth
LEC	Lymphatic Endothelial Cell
Link_TSG-6	Link Module of TSG-6
LYVE-1	Lymphatic Vessel Hyaluronan Receptor 1
mAb	Monoclonal Antibody
MACS	Magnetic Cell Sorting
MES	2-(N-morpholino)ethanesulfonic acid

MFI	Mean Fluorescence Intensity
MHC	Major Histocompatibility Complex
MDLEC	Mouse Dermal Lymphatic Endothelial Cell
MMP	Matrix Metalloproteinase
NMR	Nuclear Magnetic Resonance
OxLDL	Oxidised Low Density Lipoprotein
PBS	Phosphate Buffered Saline
PDB	Protein Data Bank
PCR	Polymerase Chain Reaction
PMA	Phorbol 12-Myrisate 13-Acetate
Prox-1	Prospero-Related Homeobox 1
QCM-D	Quartz Crystal Microbalance with Dissipation Monitoring
RPMI	Roswell Park Memorial Institute
SD	Standard Deviation
SEM	Standard Error of the Mean
SHAP	Serum-derived Hyaluronan-Associated Protein
TBS	Tris-Buffered Saline
Tween 20	Polyoxyethylene-sorbitan monolaurate
TNF	Tumour Necrosis Factor
Tris	Tris-hydroxymethylamino methane
TSG-6	TNF Inducible Gene 6
VCAM-1	Vascular Cell Adhesion Molecule 1
VEGF	Vascular Endothelial Growth Factor
VEGFR	Vascular Endothelial Growth Factor Receptor
VLA-4	Very Late Antigen-4
UV	Ultraviolet
v/v	volume/volume
w/v	weight/volume

Chapter 1.
General Introduction

1.1 The Lymphatic System

The lymphatic system comprises a network of vessels whose primary functions are the maintenance of extracellular fluid balance and the transport of antigen-presenting cells from the periphery to the lymph nodes, thus facilitating immunological surveillance (Swartz, 2001). Without this conduit between the peripheral tissues and lymph nodes, initiation of adaptive immunity to bacteria and viruses would be an impossibility, due to the unlikelihood of T or B-cells encountering their cognate antigen in the absence of antigen presentation. In pathological conditions, the lymphatics are subverted as route for dissemination of hyaluronan-encapsulated bacteria and metastatic cancers such as cutaneous melanoma and breast carcinoma. Disruption of lymphatic drainage leads to debilitating lymphedema, characterized by fluid accumulation and tissue swelling. In contrast to the blood vasculature, where the mechanisms controlling vessel permeability and cellular egress are well defined, comparatively little is known about the basic biology of the lymphatic system. With the advent of specific markers for lymphatic endothelial cells such as LYVE-1, an increased focus on the lymphatics has been realised, with the result that many of the critical features of this system have begun to be described.

1.1.1 General anatomy of the lymphatic system

The lymphatic vasculature is present in all tissues that possess a blood supply, with notable exceptions of the central nervous system and bone marrow. The two systems are connected at the point where the thoracic duct meets the subclavian vein but are otherwise physically separate (Figure 1.1, A, C). On the smallest scale, the lymphatic system comprises a network of small blind-ended capillaries, or initial lymphatics, with an internal diameter of 30 – 80 μm. These vessels are formed from a thin wall of lymphatic endothelial cells that

take on a distinctive oak-leaf morphology (Figure 1.1, D). Flap valves formed at the point of inter-digitation are the proposed sites of fluid and cellular entry to the vessel lumen (Figure 1.1, B) (Mendoza and Schmid-Schonbein, 2003; Trzewik et al., 2001). The integrity of the vessel is maintained by 'button' junctions formed of VE-cadherin, that anchor the sides of the flaps and pin individual cells together (Baluk et al., 2007). This contrasts the situation in the blood vasculature, where individual cells are closely-knit by 'zipper junctions', even in the smallest vessels. The 'zipper' arrangement is also observed in lymphatic endothelium during development, under certain conditions of chronic inflammation, and in actively-sprouting lymphatic capillaries (Yao et al., 2012). Immediately prior to birth, button-junctions begin to replace zippers on initial lymphatic vessels, a process that is complete by post-natal day 70 in the mouse. Buttons therefore represent the mature junctional-type in the peripheral lymphatics.

Unlike the capillaries of the blood vasculature, initial lymphatics lack associated pericytes and secrete only a rudimentary and discontinuous basement membrane (Pflicke and Sixt, 2009). However, lymphatic endothelial cells have been observed to contact the surrounding ECM via anchoring filaments radiating from the cell surface (Leak and Burke, 1968). These filaments consist of fibrillin microfibrils (Solito et al., 1997) and elastin fibres (Gerli et al., 1990) and function to prevent vessel collapse upon an increase in interstitial pressure (Figure 1.1, B). The overlapping nature of the flap valves prevents fluid leaking back into the interstitium thus reducing intraluminal pressure and maintaining lymph flow (Swartz, 2001).

Lymph passes from the initial lymphatics into pre-collecting vessels that are surrounded by a thin layer of smooth muscle and have an overall structure that resembles the blood capillaries (Alitalo, 2011). These vessels in turn are connected to large-diameter collecting

vessels that have defined layers of periendothelial muscle, a more extensive basement membrane and closely-knit 'zipper' junctions between individual cells (Figure 1.1 A,C,D) (Baluk et al., 2007). Intra-luminal valves positioned at intervals in the collectors consist of two semilunar leaflets of specialized endothelium and assist with unidirectional lymph flow (Figure 1.1, E) (Lauweryns and Boussauw, 1973). The collecting vessels are thus divided into segments termed lymphangions, into which fluid enters from an upstream direction, but is prevented from flowing backwards by the closing of the valve. In the peripheral vessels, lymphatic flow is maintained chiefly by interstitial fluid pressure and strain of the extracellular matrix, both of which are affected by skeletal muscle contraction and arterial pressure pulsations (Swartz, 2001). In the larger vessels, lymph propulsion is maintained by the intrinsic pumping action of smooth muscle cells, which is itself regulated by neural, hormonal and physical inputs, such as nitric oxide, prostanoids and increased lymph pressure (Zawieja, 2009).

Lymphatic collectors drain fluid into the lymph nodes, of which there are 400 – 500 in the human body, organised into clusters. The nodes are typically connected in series, with pre-nodal, or afferent lymphatics entering the outer capsule and post-nodal, or efferent draining from it (Figure 1.1, C). Lymph nodes function as filters of the lymph fluid and reservoirs of immune cells that constantly sample antigen delivered from the peripheral tissues (Swartz, 2001). Narrow fluid crevices percolate through the cortex and paracortex and are fed by the afferent lymphatics and blood vasculature, via high endothelial venules (HEVs), before eventually draining into the medullary sinus and exiting via one or more efferent lymphatic vessels (Girard et al., 2012). The node is capable of acting as a fluid exchange chamber, as the nodal vasculature can either add fluid to lymph or absorb it, depending on the relative protein concentration in the two fluids (Witte et al., 2006).

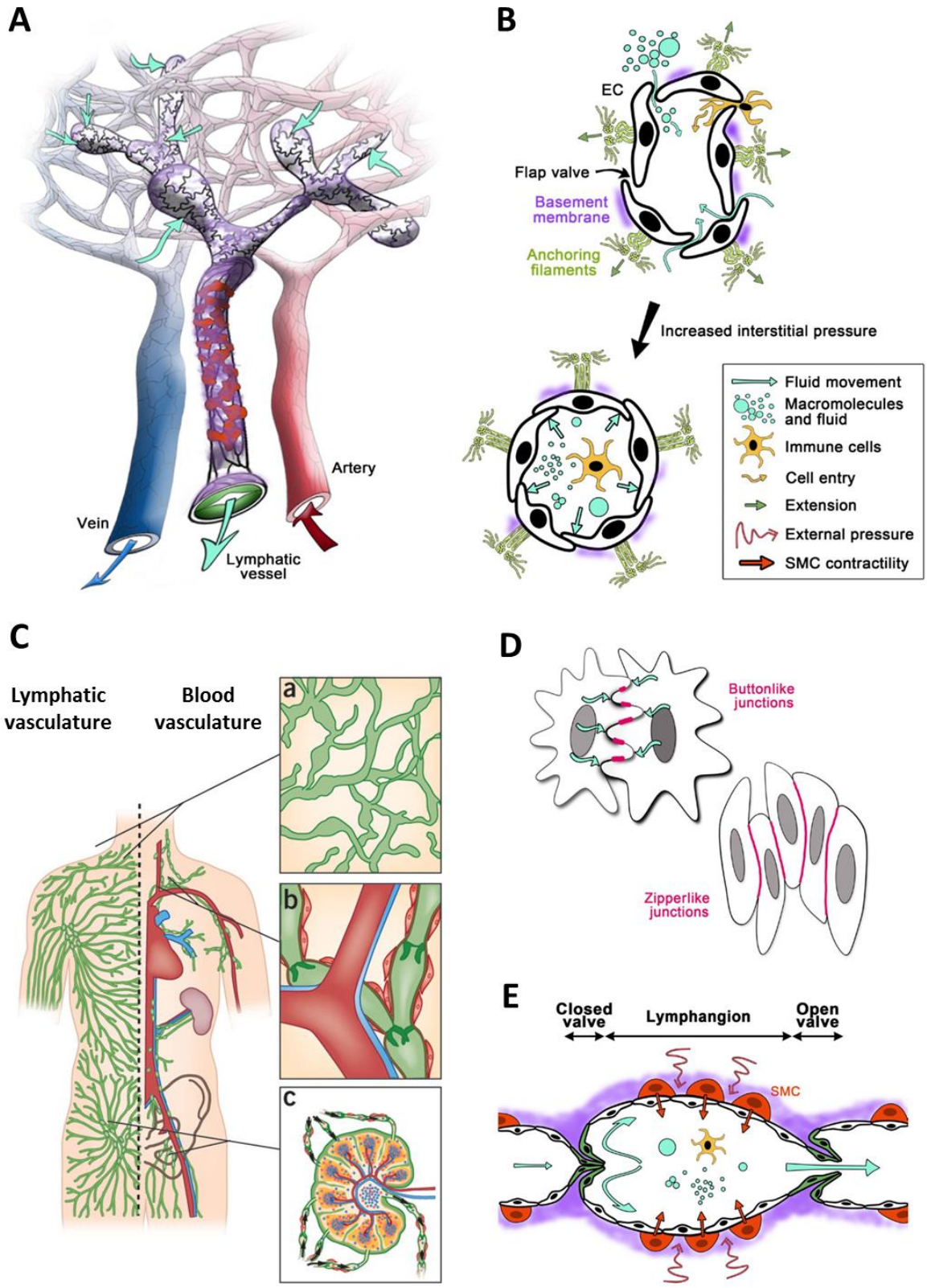


Figure 1.1. **Architecture of the lymphatic vasculature**. (A, C) The lymphatic vasculature extends throughout the body, and is found in nearly all tissues that possess a blood supply. In the periphery, a network of small blind-ended capillaries (C, a) resorbs fluid and macromolecules from the interstitium, depositing it into larger collecting vessels (C, b) that eventually drain back into the blood supply via the thoracic duct. Arranged in

clusters at various points along the network, lymph nodes (C, c) provide a reservoir for immune cells that sample lymph arriving from the tissues. This includes soluble antigen and antigen-presenting cells, that utilise the lymphatics as a conduit for migration to the lymph nodes. (B) Interstitial fluid and migratory cells penetrate lymphatic capillaries via flap-valves located between individual Lymphatic Endothelial Cells (LEC). Lymph is prevented from returning to the interstitium by anchoring filaments that attach LECs to the ECM and prevent vessel collapse. This maintains a lower luminal than interstitial pressure and thus direction of lymphatic flow (D) In lymphatic capillaries, individual cells are joined at discrete locations termed 'button junctions' that contrast markedly with the 'zipper-like junctions' of the larger collecting vessels. (E) The collecting vessels possess an extensive basement membrane, smooth muscle cells (SMCs) and intra-luminal, all of which are absent in the smaller lymphatic capillaries. Coordinated opening and closure of lymphatic valves at either end of each vessel segment, or lymphangion, is assisted by the intrinsic pumping action of SMCs that drive lymphatic flow. Adapted from (Alitalo, 2011; Schulte-Merker et al., 2011).

Lymph originating from the legs, abdomen and left arm drains ultimately into a large terminal lymphatic vessel termed the thoracic duct, which empties into the venous supply at the left subclavian vein (Swartz, 2001). Lymphatics from the intestinal, hepatic and lumbar areas drain directly into a sac-like structure termed the cisterna chyli at the distal end of the thoracic duct, while lymph originating the head and neck, right arm and thorax drains through the right lymphatic trunk into the right subclavian vein.

1.1.2 Embryonic development of the lymphatics

Lymphatic systems are found exclusively in vertebrates, including lower-order members of the phylum such as fish, amphibians and reptiles. The architecture of the mature vasculature is divergent; fish for example lack lymph nodes or lymphatic valves, while amphibians have lymphatic hearts that drive lymphatic flow, a modification not seen in mammals (reviewed in Koltowska et al., 2013). Despite this, a common program of lymphatic development has been found in various vertebrate model systems, including mice, chickens, amphibians (*Xenopus leavis*) and most recently zebrafish (*Danio rerio*)

(Schulte-Merker et al., 2011). In all cases, lymphatic progenitors arise from the cardinal vein early in development, before migrating away from the blood endothelium, sprouting to form the lymphatic vasculature, and undergoing maturation to form capillaries, pre-collecting and collecting vessels. Over twenty different genes orchestrate lymphatic development in mice and humans, many of which have been found to play to similar roles in amphibians and fish, as part of an evolutionarily-conserved developmental program.

In the mouse, a sub-population of blood endothelial cells (BECs) in the cardinal vein undergo transdifferentiation and begin to form lymphatic progenitors at embryonic day E9.5 (Figure 1.2, A). The venous origin of lymphatic progenitors had been proposed as early as 1902 by Florence Sabin, and has since been confirmed in mammals using lineage tracing experiments (Srinivasan et al., 2007). The transcription factor Prox-1 and the lymphatic vessel endothelial hyaluronan receptor (LYVE-1) are the earliest markers of lymphatic identity and their expression is restricted to the dorsolateral wall of the cardinal vein. Prox1 is a master regulator of lymphatic lineage differentiation, from the earliest developmental stages through to adulthood (Koltowska et al., 2013). *Prox1*$^{-/-}$ mice do not develop any lymphatic structures (Wigle and Oliver, 1999) and its over-expression in BECs both *in vitro* and *in vivo* is sufficient to reprogram cells to a lymphatic identity. Prox1 expression is induced by the transcription factor Sox18, which binds directly to the Prox1 promoter (Francois et al., 2008) and nuclear receptor COUP-TFII, which is essential for venous development, but also binds Prox-1 directly and assists with induction of Prox1 target genes (Figure 1.2, B) (Srinivasan et al., 2010).

Prox1^{+}/LYVE-1^{+} cells bud from the surface of the cardinal vein and migrate outwards in a dorsolateral direction in response to VEGF-C signalling from the mesoderm (Figure 1.2, A). These cells initially form ‘lymph sacs’ at various locations along the anterior-posterior

axis, before developing into a crude network of superficial vessels termed the primary lymphatic plexus. VEGF-C is a pro-lymphangiogenic growth factor that triggers sprouting behaviour in lymphatic endothelial cells (LEC) and is essential for the exit of LEC-progenitors from the cardinal vein (Karkkainen et al., 2004).

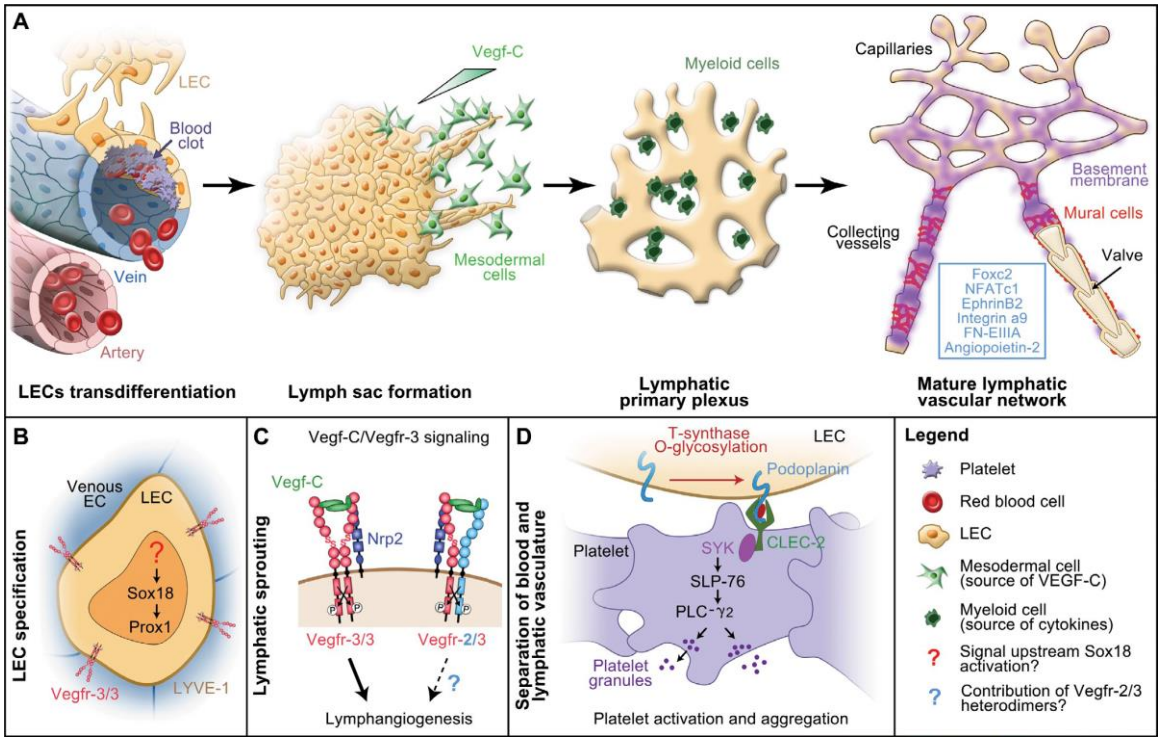


Figure 1.2. **Primary steps in mammalian lymphatic vascular development**. (A) Lymphatic development begins at E9.5 in the mouse, with the expression of LEC lineage markers Prox-1 and LYVE-1 by cells in the dorsolateral wall of the embryonic cardinal vein. These progenitors sprout toward VEGF-C–producing mesodermal cells and aggregate to form the lymph sacs that later develop into the lymphatic primary plexus. Myeloid cells produce cytokines that regulate lymphatic vascular morphogenesis. By E14.5 the primary plexus lymphatic vessels has begun to remodel to form collecting, precollecting, and capillary compartments. (Box) Genes important for collecting lymphatic vessel development. (B) LYVE-1, Prox-1 and Sox18 are the earliest known LEC markers; all three are required for lymphatic development, but Prox1 is master regulator of LEC identity from development to adulthood. (C) Signalling via Vegf-c and Vegfr-3 regulates LEC sprouting and proliferation, the latter is indispensable for these processes. The molecular details of signalling and the role of co-receptors Vegfr-2 and Nrp2 are not fully understood. (D) Separation of lymphatic and blood vasculature requires platelet aggregation, mediated by the interaction of O-glycosylated podoplanin on LECs and CLEC-2 on platelets. Taken from (Schulte-Merker et al., 2011).

Both VEGF-C and its homolog VEGF-D signal through the receptor tyrosine kinase VEGFR3, which is largely restricted to $Prox1^{+}$ endothelium, and its non-signalling transmembrane coreceptor Neuropilin-2 (Nrp2) (Figure 1.2, C). VEGFR3 is similarly required for LEC sprouting and formation of the lymph sac, alongside various intracellular components involved with its internalisation and signalling, such as claudinlike Clp24, ephrin B2 and the Rho GTPase Rac1 (reviewed in Schulte-Merker et al., 2011). Nrp2 is internalised along with VEGFR3 during VEGF-C signalling and is highly expressed in migrating cells, but is dispensable for lymph sac formation (Yuan et al., 2002). While the VEGF-C/VEGFR3 signalling axis is critical during lymphatic development, post-natal vessel growth and sprouting is independent in most tissues, with the exception of the skin. Less well understood are the roles played by the calcium binding EGF-domain containing protein 1 (Ccbe1) (Hogan et al., 2009) and adrenomedullin pathways (Fritz-Six et al., 2008), both of which have recently been implicated in lymphatic development of fish and amphibians. The function of Ccbe1 is conserved, as *Ccbe1* mutations underlie the hereditary human lymphedema syndrome, Hennekam syndrome (Alders et al., 2009).

In adult mammals the lymphatic and blood vasculatures are joined only at discrete locations where lymph fluid is returned to the venous circulation. This necessitates separation of two systems that are initially conjoined by vessels connecting the cardinal vein to the lymph sacs. Several groups have reported that platelets play an important role in sealing these connections, and that platelet depletion or deficiencies in aggregation results a failure of separation and blood-filled lymphatics (reviwed in Koltowska et al., 2013; Schulte-Merker et al., 2011). A physical barrier is formed to ‘plug’ the openings between veins and the lymph sacs following interaction of the C-type lectin receptor CLEC-2 on platelets and the mucoprotein podoplanin on lymphatic endothelial cells (Figure 1.2, D) (Uhrin et al., 2010). Engagement of CLEC-2 triggers a signalling cascade through spleen tyrosine kinase (Syk),

Slp76, and PLC-γ2 that leads to further aggregation of platelets and the formation of a blood clot. The podoplanin-CLEC-2 interaction is dependent on extensive O-glycosylation of the former by the T-synthase, and mice with defective glycosylation machinery in endothelial cells exhibit the blood-filled lymphatic phenotype (Fu et al., 2008). Whether separation of the two vascular compartments is mediated solely by platelet aggregation, or whether the platelet-LEC interaction triggers further signalling events that are also important remains to be established (Koltowska et al., 2013).

Commencing at E15.5 in the mouse, and continuing post-natally, the primary lymphatic plexus is remodelled to form a mature network of lymphatic capillaries, pre-collectors and collecting vessels (Figure 1.2, A) (Koltowska et al., 2013). Some of the key regulators of blood vascular remodelling have been found to play similar roles in lymphatic development, including the angiopoietin/Tie and Ephrin-Eph signalling pathways. Mice hypomorphic for the endothelial RTK Tie1 exhibit LEC hyperplasia, disorganised lymphatic vessels and impaired drainage (Qu et al., 2010), while mice deficient for the Tie2 ligand angiopoietin-2 lack lymphatic valves and display abnormal vessel architecture (Gale et al., 2002). Similarly mice carrying a mutation in the PDZ signalling domain of ephrin-β2 fail to remodel the primary lymphatic plexus into a hierarchal network (Makinen et al., 2005). Increases in interstitial pressure, or 'mechanoinduction' also appear to stimulate lymphatic vessel outgrowth from the lymph sac in developing mouse embryos (Planas-Paz et al., 2012)

The forkhead box protein C2 (FOXC2) plays an important role in the separation of initial and collecting vessel phenotypes, and transient up-regulation of the protein is the first sign of lymphatic collector development (Norrmen et al., 2009; Petrova et al., 2004). Mice deficient for *Foxc2* proceed through the initial stages of lymphatic development normally,

but initial lymphatic vessels later acquire an extensive basement membrane and pericyte coverage, while collecting vessels retain markers associated with initial lymphatics and fail to develop intraluminal valves. Enhancer elements bound by FOXC2 also feature binding sites for NFAT (Nuclear Factor of Activated T-cells) and the two proteins appear to work in tandem on the basis of pharmacological inhibition experiments (Norrmen et al., 2009). Foxc2, Prox1 and the zinc-finger transcription factor GATA2 are up-regulated in lymphatic valves throughout development and persist into adulthood (Koltowska et al., 2013). Valve formation correlates with the start of lymph flow, and their positioning often correlates with sites of disturbed flow, for example at points of bifurcation in collecting vessels (Sabine et al., 2012).

1.1.3 Physiological functions of the lymphatics

The lymphatic system is currently thought to have three primary functions; the maintenance of fluid balance by absorption of protein-rich fluid from the interstitium, the uptake of dietary lipids and vitamins from the gut, and the transport of leukocytes from the tissues to the draining lymph nodes (Johnson and Jackson, 2008). The latter function involves the collection of soluble antigen from the periphery and the trafficking of mature antigen-presenting cells, thus facilitating downstream monitoring by lymph-node resident immune cells. Disruption of the lymphatic system compromises immune function and fluid homeostasis, leading to pathological conditions such as lymphedema. The central functions of the lymphatic vasculature are described here, and their disruption during disease in the following section, 1.1.4.

1.1.3.1 Lymphatic drainage

A high proportion of the fluid and small molecules that egress from the blood vasculature are reabsorbed into the circulation, but ~10% remains, necessitating drainage from the interstitium. Borne within the lymphatic vessels, lymph comprises a variety of migratory leukocytes suspended in a fluid mix of proteins and small molecules, extracellular matrix components and macromolecules. The composition is essentially identical to the interstitial fluid, with the exception of the lacteal vessels of intestinal microvilli, that absorb a substantial amount of fat from the gut (reviewed in Swartz, 2001). Lymphatic capillaries exhibit little size-discrimination regarding uptake of macromolecules, preferentially absorbing 10 – 100 nm diameter particles, compared to an upper size limit of 10 nm for blood vessels. The relatively porous nature of initial lymphatics is a reflection of their architecture; individual cells are loosely connected by 'button' junctions instead of the close-knit 'zippers' found in blood endothelium (Figure 1.3) (Baluk et al., 2007). Flap valves, present at the point of LEC inter-digitation, have a diameter of 2-3 μm and are the entry points for interstitial fluid and migrating cells (Pflicke and Sixt, 2009). The cellular composition of lymph is ~85 - 90% lymphocytes, especially $CD4^+$ T-cells of both memory and naïve phenotypes, and 10 - 15% dendritic cells and monocytes (reviewed in Johnson and Jackson, 2008).

In health, the lymphatic system returns ~2 litres of fluid to the blood per day, at a rate ~100 – 500 times slower than the venous circulation (Swartz, 2001). Two factors govern the net flow rate; lymph formation, or the process of fluid adsorption from the interstitium, and lymph propulsion, the process of driving lymph along the vasculature network. An imbalance in either component results in a build-up of fluid, leading to tissue swelling or edema. In the periphery, the flow of lymph in capillaries is maintained primarily by

contraction of the skeletal muscles, pulsation of arterial blood flow and interstitial fluid pressure. The larger lymphatic collectors feature unidirectional valves, and have an intrinsic pumping action mediated by a layer of smooth muscle surrounding the vessel. Inflammation triggers lymphangiogenesis and expansion of existing vessels, resulting in increased drainage of interstitial fluid and resolution of local swelling (reviewed in Liao and Padera, 2013). However, the response to inflammation is dependent on the antigen and site of immunization, and may equally result in a decrease in lymphatic drainage, for example in response to oxazolone skin painting or intraperitoneal LPS injection. Expression of inducible nitric oxide synthase (iNOS) by infiltrating $CD11b^+$ $Gr\text{-}1^+$ cells disrupts the NO gradients produced by endothelial-NOS (eNOS) in the collecting vessels, resulting in sustained relaxation and the cessation of intrinsic pumping (Liao et al., 2011). Inflammation results in increased liberation of self-antigens that drain through the lymphatic vasculature to the lymph nodes. A decrease in drainage may therefore represent a mechanism of self-protection from autoreactive responses under conditions of sustained inflammation.

1.1.3.2 Entry and migration of leukocytes in lymphatic vessels

The lymphatic vessels are the primary conduit for migration of antigen-presenting cells from the tissues to the draining lymph nodes (Figure 1.3). The process of migration was originally believed to be a passive one, driven primarily by interstitial flow and unencumbered by the porous lymphatic endothelium (Russo et al., 2013). Consideration of lymphatic vessel architecture would suggest that this is unlikely; while flap-valves permit free-flow of interstitial fluid, their small diameter (2 – 3 μm) requires transmigrating cells to undergo a dramatic shape change in order to squeeze through (Stoitzner et al., 2002). It is now known that migration of cells towards initial lymphatics and their transmigration of

lymphatic endothelium is dependent on chemotactic guidance cues and cellular adhesion molecules, especially under conditions of inflammation. The identity of proteins involved and their mechanism of action is relatively poorly understood in comparison to the blood vasculature, but considerable advances have been made in recent years.

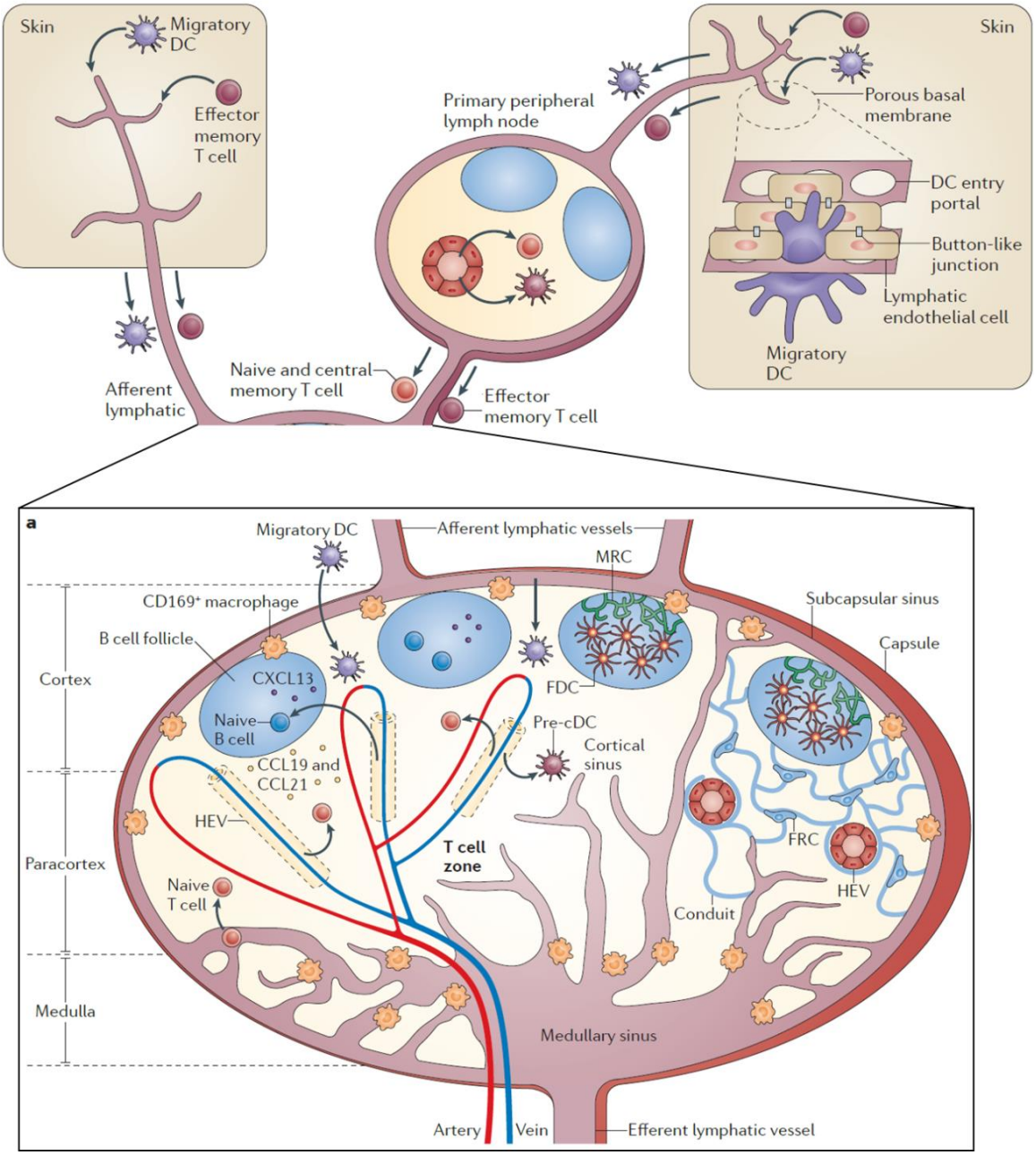


Figure 1.3. **Organisation of the lymph node and trafficking of immune cells via the lymphatic vessels.** MRC: Marginal Reticular Cell, FDC: Follicular Dendritic Cell. Adapted from (Girard et al., 2012).

1.1.3.3 Role of chemokines in leukocyte entry

The principle axis of chemotactic guidance towards lymphatic vessels consists of the chemokine receptor CCR7, which is up-regulated by migratory dendritic cells, T-cells and B-cells, and its ligands CCL21 and CCL19 (Johnson and Jackson, 2008). CCR7-deficient mice exhibit delayed immune responses to foreign antigen, especially that applied to the skin, due to a failure to mobilize epidermal DCs to the lymph nodes (Forster et al., 1999). Dermal DCs were subsequently found to accumulate in the tissues under both steady-state and inflammatory conditions, suggesting that CCR7-signalling is required for transmigration of lymphatic endothelium in addition to its chemotactic role (Ohl et al., 2004). Similarly, the absence of CCL21 and CCL19 ligands in the naturally occurring mouse strain *plt* (paucity of lymph node T-cells) results in the failure of T-cells and DCs to accumulate in the lymph node.

In mice, there are two CCL21 genes that differ by a single amino acid, CCL21-Ser and CCL21-Leu. The former is expressed mainly by lymphatic endothelium, to the exclusion of CCL19, and is the principle attractant for CCR7-expressing cells towards initial lymphatics (Forster et al., 2012; Vassileva et al., 1999). The *plt* mouse retains expression of CCL21-Leu, but lacks CCL21-Ser, which is produced by HEVs and fibroblastic reticular cells (FRCs) in the lymph node, and is essential for retaining T-cells and DCs that enter via the afferent lymphatics (Bajenoff et al., 2008; Luther et al., 2000). CCL21 features a C-terminal tract of positively-charged residues, absent from CCL19, that facilitates its immobilization in the ECM or at the cell surface via heparan sulphate moieties (Bao et al., 2010; Hirose et al., 2002). Surface-bound CCL21 enhances cell migration by triggering integrin activation and cell adhesion (Schumann et al., 2010).

Immunofluorescence studies and time-lapse microscopy have revealed the distribution of CCL21 in lymphatic vessels and the response of CCR7-expressing cells. The chemokine is present as large intracellular deposits within lymphatic endothelium, as discrete puncta on the cell surface, and as a heparan sulphate-immobilized gradient that radiates out from the vessel (Johnson and Jackson, 2010; Tal et al., 2011; Weber et al., 2013). Dendritic cells that pass within 90 µm of a lymphatic vessel are able to detect the CCL21 gradient and exhibit an increase in velocity and directedness of motion towards the capillary that is not seen in CCR7-deficient cells (Weber et al., 2013). DCs also appear to dock onto CCL21 puncta immobilized at the cell surface, before initiating the transmigration process (Tal et al., 2011).

While the CCL21-CCR7 axis appears to be the principle process guiding cells towards lymphatic vessels, other factors have been recently identified that are significant for certain subsets of migratory cells. These include CXCL12, which is upregulated by LECs in response to inflammation, and enhances migration of CXCR4-expressing dermal DCs and langerhan cells (LCs) to draining lymph nodes (dLNs) (Kabashima et al., 2007). The lipid receptor Sphingosine-1-phosphate receptor-1 ($S1P_1$) is upregulated in activated skin DCs and required for efficient trafficking of these cells to dLNs (Czeloth et al., 2005), however the involvement of $S1P_1$ in lymphatic trafficking is unclear, as deletion of S1P kinase in LECs blocks lymph node egress, but not ingress (Pham et al., 2010). Most recently CX3CL1, also known as fractalkine, has been shown to be produced by LECs in response to inflammation, and neutralizing antibodies against CX3CL1 dramatically reduce allergen-induced trafficking of cutaneous DC to dLNs (Johnson and Jackson, 2013).

1.1.3.4 Leukocyte transmigration under resting and inflammatory conditions

Dendritic cells enter the lymphatic capillaries in a two-step process, first traversing 'portals' in the surrounding basement membrane (BM), before entering the vessel lumen via flap-valves between individual cells (Pflicke and Sixt, 2009). Both dermal DCs and Langerhan cells transiently dilate gaps in the BM, before probing the surface and lumen of the vessel, in an apparent search for an entry point. The process of transmigration has been variously reported to take 20 – 30 mins (Sen et al., 2010), or 30 – 60 mins (Tal et al., 2011) and it is not uncommon to observe a second DC following the path created by a predecessor. Under steady-state conditions, entry of dendritic cells is integrin and protease-independent, but requires active cell flowing and crawling (Lammermann et al., 2008). This contrasts the situation in blood endothelium, where cellular adhesion molecules (CAMs) such as integrins are essential for extravasation. This is perhaps unsurprising given the difference in junctional arrangement in lymphatic capillaries, sparse distribution of basement membrane and the fact that LECs express do not express integrins under resting conditions (Johnson et al., 2006).

During inflammation, lymphatic endothelium is activated by inflammatory cytokines and strongly upregulates expression of ICAM-1, VCAM-1 and E-selectin together with a panel of chemokines that attract migratory cells. Ablation of DC migration to the dLNs in ICAM-$1^{-/-}$ mice (Xu et al., 2001) or by antibody blockade (Johnson et al., 2006) has demonstrated that CAMs play an important role in lymphatic entry during inflammation. The relative contribution of these receptors appears to be dependent on the antigen type and the mode of immunization, as differential expression of integrins and CCL21 chemokine by dermal LECs has been observed following inflammation induced by contact-hypersensitivity or application or complete Freund's adjuvant (Vigl et al., 2011). It is unclear whether

migratory leukocytes are able to enter pre-collecting or collecting vessels, however it has been reported that button junctions found in the initial lymphatics convert to the zipper formation during chronic inflammation (Yao et al., 2012). An emerging theme in lymphatic research is that entry into vessels appears to be more selective during certain types of inflammation. Once inside lymphatic capillaries, cells exhibit crawling behaviour, a process that requires actomyosin-mediated cellular contraction and Rho-associated protein kinase (ROCK), which mediates de-adhesion of integrins (Nitschke et al., 2012). Lymph flow in the capillaries is very low (1 – 30 μm), but increases to several mm/sec in the collecting vessels, which is sufficient to propel cells in suspension towards the lymph nodes (Russo et al., 2013).

1.1.3.5 Organisation and function of the lymph nodes

The lymph nodes have a highly organised microarchitecture designed to maximise interaction of naïve lymphocytes with antigen delivered via the lymphatics (reviewed in Forster et al., 2012; Girard et al., 2012; Liao and Padera, 2013). Three main regions, the cortex, paracortex and medulla are surrounded by a bean-shaped capsule that is penetrated by afferent lymphatics in the outer hemisphere (Figure 1.3). The node is connected to the blood supply and a downstream lymph node at the hilum, the point at which cells and fluid egress into the efferent lymphatic vessel. Lymph transported by the afferent lymphatics drains initially into the subcapsular sinus (SCS), a thin region underlying the capsule defined by a layer of weakly LYVE-1^+ endothelium, and interspersed with $CD169^+$ macrophages. Fluid then percolates into the cortex, which is comprised mainly of B-cells organised into primary lymphoid follicles, and is the site of the germinal centres that appear during an adaptive immune response. The underlying paracortex contains the T-cell zone and is punctuated by high endothelial venules (HEVs), a specialized blood endothelium

that expresses the peripheral node addressin (PNAd) and supports extravasation of naïve L-selectin$^+$ lymphocytes. Different lymph node stromal cells secrete chemokines that direct organisation of leukocytes into the appropriate compartments. HEVs and fibroblastic reticular cells (FRCs) express CCL21 and CCL19 to recruit naïve T and B cells from the circulation and direct migration of CRR7$^+$ DCs from the subcapsular sinus, thus concentrating both cell types in the paracortex and facilitating T-cell activation via antigen presentation. Follicular stromal cells and follicular DCs located in the cortex also produce CXCL13, which guides CXCR5-expressing B-cells to the B-cell follicles. Lymphocytes that do not recognize their specific antigen in a particular node follow a sphingosine-1-phosphate gradient produced by LECs and exit via the efferent lymphatic. To reach the hilum, cells transit narrow fluid-filled crevices termed cortical sinusoids, that eventually widen into the medullary sinuses. This region of endothelium is strongly LYVE-1$^+$ and in common with the subcapsular sinus is enriched with plasma cells and CD169$^+$ macrophages.

The cellular content of afferent lymph includes a majority of effector/memory T-cells, dendritic cells that have undergone antigen-stimulated maturation, and naïve T-cells that have egressed from an upstream lymph node (Forster et al., 2012). Mature dendritic cells entering the subcapsular sinus have upregulated levels of CCR7, and migrate into the T-cell zone in response to a CCL21 gradient produced by HEVs. Here they encounter naïve T-cells and present antigens engulfed in the tissues alongside co-stimulatory molecules. Soluble antigens borne in the lymph with a molecular weight <70 kDa are also able to penetrate the cortex using a fluid-filled reticular conduit system, and are engulfed by follicular DCs (Liao and Padera, 2013). Larger antigens are phagocytosed by CD169$^+$ macrophages and B-cells and are processed and presented to naïve lymphocytes. During inflammation, the increased influx of self-antigen from the inflamed tissue raises the

possibility of an autoreactive immune response, as not all self-reactive T-cells are deleted in the thymus. The lymph node compensates by down-regulating PNAd, CCL21 and CXCL13 in the initial stages of inflammation, thus reducing influx of naïve lymphocytes. In addition, both follicular DCs, LECs and FRCs contribute to peripheral tolerance by presenting self-antigens in the absence of costimulatory molecules or inflammatory cytokines. This serves to limit any self-reactive T-cell response by inducing anergy, clonal deletion and the expansion of regulatory T-cells (Liao and Padera, 2013).

1.1.4 Involvement of lymphatics in disease pathology

The lymphatic system plays important roles in the maintenance of fluid balance and immune surveillance, so it is unsurprising that disregulation or dysfunction of the vasculature has important consequences in disease. Defects in lymphatic function can lead to compromised immune function or accumulation of fluid in the interstitium, while metastasizing tumour cells exploit the lymphatic vessels as a major route for their dissemination (Alitalo, 2011; Sleeman and Thiele, 2009). In recent years, a greater appreciation of the role played by the lymphatics in a variety of disease processes had led to increased focus on the molecular mechanisms underlying lymphatic dysfunction.

1.1.4.1 The lymphoedemas

Lymphedema is characterized as a dysfunction of fluid drainage by the lymphatics, leading to non-pitting localized tissue swelling and impaired local immunity (reviewed in Lyons and Modarai, 2013). Reflux of lymph from the initial lymphatics may manifest as accumulation of lymph in the abdomen, heart, lungs or skin, progressing to subcutaneous tissue fibrosis. Patients are predisposed to episodes of cellulitis and lymphangitis and suffer from reduced mobility and pain associated with swollen tissue. Primary lymphedema

describes a group of rare hereditary diseases, many of which involve mutation of genes associated with lymphatic development and growth factor signalling. Onset of primary lymphedemas may occur in utero, neonatally, or more frequently years after birth (reviewed in Schulte-Merker et al., 2011). Lymphedemadistichiasis syndrome (LD) is an example of late-onset lymphedema where the underlying genetic component has been defined. Patients typically possess a double-row of eyelashes and present with swelling arising from lymph reflux, despite normal densities of lymphatic vessels (Fang et al., 2000). Disrupted fluid drainage arises from loss-of-function mutations in *foxc2*, resulting in a lack of intraluminal valves in the collecting vessels. By contrast, patients suffering from Milroy's disease have undeveloped or disrupted cutaneous lymphatic vessels and mis-sense mutations in the signalling domain of VEGFR-3 (Karkkainen et al., 2000). An inability to respond appropriately to the pro-lymphangiogenic growth factor VEGF-C likely accounts for the disrupted lymphatic network.

Secondary, or acquired lymphedema is the second leading cause of chronic disability, affecting ~ 15 million people worldwide (Lyons and Modarai, 2013). In the western world, secondary lymphedema typically arises from cancer treatment, especially following radiotherapy or surgical removal of lymph nodes. The condition is a relatively common post-operative complication for patients undergoing mastectomy (24 – 49%) or lumpectomy (4 – 28%). Growth factor therapy, using adenoviruses to deliver VEGF-C and promote lymphangiogenesis in mice and pigs has been successful in restoring surgical damage to the lymphatic network, and is currently being developed for use in humans (reviewed in Alitalo, 2011). Certain infectious agents are also capable of disrupting lymphatic function, and are the major cause of lymphedema in developing countries. The majority of cases are attributed to nematode worms that migrate into the lymphatic vessels and persist for many years, resulting in filiariasis or elephantitis.

1.1.4.2 Tumours of the lymphatic system

A number of tumour types are known to rise from lymphatic tissues, including lymphagiosarcoma, a malignant tumour described in patients with long-standing lymphedema. Others bear the molecular markers of lymphatic vasculature, such as Kaposi's sarcoma (KS), where blood endothelial cells transformed by infection with human herpes virus 8 (HHV8) are reprogrammed toward the LEC-lineage (Wang et al., 2004). Conversely, HHV8-infected LECs take on a spindle-like morphology and begin to express markers of blood endothelium, while a component of the viral capsid activates VEGFR-3 and induces endothelial cell proliferation and migration (Zhang et al., 2005). Blockade of VEGFR-3 with monoclonal antibodies has been shown to reduce growth and sprouting of infected LECs *in vitro* and is being assessed as a potential therapeutic (Tvorogov et al., 2010). Lymphangioleiomyomatosis (LAM) is a rare lung disease affecting women of child-bearing age and is characterized by a hyper-proliferation of smooth muscle cells that metastasize via lymphatic vessels (Seyama et al., 2010). LAM cells express high levels of VEGF-D and become covered with LECs, eventually invading the lymphatic vessels, destroying the lung parenchyma and resulting in death. Approximately one-third of patients carry mutations in the mTOR-suppressors (mammalian target of rapamycin) TSC-1 or TSC-2, and rapamycin has been trialled alongside VEGFR-3 inhibitors as potential therapies, with some success. However both strategies serve only to slow disease progression, and lung transplant remains the final treatment option in most cases.

1.1.4.3 Exploitation of the lymphatics during tumour metastasis

The lymphatic vasculature is frequently co-opted by metastasizing tumours as a route for dissemination around the body (reviewed in Alitalo, 2011; Liao and Padera, 2013). The presence of metastases in the tumour-draining or sentinel lymph node is central to staging systems used for most cancers, and is strongly prognostic of patient outcome. However, the significance of the lymphatic metastatic route, beyond its prognostic value, is controversial. The anatomical-mechanical model of tumour metastasis proposed that tumour cells spread sequentially along the chain of draining lymph nodes in a predictable fashion, before being deposited into the venous circulation. As a result, complete surgical resection of axillial lymph nodes in response to metastases in the sentinel node remains common-place in breast cancer surgery. However several large clinical trials have concluded that the effect on patient long-term survival is negligible, thus calling into question the efficacy of such radical surgical intervention (Giuliano et al., 2011; Louis-Sylvestre et al., 2004). Many tumours also exploit the blood vasculature as a route for metastasis, and there is growing evidence that genetic variation in primary tumours is an early event, leading some cells to disseminate before lymph-node metastases are apparent. The contribution of lymph-node spread to disease progression and treatment is therefore likely to be dependent on the tumour type and location.

Solid tumours frequently feature high interstitial pressure, a factor that is thought likely to encourage entry of tumour cells into lymphatic vessels, and has been positively correlated with dissemination to the draining lymph node (reviewed in Swartz and Lund, 2012). Intratumoural vessels are thought to be collapsed to the high pressure, but the density of peritumoural vessels has been correlated with metastasis in a variety of tumours, and the presence of flap-valves may facilitate easier access than is the case for blood capillaries

(Alitalo, 2011). LECs also produce CCL21 and CXCL12 in response to tumour-associated inflammation, which attracts those tumour types that express chemokine receptors CCR7 and CXCR4 (Kim et al., 2010; Shields et al., 2010). Some tumours or their tumour-associated macrophages (TAMs) also express pro-lymphangiogenic growth factors such as VEGF-C and VEGF-D, and are pre-disposed to lymph node metastasis. Tumour-induced lymphangiogenesis enhances delivery of antigens and tumour cells to the dLNs, and correlates increased metastasis and poor patient prognosis (Liao and Padera, 2013). There is evidence that the lymph nodes are pre-conditioned prior to seeding with metastasizing cells, thus enhancing the environment for these invading cells. The ability of LECs, follicular DCs and lymph-node macrophages to present antigen and participate in peripheral tolerance is also thought to work against the anti-tumour T-cell response. There is considerable interest therefore in understanding tumour-cell dissemination via the lymphatics, both as a route for metastasis and the effect on anti-tumour immune response.

1.2 Hyaluronan

1.2.1 Hyaluronan structure and solution properties

Hyaluronan is a large, uniformly repetitive, linear glycosaminoglycan composed from a disaccharide repeat unit of D-glucuronic acid (GlcA) and *N*-acetyl D glucosamine (GlcNAc) (Figure 1.4a). HA was originally purified from the vitreous humour of bovine eye, from which it derives its name; hyaloid (vitreous) and uronic acid (Meyer and Palmer, 1934). A number of years later, the repeating GlcA and GlcNAc residues were shown to be linked by alternating β1-3 and β1-4 linkages (Weissmann and Meyer, 1954). The polysaccharide is a fundamental component of the extracellular matrix within all tissues of vertebrates, but is also synthesized by some bacteria, such as group A streptococci (Kass and Seastone, 1944). Unlike other glycosaminoglycans, such as heparan, chondroitin and keratan, HA is synthesized as a free chain without attachment to a protein core, and is also non-sulphated. These chains can be very large, of the order of $10^2 – 10^4$ kDa and containing 2000 – 25 000 disaccharide repeat units, with typical lengths of 2 – 25 μm (Jackson, 2009; Toole, 2004).

In solution, HA chains are highly flexible and dynamic, undergoing rapid kinking and bending, but with an average structure akin to a stiffened random coil (Figure 1.4,b-e) (Day and Sheehan, 2001). The molecular dynamics of HA in solution have been probed using computer simulation and NMR that identify weak hydrogen bonding across the two glycosidic linkages as mediating flexibility of HA chains (Almond et al., 1998; Almond et al., 2006). Inter-chain hydrogen bonding however is uncommon, as confocal-FRAP experiments have shown convincingly that HA chains remain dispersed even at high concentration (Gribbon and Hardingham, 1998; Gribbon et al., 2000). The dynamic nature

of the carbohydrate chain and its overall negative charge attract positive counter ions; the resulting osmotic potential draws in water, with the result that HA is highly soluble. The remarkable viscosity of HA solutions is a function of concentration, chain length, salt concentration and pH (Lapcik et al., 1998). The combination of viscosity, dynamic flexibility and high levels of hydration mean that HA is an excellent coloniser of extracellular space and recovers rapidly from mechanical compression (Day and Sheehan, 2001).

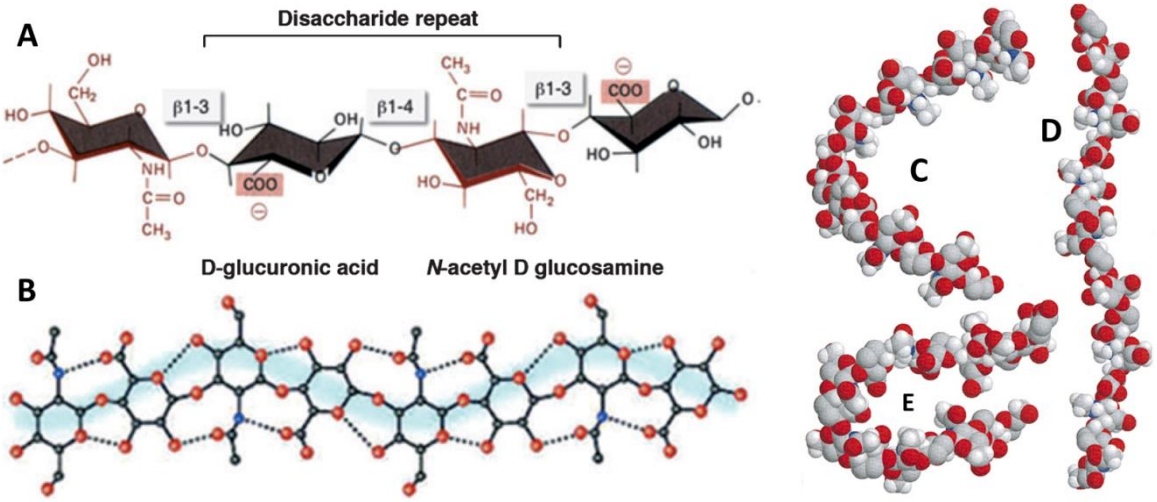


Figure 1.4. **Structure of hyaluronan.** Hyaluronan is a linear glycosaminoglycan composed from a disaccharide repeat unit of D-glucuronic acid and N-acetyl D glucosamine joined by alternating β1-3 and β1-4 linkages (A). The molecule exists as a stiffened random coil in solution (B), but is considerably more flexible than related polymers such as cellulose, thanks to a high degree of flexibility across the ß1-4 glycosidic bond. Using a combination of NMR and molecular dynamics simulations, a number of potential HA conformations have been described (C, D, E). Adapted from (Almond et al., 1998; Jackson, 2009)

1.2.2 Hyaluronan synthesis

Hyaluronan is synthesized on the inner leaflet of the plasma membrane and extruded directly into the extracellular space by members of the hyaluronan synthase (HAS) family (Prehm, 1984). This method of biosynthesis has two advantages; firstly it avoids the difficulties associated with production of other large macromolecules in the ER or golgi and secondly it permits unrestricted elongation of HA chains (Weigel and DeAngelis, 2007). Synthesis of a single HA chain of 1 MDa or more is an energetically costly process for the cell, consuming approximately 50 000 ATP equivalents, 20 000 NAD cofactors and 10 000 molecules of acetylCoA (Lee and Spicer, 2000). Elongation is achieved in most HAS by the sequential addition of UDP-GlcA and UDP-GlcNAc oligomers to the reducing end of the HA chain in the presence of Mg^{2+} (Prehm, 1984). HA polymerization may continue until chain length exceeds the unit length of the cell, with an upper molecular weight in the low megadalton range (Laurent and Fraser, 1992).

Hyaluronan synthases are divided into two major classes; Class I enzymes are located in the plasma membrane and are subdivided into those that catalyse addition of UDP-sugars to the non-reducing termini (xlHAS1 from Xenopus laevis is the only known example) and those polymerise from the reducing terminus (Weigel and DeAngelis, 2007). The only known Class II HAS is a bacterial peripheral membrane protein with distinct structural features, isolated from a pathogenic strain of Pasteurella multocida (pmHAS) (DeAngelis et al., 1998). Another HA-encapsulated bacterium, Streptococcus pyogenes, was the source of the first HAS to be cloned and characterised (DeAngelis et al., 1993). This report was followed by the isolation of three isoforms of mammalian HAS (Itano and Kimata, 1996; Shyjan et al., 1996; Spicer et al., 1996; Spicer et al., 1997; Watanabe and Yamaguchi, 1996) and the first and only example of a viral-encoded HAS from chorella PBCV-1

infected algae (DeAngelis et al., 1997). While HAS-1 is the most widely expressed of the mammalian isoforms (Spicer and McDonald, 1998), only HAS-2 has be shown to be essential for embryonic development; HAS-2 deficient mice die at embryonic day 9.5-10 from severe cardiac and vascular abnormalities, while HAS-1 and HAS-3 deficient mice are viable (Camenisch et al., 2000). While these observations suggest a level of redundancy, it has been reported that HAS-1 and HAS-3 expressing COS-1 cells secrete HA with size distributions from 0.2 to 2.0 MDa, whereas HAS-2-expressing cells make larger HA with an average molecular mass of >2 MDa (Itano et al., 1999).

Two competing models have been proposed for the mechanism of HA synthesis by HAS enzymes; the so-called 'pore hypothesis' (Tlapak-Simmons et al., 1999) and the ABC transporter model (Ouskova et al., 2004; Prehm and Schumacher, 2004). The former proposes that an intra-HAS pore traverses the plasma membrane and simultaneously traps the HA chain, to permit addition of further UDP-glucose, and then releases it to facilitate translocation to the exterior. A key conceptual problem with this model is that twelve transmembrane spans are typically required for a functional pore, whereas active HAS have only 6-8, supported by a number of cardiolipin molecules (Tlapak-Simmons et al., 1998). The latter proposes that HAS synthesizes intracellular HA, which is recognized and transported by a membrane-bound ABC transport system, a mechanism exploited by bacteria for the export of other polysaccharides. However, recent observations have tipped the balance firmly in favour of the pore hypothesis. HA synthesis proceeds uninhibited by ABC transporter inhibitors in breast carcinoma cell lines (Thomas and Brown, 2010), while purified S. equisimilis HAS (SeHAS) reconstituted in liposomes displays pore activity that mediates dye translocation (Medina et al., 2012) and also HA translocation to the lumen (Hubbard et al., 2012).

1.2.3 Hyaluronan turnover and degradation

The total HA content of the human body has been estimated at ~15g, of which one-third is degraded and replaced daily (Fraser et al., 1997). The rate of turnover varies markedly between tissues; the half-life of HA in the blood is as short as 2-5 minutes, and as long as 1-3 weeks in synovial cartilage (Stern, 2003). In the skin, which accounts for 50% of the total body HA, constant synthesis by keratinocytes and shedding of the epidermis results in a half-life of 1-1.5 days (Laurent and Fraser, 1992; Reed et al., 1990). During inflammation, injury and infection the rate of degradation can increase drastically; HA can be released from hyaladherins by matrix metalloproteinases (Chockalingam et al., 2004), degraded by the neutrophil oxidative burst (Greenwald and Moak, 1986) or digested by metastasizing tumour cells (Sugahara et al., 2003). The resulting low molecular weight degradation products are subsequently detected as an increase in lymph or plasma HA levels (Laurent et al., 1996).

Under steady-state conditions, the majority of HA degradation is thought to occur locally through uptake by cells such as macrophages and fibroblasts (Armstrong and Bell, 2002). Low to medium weight HA chains originating in peripheral tissues are drained by the lymphatic system and ultimately taken up by the HA receptor on endothelium (HARE), also known as Stabilin-2 (Falkowski et al., 2003; Harris et al., 2007). A smaller proportion still passes through to the blood circulation where it is rapidly removed by HARE molecules present on liver and spleen sinusoidal endothelium.

There are six human hyaluronidase-related genes clustered on two chromosomal loci, 3p21.3 (*HYAL1*, *HYAL2*, and *HYAL3*) and 7q31.3 (*HYAL4*, *HYALP1*, and *SPAM1*) (Csoka et al., 1999). *HYALP1* is a pseudogene, *HYAL4* encodes a chrondroitinase with no activity against HA (Csoka et al., 2001) and *SPAM1* is responsible for the sperm acrosome

hyaluronidase PH-20 (Cherr et al., 2001). Hyal-3 has a restricted expression pattern and its ability to degrade HA is questioned due to a lack of Fl-HA uptake when over-expressed in HEK 293T cells (Harada and Takahashi, 2007). The more widely expressed Hyal-1 and the GPI-anchored Hyal-2 have therefore been proposed to play the major roles in constitutive HA degradation *in vivo* (Stern, 2003). A model has been proposed whereby HA tethered to cell surfaces by CD44 or HARE is concentrated in caveolin-rich lipid rafts, cleaved by GPI-anchored Hyal-2 into intermediate-size fragments and further degraded to oligosaccharides within the lysosome by Hyal-1, in coordination with β-glucuronidase and β-N-acetyl-glucurosaminidase (Stern, 2004).

Recently, this model has been called into question following the discovery that KIAA1199, a deafness gene of previously unknown function, is a novel hyaluronidase lacking sequence homology with other known hyaladherins (Yoshida et al., 2013). Yoshida and colleagues noted a number of inconsistencies with the existing description of HA turnover, including the absence of Hyal1 and 2 in the brain, a reported lack of hyaluronidase activity by Hyal2, the presence HA degradation products in tissue exceeding the size generated by Hyal1, and the lack of significant HA accumulation in mice deficient for Hyal1 or 2. KIAA1199 was identified by microarray analysis of primary human fibroblasts, prompted by the observation that HA depolymerisation continues despite knockdown of CD44, Hyal-1 or Hyal-2. Conversely, HA degradation is abolished in these cells following knockdown of KIAA1199, and enhanced degradation of HA in synovial fibroblasts from patients with osteoarthritis or rheumatoid arthritis is correlated with increased expression of the protein. HA catabolism proceeds independently of CD44 or Hyal enzymes, but does involve clathrin-mediated endocytosis and endo-β-N-acetylglucosaminidase. This suggests that KIAA1199 is central to HA turnover in the skin under steady-state conditions.

1.2.4 Hyaluronan function

Hyaluronan is a polymer with simple chemistry, yet is involved in a diverse array of biological processes, from space-filling and scaffolding roles, to the modulation of cell behaviour and progression of disease. This diversity is a reflection of the large number of proteins with which it interacts, each with their own or inter-connected functions (Day and Prestwich, 2002). In many instances, HA provides the scaffold for organisation into higher-order architectures with specific structural or instructional roles. Hence, the function of HA is primarily dictated by the proteins with which it interacts, a number of which are described in Section 1.3.

In addition to the HA binding proteins, there is a clear relationship between HA size, specifically chain length, and functional outcomes. By far the greatest proportion of HA in the body is high molecular weight (HMW), defined as exceeding 100 kDa, and representing the resting state of the extracellular matrix. HMW HA has primarily structural, lubricating and shock-absorbing properties; it is abundant in the synovial fluid of the joints, and in complex with aggrecan and cartilage Link protein, is a major constituent of intra-articular cartilage (Figure 1.5) (Schmidt et al., 2007).

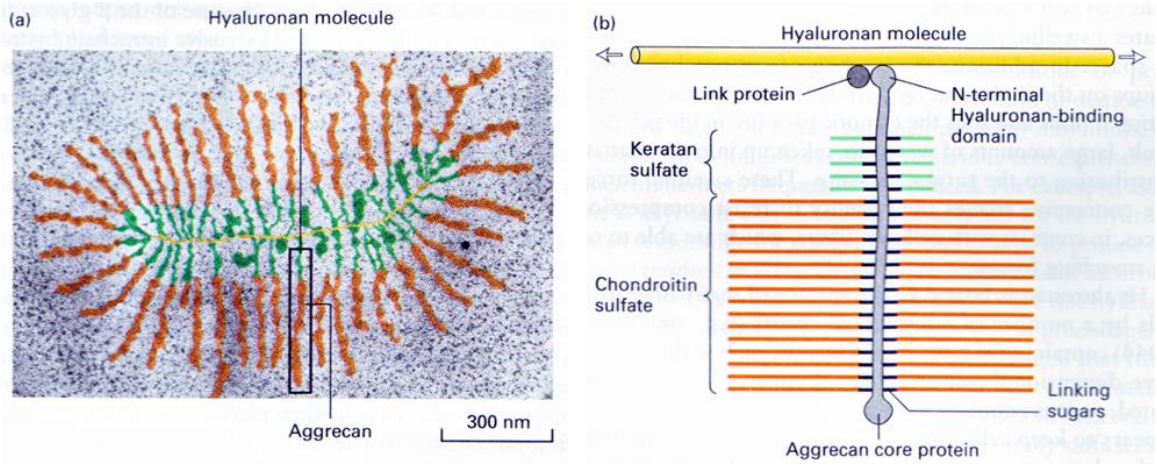


Figure 1.5. **False colour electron micrograph and schematic of an Aggrecan-decorated HA chain from cartilage.** Adapted from (Lodish, 2004)

HMW HA predominates under resting conditions and has a down-modulating effect on surrounding cells; as such it is commonly described as an inert or anti-inflammatory matrix component. Various reports have described anti-angiogenic effects on endothelial cells in adults (Deed et al., 1997), and during development (Rooney and Kumar, 1993), suppression of inflammation following lung injury (Jiang et al., 2005), reduced phagocytosis by macrophages (Forrester and Balazs, 1980) and restriction of antibody-antigen interactions (Delmage et al., 1986). Cross-linking of CD44 by HMW HA induces Foxp3 expression in $CD4^+$ $CD25^+$ T_{Regs}, promoting their persistence and thus immune tolerance (Bollyky et al., 2009). In the bone marrow, HA is required for haematopoiesis, as shown by the decrease in number and reduced activity of hematopoietic stem/progenitor cells (HSPC) in HAS1,2,3 triple knockout mice (Goncharova et al., 2012). Following tissue injury, monocytes migrate into the wound site and differentiate into fibrocytes, a fibroblast-like cell type that mediates tissue repair. The differentiation process is potentiated by HMW HA, but inhibited by low molecular weight HA fragments (Maharjan et al., 2011).

Under certain pathological conditions, lower molecular weight (LMW) HA chains predominate following HA degradation by hyaluronidases or the oxidative burst of neutrophils (Agren et al., 1997). The smallest of these fragments are bound by Toll-like receptors such as TLR-4 (Termeer et al., 2002) and are pro-inflammatory, inducing chemokine expression by alveolar macrophages (McKee et al., 1996), activating tissue resident dendritic cells (Termeer et al., 2000) and prompting endothelial cells to initiate wound repair following injury (Taylor et al., 2004). Cytokines released by these cells, such as IL-1β, TNF-α, and IL-12 initiate the inflammatory or wound healing response, attracting leukocytes to the site of inflammation (Termeer et al., 2002). HA oligosaccharides are also pro-angiogenic, inducing proliferation and migration of vascular endothelial cells during

the wound healing response (Slevin et al., 1998; Slevin et al., 2002; West et al., 1985) and neovascularization of tumours (Rooney et al., 1995).

HA degradation products are commonly detected in diseases and inflammatory conditions, such as arthritis and cancers (Ghosh, 1994; Sugahara et al., 2003). The reduced average molecular weight of HA in synovial fluids from patients with osteoarthritis (OA) or rheumatoid arthritis (RA) decreases synovial viscosity and is associated with intra-articular inflammation (Soltes et al., 2006; Vuorio et al., 1982). Injections of high molecular weight HA have been used to alleviate symptoms by restoring the elastic and viscous properties of the synovial fluid, decreasing inflammatory cell count and stimulating chrondrocyte proliferation (Kogan et al., 2007). While the origins of inflammatory bowel disease (IBD) are unknown, increased HA staining has been observed in inflamed tissue sections from patients with ulcerative colitis or Crohn's disease (de La Motte et al., 1999). HA deposition is associated with remodelling into HA cable structures, and precedes the onset of inflammation and arrival of leukocytes that bind cables via CD44 (de la Motte et al., 2003; Kessler et al., 2008).

1.2.5 Hyaluronan and cancer

Hyaluronan is a prominent component of the tumour microenvironment, where it influences tumour growth and metastasis and can be prognostic for tumour progression (Toole, 2009) (Figure 1.6). This includes HA directly associated with tumour cells and in the peritumoural stroma (Tammi et al., 2008). The picture of HA interactions within tumours is complex; significant parameters include turnover rate, absolute concentration, chain length and association with hyaladherins. The outcome arising from these parameters is dependent on the tumour site, the tumour type, tumour stage, expression of HA binding

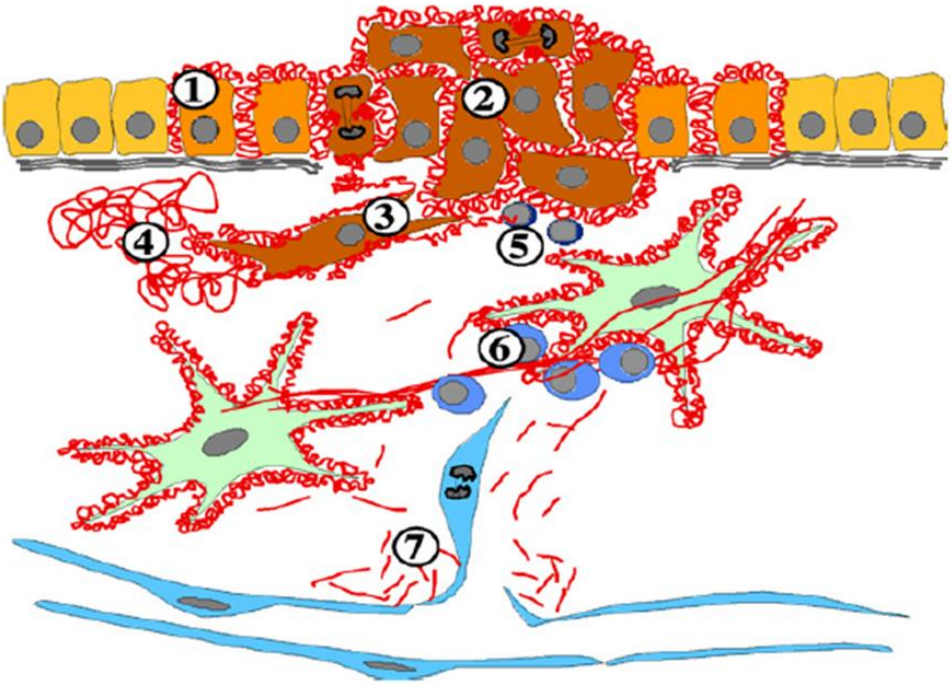
proteins, signalling outcomes resulting from interaction with HA and the response of other cell types, particularly immune cells that may attack the tumour.

A reflection of this complexity is the degree of contradiction in the literature surrounding the significance of HA in tumours. However, some general themes have emerged. HA often accumulates in cancer tissues, and this is particularly noticeable at sites that typically lack significant amounts of HA (Tammi et al., 2008). Examples include tumours originating from connective tissue or of epithelial origin, such as carcinomas of the head and neck, breast, ventricle, pancreas and colon (Knudson et al., 1989). In most of these cases, HA accumulation is prognostic, usually of poor patient outcome (Toole, 2002). Conversely, at sites where hyaluronan is abundant under non-pathological conditions, reduced levels of HA is associated with poor prognosis, as reported for oral squamous cell carcinoma (Kosunen et al., 2004) and cutaneous melanoma (Karjalainen et al., 2000).

HA accumulation or decrease in the tumour stroma may arise from changes in synthesis or degradation. For example, HAS-2 is up-regulated in breast cancer stem-like cells (CSC) and plays a critical role in the generation of a prometastatic microenvironment, through attraction of tumour-associated macrophages (Okuda et al., 2012). However there can also be an optimum level of HA synthesis, as tumourigenicity of transformed fibroblasts increases with HAS expression only up to a point, beyond which growth is inhibited (Itano et al., 2004). Recently, the well-documented cancer resistance of the naked mole rat has been attributed to high concentration of HA in the skin, and a global increase in sensitivity to HA-induced signalling (Tian et al., 2013). Naked-mole rats express a novel HAS-2 mutant that synthesizes very high molecular weight HA (6-12 MDa) that is approximately five times larger than that found in humans or mice. Increased Hyal-1 hyaluronidase activity is also a strong negative prognostic indicator in prostate and bladder cancers

(Tammi et al., 2008), however both elevated and lowered levels have been reported to enhance malignancy in the former (Lokeshwar et al., 2005)

The mechanisms by which HMW HA and its degradation products influence tumour growth has recently been reviewed by Tammi et al. (2008) (Figure 1.6). Citing the example of an epithelia layer, where HA is not typically abundant, transformation of cells is followed by significant aberrant HA synthesis. The local response is similar to that expected during inflammation or injury; HMW HA stimulates cell proliferation, epithelial to mesenchymal transition, and enhances cell locomotion, particularly at the invading edge. Engagement through CD44, a common marker of cancer stem cells, triggers signalling cascades that prevent apoptosis. Monocyte-derived macrophages are drawn into the tumour mass by inflammatory cytokines, but are immobilized and deactivated through binding to HA cables that arise during inflammation. Finally, HA oligosaccharides generated during matrix remodelling have pro-angiogenic effects on local vascular endothelium, resulting in *de novo* synthesis of blood capillaries that enhance oxygen and nutrient supplies to the tumour mass.



1. Hyaluronan is not present in normal simple epithelia, but emerges in epithelial inflammation or injury, presumably to enhance cell proliferation and migration to cover the defect.
2. Hyaluronan is also upregulated when the epithelial cells undergo malignant transformation. It supports cell proliferation, prevents apoptosis, maintains intercellular space to facilitate nutrient diffusion, and enhances cell locomotion that stimulates invasion.
3. Hyaluronan synthesis enhances epithelial to mesenchymal transition in the cancer cell phenotype which releases the cells from their epithelial compartment for invasion.
4. Accumulation of hyaluronan in the stroma opens the fibrillar matrix for cell migration.
5. A coat of hyaluronan on cancer cells shields them from the cytotoxic effects of T-lymphocytes.
6. Free hyaluronan, arranged as "cables" in fixed cell preparations, binds tissue macrophages and modulates their activity to favor tumor growth.
7. Fragments of hyaluronan (oligosaccharides) stimulate endothelial cell proliferation and budding of new capillaries that allow tumor expansion.

Figure 1.6. **Localization of hyaluronan and potential roles in a malignant invasive tumour arising from simple epithelia.** Hyaluronan is shown in *red*, normal and transformed epithelia in *yellow* and *orange*, respectively, tumour cells in *brown*, vascular endothelium in *light blue*, T-cells in *navy* and activated and quiescent tumour-associated macrophages in *green* and *dark blue*, respectively. Adapted from (Tammi et al., 2008).

1.3 Hyaluronan binding proteins

Hyaluronan is bound by a variety of HA-binding proteins, or hyaladherins, many of which are members of the Link module superfamily (Day and Prestwich, 2002) (Figure 1.7). Members of this family contain one or more copies of the HA-binding Link domain, a conserved sugar-binding module of approximately 100 residues that resembles the C-type lectin fold (Brissett and Perkins, 1996; Kohda et al., 1996). The fold comprises two antiparallel ß-sheets made from a total of six ß-strands (ß1-6) and two α-helices stabilized by a pair of conserved disulpide bridges and was first identified as a structural domain in Link protein purified from cartilage (Neame et al., 1986). The consensus Link module is found as both a single unit, as in TSG-6 (tumor necrosis factor-stimulated gene-6), and tandem modules that are a feature of chondroitin sulphate proteoglycans (CSPG) such as aggrecan, versican, brevican and neurocan, that aggregate HA in cooperation with the Link protein (Day and Prestwich, 2002). An extended Link domain (ELD) is found in a third group of membrane-anchored receptors that has two known members, CD44 and LYVE-1 (Banerji et al., 1998; Banerji et al., 2010).

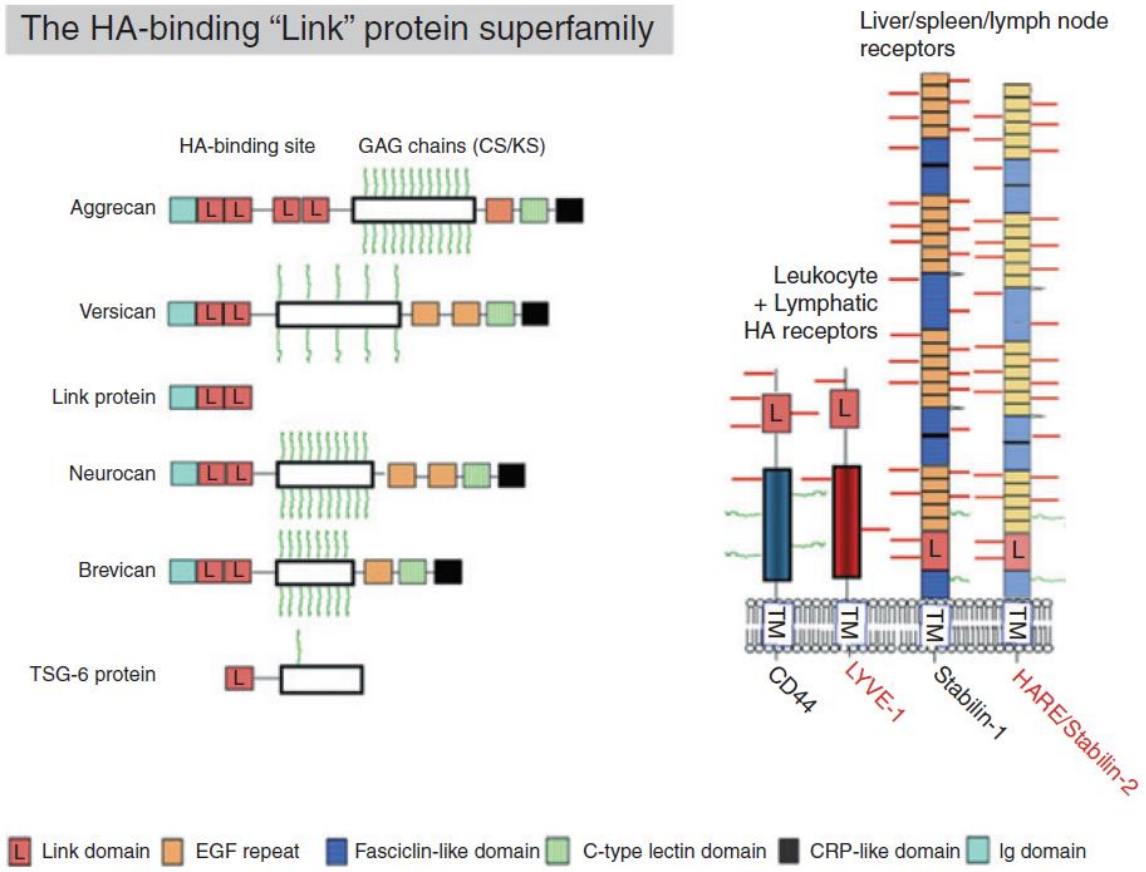


Figure 1.7. **The Link superfamily of hyaluronan binding proteins.** Members include proteoglycans associated with the extracellular matrix (*left*) as well as a small group of membrane bound receptors (*right*). Major structural domains are indicated as per the key. N-linked and O-linked glycans are denoted by *red* and *green* lines respectively.

1.3.1 Type A hyaluronan binding domains

The hyaluronan binding domains of Type A HABPs are the smallest of the Link family and only one of them is present in each molecule (Day and Prestwich, 2002). The archetypal member of this sub-group is TSG-6, the structure of which has been solved using x-ray crystallography and NMR in the presence and absence of HA oligosaccharides (Figure 1.8) (Blundell et al., 2003; Higman et al., 2007; Kohda et al., 1996). A reflection of the compact nature of Type A HABDs is the minimal HA chain that may be bound efficiently, which is HA_7 for TSG-6 and slightly larger for the extended link domain of

CD44, at HA_8 (Banerji et al., 2007; Blundell et al., 2003). The functional Link module of TSG-6 comprises 98 residues formed into two antiparallel ß-sheets made from a total of six ß-strands (ß1-6) and two α-helices stabilized by a pair of conserved disulphide bridges (Kohda et al., 1996). Comparison of free and ligand-bound solution structures has revealed that binding of the HA oligosaccharide opens a shallow binding groove (Blundell et al., 2003; Higman et al., 2007). The transition occurs mainly through the movement of the Cys47–68 disulfide bond and rearrangement of the β4/β5 loop, which exposes critical HA-binding residues. Two residues, Pro60 and Gly74 form the hinge for this movement and are conserved throughout the Link superfamily, suggesting that this may be a common mechanism (Blundell et al., 2003).

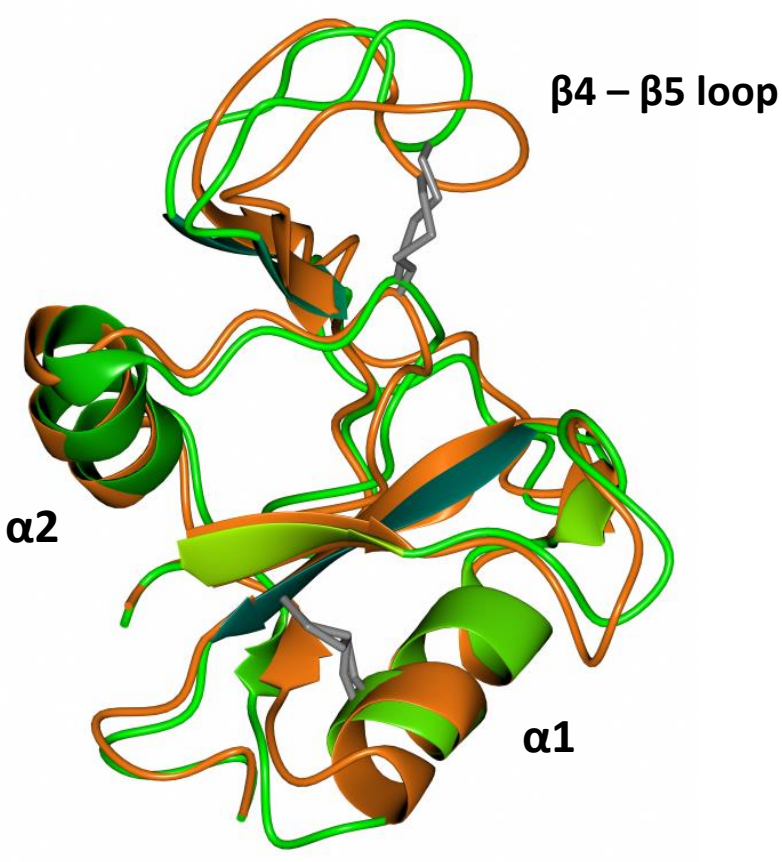


Figure 1.8. **Solution structure of the Link module from TSG-6 in the presence (green) and absence (orange) of a hyaluronan octasaccharide**. Note the change in position of the β4 - β5 loop from the open conformation (orange) to the ligand bound position (green). Coordinates from (Blundell et al., 2003).

1.3.1.1 TSG-6

TNFα stimulated gene 6 protein (TSG-6) is a naturally occurring hyaluronan cross-linker that plays important roles in inflammation and ovulation (Baranova et al., 2011; Fulop et al., 2003). Expression of TSG-6 is tightly controlled, with little or no constitutive expression in adult tissues, but the protein is synthesized by a variety of cell types in response to pro-inflammatory mediators or certain growth factors. TSG-6 has been shown to modulate the interaction between hyaluronan and CD44, enhancing or inducing binding by the HA receptor on constitutive and inducible cell backgrounds, respectively (Lesley et al., 2004). As such, TSG-6 mediated cross-linking of HA has been proposed as a functional mechanism for regulation of leukocyte adhesion (Baranova et al., 2011; Day and de la Motte, 2005). The protein is composed mainly of two contiguous domains, a Link module, responsible for HA binding, and a C-terminal CUB module, the function of which is unclear, but is thought to include mediating TSG-6 oligomerization. The full length protein is also required for the enzymatic properties of TSG-6 (see below) (Getting et al., 2002; Rugg et al., 2005) and the CUB module has also recently been shown to mediate binding to fibronectin (Kuznetsova et al., 2008).

In addition to its function as an HA cross-linking protein, TSG-6 catalyses the only naturally-occurring covalent modification of HA; modification with heavy chains (HCs) donated from inter-α-inhibitor (IαI) (Jessen and Odum, 2003; Mukhopadhyay et al., 2004; Rugg et al., 2005). The ensuing HA•HC complex is also known as serum-derived hyaluronan-associated protein (SHAP) complex (Yingsung et al., 2003; Zhao et al., 1995) and has been found in the sera of patients with ovarian cancer (Obayashi et al., 2008) and the synovial fluid of arthritic joints (Kida et al., 1999), amongst others. Heavy-chain HA is an important component of the cumulus-cell-oocyte complex in the ovary, where it cross-

links the HA matrix and is crucial for successful ovulation and fertility (Fulop et al., 2003; Mukhopadhyay et al., 2004; Mukhopadhyay et al., 2001). The formation of HA•HC complex has also been shown to promote leukocyte adhesion to HA matrices (de la Motte et al., 2003) in a CD44-dependent manner (Zhuo et al., 2006). In response to the viral mimic poly(I:C), airway smooth muscle cells produce similar HA•HC cable structures up to 200 μm in length, with enhanced leukocyte binding (Lauer et al., 2013).

1.3.2 Type B hyaluronan binding domains

There are two members of the type B sub-group of Link superfamily members, LYVE-1 and CD44, both of which are membrane-bound proteins and are characterised by the presence of an extended link module. In CD44, the importance of additional sequence elements outside the consensus link domain (CLD) became apparent for a number of reasons. These included the observation that recombinant CLD fails to refold following expression by *E. coli* (Banerji et al., 1998) and the identification in the flanking sequences of residues that participate in HA binding using site-directed mutagenesis (Peach et al., 1993). Using a combination of NMR and x-ray crystallography, the structure of the extended link domain has been described in detail for CD44 (Banerji et al., 2007; Teriete et al., 2004), and is also an apparent feature of its close homolog, LYVE-1 (Banerji et al., 2010).

1.3.2.1 CD44

CD44 is a type-I integral membrane glycoprotein widely expressed in the human body, and is the primary receptor through which migratory cells contact hyaluronan (Ponta et al., 2003). Binding of hyaluronan, the primary ligand for CD44, is functionally regulated and may be activated when resting leukocytes are exposed to pro-inflammatory cytokines and

begin to migrate (Pure and Cuff, 2001). In this way, discrete populations of circulating cells can be directed to transmigrate at inflammatory sites, where they recognise and respond to HA presented by CD44-expressing endothelial cells (Lesley et al., 1997; Mohamadzadeh et al., 1998). Expressed in the form of different splice variants, the receptor participates in many different cellular processes including regulation of growth, survival, differentiation and motility (Ponta et al., 2003). The most common form, CD44H, a term that arises from its abundance on hematopoietic cells, is invariant, and has an apparent molecular weight of 80-100 kDa, including a significant contribution from N- and O-linked glycans. Disregulation of CD44 is associated with a number of diseases, and the interaction of tumour cells with HA via CD44 is a target for cancer therapy (Misra et al., 2011). Mice deficient in CD44 have a mild phenotype however, with abnormalities in myeloid progenitor colonisation of bone marrow (Schmits et al., 1997) and recirculation of lymphocytes to the thymus and lymph node (Protin et al., 1999).

CD44 comprises a single extracellular Link domain that is N-glycosylated at 5 separate sites and separated from the membrane by an O-glycosylated juxta-membrane stalk. Glycosylation is known to play a prominent role in HA binding; although not absolutely required, as shown by the ability of *E. coli* expressed protein to bind HA, cell-specific and splice-variant specific glycosylation patterns can positively and negatively regulate binding (English et al., 1998; Skelton et al., 1998). The Link domain is extended beyond the conserved fold, with four additional ß-strands (ß0, ß7-9) and flanking sequences that are stabilised by a third disulfide (Teriete et al., 2004) (Figure 1.9). The crystal structures of the HA-binding domain in both human (Teriete et al., 2004) and mouse CD44 (Banerji et al., 2007) have been solved, and in the case of the mouse protein, a ligand-bound co-crystal revealed the precise details of hyaluronan binding. HA-contact residues are directly conserved between the two species (Figure 1.14, page 73) and there is evidence from the

mouse crystal structure that the protein can adopt two different conformations that may correspond to a high and a low affinity state for HA-binding. The two structures differ in the orientation of the β1-α1 loop, which is reorganized in the high affinity complex such that Arg^{45} is brought into contact with HA via a H_2O-mediated hydrogen bond. Although the Link extension does not play a major role in binding of hyaluronan, it may play a role in allosteric regulation of the receptor, perhaps contributing to switching between these two conformations (Banerji et al., 2007).

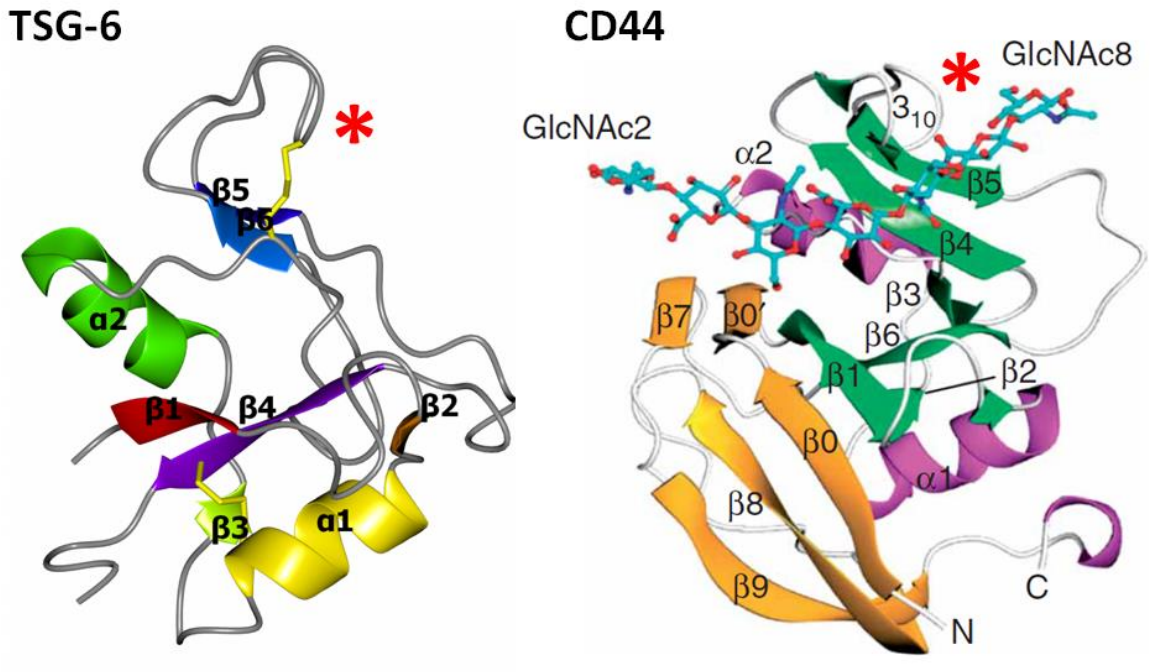


Figure 1.9. **The consensus Link domain of TSG-6 and the extended Link domain of CD44.** Each member of the Link superfamily contains a copy of the consensus Link domain (CLD), exemplified by the solution structure of human TSG-6 (left) (Blundell et al., 2003). In CD44, this domain is extended (gold lobe) by an additional 4 ß-sheets and a 3rd disulphide that stabilises the structure. However, the majority of contact with an HA octasacchride in the crystal structure of murine CD44 occurs within the CLD (Banerji et al., 2007).

Analysis of CD44 interactions with HA in an artificial membrane system monitored by Quartz Crystal Microbalance with Dissipation monitoring (QCM-D) have revealed that the

amount of HA binding to densely CD44-coated bilayers increases as a function of HA size (Wolny et al., 2010). Binding was reversible for smaller HA species (≤ 10 kDa) and essentially irreversible with large polymers. Furthermore, the amount of bound HA decreased with decreasing receptor surface density. These data match the findings of other authors who have observed an expression threshold for HA binding in AKR1 T-lymphoma cells (Perschl et al., 1995), and an increase in avidity with HA chain length, that defines multivalent interactions as the primary feature of HA binding by cell surface CD44 (Lesley et al., 2000). These conclusions were built on initial findings that HA binding could be induced in CD44-expressing cell lines by bivalent CD44 mAbs IRAWB14 and B26, but not by their monovalent Fab fragments (Lesley et al., 1993). Clustering of CD44 receptors by these antibodies is reported to have little effect on binding kinetics, but greatly delays dissociation of HA from the cell surface due to an increase in avidity (Lesley et al., 2000).

1.3.3 Type C hyaluronan binding domains

Type C members of the Link superfamily are characterized by a hyaluronan binding domain comprised of tandem-Link modules coupled to an Ig-like domain (Day and Prestwich, 2002). Members can be divided further into chondroitin sulphate proteoglycans (CSPG, also termed lecticans), such as versican, aggrecan, neurocan and brevican, and the HA and Proteoglycan Binding Link Protein (HAPLN1 to 4) family, that includes cartilage Link protein (cLP) and brain Link proteins 1 and 2 (HAPLN2 and 4). The former have aggregating properties, producing higher-order HA architectures with structural and load-bearing properties, while the latter stabilise binding of the CSPGs to the HA chain. Genes encoding separate components of functional protein complexes are rarely co-localized in vertebrate genomes, but strikingly all four *HAPLN* genes are located immediately adjacent

to the four *CSPG* core protein genes, creating four paralogous *CSPG-HAPLN* gene pairs (Spicer et al., 2003).

While the tertiary structures of lecticans and HAPLNs are currently unavailable, a considerable amount of information regarding their mode of binding has been gleaned using surface plasmon resonance and molecular modelling. Watanabe and colleagues (1997) demonstrated that the tandem Link module of aggrecan is required for HA binding, and that none of the individual Link or Ig-like domains were capable of binding in isolation. A construct incorporating both the tandem Link module and Ig-like domain had the highest HA binding affinity, indicating that the latter enhances HA binding by aggrecan Link domains. More recently, the Ig-like domain of versican has been shown to enhance HA binding by its tandem Link module (Matsumoto et al., 2003). The authors were also able to demonstrate that versican forms proteoglycan aggregates with cartilage Link protein (HAPLN1), and that the interaction is mediated by the versican tandem Link module, instead of the Ig-like domain as is the case for aggrecan.

Molecular modelling of the tandem Link domain of HAPLN1 using the HA-bound solution structure of TSG-6 has revealed interesting features of Type C HABD binding to HA chains (Blundell et al., 2005). Four aromatic and two large hydrophobic residues are found at the Link-Link interface and are thought to mediate close contact of the domains. These residues are also well conserved across the type C sub-group, but are not routinely found in type A or type B family members. Residues with similar properties are clustered at the free ‘ends’ of the HAPLN1 model, which may represent the point of interaction with aggrecan or versican. Furthermore, as a consequence of the wedge-shape of the HABD, HAPLN1 binding to HA may propagate a helical structure in the chain (Figure 1.10).

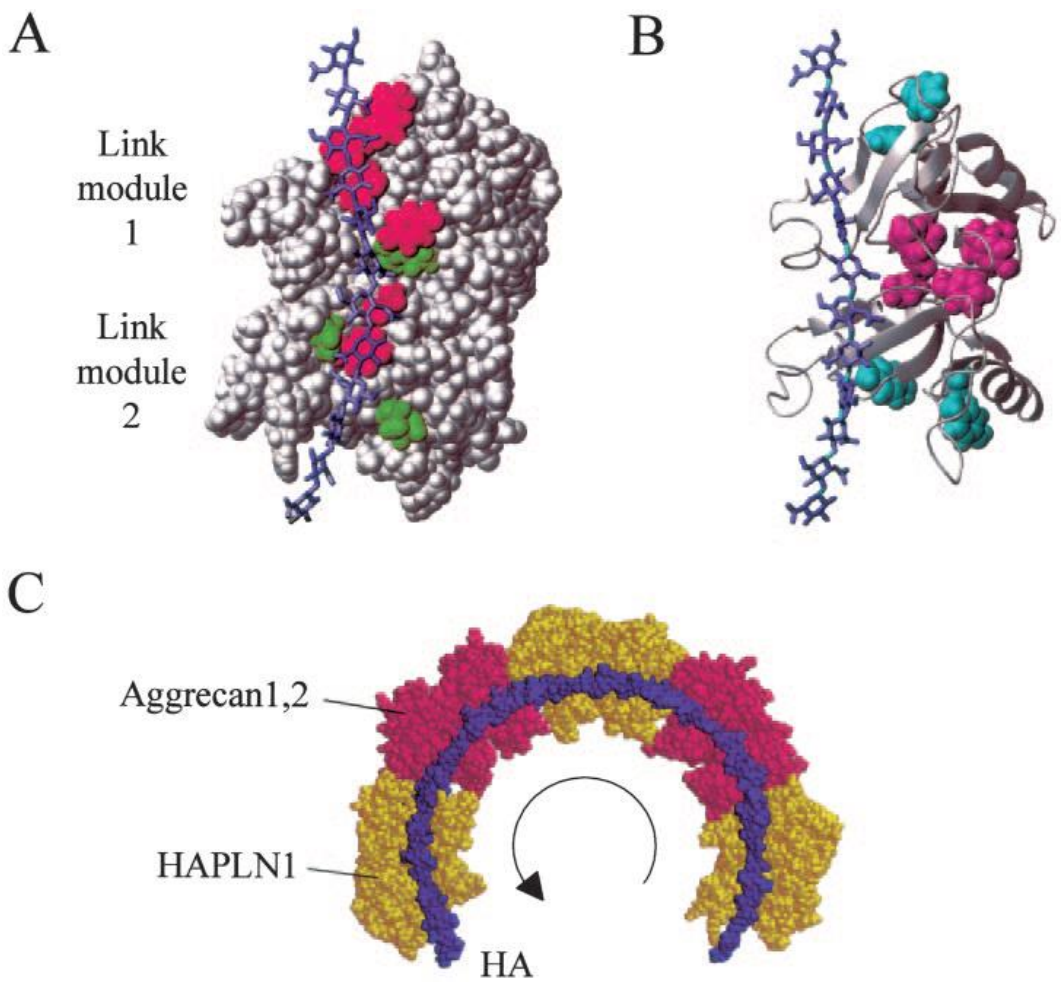


Figure 1.10. **Homology models of cartilage link protein (HAPLN1) with an HA dodecamer.** (A) Space-filling view of the HAPLN1 model, with predicted HA-binding residues shown in *red* (aromatic) and *green* (basic) and bound HA shown as *blue sticks*. The first Link module in the model makes six contacts with HA, but the second makes only four. (B) Secondary structure view of the model (50° rotation about the *y*-axis relative to (A)), with the hydrophobic side chains predicted to form the inter-module interface shown as *magenta spheres*. Hydrophobic residues on the external faces at either end of the Type C domain, which may be involved in interprotein interactions, are shown in *cyan*. *C*, The wedge-shape of Link modules, coupled with the curve of bound HA, suggests that side-by-side binding of Type C HABD domains will the HA chain in a helical structure. Taken from (Blundell et al., 2005).

1.3.3.1 Aggrecan

In the joints, HA produced by chondrocytes is secreted into the synovial fluid where it forms complexes with cartilage Link protein (cLP) and aggrecan. These complexes were first described by Heinegård and Hascall, who in the 1970s described the interaction between the aggrecan G1 domain, cLP and hyaluronan (Hascall and Heinegard, 1974a, b; Heinegard and Hascall, 1974). The G1 domain lies at the N-terminus of the protein and comprises an Ig-like repeat (A subdomain) and twin Link molecules in tandem (B and B′ subdomains) (Figure 1.11). A second globular domain, unique to aggrecan, is located C-terminal to G1. G2 is highly conserved but has no known function, and does not interact with HA or Link protein (Fosang and Hardingham, 1989). A C-terminal G3 domain contains four structural motifs that link aggrecan/LP/HA complexes to the wider extracellular matrix (reviewed in Aspberg, 2012). These include two epidermal growth factor (EGF)–like repeats, followed by a C-type lectin domain (CLD) and a complement regulatory protein (CRP). Protein ligands identified for the CLD domain are all dimeric or multimeric ECM proteins, such as tenascin-R, tenascin-C, fibulin-1 and fibrillin-1. These interacting partners have been shown in principle to mediate cross-linking and aggregation of HA/cLP/aggrecan complexes under native conditions using molecular electron microscopy (Lundell et al., 2004; Olin et al., 2001). The extended polypeptide chain lying between G2 and G3 is extensively modified by keratan and chondroitin sulphate chains. The negative charge of these GAG chains, coupled with the intrinsic negative charge of HA, attracts positive counter ions, and the resulting osmotic potential draws water into the cartilage. This causes a swelling pressure within the articular tissues that resists compression and provides the viscoelastic properties of cartilage that allow load distribution in the skeletal joints (Aspberg, 2012).

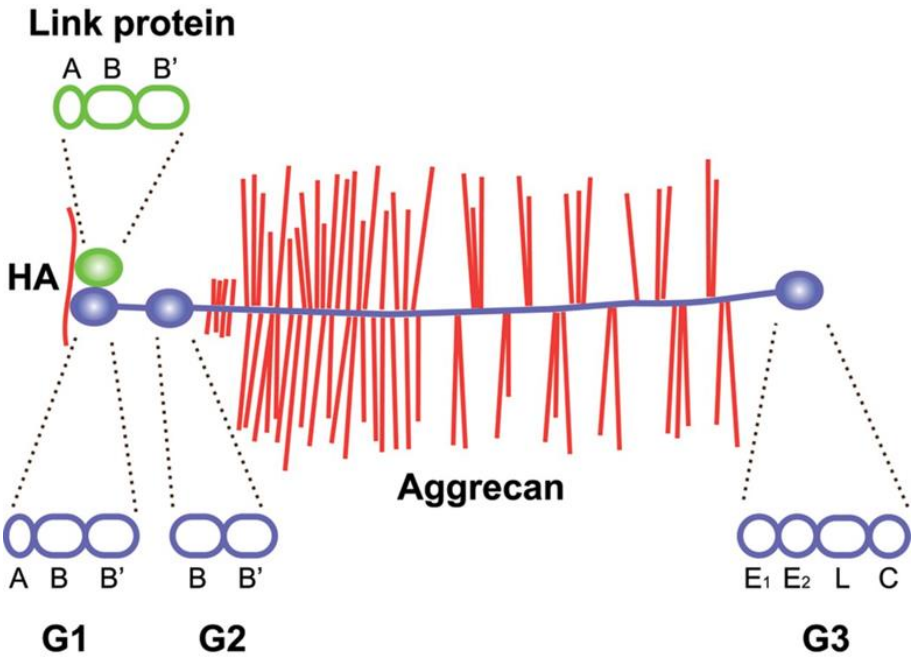


Figure 1.11. **The domain structure of aggrecan and link protein and sites of interaction with HA**. Aggrecan binds hyaluronan through its N-terminal G1 domain in ternary complex with link proteins. The G1 domain and link proteins are homologous, with an immunoglobulin-like repeat (A) followed by two Link modules in tandem (B and B′). In aggrecan, but not in other lecticans, the G1 is followed by a second globular domain (G2) that also contains B and B′ but not the A domain. G2 and G3 are separated by a long glycosaminoglycan attachment region, that is modified with keratan sulphate and chondroitin sulphate chains (*red lines*). The C-terminal G3 domain consists of an epidermal growth factor (EGF) repeat (E1), a calcium-binding EGF repeat (E2), a C-type lectin domain (L), and a complement regulatory protein repeat (C). Adapted from (Aspberg, 2012).

1.3.3.2 Versican

Versican, the largest of the lecticans family of chondroitin sulphate proteoglycans (CSPG), is widely expressed in the epidermis, connective tissues, neural tissue, cartilage, lung and skeletal muscle (Bode-Lesniewska et al., 1996). The gross architecture of the protein resembles that of aggrecan; a N-terminal G1 domain mediates HA binding through a tandem Link module, a G3 domain mediates interactions with other proteins, and the interceding GAG attachment region is extensively modified with chondroitin sulphate (CS)

chains (Zimmermann and Ruoslahti, 1989). There is no G2 domain in versican however, and the interaction with Link protein is mediated via the tandem Link module (B, B′ subdomain) rather than the Ig-like fold (A subdomain), as is the case in aggrecan (Matsumoto et al., 2003). Four isoforms may arise through alternative splicing, the largest of which, V_0, has 20 potential CS-attachment sites and a total molecular weight exceeding 1 MDa (Wight, 2002). The V_1 isoform lacks the exon the GAGβ region, reducing the number of CS chains to ~14, the V_2 isoform lacks GAGα and bears 6 CS chains, while the smallest variant V_3, lacks the entire GAG-attachment region. The length of the CS chains varies with tissue type and can be modified in response to growth factor signalling (Cardoso et al., 2010). Versican is also a substrate for MMP and ADAMTS enzymes that generate cleavage products with a variety of functions, such as supporting the role of FGFs and BMPs during interdigital tissue remodelling (McCulloch et al., 2009)

Versican plays a number of roles in adult and developmental tissues, including regulation of cell proliferation, migration, extracellular matrix assembly and cell adhesion, and as a component of cartilage (Wight, 2002). The larger isoforms with their negatively-charged CS chains are anti-adhesive and are typically involved in remodelling events; versican deficient mice for example die at embryonic day 10.5 due to malformation of the heart (Mjaatvedt et al., 1998). During ovulation, V_0 and V_1 are also critical components of the hyaluronan-rich cumulus-oocyte-complex and are cleaved by ADAMTS proteases during follicle maturation (Brown et al., 2010; Russell et al., 2003). Increased levels of versican have been reported to be a negative prognostic marker in many cancers, increasing both tumour cell proliferation and migration (reviewed in Ricciardelli et al., 2009). In many cases, the CS-free V_3 isoform or metalloproteinase fragments of versican are reported to compete with V_0 and V_1 for binding of HA and can reverse the biological effects of the larger proteoglycans. Recently, the G1 domain of versican has been used as a model of

these shorter isoforms and shown to reverse both CD44 binding of end-grafted HA films using QCM-D, and TSG-6-mediated enhancement of HA binding by CD44-transfected cells (Foulcer, 2012, PhD thesis).

1.3.3.3 Neurocan and Brevican

Each of member of the lectican family has a characteristic distribution pattern; aggrecan is the most abundant CSPG in cartilage, versican is the mostly ubiquitously expressed, while neurocan (Prange et al., 1998) and brevican (Yamada et al., 1994) are largely restricted to the neural tissues (reviewed in Yamaguchi, 2000). A restricted expression pattern is also observed for the brain specific Link proteins BRAL-1 (HAPLN2) (Hirakawa et al., 2000) and BRAL-2 (HAPLN4) (Bekku et al., 2003) that enhance HA binding of neural-resident lecticans. Bral-2 has recently been shown to be indispensable for the proper localization of brevican and the integrity of structures termed perineuronal nets (PNN) (Bekku et al., 2012). PNNs are a specialized form of extracellular matrix (ECM) comprising HA, lecticans, link proteins (cLP, Bral-1 and Bral-2), and a number of cross-linking proteins that interact with the lectican G3 domain, such as tenascin-R (Carulli et al., 2006). These structures enwrap the cell body and proximal dendrites of many adult neurons and play an important role in plasticity. The function of the lecticans at these sites is not entirely clear, but their negative charge is thought to attract positive counter ions, thus providing a ready pool for ion flux during neuronal firing (Oohashi et al., 2002). Mice deficient in Bral1 have abnormally diffuse hyaluronan-associated ECM and decreased conduction velocity in the spinal cord ((Bekku et al., 2010), while the targeted mutation of brevican leads to a defect in long term potentiation, but no obvious defects in memory or learning (Brakebusch et al., 2002).

1.4 LYVE-1

In 1999, a BLAST search of the combined Human Genome Sciences/TIGR EST databases identified a new homologue of CD44 that would subsequently be named the lymphatic vessel endothelial hyaluronan receptor (LYVE-1) (Banerji et al., 1999). With 41% overall sequence similarity to CD44 and 57% within the consensus Link domain, LYVE-1 was clearly a new member of the Link protein superfamily and the second member of a sub-group of type I integral membrane proteins. An Fc fusion protein of LYVE-1 with the hinge, CH2, and CH3 domains of human IgG_1 was shown to bind soluble or immobilized HA in a concentration-dependent manner, reminiscent of CD44 Fc protein. The specificity of binding to HA was also apparent from the absence of competition with free glycosaminoglycans, such as chondroitin-4-SO_4, chondroitin-6-SO_4, and heparan sulphate and contrasting sensitivity to inhibition with free HA (Banerji et al., 1999; Prevo et al., 2001). The similarities with CD44 ended however with the realization that LYVE-1 expression is highly restricted, in stark contrast to the growing list of CD44-expressing cell types.

1.4.1 Tissue specific expression of LYVE-1

Whereas CD44 is found in a wide range of tissues, LYVE-1 expression is largely restricted to lymphatic endothelium, to the exclusion of CD44 (Banerji et al., 1999). Electron microscopy has been used to demonstrate that LYVE-1 is present on both the luminal and abluminal faces of lymphatic vessels and is entirely absent from CD44-positive blood endothelium (Prevo et al., 2001). Expression of the receptor extends the length of the lymphatic tree, from the smallest blind-ended capillaries, through larger afferent and collecting vessels, to the floor of the subcapsular sinus in the lymph node (Girard et al.,

2012). LYVE-1 is particularly enriched at the tips of flap valves between individual endothelial cells in afferent or initial lymphatic vessels (Figure 1.12) (Baluk et al., 2007). These specialized structures lie beneath pre-formed pores in the basement membrane surrounding the vessel, and function as the site of entry for transmigrating cells, such as dendritic cells (Pflicke and Sixt, 2009).

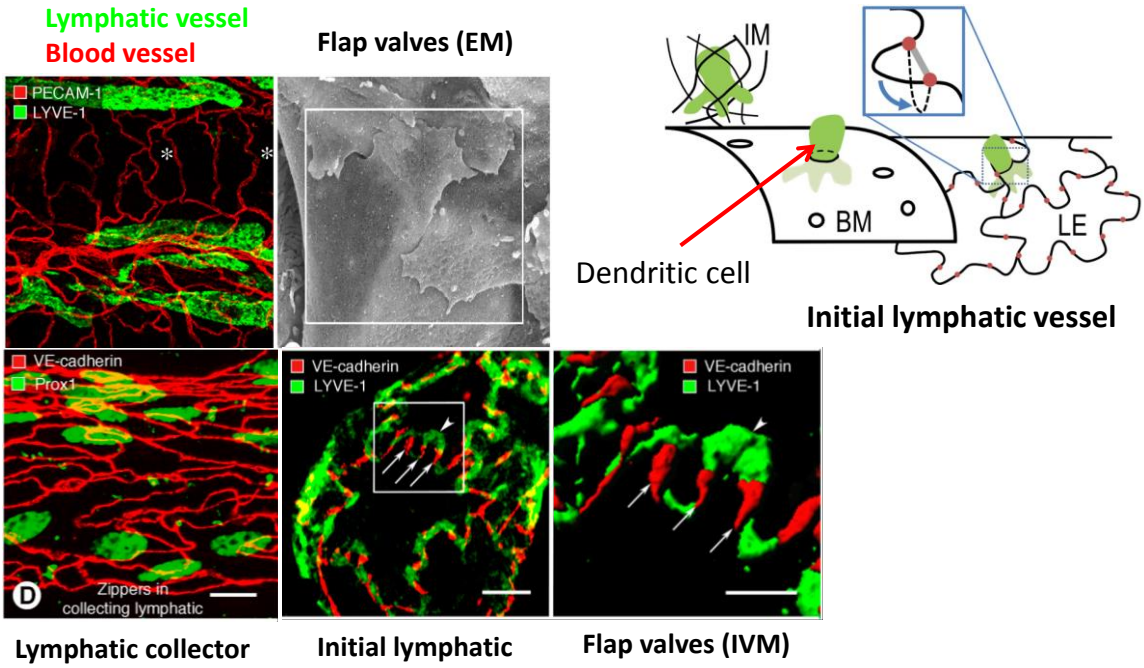


Figure 1.12. **Functionally specialized junctions between endothelial cells of lymphatic vessels**. Confocal images showing lymphatic vessels (green, LYVE-1) and blood vessels (red, PECAM-1) in whole mount of mouse trachea, alongside an electron micrograph (EM) of inter-digitating lymphatic endothelial cells (LEC). LEC adopt a distinctive oak-leaf morphology in initial lymphatics, supported by 'button' junctions comprised of VE-cadherin at the point of inter-digitation, and enriched LYVE-1 expression at the 'fingertips', or flap valves. Cells comprising the larger collecting vessels have a spindle-like shape reminiscent of blood endothelium, with distinctive 'zipper-like' junctions. Intravital microscopy has been used to further demonstrate that dendritic cells enter lymphatic vessels through these valves, having first transited through pre-formed discontinuities in the surrounding basement membrane. (Adapted from Baluk et al., 2007; Pflicke and Sixt, 2009).

The specificity of LYVE-1 expression by lymphatic endothelium and the availability of several polyclonal and monoclonal antibodies has led to its wide-spread use as a marker of lymphatic vessels, particularly for imaging studies. Over time this has led to the serendipitous discovery of additional sites of LYVE-1 expression, including liver sinusoidal endothelium, a major site of HA catabolism, and $CD68^+$ liver-resident macrophages, termed Kuppffer cells (Mouta Carreira et al., 2001). More recently, additional macrophage populations have been identified, including a subset of CD11b+, F4/80+ tissue macrophages that preferentially co-expressed stabilin-1, and are proposed to trans-differentiate into *de novo* lymphatic vessels in tumour tissue (Schledzewski et al., 2006). Bone marrow-derived LYVE-1^+ macrophages have also been observed in the dense vascular network (DVN) in the tip portion of epididymal (testicular) adipose tissue in adult mice (Cho et al., 2007). The function of LYVE-1 in this setting is unclear, but macrophages were essential for DVN formation and angiogenesis.

1.4.2 Structure of the LYVE-1 protein

Both LYVE-1 and CD44 are type I integral membrane proteins, and share a gross overall architecture, with an extended Link domain positioned at the N-terminus of a heavily O-glycosylated juxta-membrane stalk (Figure 1.13). The greatest degree of homology lies within the Link domain (57% similarity) including a number of conserved HA contact residues, three structural disulphides, and a N-glycosylation site (N130 in hLYVE-1) (Figure 1.14). Outside of this region the sequences are divergent, the LYVE-1 gene encoding a smaller 322-residue polypeptide, with no evidence of alternative splicing that generates the various CD44 isoforms (Prevo et al., 2001). Comparison of LYVE-1 sequences from various species (human, mouse, bovine, rat and chicken) reveals striking regions of conservation, particularly in the extended Link domain and cytoplasmic tail,

which is almost invariant (Nightingale, 2004). The greatest degree of divergence lies in the stalk region, but with notable exceptions, including thirteen potential O-glycosylation sites and a tract of basic residues centred around an unpaired cysteine (C201 in human) (Prevo et al., 2001). Using a combination of truncation and site-directed mutagenesis, Cys 201 has been identified as the residue responsible for a population of disulphide-linked dimers observed by western blot of protein from primary LEC (Figure 1.13) (Nightingale, 2004). The presence of a free thiol that can support inter-chain disulphide bond formation is a unique feature of LYVE-1 amongst the Link SF, but the function of LYVE-1 homodimers has yet to be elucidated.

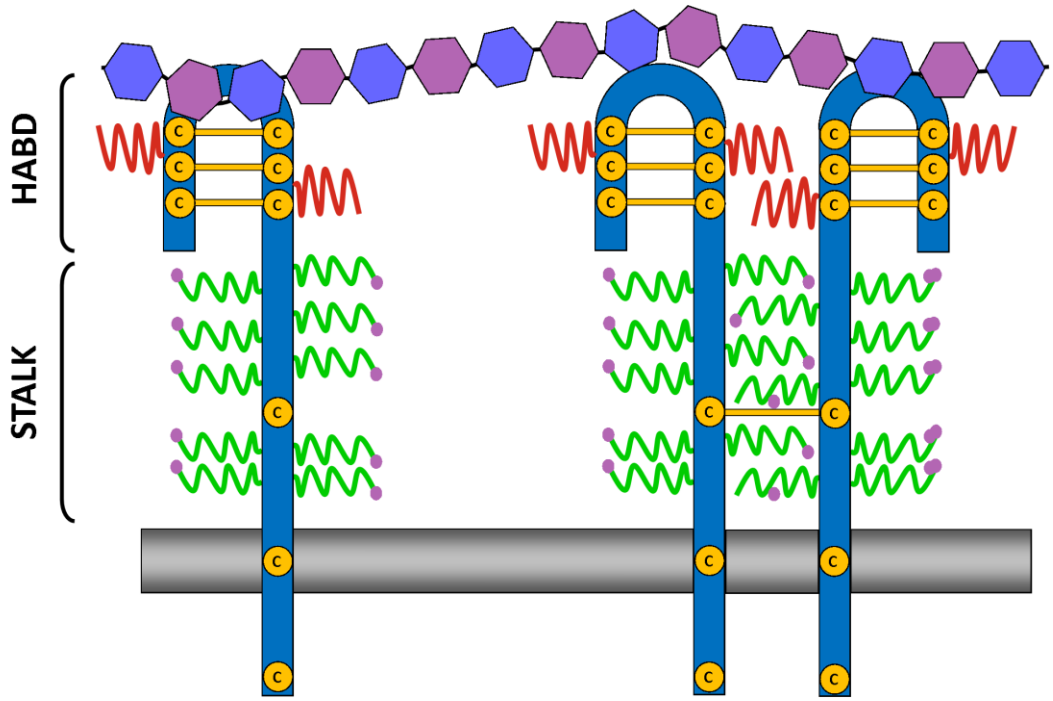


Figure 1.13. **Schematic of LYVE-1 monomer and dimer bound to an HA chain.** LYVE-1 is a 65kDa (monomer, *left*) type I integral membrane protein. An N-terminal HA-binding domain contains an extended form of the conserved Link module that is N-glycosylated (*shown in red*) at two sites; both are required for efficient HA-binding. The stalk region is extensively modified with O-glycans (*green*) that have sialic acid (*purple*) at their termini. Sialic acid, operating through an unknown mechanism, has been shown to mediate inhibition of HA binding in primary lymphatic endothelial cells. Three unpaired cysteine residues are located in the stalk, transmembrane helix and cytoplasmic tail respectively, the former has been identified as the thiol responsible for a population of dimeric LYVE1 (*right*) identified by western blot of protein from primary cells.

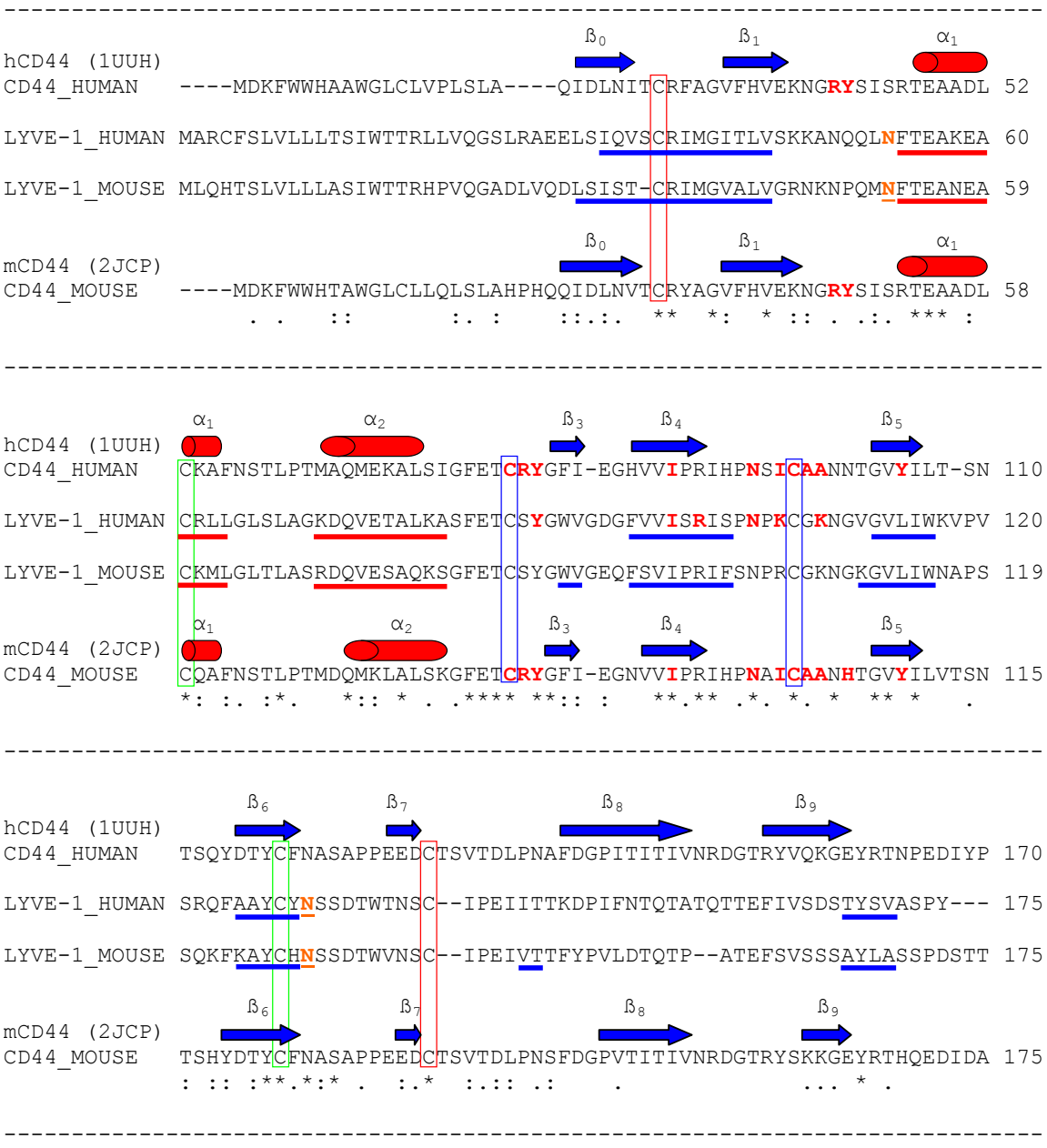


Figure 1.14. **Multiple sequence alignment of LYVE-1 and CD44 from human and mouse.** The first 175 residues of LYVE-1 and CD44 from human and mouse were aligned using ClustalW2 (Larkin et al., 2007). Residues marked with an *asterisk* are directly conserved, *paired* or *single dots* indicate conservative or semi-conservative substitutions, respectively. Secondary structure elements derived from the relevant crystal structures for human and mouse CD44 are indicated with *red* cylinders for α-helices and *blue* arrows for ß-strands. Secondary structure predictions by Jpred 3 (Cole et al., 2008) for LYVE-1 sequences are indicated with *red* lines for α-helices and *blue* lines for ß-strands. Conserved cysteines involved in disulphide bonds are *boxed*, and the colour of the boxes illustrates which cysteines are paired. *Red* lettering indicates residues critical for HA-binding in CD44 and conserved equivalents in hLYVE-1. Residues *underlined in orange* are predicted sites of N-glycosylation.

While the crystal structure of LYVE-1 has yet to be solved, a considerable amount of structural information has been deduced using truncation and site-directed mutagenesis of the human receptor (Banerji et al., 2010). Through testing of HA-binding by a series of graded truncation mutants, it has been possible to demonstrate that the functional HA binding unit in LYVE-1 extends beyond the conserved Link domain. This places the receptor alongside CD44 in the 'type B' sub-group of Link SF members that feature an Extended Link Domain (ELD) (Figure 1.15). Four additional β-strands, β0 and β7-9 comprise the Link extension, which is stabilised by a third disulphide linkage conserved in both proteins (Figure 1.14) (Teriete et al., 2004). A combination of secondary structure prediction and *in silico* modelling of the human LYVE-1 HABD strongly suggest that an equivalent ELD is present in LYVE-1 (Figure 1.15) (Banerji et al., 2010).

Site-directed mutagenesis of the human receptor has revealed a number of conserved HA-binding residues in human LYVE-1, as well as the epitope of an HA-blocking monoclonal antibody 3A, which overlaps the HA-binding site (Figure 1.15) (Banerji et al., 2010). The binding site in hLYVE-1 maps to a position similar to that of the HA-binding site in CD44, beneath the hook-like β4-β5 loop region, but is more compact, and lacks additional residues found in the $ß_1$-α_1 loop (e.g. Arg-41, Tyr-42). The binding surface in hLYVE-1 is dominated by charged or polar residues (Arg-99, Asn-103, Lys-105 and Lys-108), compared to the largely aliphatic makeup of the CD44 binding site, and this is reflected in a marked sensitivity to ionic strength not seen in the latter (IC_{50} of 150 mM NaCl for hLYVE-1, compared to IC_{50} >2M NaCl for CD44). In this regard, the mode of HA binding by LYVE-1 resembles that of the selectins, which bind the prototype fucosylated tetrasaccharide sialyl Lewis-X through recognition of the negatively charged carboxylate group of NeuNAc by primarily lysine and arginine residues (Banerji et al., 2010; Bouyain et al., 2001).

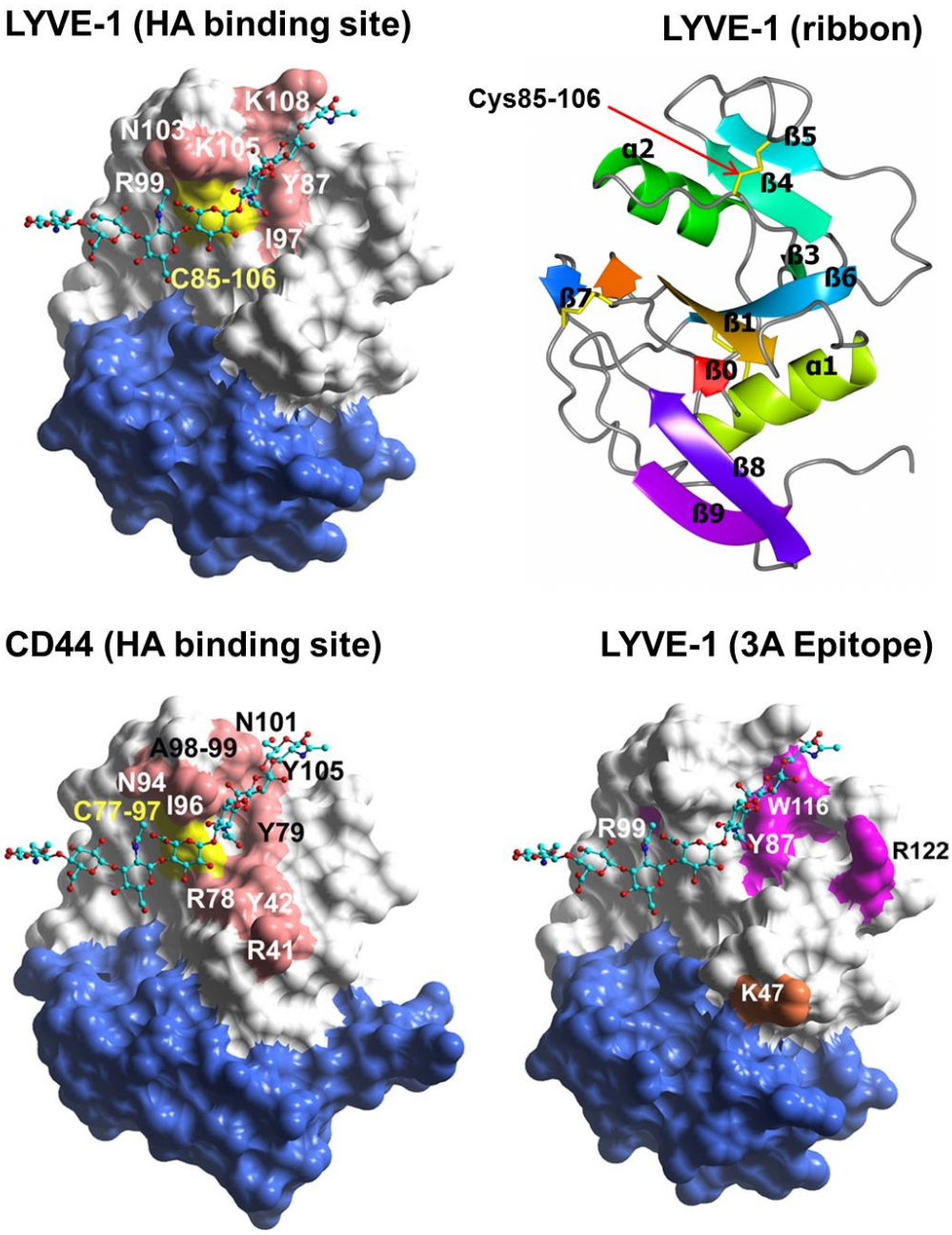


Figure 1.15. **Structure-based model of the extended Link domain and HA-binding surface in LYVE-1.** Representations of the hLYVE-1 HABD modelled using coordinates of the mCD44 crystal structure B (Banerji et al., 2007). In space-filled representations, an HA octasaccharide is shown docked into the putative binding site, the Cys85-106 structural disulphide (C77-97 in CD44) is shown in yellow, and the region corresponding to the Link module extension is coloured blue. *Top left*: Key residues comprising the predicted ligand-binding surface in hLYVE-1 shown coloured pink. *Top right:* Secondary structure elements, including the Cys85-106 disulphide, are indicated on a ribbon diagram of the hLYVE-1 HABD. *Bottom left:* HA contact residues in human CD44 shown coloured pink. *Bottom right:* Residues identified as part of the epitopes for the Lyve-1-specific mAbs 3A and 8C coloured magenta and orange, respectively. Adapted from (Banerji et al., 2010).

1.4.3 Regulation of hyaluronan binding

The interaction of hyaluronan expressed in lymphatic endothelium, like that of CD44 in leukocytes appears to be highly regulated. When over-expressed in cell backgrounds such as HEK 293T fibroblasts, or as a soluble recombinant Fc fusion protein, LYVE-1 demonstrates saturable levels of binding to fluoresceinated (Fl-HA) or biotinylated HA (bHA), which may be blocked using LYVE-1 mAbs or an excess on unlabelled hyaluronan (Banerji et al., 1999; Prevo et al., 2001). The situation for the endogenous receptor however is much different; lymphatic vessels in human or mouse tissue fail to co-localize with endogenous or exogenously added HA, while cultured lymphatic endothelial cells extracted from either source display only residual binding to Fl-HA or bHA (Nightingale et al., 2009). This suggested that LYVE-1 may be functionally silenced in lymphatic endothelial cells, and that mechanisms must exist to relieve this inhibition in certain contexts. Cell-specific regulation is a known feature of CD44; although widely expressed by a variety of cell types, most primary CD44-positive cells fail to exhibit HA receptor function until activated to do so (Pure and Cuff, 2001).

Regulation of hyaluronan binding by LYVE-1 glycosylation has been addressed using a combination of mutagenesis and expression in Chinese hamster ovary (CHO) cell lines with deficient glycosylation machinery (Nightingale et al., 2009). Mutation of the two N-glycosylation sites in hLYVE-1 revealed that N-glycans play a positive role in HA-binding. This contrasts the situation in CD44, where sialic acid on the tips of N-glycan chains is inhibitory (English et al., 1998) and cleavage by sialidase Neu1 results in activation of HA binding in T helper type 2 (Th2) cells (Katoh et al., 2010). A series of truncation mutants that progressively delete the Ser/Thr-rich stalk region demonstrated that it is in fact the O-glycans that play the inhibitory role in LYVE-1. Expression of LYVE-1 in a panel of CHO

glycosylation mutants suggested that the inhibitory mechanism is reversible and is exerted by terminal sialylation, most likely through α2-3 or α2-6 linkage to O-glycans. This mechanism also appears to function *in vivo*, as the endogenously-expressed receptor is extensively sialylated, and LYVE-1 Fc fusion protein expressed in lymphatic endothelial cells (LEC) can be activated to bind HA following treatment with neuraminidases that cleave sialic acid. Curiously, the inhibitory sialyl moieties are inaccessible in intact cells, as neuraminidase treatment is effective against other membrane proteins, but can only remove sialic acid from LYVE-1 if first immunoprecipitated from lysed cells (Nightingale et al., 2009).

To date, no physiological factors have been identified that promote de-sialylation and subsequent unmasking of HA binding by LYVE-1 in primary cells. Stimulation of LYVE-1-expressing HEK 293T cells with the phorbol ester PMA leads to a 4-5 fold increase HA binding, coupled with *de novo* synthesis of the receptor with reduced levels of glycosylation (Nightingale, 2004). Although a similar effect has been observed with CD44-expressing cells, PMA treatment of lymphatic endothelial cells is ineffective (Dr. S. Banerji, unpublished observations). Far from activating the receptor, pro-inflammatory cytokines TNFα and TNFβ promote rapid but reversible internalisation and degradation of LYVE-1 in lysosomes, coupled with a shutdown in gene expression (Johnson et al., 2007). Down-regulation of LYVE-1 was also found to be reversible, as expression levels recover within 48 hours of TNFα withdrawal. Crucially, internalization of LYVE-1 does not result in significant uptake of HA, a process that proceeds almost equally in resting and inflammation-activated LEC and is unaffected by hLYVE-1 HA blocking mAb 3A. A wider screen of cytokines, chemokines and growth factors found no influence on LYVE-1 surface expression or HA binding. This prompted a wider search, both for alternative LYVE-1 ligands and the circumstances under which HA binding does occur.

1.4.4 Potential interactions of LYVE-1 with ligands other than HA

1.4.4.1 Binding of growth factors containing cell surface retention sequences

In 1995, *Boensch et. al.* described a protein purified from bovine liver that they designated Cell Surface Retention Sequence Binding Protein-1 (CRSBP-1) (Boensch et al., 1995). CRSBP-1 was identified by its ability to bind so-called cell surface retention sequence (CRS) peptides, that are 11-15 amino acids in length and contain 7 or 8 basic residues. CRS sequences had been identified previously in certain growth factors and cytokines, such as VEGF-A and PDGF-BB and were proposed to function as retention sequences mediating autocrine signalling via an unknown receptor (LaRochelle et al., 1991). Later, the interaction with CRS peptide from PDGF-BB with CRSBP-1 was demonstrated in cells transformed with simian sarcoma virus (Boensch et al., 1999), followed by the cloning and characterization of CRSBP-1 from a bovine cDNA library (Huang et al., 2003). Comparison of the CRSBP-1 sequence with existing records in genome databases revealed it to be identical to bovine LYVE-1, the direct homolog of the murine and human receptors (Banerji et al., 1999; Prevo et al., 2001). The authors of these studies have since described a role for CRSBP-1 in the autocrine retention of hyaluronan, VEGF-A and PDGF-BB CRS peptides, with resulting uncoupling of VE-cadherin junctions in lymphatic endothelial cells (Hou et al., 2011; Hou et al., 2012).

However, there are a number of inconsistencies that give rise to reasonable scepticism. Firstly, the polyclonal anti-CRSBP-1 antiserum used in all of these studies was generated against a N-terminal peptide from bovine CRSPB-1 fused to bovine thyroglobulin. This peptide is not present in human or mouse LYVE-1, yet the antiserum has been used to characterize CRSBP-1 in human and mouse tissues. This may explain why CRSBP-1 was reported to be present on all cell types tested (Huang et al., 2003) and is found primarily in

the endoplasmic reticulum, rather than on the cell surface, a distribution pattern that is distinct from that reported by many authors using the wide variety of anti-LYVE-1 antibodies available. Secondly, CRS sequences are not commonly supported in the literature, with no reports post-dating 1995. Furthermore, when tested for binding to LYVE-1 using surface plasmon resonance, CRS peptides exhibited very weak binding that was no greater than a scrambled peptide control (Dr. S. Banerji, unpublished observations).

1.4.4.2 Interaction with Fibroblast Growth Factor 2

The repertoire of lymphangiogenic factors has expanded in recent years to include the fibroblast growth factors 1 and 2, which act to stimulate proliferation and migration of lymphatic endothelial cells and have been shown act reciprocally with VEGF-C in tumours, leading to additive effects on lymphangiogenesis and metastasis (Cao et al., 2012; Chang et al., 2004; Shin et al., 2006). Recently LYVE-1 has been shown to interact with FGF-2 when surface immobilized or in solution, using a combination of Alphascreen technology, chemical cross-linking and co-immunoprecipitation (Platonova et al., 2013). The authors reported an apparent binding affinity of ~100 nM, that was completely ablated following deglycosylation using PNGaseF. Interestingly, FGF-2 binding could be displaced by combination with PDGF-BB or heparan, supporting earlier reports of a interaction with LYVE-1 from Boensch and colleagues. When over-expressed in CHO cells, LYVE-1 significantly increased binding of FGF-2 to so-called low-affinity sites. Binding of FGFs involves a combination of these sites and heparan sulphate proteoglycans, in addition to high affinity interactions with FGF receptors (Roghani and Moscatelli, 1992). HSPG and low-affinity interactions are thought to be particularly important for internalisation of and signalling by FGF-2.

In primary lymphatic endothelial cells, soluble recombinant LYVE-1 or siRNA knockdown or the receptor impaired FGF-2 signalling and function, despite the presence of the high affinity FGF receptor-3. No effect on VEGF-C mediated lymphangiogenesis was detected, despite recent reports of a synergistic effect with VEGF-C and FGF-2 (Cao et al., 2012). Conversely, FGF-2 treatment enhanced LYVE-1 expression, and effectively protected against the previously reported TNFβ-mediated down-regulation and degradation of the receptor (Johnson et al., 2007). This suggests that FGF-2 and LYVE-1 may be integrated in a regulatory loop, in which FGF-2 activates LYVE-1 expression, which in turn, limits FGF-2 activity by directly interacting with the growth factor (Platonova et al., 2013).

1.4.5 Potential physiological functions of LYVE-1

Prior to the start of my DPhil, a considerable body of work had been undertaken within the Jackson Laboratory aimed at defining the biological function of LYVE-1. This included characterisation of LYVE-1 deficient mice, the generation and use of mouse LYVE-1 specific monoclonal antibodies (mAbs) in animals model of inflammation and disease, and the biochemical characterisation of the receptor and its interaction with the only known ligand, hyaluronic acid. Based on the homology of LYVE-1 with CD44, and the specific expression pattern of the receptor, an early hypothesis imagined a role for LYVE-1 in adhesion and transmigration of lymphatic endothelium (Prevo et al., 2001).

However, two key observations appeared to suggest that such a function was unlikely; firstly that LYVE-1 is rapidly internalized and degraded in acute inflammation, both in primary human dermal lymphatic endothelial cells (LEC) and intact lymphatic vessels in mouse dermis (Johnson et al., 2007), and secondly, that LYVE-1-deficient mice exhibit no overt defects in DC trafficking from inflamed skin to the draining lymph nodes (Gale et

al., 2007). Normal fluid balance, HA levels in tissue and the blood, and lymphatic development and vessel ultrastructure ruled out secondary roles for the receptor, such as clearance of HA from lymph.

However, more recent studies have revealed an intriguing effect of blockade of mouse LYVE-1 using specific monoclonal antibodies in animal models of inflammation and disease. In a transmigration assay of cultured mouse dermal LEC, anti-mouse LYVE-1 mAb C1/8 effectively blocked adhesion and transmigration by ex vivo cultured dendritic cells (DCs) (Johnson & Jackson, unpublished observations). Subsequent experiments revealed a similar blockade of $CD11c^+$ $FITC^+$ endogenous DC trafficking from inflamed skin to lymph nodes in mice following contact hypersensitivity. Another mouse LYVE-1-specific mAb, B1/10, had no significant effect. Furthermore, C1/8 appears to inhibit entry of adoptively transferred bone marrow-derived DCs to afferent lymphatics following contact hypersensitivity in mice, whereas DCs are efficiently cleared from the dermis of mice treated with irrelevant rat IgG or B1/10.

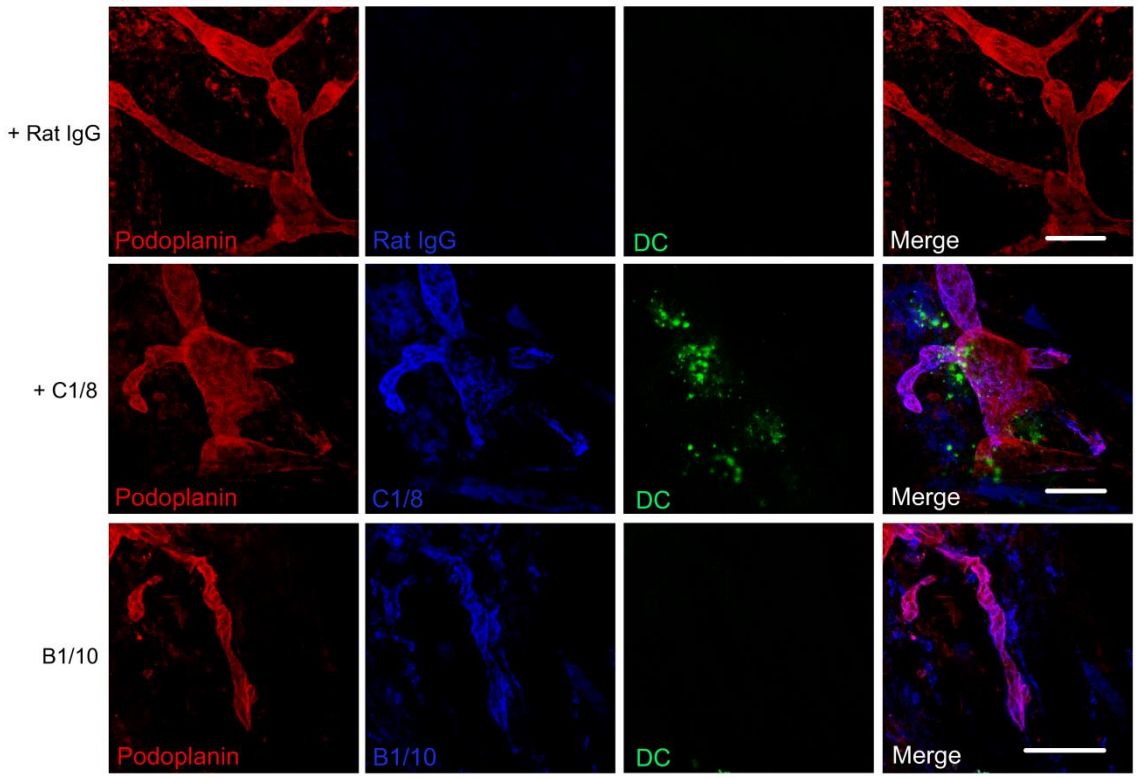


Figure 1.16. **LYVE-1 function-blocking mAbs inhibit entry of dendritic cells to afferent lymphatic vessels of the skin.** Mouse LYVE-1 mAb C1/8 inhibits entry of adoptively transferred bone marrow-derived DC to afferent lymphatics following contact hypersensitivity in mice, whereas DC were efficiently cleared from the dermis of mice which had received either irrelevant rat IgG or B1/10 mAb. Bar = 100 µm. Johnson and Jackson, unpublished observations.

In light of the finding that LYVE-1 plays a role in adhesion and transmigration of lymphatic endothelium by dendritic cells, function blocking experiments with LYVE-1 specific mAbs were expanded to investigate trafficking of other cell types, including metastasizing tumour cells. However in contrast to expectations, systemic administration of LYVE-1 mAb B1/10 to wild type (LYVE-$1^{+/+}$) mice was observed to potentiate nodal dissemination of spontaneously metastasizing primary T-241/VEGF-C fibrosarcomas, and induce *de novo* nodal metastasis in parental 'non-metastasizing' T-241 tumours (Royston, 2011). Administration of the C1/8 antibody however, had no significant effect. Furthermore, a similar increase in T-241/VEGF-C metastasis and *de novo* metastasis of T-241 tumours

was seen when both tumours were implanted into LYVE-1-/- mice. These results predict a protective role for LYVE-1 against lymphatic-borne tumour dissemination, which can be disrupted by B1/10, but not the C1/8 antibody.

Although largely restricted to the lymphatics, LYVE-1 is also expressed in murine lung by type I alveolar epithelial cells (AECs) (Prevo et al., 2001; Royston, 2011). While alveolar development in LYVE-1-deficient mice is normal, these mice do exhibit a serious defect in the resolution of acute lung injury, which can phenocopied in wildtype mice by administration of LYVE-1 blocking mAb (Royston & Jackson, manuscript in preparation). In wildtype (LYVE-$1^{+/+}$) animals, intratracheal injection of bleomycin induces a self-limiting and reversible acute inflammatory lung disease, however the same treatment in LYVE-1 deficient mice resulted in a progressive pulmonary infiltrate of neutrophils and macrophages, destruction and loss of functional lung tissue and eventually death. A similar lung pathology was observed in wildtype mice (LYVE-$1^{+/+}$) mice receiving a single intratracheal injection of LYVE-1 mAb C1/8 prior to bleomycin treatment, while disease progression in mice treated with the B1/10 mAb closely resembled that of mice receiving an irrelevant IgG control. Accumulation of leukocytes in the alveolar space appears to be a consequence of defective LYVE-1-mediated migration of inflammatory macrophages across the alveolar epithelium into the interstitium in a luminal-basolateral direction. Whether or not hyaluronan plays a role in this process is unclear, as previous work by Jorge Espinosa, a former DPhil student in our lab, demonstrated that LYVE-1 deficient mice have no defect in clearance of pulmonary HA.

1.5 Aims of this thesis

Anomalous features of HA binding by LYVE-1, such as inhibition by modification with sialic acid, fuels the question of what functions LYVE-1 mediates *in vivo* and whether these functions involve HA. In particular, the disparate effects observed following administration of anti-mLYVE-1 monoclonal antibodies highlights the importance of determining whether LYVE-1 mediates *in vivo* functions through binding of hyaluronan, an alternative ligand, or some other process. These problems can be tackled by identifying the HA-binding site in mouse LYVE-1 in the relation to the epitope bound by each antibody, which has yet to be defined, and the relative ability of each antibody to block HA binding (see Chapter 3).

Much of the past effort aimed at inducing hyaluronan binding to LYVE-1 in lymphatic endothelial cells has focussed on defining conditions that stimulate removal of inhibitory sialic acid from the receptor. However, the necessary conditions remain obscure and this has prompted consideration of additional, and potentially more rapid mechanisms of LYVE-1 regulation, many of which have been inspired by previous work on induction of HA binding by CD44. Recent QCM-D analysis of CD44-hyaluronan binding in an artificial membrane system has reminded how multiple weak individual interactions can tie down a large polyvalent ligand through the power of avidity (see Chapter 6). A key aim of this thesis will be to determine the extent to which avidity affects the binding of HA by LYVE-1, and whether receptor clustering represents a mechanism for regulating LYVE-1 function, by increasing the valency of the LYVE-1-HA interaction (see Ch. 4).

As described in the introduction, there are numerous examples in the literature where association of HA with one hyaladherin can influence binding of a second, and often with

consequences for the expressing cell. To date, studies of LYVE-1 interactions with HA have focussed on binding of free native HA chains, or fluorescein/biotin-labelled derivatives thereof. These forms of HA are not bound constitutively by primary lymphatic endothelial cells, but it would be intriguing to determine whether cross-linking of the ligand has a similar effect on LYVE-1 distribution. Previous studies have shown that cross-linking of HA by proteins such as TSG-6 can enhance or even induce binding by CD44-expressing cells. Tethering several HA chains together is likely to restrain their motion and present a larger array of binding sites to a membrane-bound HA receptor. There is ample scope therefore to explore the effect of cross-linking, multimerization or close array of HA chains on binding by LYVE-1 (see Chapter 5).

The role played by LYVE-1 homodimers is currently elusive; although they clearly exhibit greater affinity for HA than monomeric LYVE-1, the latter can be sufficient for HA binding, depending on cell background and capacity for receptor sialylation. While dimeric LYVE-1 is readily detected in both primary and transfected cells, little is known about its sub-cellular location or what controls the ratio of monomeric to dimeric LYVE-1. The relatively weak HA binding affinity of individual LYVE-1 molecules suggests a requirement for multivalent interactions, particularly under conditions of heavy sialylation in lymphatic endothelium, where a dimeric receptor may well play a critical role in stabilizing HA binding. Understanding the full functional significance of LYVE-1 homodimerization would therefore be aided by cell biological studies using both primary LEC and other transfected cell backgrounds. In addition, this would be complemented by studies with purified LYVE-1 proteins using a fully defined cell free system, such as QCM-D, where individual aspects of LYVE-1 regulation may be probed in isolation (see Chapter 6).

Chapter 2.
Materials and Methods

2.1 Materials and Reagents

General laboratory chemicals and reagents were purchased from Sigma-Aldrich, Fisher-Scientific, Merk, Life Technologies, QIAGEN and New England Biolabs (NEB). In general, reagents of molecular biology grade or higher were used, dependent on the application; for example cell-culture grade reagents were used for live-cell experiments. Reagents of particular significance to this project are listed below or associated with the relevant protocol.

2.1.1 Chemicals and buffers

- FACS incubation buffer: 5% (v/v) FCS, 5mM EDTA, 0.05% (w/v) NaN_3 in PBS.
- FACS Fix: 2% (v/v) formaldehyde, 0.02% (w/v) NaN_3 in PBS.
- ELISA buffer: 0.2% BSA, 0.1% Tween 20, 0.02% NaN_3 in PBS.
- ELISA wash: 0.1% Tween in PBS.
- Coating buffer: 15mM sodium carbonate, 34 mM sodium bicarbonate, pH 9.3.
- PBS-Tween: 0.1% (v/v) Tween 20 in PBS.

2.1.2 Reagents for molecular biology

- Hyaluronan from rooster comb was purchased from Sigma-Aldrich.
- High molecular weight medical-grade hyaluronan was obtained from Genzyme.
- High molecular weight (1.540 MDa), low-endotoxin hyaluronan was purchased from R&D Systems.
- End-biotinylated 30 kDa and 300 kDa hyaluronan was a kind gift from Professor Paul DeAngelis, University of Oklahoma Health Sciences Centre, USA.
- Restriction enzymes were purchased from NEB.
- T4 DNA ligase was purchased from NEB.
- Pfu Ultra HF DNA polymerase was purchased from Agilent.

2.1.3 Reagents for cell culture

- Accutase® (a proprietary cell detachment solution) was purchased from Sigma.
- Endothelial Cell Basal Medium 2 (EBM2) and the microvascular cell supplement kit (EGM2-MV) was purchased from Lonza.
- 2% gelatin solution was purchased from Sigma-Aldrich.
- Anti-mouse IgG microbeads were purchased from Miltenyi Biotec.

2.1.4 Antibodies

Specificity	Clone	Host	Source
hLYVE-1	8C (IgG_1)	Mouse	Jackson laboratory
hLYVE-1	6A (IgG_1)	Mouse	Jackson laboratory
hLYVE-1	7C (IgG_1)	Mouse	Jackson laboratory
hLYVE-1	3A (IgG_1)	Mouse	Jackson laboratory
hLYVE-1	891 (IgG_{2b})	Mouse	R&D Systems
hLYVE-1	892 (IgG_1)	Mouse	R&D Systems
hLYVE-1	893 (IgG_{2b})	Mouse	R&D Systems
hLYVE-1	Polyclonal	Rabbit	Jackson laboratory
hLYVE-1	Polyclonal (AF2089)	Goat	R&D Systems
hLYVE-1	Biotinylayed Polyclonal (AF2089)	Goat	R&D Systems
mLYVE-1	B1/10 (IgG_1)	Rat	Jackson laboratory
mLYVE-1	C1/8 (IgG_{2a})	Rat	Jackson laboratory
mLYVE-1	2125 (IgG_{2a})	Rat	R&D Systems
mLYVE-1	ALY7 (IgG_1)	Rat	e-biosciences
mLYVE-1	E9VA4 (IgM)	Rat	Santa Cruz Biotechnology
mLYVE-1	4D17 ('IgG_2')	Rat	Novus Biologicals
mLYVE-1	14-4 (IgG_{2a})	Rat	MBL Ltd.
mLYVE-1	Polyclonal	Rabbit	Jackson laboratory
mLYVE-1	Polyclonal (AF2125)	Goat	R&D Systems
CD31	JC70A (IgG_1)	Mouse	Dako
Podoplanin	NZ-1 (IgG_{2a})	Rat	AngioBio
Prox-1	Polyclonal (AF2727)	Goat	R&D Systems
Human CD44	BRIC235 (IgG_{2b})	Mouse	IBGRL

Specificity	Clone	Host	Source
Inter-α-inhibitor (Human)	Polyclonal	Rabbit	Dr. M. Lauer, Lerner Research Institute, under Award Number P01HL107147 from the National Heart, Lung and Blood Institute

Table 2.1. **List of antibodies; isotype, host and source.**

Secondary antibodies and streptavidin conjugates for flow cytometry and immunofluorescence microscopy were from the Alexa Fluor® range of dye-conjugated polyclonal antibodies and streptavidin conjugates available from Life Technologies®. Horseradish-peroxidase (HRP)-conjugated streptavidin or polyclonal secondary antibodies for use in ELISA were purchased from Pierce. IRDye-conjugated polyclonal secondary antibodies for use in infrared-fluorescent western blots were purchased from LI-COR.

2.1.5 Labelling of hyaluronan

Fluorescein labelled hyaluronan (Fl-HA) was prepared from high molecular weight rooster comb HA (Sigma) based on the method of de Belder and Wik (1975). Briefly, 10 mg of HA was dissolved in 8 ml of ultrapure water and mixed with 4 ml of DMSO. In a separate vial, 5 µl of acetaldehyde, 5 µl of cyclhexylisocyanide and 5 mg of fluoresceinamine were mixed in 300 µl of DMSO, before combining with the HA solution and incubating at R.T. for 5 hours. Ice-cold ethanol (160 ml) was then added to the reaction mix, followed by saturated NaCl solution until a precipitate formed (~2 ml). The precipitate was pelleted by centrifugation at 3 400 × g for 5min and then dissolved in 10 ml ultrapure water. Ice-cold ethanol (100 ml) was added once more to the Fl-HA solution, and the precipitate recovered as before, before dissolving in 5 ml H_2O. Fl-HA was dialysed overnight against 2L of H_2O

containing 0.05 % NaN_3, with periodic changes of the dialysis solution. Fl-HA was titrated against LYVE-1 or CD44-expressing cells to determine whether the HA had been over-modified (in which case the labelling time was reduced for subsequent preparations).

Biotinylated HA (bHA) was prepared from high molecular weight rooster comb HA (Sigma). HA was dissolved in 0.1M 2-(N-morpholino)ethanesulfonic acid (MES) pH 5.5 at 5 mg/ml and combined with *N*-(3-Dimethylaminopropyl)-*N'*-ethylcarbodiimide hydrochloride (EDAC) dissolved in 0.1M MES pH5.5 at 6.25, 12.5 or 25 mg/ml (final concentrations of 81.3, 162.5 or 325 µg/ml respectively). Biotin-LC-hydrazide (Pierce) made up in DMSO (50 mM) was added to a final concentration of 1 mM and stirred overnight at R.T. Each sample was dialysed against 2L of H_2O containing 0.05 % NaN_3, with periodic changes of the dialysis solution. Samples were then titrated against LYVE-1 or CD44-expressing cells to determine the optimum degree of HA-biotinylation for binding and detection by flow cytometry.

2.2 Bacterial Culture

2.2.1 Bacterial Strains

Two competent strains of *Escherichia coli* were used; DH5α (either NEB 5-alpha F'I^q or Invitrogren OmniMAX 2-T1^R), for cloning involving the pRcCMV expression vector and MC1061/p3 (Invitrogen), for cloning involving the pCDM7Ig expression vector.

2.2.2 Bacterial media and culture conditions

E. coli were grown in Luria-Bertani media (LB) 10 g/L tryptone, 5 g/L sodium chloride (or 10 g/L, when purifying plasmid DNA), 5 g/L yeast extract, and 100 µg/ml ampicillin (DH5α transformed with pRcCMV) or 25 µg/ml ampicillin, 7.5 µg/ml tetracycline (MC1061/p3 transformed with pCDM7Ig) at 37^{o}C. Agar plates were made with LB, bacto-agar (16 g/L) and antibiotics at the concentrations described, and inoculated using bacterial spreaders under an open flame. SOC medium, used during transformation of competent cells, was purchased from Invitrogen or NEB.

2.2.3 Transformation of competent cells

Transforming DNA (400-1200 ng) was added to a 25 µl aliquot of competent cells and incubated on ice for 30 min. Cells were heat-shocked at 42^{o}C for 30 secs, before returning to ice for 2 min. Pre-warmed SOC (125 µl) was added to the cells, followed by horizontal shaking incubation at 37^{o}c for 1.5 hours. A portion of the cells (25 – 50 µl) were spread onto LB-agar plates containing the appropriate antibiotic(s) and incubated at 37^{o}C overnight.

2.2.4 Preparation of glycerol stocks

Glycerol stocks of all transformed *E. coli* were prepared by mixing 750 µl of bacterial culture with 200 µl 80% (v/v) glycerol and freezing at –80 ^{o}C. DNA sequencing was used to determine which transformations contained the desired plasmid or construct, and all other glycerol stocks discarded.

2.3 Molecular Biology

2.3.1 Plasmids and constructs

Plasmid/vector	Source	Notes
pRcCMV	Invitrogen	Eukaryotic expression vector with ampicillin resistance
pCDM7Ig	Dr. A. Aruffo, Bristol-Myers Squibb, Seattle, WA.	For expression of soluble Ig fusion proteins
pHR-SIN	Davis laboratory, WIMM, Oxford	Lentiviral expression vector comprising the HIV-1 LTR and a CMV promoter
pHRI-SIN		Lentiviral expression vector comprising the HIV-1 LTR and a 5x/GRE promoter
pEE14		Expression vector of the CHO GS expression system (Lonza) encoding glutamine synthase, in addition to gene of interest
Construct		**Source**
Full length human LYVE-1 in pRcCMV		Dr. S. Banerji, Jackson Laboratory, WIMM, Oxford
Full length mouse LYVE-1 in pRcCMV		
Human LYVE-1 residues 1-232 in pCDM7Ig		
Mouse LYVE-1 residues 1-165 in pCDM7Ig		
Human LYVE-1-GFP in pHR-SIN		
Human LYVE-1 C201A-GFP in pHR-SIN		
Human LYVE-1 residues 1-238, 10 Histidine C-terminal tag, in pEE14		
Human LYVE-1 in pHR-SIN		William Lawrance, Jackson Laboratory, WIMM
Human LYVE-1 in pHRI-SIN		
Mouse LYVE-1 in pHR-SIN		
Mouse LYVE-1 in pHRI-SIN		

Table 2.2. **List of expression plasmids and constructs used in this project**.

2.3.2 Purification of plasmid DNA from bacterial cultures

For small scale purification of plasmid DNA (5-15 µg), 4ml of high-salt LB containing the appropriate antibiotic was inoculated from a glycerol stock of the desired bacterial line, and incubated at 37^{o}C, 225 rpm, for ~16 hours. Plasmid DNA was purified from the

resulting culture using a QIAGEN QIAprep miniprep kit, according to the manufacturer's instructions. For larger scale purification of plasmid DNA (up to 2.5 mg), a 4 ml starter-culture was setup as described, and 1ml used to inoculate a 500 ml volume of high-salt LB containing the appropriate antibiotic. This culture was incubated 37ºC, 225 rpm, for ~16 hours and the cells harvested by centrifugation at 6 000 rpm for 30 min. The pellet was weighed, and plasmid DNA harvested using a QIAGEN QIAprep miniprep kit, according to the manufacturer's instructions, and adjusting for the weight of cells used. In both cases, the yield of DNA was measured using a Nanodrop spectrophotometer.

2.3.3 PCR (Polymerase Chain Reaction)

PCR for routine amplification or mutagenesis was conducted using *Pyrococcus furiosus* (Pfu) Ultra High Fidelity (HF) (Agilent) and a TPersonal thermocycler (Biometra). Typical PCR reactions used in this project are listed below. Primers were designed with consideration for the sequence of the target gene and properties of any relevant restriction enzymes, and evaluated for melting temperature and secondary structure using the NETprimer tool at http://www.premierbiosoft.com. Where required for downstream applications, the PCR product was purified from the reaction mix using a PCR cleanup kit (Qiagen), or loaded onto a 0.8% agarose gel, fractionated by electrophoresis and purified from the appropriate gel slice using a Gel Extraction Kit (Invitrogen).

Amplification of a 1.5 kb gene from plasmid DNA using primers designed to add 5' and 3' restriction digest sites			
Composition of 50 µl reaction:			
50 – 200 ng of template DNA			
Forward and reverse primers at 500 nM			
1x Pfu Ultra HF buffer			
25 nM dNTPs			
Pfu Ultra HF at 2.5 U/µl			
Water to 50 µl			
Segment	**Cycles**	**Temp (°C)**	**Duration (min)**
1	1	95	2
2	5	95	0.5
		55	1.5
		72	2
3	25	95	0.5
		62	1
		72	2
4	1	72	10
Site-directed mutagenesis of a 1.5 kb gene encoded by a 5.5 kb plasmid, based on the Stratagene Quickchange II protocol			
Composition of 50 µl reaction:			
20 – 50 ng of template DNA			
100 ng of both forward and reverse primers			
1x Pfu Ultra HF buffer			
25 nM dNTPs			
Pfu Ultra HF at 2.5 U/µl			
Water to 50 µl			
Segment	**Cycles**	**Temp (°C)**	**Duration (min)**
1	1	95	1
2	20	95	0.5
		55	1
		68	10
3	1	68	10

Table 2.3. **PCR parameters for routine amplification and site-directed mutagenesis.**

2.3.4 Agarose gel electrophoresis

Agarose gels were made in Tris-Borate EDTA (TBE) buffer (90 mM Tris-Borate, 2 mM EDTA), with SYBR safe DNA stain at 1/10 000. For routine visualization and fractionation

of PCR products, 1% (w/v) agarose gels were used, or 0.8% (w/v) where fractionation of restriction digests was required. DNA samples were mixed with a 1/6 volume of loading buffer (2.5 mg/ml bromophenol, 30% (v/v) glycerol), loaded onto agarose gels and run at constant voltage (100V) alongside 1 kb or 100 bp DNA ladder (QIAGEN). Gels were visualized using a UVP UV transilluminator.

2.3.5 Digestion of DNA with restriction endonucleases

Restriction enzymes and buffers from New England Biolabs (NEB) were used to digest plasmid DNA or PCR products according to the manufacturer's instructions. Typically this involved a 50 µl reaction volume containing 0.5-10 µg of DNA, the appropriate reaction buffer, BSA if required, and restriction enzymes at a concentration of 1-5 units/µg of DNA, while maintaining a glycerol concentration of <10% (v/v).

2.3.6 Purification of DNA fragments

DNA fragments generated by restriction enzyme digest were fractionated using 0.8% TBE agarose gel electrophoresis. Bands corresponding to the desired fragment sizes were excised under UV illumination and DNA extracted from the resulting gel slices using a Gel Extraction Kit (Invitrogen) according to the manufacturer's instructions.

2.3.7 Ligation of DNA fragments

Purified DNA fragments were ligated using 200 units of T4 DNA ligase (NEB) in a 10 µl reaction containing 1x T4 DNA ligase buffer and the DNA of interest, at a total concentration of 1 – 10 µg/ml and an insert:vector molar ratio varying between 2:1 and 6:1. Ligation was performed for 2 hours at 16^{o}C.

2.4 Cell culture and generation of cell lines

2.4.1 Cell lines

Cell line	Source
Primary Human Dermal Lymphatic Endothelial Cells	Patients undergoing elective plastic surgery at the John Radcliffe Hospital, Oxford
HEK 293T Fibroblasts	CRUK cell bank
Jurkat	Davis laboratory, WIMM
Human and mouse LYVE-1 HEK 293T	Dr. S. Banerji, Jackson Laboratory, WIMM
Human LYVE-1 CHO K1	Dr. T. Nightingale, former Jackson Laboratory
Human LYVE-1 CHO LEC2	Dr. T. Nightingale, former Jackson Laboratory
Human LYVE-1 pHR and pHRI Jurkat	William Lawrance, Jackson Laboratory
Mouse LYVE-1 pHR and pHRI Jurkat	William Lawrance, Jackson Laboratory
Human LYVE-1-GFP pHR Jurkat	Dr. S. Banerji, Jackson Laboratory, WIMM
Human LYVE-1 C201A-GFP pHR Jurkat	Dr. S. Banerji, Jackson Laboratory, WIMM
Human LYVE-1 Δ238 10 His CHO K1 (CHO17 clone)	Mrs. Janet Fennelly, Davis Laboratory, WIMM

Table 2.4. **Table of cell lines utilised in this DPhil project.**

2.4.2 Isolation of primary Human Dermal Lymphatic Endothelial Cells (HDLEC)

HDLECs were prepared from healthy adults undergoing elective plastic surgery (breast reduction and abdominoplasty). Skin was digested overnight at 4°C with 2 mg/ml Dispase (Calbiochem) in PBS, and the epidermis removed using forceps. Dermal cells were released from the tissue by scraping, passed through a 70-μm cell strainer, and expanded in 0.1% gelatine-coated flasks in complete medium (EGM-2 MV; Lonza) at 37°C, 5% CO_2 in a humidified atmosphere. HDLECs were lifted with Accutase (PAA Laboratories) and immunoselected with mouse anti–human LYVE-1 mAb 8C, followed by magnetic retrieval with anti-mouse IgG MACS bead preparations (Miltenyi Biotec). The resulting cells were

cultured in EGM-2 MV using plastic tissue culture flasks pre-coated with 0.1% gelatin (Sigma). Expression of lymphatic endothelial cell markers (Prox-1, LYVE-1, Podoplanin) the pan-endothelial marker CD31, and an absence of blood endothelial cell markers (PAL-E, CD44), was confirmed at early passage by immunofluorescence microscopy and flow cytometry.

2.4.3 Cell culture conditions

All cell types were cultured at 37ºC in a 5% CO_2 humidified atmosphere. Primary HDLEC were cultured on 0.1% gelatin-coated T75 tissue-culture flasks in 12ml of EGM2-MV media (Lonza). Once the cells had formed a confluent monolayer (typically 48 hours), the media was removed, cells washed with PBS and then incubated with Accutase solution for 5-10 min at 37ºC to dissociate cells from the cell culture plastic. Cells were harvested, and removed from the Accutase solution by centrifugation at 300 ×g for 4 min. Cells were then re-suspended in sufficient fresh media for a 1:2 split.

Human and mouse LYVE-1 transfected cell HEK 293T, CHO K1, and CHO LEC2 cells were cultured on 15cm diameter tissue-culture plates in R10 (RPMI 1640 (Sigma) supplemented with 10% (v/v) FCS (Sigma), 1% (v/v) L-Glutamine, 1% (v/v) Penicillin/Streptomycin). Cells were typically passaged 1:5 every 3 days, using Trypsin 5mM EDTA solution (Lonza) in place of Accutase. LYVE-1 transfected Jurkat cells were cultured in JMEM (RPMI 1640 supplemented with 10% (v/v) FCS (Sigma), 1% (v/v) L-Glutamine, 1% (v/v) Penicillin/Streptomycin, 10 mM HEPES, 1 mM sodium pyruvate) and passaged 1:10 into fresh media every 2-3 days. When transfecting HEK 293T fibroblasts, cells were cultured in D10 sera (DMEM supplemented with 10% (v/v) FCS (Seralabs), 1% (v/v) L-Glutamine, 1% (v/v) Penicillin/Streptomycin) which facilitates enhanced transfection efficiency compared to R10 (Dr. S. Banerji, unpublished observations).

2.4.4 Cryopreseveration

Confluent monolayers of adherent cells were lifted using Accutase (primary HDLEC) or Trypsin-5mM EDTA solution (all others) and centrifuged at 300 ×g for 4 min. The supernatant was removed and cells re-suspended in 10% DMSO (v/v) in FCS at different cell densities, dependent on the cell type, and divided into 1 ml aliquots for freezing. For primary HDLEC this corresponded to 2 cryovials per T75 tissue culture flask, for all other adherent cell types, 5 cryovials per 15cm diameter plate. Jurkat cells were frozen in 1ml aliquots of 5 million cells. All cell types were initially frozen in a -80^{o}C freezer, prior to transfer to liquid nitrogen for long-term storage.

2.4.5 Recovery of frozen cells

Cryovials were thawed rapidly in a 37^{o}C water bath and cells transferred to 10 ml of pre-warmed media. Cells were pelleted by centrifugation at 300 ×g for 4 min, re-suspended in fresh media and transferred to tissue culture flasks or dishes.

2.4.6 Transient transfection of HEK 293T fibroblasts

HEK 293T cells cultured in D10 (DMEM supplemented with 10% (v/v) FCS, 1% (v/v) L-Glutamine, 1% (v/v) Penicillin/Streptomycin) were seeded onto 6-well tissue culture plastic and grown to 80-90% confluency on the day of transfection. For each transfection, 4 µg of plasmid DNA was mixed with 200 µl DMEM and polyethyleneimine (PEI) at a final concentration of 70 µg/ml. The mixture was incubated at room temperature for 10 minutes and added drop-wise to the culture medium. Cells were returned to a 37^{o}C incubator for 24 hours for transfection to occur, before replacing the media.

2.4.7 Lentiviral vector production and infection of cell lines

Lentivirus were produced in HEK 293T fibroblasts following transfection with three separate plasmid vectors; (i) *pHR-SIN*, encoding the gene of interest, under the control of a CMV promoter, and the HIV genome long terminal repeat (LTR), or pHRI-SIN, an equivalent vector with a 5x/GRE promoter, that drives ~100-fold lower levels or protein expression than CMV, (ii) *p8.91 Ex QV*, encoding the viral gag, polymerase, rev and tat proteins, and (iii) *pMD-G*, encoding the vsv-g envelope protein. HEK 293T cells were first seeded onto 6-well tissue-culture dishes and grown to ~70% confluency, before changing the media to that required by the cell type targeted for infection. Each well required a transfection mix containing 0.5 µg of p8.91, pMD-G and pHR-SIN in ~20 µl H_2O, together with 4.5 µl of genejuice transfection reagent (Merckmillipore) and 100 µl of DMEM, incubated together for 30 min at room temperature. The transfection mix was added drop-wise to the culture medium, and cells incubated at 37ºC for 48-72 hours, to allow transfection and viral expression to occur. The viral supernatant was harvested, centrifuged at 500 ×g for 5 min to remove the majority of cells, and passed through a 0.45 µm filter to remove cell debris. When infecting adherent cell types, cells were typically seeded onto 6-well tissue-culture dishes and grown to 50% confluency, prior to removal of media and additional of 2ml of viral supernatant. Suspension cells, such as Jurkats, were re-suspended in viral supernatant, typically 1 million cells in 2-4 mls. Twenty-four hours later, 2 mls of fresh media was added and cells expanded in culture, as appropriate.

2.4.8 Fluorescence-activated cell sorting

Fluorescence-activated cell sorting (FACS) was used to purify LYVE-1-expressing cells following transfection or infection with LYVE-1-bearing plasmid or lentiviral vectors. Adherent cells were first lifted using Accutase, a cell-detachment reagent that has

previously been shown to have no enzymatic activity against LYVE-1 (Dr. D. Rigby, Jackson laboratory, WIMM). Adherent or suspension cells were pelleted by centrifugation, washed once with PBS, and re-suspended in FACS incubation buffer (5% FCS, 5mM EDTA in PBS) containing a LYVE-1 specific mAb (either 8C, 891 or 2125, depending on cell type) at 25 µg/ml and incubated for 20 min at 4^{o}C. Cells were then pelleted by centrifugation, washed once with FACS incubation buffer, and re-suspended in fresh buffer containing anti-mouse or anti-rat IgG Alexa 488 (Life technologies) at 20 µg/ml for 20 min at room temperature. Cells were twice pelleted by centrifugation and washed with FACS incubation buffer, before re-suspending in 1ml of buffer at 1-10 × 10^6 cells/ml. This cell suspension was passed through a single-cell filter and sorted for LYVE-1-expressing cells by Dr. Craig Waugh (FACS facility, WIMM) using an unlabelled sample of cells as a reference. LYVE-1$^+$ cells were pelleted by centrifugation and re-suspended in 2-4 mls of the appropriate cell-culture media and transferred to a T25 tissue-culture flask.

2.5 Recombinant protein and monoclonal antibodies

2.5.1 Expression of LYVE-1-Fc fusion proteins by transiently-transfected HEK 293T fibroblasts

HEK 293T cells cultured in D10 (DMEM supplemented with 10% (v/v) FCS, 2 mM L-Glutamine, 50 µg/ml Penicillin/Streptomycin) were seeded onto 15 cm diameter tissue culture plastic dishes and grown to 80-90% confluency on the day of transfection. For each transfection, 40 µg of plasmid DNA was mixed with 2 ml DMEM and polyethyleneimine (PEI) at a final concentration of 70 µg/ml. The mixture was incubated at room temperature for 10 minutes before adding it to the culture medium. Cells were returned to a 37^{o}C incubator for a period of 12-16 hours before exchanging the D10 medium for expression media (CHO-SF-MII [Gibco] supplemented with 2 mM L-Glutamine, 50 µg/ml Penicillin/Streptomycin, 25 µg/ml fungizone). After a period of 72 hours, the cell culture supernatant containing LYVE-1-Fc fusion protein was harvested and cleared of cellular debris by filtration through a Steritop filter unit with a 0.22 µm pore size (Millipore). The pH of the supernatant was adjusted to pH 8.0 by addition of 1/20 volume of 2M Tris pH 8.0, before passing over Protein A Fastflow Sepharose 4B (Sigma) at 4^{o}C at a flow-rate of 1 – 5 ml/min for a period of 24 – 48 hours. The protein A column was washed with 10 column volumes of PBS, and bound LYVE-1 Fc eluted by addition of 0.1M glycine-HCl pH3.0 in fractions of 1ml. These fractions were adjusted to neutral pH by addition of 2M Tris pH8.0 and the protein content assessed using a Nanodrop spectrophotometer. LYVE-1 Fc fusion proteins were further purified by size-exclusion chromatography on a superdex S200 10/300 column (GE) using PBS as the buffer. Fractions corresponding with the predicted molecular weight of LYVE-1 Fc were combined and concentrated using 10 kDa

molecular weight cut-off, centrifugal filtration devices (Amicon) and the purity of final protein assessed by LDS-PAGE and western blotting.

2.5.2 Expression and purification of recombinant histidine-tagged LYVE-1 extracellular domain from Chinese Hamster Ovary (CHO) cells

Human LYVE-1 Δ238 with a C-terminal 10 histidine tag was produced by a CHO K1 clone (CHO17) transfected with vector pEE14 bearing hLYVE-1 Δ238 10His and isolated for high expression using the glutamine synthetase system (Lonza) by Janet Fennelly (Davis laboratory, WIMM) and Dr. S. Banerji (Jackson laboratory, WIMM). CHO17 cells were cultured in selection media (DMEM [-] L-glutamine [Gibco] supplemented with 10% heat-inactivated, dialysed [10 kDa MWCO] FCS, 50 µg/ml penicillin/streptomycin, 1x amino acid/nucleoside supplement, sodium pyruvate and 40 µM MSX) and expanded until a final 1:2 split into expression media (selection media minus MSX and containing regular FCS). Once the cells reached confluency, sodium butyrate was added to a final concentration of 2 mM and cells maintained in culture for a further five days. Cell culture supernatant was harvested, cleared of cellular debris by centrifugation and filtration through steritop filter units (0.22 µm pore size) and diluted with 2 volumes of PBS. NaCl and imidazole were added to final concentrations of 500 mM and 40 mM respectively, before passing the supernatant over an immobilized metal ion affinity chromatography (IMAC) column (5ml Ni^2-loaded Histrap, GE) at 4ºC and at a flow rate of 1-2 ml/min. After every 500ml of supernatant the IMAC column was cleared of non-specifically bound protein using 25 ml of wash buffer 20mM phosphate + 40mM imidazole + 500mM NaCl. Recombinant hLYVE-1 Δ238 10His was eluted by addition of 10 ml of 20mM phosphate + 500mM imidazole + 500mM NaCl and further separated into monomeric and dimeric species by

two consecutive rounds of size-exclusion chromatography (SEC) on a superdex S200 10/300 column.

2.5.3 Hybridoma cell culture and affinity purification of monoclonal antibodies

LYVE-1 mAb hybridoma cells lines were cultured in RPMI 1640 supplemented hypoxanthine and thymidine (HT) supplement (Gibco), 2 mM L-Glutamine, 50 µg/ml penicillin/streptomycin and FCS at varying concentrations during the culture process. Frozen aliquots containing 2 million cells were initially revived in 10 ml of media containing 10 % FCS, before expanding with periodic additions of fresh media to 200 ml at a cell density of 1 -5 million cells/ml. Cells were split 1:5 into fresh media containing 5% FCS (1L total) and expanded in culture, before a final 1:2 split into media containing 1% FCS (2L final). After a period of 7 – 10 days, the cell culture supernatant was harvested by centrifugation at 15 000 rpm for 5 min, followed by filtration using Steritop filter units with a 0.22 µm size-exclusion limit (Millipore) to remove cell debris. The pH of the supernatant was adjusted to pH 8.0 by addition of 1/20 volume of 2M Tris pH 8.0, before passing over Protein A or G (as appropriate for the antibody isotype) Fastflow Sepharose 4B (Sigma) at 4^{o}C at a flow-rate of 1 – 5 ml/min for a period of 24 – 48 hours. The protein G column was washed with 10 column volumes of PBS, and bound IgG eluted by addition of 0.1M glycine-HCl pH3.0 in fractions of 1ml. These fractions were adjusted to neutral pH by addition of 2M Tris pH8.0 and the IgG content assessed using a Nanodrop spectrophotometer. The protein G column was regenerated by sequential addition of 10 column volumes of 0.1M glycine-HCl pH3.0, 2 M Urea, 1 M LiCl, 0.1M glycine-HCl pH3.0, followed by 20 column volumes of storage buffer (0.05 % NaN_3 in PBS). Where required by the downstream application, eluted IgG was further purified by size-exclusion chromatography on a superdex S200 10/300 column (GE).

2.6 Protein biochemistry

2.6.1 Preparation of protein from whole-cell lysates

2.6.1.1 TCA precipitation of protein

Culture media was removed, cells washed with PBS, and then lifted at 4ºC with 5 mM EDTA in PBS. Cells were washed once with PBS, before re-suspending in PBS. Trichloroacetic acid (TCA) was then added to a final concentration of 10% (w/v) and samples placed on ice for 10 minutes. Precipitated protein was spun-down briefly in a microcentrifuge and the pellet washed with ice-cold acetone to remove any remaining TCA. The acetone was discarded, and the pellet allowed to air-dry, before re-suspending at 95ºC in 1x LDS sample buffer (Invitrogen). Where reducing conditions were desired, DTT was added to a final concentration of 50 mM.

2.6.1.2 Lysis using LDS-sample buffer

Tissue culture medium was removed from adherent cell monolayers and cells washed with PBS. Lithium dodoceyl sulphate (LDS) sample buffer (1x, Invitrogen) was added directly to cells and the lysate collected in an eppendorf tube, before heating to 95ºC for 5 minutes. DNA was sheared by repeat 15-second bursts of sonication in an ice-water bath sonciator. If reducing conditions were required, DTT was added to the sample at a final concentration of 50 mM.

2.6.2 LDS Polyacrylamide gel electrophoresis (LDS-PAGE)

Between 1 and 10 µg of protein was denatured at 95ºC for 5 min in 1x LDS sample buffer (Invitrogen) under reducing (50 mM DTT) or non-reducing conditions. These samples, or

those prepared from whole-cell lysates, were fractionated on 4-12% Bis-Tris polyacrylamide gels (Invitrogen) alongside Novex pre-stained protein standards (Life technologies) using 1x MES or MOPS running buffer (Life technologies), as appropriate for the molecular weight of the protein of interest. Gels were rinsed with distilled water and stained with SimplyBlue SafeStain (Life technologies) for direct visualisation, or subsequently probed by western blot for specific proteins.

2.6.3 Western blotting

Protein gels were blotted onto activated Immobilin-PL PVDF membrane (Li-Cor) using 1x transfer buffer (3.033 g/L Tris-base, 14.4 g/L glycine, 20% v/v methanol in distilled water) using a semi-dry Bio-Rad blotting apparatus (20V, 30 min). Western blots were blocked using blocking buffer (Li-Cor) for 1 hour at room temperature before incubating with primary antibodies (typically, goat anti human or mouse LYVE-1 polyclonal (R&D systems) at 0.3 µg/ml) overnight at 4^{o}C. Membranes were washed 3x with PBS-0.1% Tween before incubating with appropriate secondary antibodies (typically, donkey anti goat IgG Fc IRDye 800CW, at 1/15 000 from Li-Cor) in blocking buffer, for 1 hour at room temperature. Where IRDye 680 conjugates were used, the blocking buffer was supplemented with 0.01% (v/v) SDS and 0.1% (v/v) Tween, to reduce background. Western blots were washed 3x with PBS-Tween, 1x with PBS and allowed to dry, before imaging with a Li-Cor ODYSSEY scanner.

2.7 Experimental protocols

2.7.1 Generation of mouse LYVE1 site-directed mutants

Primers were designed for the PCR mutagenesis of forty-two individual amino acids to alanine (see Appendix 1, Table 7.1). Full length mLYVE-1 in pRcCMV was used as a template in a PCR protocol based on the Quickchange II Site-Directed Mutagenesis Kit (Stratagene). Following digestion of methylated template DNA with DpnI, PCR products were used to transform OmniMAX 2-T1R E. coli (Invitrogen) as per the manufacturer's instructions. Successful transformations were identified as colonies that grew on ampicillin-LB-agar plates. Individual colonies were expanded in small (4ml) LB + ampicillin cultures prior to purification of high purity plasmid DNA using a Qiaprep spin miniprep kit (QIAGEN). Samples of each plasmid were submitted for sequencing to confirm error-free amplification and successful mutation at the site of the target residue.

2.7.2 Transient transfection of HEK 293T cells with mouse LYVE-1 mutants

HEK 293T cells cultured in D10 (DMEM supplemented with 10% (v/v) FCS, 1% (v/v) L-Glutamine, 1% (v/v) Penicillin/Streptomycin) were seeded onto 6-well tissue culture plastic at a cell density that gave 80-90% confluency on the day of transfection. In each experiment, cells were transfected in triplicate with either wildtype mLYVE-1, mutant mLYVE-1, mock (no DNA) or eGFP (Invitrogen). For each transfection, 4 µg of plasmid DNA was mixed with 200 µl DMEM and polyethyleneimine (PEI) at a final concentration of 70 µg/ml. The mixture was incubated at room temperature for 10 minutes before adding it to the culture medium. Cells were returned to a 37^{o}C incubator for 24 hours for transfection and protein expression to occur. An estimate of transfection efficiency was made by a visual check for eGFP expression using an epifluorescence microscope.

2.7.3 Assessment of antibody and hyaluronan binding to HEK293T cells transfected with mLYVE-1 mutants

Twenty-four hours post transfection, cells were washed with PBS and then lifted in 5mM EDTA, 0.05% sodium azide in PBS. Cells were then re-suspended in 700 µl blocking buffer (5% goat serum, 1% BSA, 0.05% Sodium Azide, 5mM EDTA, in PBS) and incubated for 10 mins at 4ºC. Next, each transfection was split into 8x 50 µl volumes in a 96-well plate. Cells were pelleted, the blocking buffer discarded, and then re-suspended in 100 µl blocking buffer containing the primary antibodies listed in Table 2.5. Cells were incubated with primary antibodies for 45 minutes at 4ºC, before washing 2x with FACS wash (5% FCS, 0.05% sodium azide in PBS). Cells were then incubated in 75 µl blocking buffer containing appropriate secondary antibodies (listed in Table 2.5) for 45 minutes at 4ºC. Cells were washed with FACS wash a further 2x before re-suspending in FACS fix (1% formaldehyde, 0.02% sodium azide in PBS).

	Primary antibodies	Conc. (µg/ml)	Secondary antibodies	Conc. (µg/ml)
1	Rabbit anti-mLYVE1 poly. (total Ig from rabbit)	80	goat anti rabbit IgG Alexa 488	10
2	Rat anti-mLYVE1 B1/10 mAb	80	goat anti rat IgG Alexa 488	10
3	Rat anti-mLYVE1 C1/8 mAb	80	goat anti rat IgG Alexa 488	10
4	Rat anti-mLYVE1 mAb MAB2125 (R&D Systems)	10	goat anti rat IgG Alexa 488	10
5	Rat anti-mLYVE1 mAb ALY7 (e-biosciences)	10	goat anti rat IgG Alexa 488	10
6	Rabbit IgG isotype control (R&D Sys.)	80	goat anti rabbit IgG Alexa 488	10
7	Rat IgG isotype control (Sigma)	80	goat anti rat IgG Alexa 488	10
8	Fluorescein-labelled HA (Fl-HA)	10% (v/v)	None	10

Table 2.5. **Primary and secondary antibodies used for epitope mapping studies.**

Samples were analysed on a LSRII flow cytometer equipped with a high-throughput autosampler (Beckton-Dickinson). Unstained wildtype-LYVE-1 transfected cells were

used to set forward and side scatter voltages, and adjust the voltage of the excitation laser such that unstained cells had a mean fluorescence close to zero. Doublets were excluded from the analysis using a plot of forward scatter height vs. forward scatter width. The mean fluorescence value of each sample in the FITC channel was calculated, and the value for polyclonal-stained cells used as a measure of total expression for each mutant. Binding of monoclonal antibodies, isotype controls, or Fl-HA was corrected for expression, by dividing the mean fluorescence value of these samples by the value for polyclonal. These calculations were performed for each technical replicate, and from the resulting values, a mean and standard error derived for each mutant.

2.7.4 Generation of an *in silico* structural model of mouse LYVE-1

A computer generated model of mLYVE-1 was produced using the ModWeb program available at https://modbase.compbio.ucsf.edu/scgi/modweb.cgi. Users submit modelling tasks by inputting the UniProt identifier of a protein of interest (in this case, mouse LYVE-1, Q8BHC0). ModWeb then runs a BLAST query on the protein sequence to identify homologs, and a PDB search to identify any known crystal or solution structures that can be used as a template. In this instance, ModWeb identified the closest homology between residues 29-176 of mLYVE-1 and the crystal structure of human CD44 (PDB code 1UUH), which covers residues 23-165. The resulting model closely resembles human CD44, and a model of human LYVE-1 previously generated using Modeller 9v6 and published here (Banerji et al., 2010). The model has a GA341 score of 1.0, on a scale of 0 to 1, with 1 indicating a native-like fold. However, the ModPipe Protein Quality Score (MPQS), a composite score comprising sequence identity to the template, coverage, and the three individual scores of evalue, z-Dope and GA341, was 0.935. A MPQS of >1.1 is considered

optimal, however this model scores lower than it otherwise might, because the template only covers the Link domain, and not the full 318 amino acids.

2.7.5 Assay for blocking of hyaluronan-binding to mLYVE-1 by anti-mLYVE-1 monoclonal antibodies (ELISA)

A maxisorb plate (Nunc) was coated overnight at R.T. with mLYVE-1 Δ165 TEV Fc at 10 µg/ml, 50 µl per well in coating buffer. The plate was washed 2x with PBS and then blocked with 1% BSA in PBS – 0.1% Tween. Mouse LYVE-1 mAbs B1/10, C1/8, MAB2125 and ALY7 or Rat IgG (Sigma) were applied in triplicate in PBS – 0.1% Tween at concentrations of 0, 10, 20, 40 or 80 µg/ml, 45 µl per well, for 30 mins, at R.T. The plate was washed 5x with PBS-Tween before applying bHA at 10 µg/ml, 50 µl per well in PBS-Tween, for 30 minutes, at R.T. The plate was washed and bound bHA detected using streptavidin-HRP (Pierce), 1/500 dilution in PBS-Tween, 50 µl per well, for 30 mins at R.T. The plate was washed a final time and developed with Sigmafast OPD HRP-substrate (Sigma) as per the manufacturer's instructions and then quenched with 2M H_2SO_4. The absorbance at 490 nm was detected using a Bio-Rad 680 Microplate Reader, and the average absorbance of samples that did not receive bHA subtracted from the absorbance of all other samples.

2.7.6 Assay for binding of anti-mLYVE-1 monoclonal antibodies to mLYVE-1 Δ165 and Δ232 Fc (ELISA)

A maxisorb plate (Nunc) was coated overnight at room temperature with mLYVE-1 Δ165 TEV Fc or mLYVE-1 Δ232 TEV Fc at 5 µg/ml, 50 µl per well in coating buffer (15mM sodium carbonate, 34 mM sodium bicarbonate, pH 9.3). The plate was washed 2x with PBS and then blocked with 1% BSA in PBS – 0.1% Tween. Monoclonal antibodies raised against mLYVE-1 (B1/10, C1/8, MAB2125 (R&D sytems), ALY7 (e-biosiences)) or Rat

IgG (Sigma) were applied in triplicate in PBS – 0.1% Tween at concentrations of 0, 10, 20, 40, 60 or 80 µg/ml, 45 µl per well, for 60 mins, at room temperature. The plate was washed (3x PBS, 1x PBS-Tween, 3x PBS) before applying anti Rat IgG Fc HRP conjugate (Pierce) 1/2000, 50 µl per well in PBS-Tween, for 45 minutes, at room temperature. The plate was washed a final time and developed with Sigmafast OPD HRP-substrate (Sigma) as per the manufacturer's instructions and then quenched with 2M H_2SO_4. The absorbance at 490 nm was detected using a Bio-Rad 680 Microplate Reader, and the average absorbance of samples that did not receive any antibody was subtracted from the absorbance of all other samples that did receive antibody. The mean and standard error of triplicate samples was then calculated.

2.7.7 Assays for constitutive HA binding by LYVE-1 transfected cells and the influence of LYVE-1 mAbs on HA binding

Human or mouse LYVE-1 transfected HEK 293T cells were cultured in 6-well tissue-culture dishes until a confluent monolayer had formed. Cell culture media was removed, cells were washed with PBS and then lifted at 4°C in 5mM EDTA in PBS. Cells were resuspended in sufficient FACS incubation buffer to yield 6x 150µl samples, and incubated at 4°C for 10 min. Human or mouse LYVE-1 transfected Jurkat cells were pelleted by centrifugation and resuspended at 1.66 x 10^6 cells/ml in buffer, and incubated at 4°C for 10 min. Both LYVE-1 transfected Jurkat and HEK 293T cells were divided into 150 µl (~250 000 cells) samples in a 96-well plate. Cells were pelleted by centrifugation and resuspended in 150 µl buffer containing biotinylated HA (bHA) (5 µg/ml) either alone, or in combination with LYVE-1 mAbs (5 µg/ml), or isotype-matched Ig (5 µg/ml), or unlabelled HA (200 µg/ml) and incubated for 40 mins at 4°C. Cells were washed 3x with buffer, before resuspending in 100 µl of buffer containing the appropriate secondary antibody at 10 µg/ml

and streptavidin Alexa 647 at 5 µg/ml, and incubated at 4°C for 30 min. Cells were washed 3x with buffer, before resuspending in FACS Fix. The fluorescence intensity was measured for 20 000 cells using flow cytometry.

In some experiments, this protocol was modified to address specific questions. To determine the concentration of bHA required for saturated binding, LYVE-1 transfected cells were incubated with bHA alone at a range of concentrations. To determine the influence of antibody concentration on bHA binding, cells were incubated with bHA at a fixed concentration of 5 µg/ml, while the Ig concentration was varied across the range indicated. In some experiments, the sequence of incubation with LYVE-1 mAbs or bHA was varied to determine the influence on bHA binding, with three washing steps between reagents. All other parameters were maintained as described.

2.7.8 Cross-blocking assay for mLYVE-1 monoclonal antibodies

Samples of mLYVE-1 mAbs B1/10 and C1/8 were conjugated with DyLight 488 and DyLight 650 respectively, as per the manufacturer's instructions (Pierce). Mouse LYVE-1 pHR Jurkat cells were incubated at 1.66 x 10^6 cells/ml in FACS incubation buffer separately with B1/10-488, C1/8-650, MAB2125-R-PE, or ALY7-Alexa488 at increasing Ig concentration, for 45 min at 4°C. Cells were washed 3x with buffer, resuspended in FACS fix, and analysed by flow cytometry to determine the saturating Ig concentration for each antibody. Fresh cells were then incubated in triplicate with dye-conjugated mLYVE-1 mAbs either alone, or simultaneously with a second mAb bearing a distinct fluorophore, or isotype-matched control IgG. A saturating concentration of Ig was used in all cases. The fluorescence intensity was measured for 20 000 cells using flow cytometry.

2.7.9 Influence of LYVE-1 expression level on HA binding in transfected cells

Separate Jurkat cell lines were established by infection with lentivirus bearing the full-length cDNAs encoding either human and mouse LYVE-1, under the control of either a CMV promoter (pHR, high levels of expression) or 5x/GRE promoter (pHRI, low expression level) (see 2.4.7, 2.4.8). Human or mouse LYVE-1 pHR or pHRI Jurkat cells were assayed for bHA binding and LYVE-1 expression using flow cytometry, as described in protocol 2.7.7. To assess the relationship with LYVE-1 expression level and bHA binding, cells were incubated with bHA first, washed 3x with buffer, and then incubated with LYVE-1 antibodies.

2.7.10 Super-transfection of primary HDLEC with LYVE-1

Primary HDLEC were infected using a lentiviral vector (pHR) bearing the coding sequence of full length human hLYVE-1, hLYVE-1-GFP, or hLYVE-1 C201A-GFP and expanded in culture. *Influence on LYVE-1 expression and HA binding detected by flow cytometry*: Cells were lifted with Accutase®, washed with FACS incubation buffer, and incubated with bHA either alone or in combination hLYVE-1 Abs (5 µg/ml), or isotype-matched controls (5 µg/ml), or an excess of unlabelled HA (200 µg/ml) for 40 min at 4ºC. Cells were washed 3x with buffer, incubated with appropriate secondary reagents for 30 min at 4ºC, washed again and resuspended in FACS fix. The fluorescence intensity was measured for 20 000 cells using flow cytometry.

2.7.11 LYVE-1 distribution and HA binding in adherent wildtype and LYVE-1 super-transfected HDLEC.

Primary HDLEC, or HDLEC over-expressing GFP-tagged hLYVE-1 (hLYVE-1-GFP pHR HDLEC) were cultured on gelatin-coated 8-chamber slides. Media was removed and

the cells were blocked with 5% FCS, 0.05% sodium azide in PBS, prior to incubation with bHA (5 µg/ml) either alone, hLYVE-1 mAbs alone, or bHA in combination with hLYVE-1 mAbs or isotype-matched controls (7.5 µg/ml) in this buffer for 30 min at room temperature. Cells were fixed with freshly depolymerised formaldehyde, blocked once more, and incubated with goat-anti hLYVE-1 polyclonal (hLYVE-1 poly) at 1 µg/ml overnight at 4°C. LYVE-1 Abs and bHA detected by incubation with appropriate secondary antibodies (10 µg/ml) and Alexa dye-conjugated streptavidin (5 µg/ml) respectively, for 45 mins at room temperature. Cells were fixed once more, and mounted with coverslips using VECTASHELD with DAPI mounting medium to stain cell nuclei. Images were captured using an inverted epifluorescence microscope (Zeiss Axiovert S100) fitted with a 100x oil-immersion objective and a Hammatsu digital camera.

2.7.12 Influence of LYVE-1 mAbs on HA binding by primary HDLEC

Primary HDLEC cultured on gelatin-coated tissue-culture plastic were lifted with Accutase and resuspended in FACS incubation buffer for 10 min at 4°C. Each T75 flask yielded 24 samples containing ~250 000 cells. To establish the purity of the HDLEC batch, samples were incubated with antibodies specific for LEC-lineage markers LYVE-1 (hLYVE-1 polyclonal, R&D) and Podoplanin (NZ-1), BEC-lineage marker CD44 (BRIC235) and the pan-endothelial marker CD31 (JC70A), for 40 min at 4°C. Additional samples were incubated with bHA (5 µg/ml) in 150 µl of buffer either alone, or in combination with individual LYVE-1 mAbs (5 µg/ml), isotype-matched control Ig (5 µg/ml), or an excess of unlabelled HA (200 µg/ml), for 40 min at 4°C. In addition, the sequence of incubation with LYVE-1 mAbs or bHA was varied, with three washing steps between reagents. Cells were washed 3x with buffer, before resuspending in 100 µl of buffer containing the appropriate secondary antibody at 10 µg/ml and streptavidin Alexa 647 at 5 µg/ml, and incubated at

4ºC for 30 min. Cells were washed 3x with buffer and resuspended in FACS fix. The fluorescence intensity was measured for 20 000 cells/sample using flow cytometry.

2.7.13 Generation of Fab fragments of LYVE-1 mAbs and their influence on LYVE-1 distribution and HA binding in HDLEC

Fab fragments of hLYVE-1 mAbs 8C and 6A were generated by Ficin digest according to the manufacturer's instructions (Mouse IgG_1 Fab preparation kit, Pierce). Samples of intact antibody and Fab fragments were further purified by size-exclusion chromatography using a superdex S200 10/300 column (GE). Fractions spanning the appropriate peaks were pooled and analysed for purity by non-reducing LDS-PAGE. Fab fragments and intact Ig were tested for their influence on bHA binding by HDLEC at varying Ig-concentration using flow cytometry protocol 2.7.12. Fab fragments and intact Ig were also tested for their influence LYVE-1 distribution in adherent HDLEC and hLYVE-1-GFP pHR HDLEC by immunofluorescence microscopy as described in protocol 2.7.11.

2.7.14 Influence of anti-hLYVE-1 monoclonal antibodies on HA binding by recombinant hLYVE-1 monomer and dimer

Recombinant human LYVE-1 extracellular domain bearing a C-terminal 10 His tag was separated by size-exclusion chromatography into separate samples of monomeric and dimeric protein. In one experiment, both species were serially diluted from a starting concentration of 1.25 µg/ml and immobilized by incubation with Ni-NTA coated HiSorb plates (Qiagen). Incubation was performed in ELISA buffer at R.T., for 90 mins, before washing 5x with ELISA wash. Triplicate samples were incubated with bHA (2.5 µg/ml) in ELISA buffer either alone, or in combination with 8C mAb (7.5 nM) or 8C Fab (15 nM), for 45 mins at R.T. In a separate experiment, hLYVE-1 monomer and dimer were incubated with HiSorb plates at 1 and 2 µg/ml respectively. Triplicate samples were incubated with

bHA (2.5 µg/ml) either alone or in combination with either hLYVE-1 mAb (7.5 nM), Fab (15 nM), isotype-matched control Ig (7.5 nM), or an excess of unlabelled HA (100 µg/ml), for 45 min at R.T. Separate samples were incubated with biotinylated anti-hLYVE-1 polyclonal (R&D, 0.2 µg/ml). In both experiments, samples were washed 5x with ELISA wash and incubated with streptavidin-HRP (1 µg/ml in ELISA buffer) for 30 min at R.T. Samples were washed once more and incubated with OPD colorometric substrate (Sigma-Aldrich) according to the manufacturer's instructions, before quenching the reaction with an equal volume of 2M H_2SO_4. The optical density at 490nm wavelength was measured with a plate reader (BIORAD iMark).

2.7.15 Effect of streptavidin crosslinking of biotinylated HA on binding by human LYVE-1 expressing Jurkat cells

Streptavidin Alexa 647-complexed biotinylated HA (bHA-S647) was formed by pre-incubation of bHA at 5 µg/ml for 30 min at R.T. with streptavidin Alexa 647 (SA647) at a range of concentrations between 20 and 0.002 µg/ml. Human LYVE-1 pHR Jurkat cells were incubated at 1.66×10^6 cells/ml in FACS incubation buffer for 10 min at 4ºC. Cells were then resuspended in buffer containing bHA-SA647 or bHA (5 µg/ml bHA) either alone, or in combination with LYVE-1 HA blocking mAb 891 (20 µg/ml) or an excess of unlabelled HA (200 µg/ml) and incubated for 40 min at 4ºC. Cells were washed 3x with buffer and incubated with streptavidin Alexa 647 (5 µg/ml) in buffer for 30 min at 4ºC. Cells were then washed 3× and resuspended in FACS fix. The fluorescence intensity was measured for 20 000 cells/sample using flow cytometry.

2.7.16 Assays for TSG-6-mediated enhancement of HA binding by LYVE-1 transfected Jurkat cells

Fluoresceinated HA (Fl-HA) or biotinylated HA (bHA) was pre-incubated with the Link module from TSG-6 (Link_TSG-6) or the full length protein (FL_TSG-6) at a ratio of 5:1 (w/w) to form TSG-6:HA complexes. Pre-incubation with HA was performed in 40mM Na-HEPES pH 6.0 at R.T. for 30 min (final conc. 200 µg/ml and 40 µg/ml respectively). TSG-6:HA complexes were subsequently diluted into FACS incubation buffer to a concentration of 2 µg/ml HA and serial dilutions prepared from this top concentration. Human LYVE-1 pHR Jurkat cells were incubated at 2×10^6 cells/ml in buffer for 10 min at 4^{o}C. Cells were then incubated with Fl-HA/bHA alone or Fl-HA/bHA:TSG-6 complexes at a range of HA concentrations, for 30 min at R.T. Cells were washed 3x with buffer; those that had been incubated with Fl-HA were resuspended in FACS fix, while those that received bHA were incubated with streptavidin Alexa 647 (5 µg/ml) in buffer for 30 min at R.T. The latter were subsequently washed 3x with buffer, and resuspended in FACS fix. The fluorescence intensity was then measured for 20 000 cells/sample using flow cytometry.

2.7.17 Assays for TSG-6-mediated enhancement of bHA binding by HDLEC

Biotinylated HA (bHA) was pre-incubated with the Link module from TSG-6 (Link_TSG-6) or the full length protein (FL_TSG-6) at a ratio of 10:1 or 5:1 (w/w) respectively, to form TSG-6:bHA complexes. Pre-incubation with HA was performed in 40mM Na-HEPES pH 6.0 at R.T. for 30 min. TSG-6:HA complexes were subsequently diluted into FACS incubation buffer to a final concentration of 5 µg/ml bHA. Primary or LYVE-1 super-transfected HDLEC were lifted with Accutase, washed, and then incubated in buffer for 10 min at 4^{o}C. Cells were divided into samples of ~250 000 cells and incubated with

bHA alone (5 µg/ml), bHA and TSG-6 (5 µg/ml bHA & 50 µg/ml Link_TSG-6 or 25 µg/ml FL_TSG-6, mixed immediately prior to incubation), or bHA:TSG-6 complexes either alone, or in combination with LYVE-1 mAbs (10 µg/ml), isotype-matched controls (10 µg/ml), or an excess of unlabelled HA (200 µg/ml) for 40 min at 4ºC. Cells were washed 3x with buffer and incubated with streptavidin Alexa 647 (5 µg/ml) in buffer for 30 min at 4ºC. Cells were subsequently washed 3x with buffer, and resuspended in FACS fix. The fluorescence intensity was then measured for 20 000 cells/sample using flow cytometry.

2.7.18 Influence of TSG-6:HA complexes on HA binding and LYVE-1 distribution in adherent HDLEC monolayers.

Primary HDLEC were cultured on gelatin-coated 8-chamber slides. Complexes of bHA and Link_TSG-6 or FL_TSG-6 were formed as described in protocol 2.7.17. Cells were blocked with 5% FCS, 0.05% NaN_3 in PBS (buffer) for 5 min at R.T. and then incubated with bHA, bHA-Link_TSG-6 or bHA-FL_TSG-6 (5 µg/ml) in buffer for 30 min at R.T. Cells were washed 5x with buffer and fixed with freshly depolymerised formaldehyde (2% in PBS) for 20 min at R.T. Cells were washed 3x with buffer and incubated with streptavidin Alexa 647 (5 µg/ml) and Dylight488-conjugated 8C mAb (10 µg/ml) for 30 min at R.T. Cells were washed 5x with buffer, fixed once more, and mounted with VECTASHIELD mounting medium with DAPI, to stain nuclei, and a coverslip. Images were captured using an inverted epifluorescence microscope (Zeiss Axiovert S100) fitted with a 40x objective and a Hammatsu digital camera.

2.7.19 Modification of HA with heavy chains from inter-α-inhibitor and the influence on HA binding by LYVE-1 transfected Jurkat cells

Fluoresceinated or biotinylated HA (Fl-HA/bHA) were pre-incubated at 40 µg/ml in PBS in the presence of human serum (4% v/v, Lonza) (HA + serum), recombinant full length

TSG-6 (40 µg/ml) (HA + TSG-6), or serum and TSG-6 (HA + serum + TSG-6) for 3 hours at R.T. Samples were then diluted to 5 µg/ml Fl/bHA in buffer (1% BSA, 5 mM EDTA, 0.05% NaN_3 in PBS). Human LYVE-1 pHR Jurkat cells were incubated at 1.66 x 10^6 cells/ml in buffer for 10 min at 4ºC. Cells were then divided into samples of 250 000 cells and incubated with HA alone, HA + serum, HA + TSG-6 or HA + serum + TSG-6 either alone, or in combination with individual hLYVE-1 mAbs (10 µg/ml), an excess of unlabelled HA (200 µg/ml) or control Ig, for 35 min at 4ºC. Cells were washed 3x with buffer, those receiving Fl-HA were resuspended in FACS fix, while those receiving bHA were incubated with appropriate secondary antibodies (10 µg/ml) and/or streptavidin Alexa 647 (5 µg/ml) for 35 min at 4ºC. Cells were washed 3x and fixed. The fluorescence intensity was then measured for 20 000 cells/sample using flow cytometry.

2.7.20 Binding of hyaluronan-coated fluorescent microspheres by HDLEC

Dragon-green® fluorescent, streptavidin-coated, 1 µm-diameter polystyrene microspheres (Bangs Laboratories) were coated with end-biotinylated 30 kDa or 300 kDa HA or randomly-biotinylated HA (average mw = 750 kDa). To do this, the number of HA molecules required to saturate the available streptavidin sites in a given number of microspheres was calculated using the biotin-FITC binding capacity supplied by the manufacturer. Microspheres were incubated in PBS with the appropriate amount of 30 kDa, 300 kDa or 750 kDa biotinylated HA for 1 hour at R.T. Microspheres were pelleted by centrifugation at the 1 200 × g for 15 mins and washed with a 100x volume of PBS. This wash step was repeated 10x, before resuspending microspheres to a final concentration of 0.5 mg/ml. Primary HDLEC, or LYVE-1 super-transfected HDLEC cultured on gelatin-coated 8-chamber glass slides were blocked with 5% FCS, 0.05% NaN_3 in PBS (buffer) for 10 min at R.T. Cells were incubated with HA-coated or unlabelled microspheres either

alone or in combination with hLYVE-1 mAb 891 (10 µg/ml) for 30 min at R.T. Cells were washed 5x with buffer and fixed with freshly depolymerised formaldehyde (2% in PBS) and incubated with goat-anti hLYVE-1 polyclonal (1 µg/ml) for 45 min at R.T. Cells were washed 5x with buffer and incubated with anti-goat IgG Alexa 647 secondary antibody (5 µg/ml). Cells were washed once, fixed and then mounted onto coverslips using VECTASHIELD mounting medium with DAPI, to stain cell nuclei. Images were captured using an inverted epifluorescence microscope (Zeiss Axiovert S100) fitted with 40 and 100x objectives and a Hammatsu digital camera.

2.7.21 Quantitation of LYVE-1 monomer:dimer ratio in different fractions of total cellular protein from HDLEC

Three batches of primary HDLEC were analysed for LYVE-1 monomer:dimer ratio in different fractions of cellular protein using a combination of surface biotinylation and western blot. A *surface plasma membrane fraction* was prepared from 3x T75 flasks of 90% confluent HDLEC using a Cell Surface Protein Isolation Kit (Pierce) with some protocol modifications, so that a non-reduced sample could be obtained. Specifically, this involved additional quenching of un-reacted biotinylation reagent by washing cells 3x with TBS, and boiling the contents of the Neutravidin® column in sample buffer for 5 min to elute biotinylated proteins, rather than using an excess of DTT. *Total cellular protein* was prepared from one T75 of 90% confluent HDLECs. Cells were lifted with a cell scraper in PBS-5mM EDTA, spun down and resuspended in lysis buffer with protease inhibitors, as per the protocol included with the biotinylation kit. Cells were sonicated in the same manner as the biotinylated cells, and LDS sample buffer added, with or without 50mM DTT, to the solubilised total cellular protein. A crude fraction of *intracellular protein* was collected by harvesting and concentrating the flow-through from the Neutravidin column.

Reduced and non-reduced samples were run on LDS-PAGE gels, blotted onto PVDF membrane and probed for LYVE-1 or ERK1/2 using goat-anti-hLYVE-1 polyclonal (R&D) or rabbit anti-Erk1/2 monoclonal (Sigma). Bound antibody was detected with anti-goat-IgG IRDye 800CW (*green*) and anti-rabbit-IgG IRDye 680LT (*red*) and a Li-Cor Odyssey Imager.

2.7.22 Comparison of hyaluronan binding by recombinant hLYVE-1 samples using ELISA

A maxisorb plate (Nunc) was coated overnight at R.T. with goat anti-mouse IgG Fc (M4280, Sigma) at 3 µg/ml in coating buffer. The plate was blocked with 1% BSA in PBS-Tween for 2 hours at R.T and then incubated with hLYVE-1 mAb 8C at 5 µg/ml in PBS-Tween for 1 hr at R.T. Serial dilutions of untreated, neuraminidase-digested or alkylated hLYVE-1 Δ238 10His monomer and dimer produced in CHO cells were prepared from a top concentration of 4 µg/ml, in PBS-Tween, and added to the plate for 1 hour at R.T. Samples were then incubated with bHA at 10 µg/ml in PBS-Tween, for 60 minutes, at R.T. Bound bHA was detected using streptavidin-HRP (21126, Thermo), 1/1000 dilution in PBS-Tween, for 30 mins at R.T. The plate was washed 5x between steps using PBS-Tween and developed with Sigmafast OPD HRP-substrate (Sigma) as per the manufacturer's instructions and then quenched with 2M H_2SO_4. The absorbance at 490 nm was then measured using a Bio-Rad iMark Microplate Reader.

2.7.23 Quartz Crystal Microbalance with Dissipation monitoring (QCM-D)

All QCM-D experiments were performed in the laboratory of Dr Ralf Richter (CIC biomaGUNE, San Sebastian, Spain) under the direction of Dr. Galina Dubacheva. Data were collected using a Q-Sense E4 system (Q-Sense) in flow mode and at a working

temperature of 23°C. In all experiments, supported lipid bilayers (SLBs) were formed on the surface of silica-coated QCM-D sensors (QSX303; Q-Sense). Prior to use, the QCM-D sensor was washed overnight in an aqueous solution of 2% (w/v) SDS, rinsed abundantly with ultrapure water, blow-dried in N_2, and treated with UV/ozone (Bioforce Nanoscience) for 30 minutes. All experiments were conducted in HEPES buffer (150 mM NaCl, 10 mM HEPES, pH 7.4). Hyaluronan 262 ± 13 kDa (SelectHA-250) was purchased from Hyalose, while lyophilized 1,2-dioleoyl-*sn*-glycero-3-phosphocholine (DOPC) and Tris-NTA-functionalized octadec-9-enyl-octadecyl-amine (OEOA-Tris-NTA) were obtained from Avanti Polar Lipids and Prof. Jacob Piehler (Universität Osnabrück, Germany) respectively. Small unilamellar vesicles (SUVs) were prepared by sonication of 5% OEOA-Tris-NTA, 95% DOPC lipid mixtures prepared in chloroform as previously described (Eisele et al., 2010; Richter et al., 2003). SLBs were formed by the spreading of SUVs (50 µg/ml) in HEPES buffer supplemented with 10 mM NiCl onto the surface of silica sensors at 10 µl/min. Changes in frequency and dissipation were monitored using the Q-sense E4 system and compared to previously obtained values for optimum formation of OEOA-Tris-NTA/DOPC SLBs (Dr. Nico Eisele, unpublished observations). Following formation, SLBs were washed extensively with HEPES buffer to establish a baseline. The frequency response (Δf) and dissipation (ΔD) were recorded for 13 overtones, Δf and ΔD are shown for the 3rd and 5th overtones respectively.

2.7.23.1 Adsorption of LYVE-1 samples onto SLBs and binding of 250 kDa hyaluronan

Single-use aliquots of untreated or neuraminidase-digested hLYVE-1 Δ238 10His monomer and dimer were thawed and diluted in HEPES buffer to a final concentration of 10 µg/ml and introduced onto SLBs comprising 5% OEOA-Tris-NTA, 95% DOPC lipids, or DOPC lipids only at a flow rate of 10 µl/min. Protein was injected until saturation point

was reached (i.e. no further change in f) over a period of ~50 mins, or alternatively, samples were diluted to 1 µg/ml and injected until a pre-determined frequency shift was achieved, typically Δf = 25 Hz. LYVE-1-engrafted SLBs were then washed extensively with HEPES buffer (~60 mins), before injecting HA (mw 250 kDa) at 10 µg/ml in HEPES buffer, until the frequency response had plateaued. In addition, HA was introduced to SLBs comprised of DOPC lipids only, to determine the specificity of the HA interaction. The stability of HA binding by LYVE-1 was then assessed over an extended period of rinsing in HEPES buffer (1 – 3 hours).

2.7.23.2 Influence of LYVE-1 mAbs on HA-binding by monomeric LYVE-1

SLBs were formed on four silica sensors and untreated hLYVE1 monomer injected at 1 µg/ml until Δf = -25Hz as described in section 2.7.23.1. Human LYVE-1 mAbs 891 and 6A were injected at 10 µg/ml onto separate SLBs, IgG_{2b} isotype control onto a third, while a fourth was left untreated. Hyaluronan (mw 250kDa) was injected at 10 µg/ml until binding to LYVE-1 reached saturation point. The stability of binding during rinsing was monitored over time.

Chapter 3. Characterization of mouse LYVE-1-specific monoclonal antibodies with function blocking properties

3.1 Introduction

While the crystal structure of LYVE-1 has yet to be solved, a considerable amount of structural information has been deduced using truncation and site-directed mutagenesis of the human receptor (Banerji et al., 2010). Through testing of HA-binding by a series of graded truncation mutants, it has been possible to demonstrate that human LYVE-1 has the same structural elements of the extended Link domain found in CD44. Site-directed mutagenesis of the receptor also revealed a number of HA-binding residues in hLYVE-1 that are conserved with those in CD44 (see General Introduction, Figure 1.15), as well as the epitope of an HA-blocking monoclonal antibody 3A, which overlaps the HA-binding site. The HA binding site in hLYVE-1 maps to a position similar to that of the HA-binding site in CD44, but is more compact, and lacks additional residues found in the $ß_1$-α_1 loop. However the predicted HA binding surface in hLYVE-1 is dominated by charged residues, compared to the largely aliphatic makeup of the CD44 binding site, and this is reflected in a marked sensitivity to ionic strength not seen in the latter (IC_{50} of 150 mM NaCl for hLYVE-1, compared to IC_{50} >2M NaCl for CD44). Based on the close sequence homology between human and mouse LYVE-1 (69% identity, Figure 1.14), the murine receptor is predicted to share many of the features of the human LYVE-1 HABD. However, this has not been formally demonstrated beyond experiments showing that mouse LYVE-1 is a *bona fide* HA receptor when expressed on the surface of 293T fibroblasts or as Fc fusion protein (Prevo et al., 2001).

Previous work within the Jackson Laboratory aimed at defining the biological function of LYVE-1 has focussed on characterisation of LYVE-1 deficient mice, the generation and use of mouse LYVE-1 specific monoclonal antibodies (mAbs) in animals model of inflammation and disease, and the biochemical characterisation of the receptor and its

interaction with hyaluronan (HA). Recent studies have revealed an intriguing effect of blockade of mouse LYVE-1 using specific monoclonal antibodies, which in many cases is dependent on the antibody used. For example, anti-mouse LYVE-1 mAb C1/8 was found to effectively block transmigration of lymphatic endothelium by dendritic cells, both *in vitro* and during trafficking from inflamed skin to lymph nodes in mice (Johnson & Jackson, unpublished observations). These data suggest that LYVE-1 plays a role in regulating cellular traffic into lymphatic vessels during inflammation, most likely at the entry points into lymphatic capillaries, which consist of LYVE-1-enriched flap valves between individual cells (Baluk et al., 2007; Pflicke and Sixt, 2009). However, for reasons that are not currently clear, blockade of mLYVE-1 using the related mAb B1/10 did not influence DC trafficking.

In light of the initial evidence that C1/8 blockade of LYVE-1 inhibits transmigration of lymphatic endothelium by dendritic cells, function blocking experiments with LYVE-1 mAbs were expanded to investigate trafficking of other cell types, including metastasizing tumour cells. However in contrast to expectations, intraperitoneal injection of C1/8 mAb to wild type (LYVE-$1^{+/+}$) mice had no effect on nodal dissemination of spontaneously metastasizing primary T-241/VEGF-C fibrosarcomas (Royston, 2011). Conversely, treatment with B1/10 mAb enhanced the rate of metastasis, and induced *de novo* nodal metastasis in parental 'non-metastasizing' T-241 tumours. Furthermore, a similar increase in T-241/VEGF-C metastasis and *de novo* metastasis of T-241 tumours was seen when both tumours were implanted into LYVE-$1^{-/-}$ mice. These results predict a role for LYVE-1 in regulating tumour cell entry into lymphatic vessels, which curiously can be disrupted by B1/10, but not the C1/8 antibody.

While alveolar development in LYVE-1-deficient mice is normal, these mice do exhibit a serious defect in the resolution of acute lung injury, which can be phenocopied in wildtype mice by administration of LYVE-1 blocking mAb (Royston, Espinosa & Jackson, manuscript in preparation). Again, this phenomenon is dependent on the antibody used; wildtype mice (LYVE-$1^{+/+}$) mice receiving a single intratracheal injection of LYVE-1 mAb C1/8 prior to inducing lung injury, exhibit similar lung pathology and terminal disease progression to LYVE-$1^{-/-}$ mice, while those treated with the B1/10 mAb recover at the same rate as mice receiving an irrelevant IgG control. Accumulation of leukocytes in the alveolar space appears to be a consequence of defective LYVE-1-mediated migration of inflammatory macrophages across the alveolar epithelium into the interstitium in a luminal-basolateral direction. Whether or not hyaluronan plays a role in this process is unclear, as LYVE-1 deficient mice have no apparent defect in clearance of pulmonary HA, at least under homeostatic conditions (Jorge Espinosa, Jackson laboratory, unpublished observations).

Involvement of HA in the inflammatory and disease processes described here is uncertain. While hyaluronan is bound readily by cells over-expressing LYVE-1, primary lymphatic endothelial cells isolated from human and mouse display little or no constitutive HA binding (Nightingale et al., 2009). Furthermore, LYVE-1 does not appear to co-localize with endogenous or exogenously-added HA in frozen sections of mouse ear. The reason for this apparent lack of HA binding is that the receptor is constitutively inactivated *in vivo* by terminal sialylation of O-glycans in the stalk region of the extracellular domain (Nightingale et al., 2009). The mechanism by which this inhibition is alleviated remains uncertain, although HA binding by recombinant LYVE-1 is enhanced following enzymatic desialylation. It has yet to be determined whether LYVE-1 is 'activated' to bind HA under certain conditions, and indeed whether HA binding plays a role in transmigration of

lymphatic vessels by the various cell types described here. Preliminary analysis of the HA blocking capacity of mAbs B1/10 and C1/8 using recombinant mLYVE-1 Fc fusion protein suggests that neither antibody is a potent HA blocking antibody, suggesting that hyaluronan may not be involved in (Dr. L. Johnson, unpublished observations). Furthermore, the particular influence of mAbs B1/10 and C1/8 on transmigration of lymphatic endothelium appears to be dependent both on context and on the cell type undergoing transit (ie dendritic cells or tumour cells). This suggests that the two antibodies may recognise separate epitopes, and/or block separate mechanisms.

3.2 Aims

The disparate effects observed following administration of anti-mLYVE-1 monoclonal antibodies highlights the importance of determining whether LYVE-1 mediates *in vivo* functions through binding of hyaluronan, an alternative ligand, or some other process. These problems can be tackled by identifying both the HA-binding site in mouse LYVE-1 and the epitope of the relevant antibodies. It will be intriguing to determine whether the epitope of either antibody overlaps the HA-binding groove, suggesting a role for hyaluronan in transmigration, or whether a separate site is involved. Equally important will be to determine whether B1/10 and C1/8 have different effects because they bind separate epitopes, and what these epitopes tell us about LYVE-1 structure and regulation of function.

1. Delineate the hyaluronan binding site in mouse LYVE-1.

2. Determine whether mLYVE-1-specific monoclonal antibodies with function blocking properties are also capable of blocking hyaluronan binding by LYVE-1.

3. Investigate the relationship between the four mAb epitopes through cross-blocking studies.

4. Map the epitopes for the LYVE-1 function-blocking antibodies B1/10 and C1/8 in relation to the hyaluronan binding site and the epitopes of potent HA blocking mAbs ALY and 2125.

3.3 Results

3.3.1 Selection of target residues for site-directed mutagenesis of mouse LYVE-1

In order to determine whether the epitopes recognised by mLYVE-1 mAbs B1/10 and C1/8 overlap the hyaluronan binding site, it was necessary to identify the residues making up the HA binding surface in mouse LYVE-1. Site-directed mutagenesis has previously been used to identify residues within the HA binding surface in human LYVE-1, as well as those contributing to the epitope of the HA-blocking mAb 3A (Banerji et al., 2010) (Figure 3.2, A). In these previous studies, single residue mutants expressed in HEK 293T cells were screened for their capacity to bind fluorescein-labelled HA (Fl-HA) compared to wildtype LYVE-1. A similar approach was used here to delineate the hyaluronan binding site in mouse LYVE-1, and to map the epitopes of four anti-mouse LYVE-1 monoclonal antibodies. These included the two function-blocking antibodies, B1/10 and C1/8, and two commercially available monoclonals, ALY7 (e-biosciences) and MAB2125 (R&D Systems), that have been characterised as HA blocking antibodies by the manufacturer.

Two complimentary approaches were used to inform selection of target residues for site-directed mutagenesis. In the first, binding of all four monoclonals to recombinant Fc fusion proteins comprising mLYVE-1 Δ165 Fc (representing the N-terminal hyaluronan binding domain [HABD] only) or mLYVE-1 Δ232 Fc (representing the full extracellular domain, including the HABD) was assessed by ELISA and found to be equivalent (Figure 3.1). This implied that the epitopes are in each case confined within the consensus HA binding domain and hence further mapping focussed on this region. Secondly, a structural model of mLYVE-1 was generated using the ModWeb program (Pieper et al., 2009) using the non-ligand bound crystal structure of human CD44 (1UUH) (Teriete et al., 2004) as a

template (Figure 3.2, B). Forty-two residues were selected for mutation, using the mLYVE-1 model to increase the likelihood of targeting 'surface' residues and on the basis of homology to HA binding residues in hLYVE-1 (a full list of mutations can be found listed in appendix 1, Table 7.1). An effort was also made to achieve as broad a coverage of the protein surface as possible.

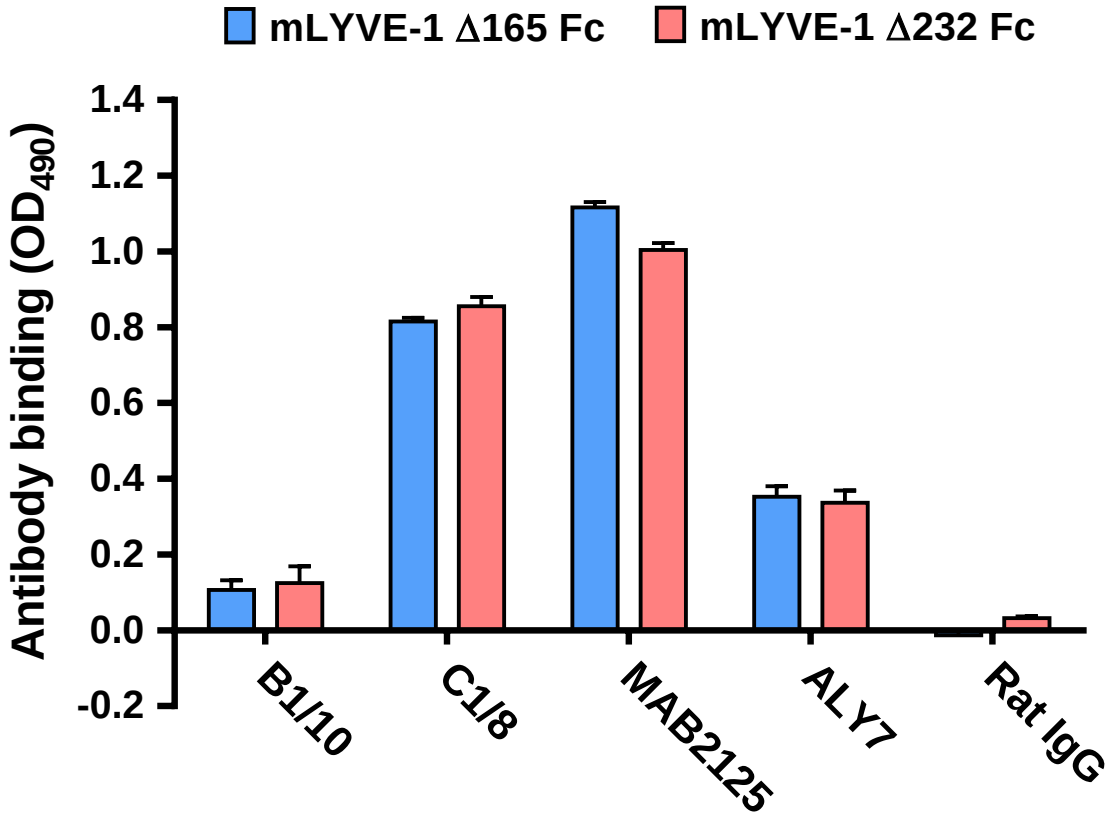


Figure 3.1. **Binding of anti-mLYVE-1 monoclonal antibodies (mAbs) to recombinant Fc fusion proteins of mouse LYVE-1.** Binding of mLYVE-1-specific mAbs to Fc fusion proteins comprising the mLYVE-1 Hyaluronan Binding Domain (HABD, Δ165) or mLYVE-1 Full Length Extracellular Domain (FL ECD, Δ232) was assessed by ELISA. Mouse LYVE-1 Fc proteins were coated directly onto 96-well plates at 10 µg/ml, overnight incubation at 4°C. All wells were blocked with BSA prior to subsequent incubation with mLYVE-1-specific mAbs at 10 µg/ml, 45 min at room temperature. Bound mAb were detected using a Rat IgG-specific HRP conjugate, 45 min incubation at room temperature. Data are the mean ± SD (n = 3), less the background signal observed in wells lacking mLYVE-1 Fc fusion protein, from a single experiment.

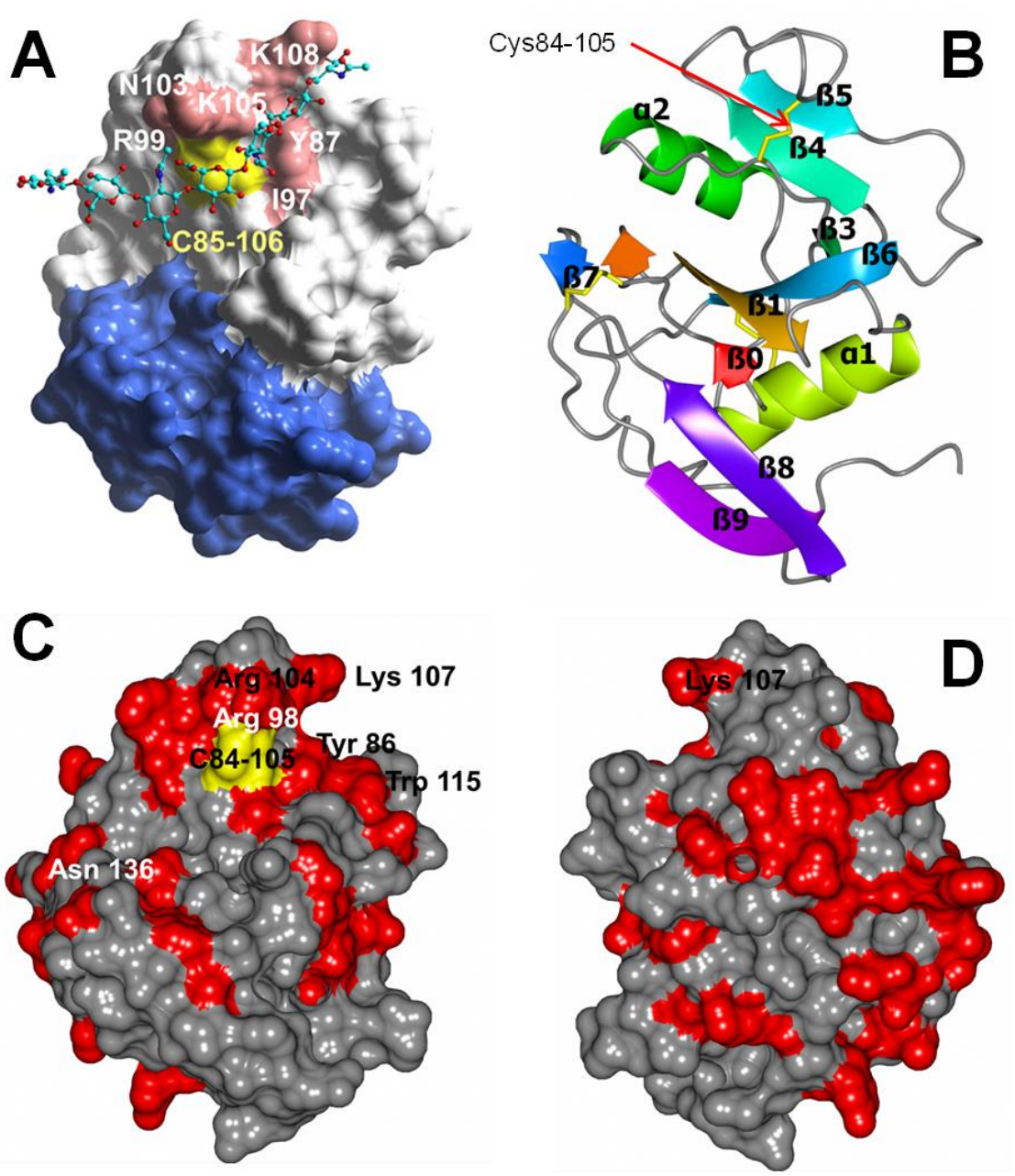


Figure 3.2. **Selection of target residues for site-directed mutagenesis using structure-based modelling of the mouse LYVE-1 HABD**. (A) Model of the hLYVE-1 HA-binding domain from (Banerji et al., 2010) based on the crystal structure of hCD44 (PDB, 1UUH), shown with an HA-octasaccharide docked into the putative ligand-binding site and critical HA-contact residues identified in pink. The Cys85 - Cys106 structural disulfide is highlighted in yellow. (B) Computer-generated model of mLYVE-1, also based on 1UUH, shown in the same orientation as panel A. Secondary structure elements are labelled, and the position of the equivalent Cys84 – Cys105 disulfide marked with a red arrow. (C) Residues (red) targeted for site-directed mutagenesis plotted onto the mLYVE-1 model. For the purpose of orientation, equivalent residues from the ligand-binding site of hLYVE-1 are labelled, including the structural disulfide Cys84 – Cys105 (shown in yellow). (D) A 180^{o} rotation about the y-axis from panel C).

3.3.2 Site-directed mutagenesis of mouse LYVE-1 and assay development

Following selection of target residues, primers were designed for the PCR mutagenesis of forty-two individual amino acids to alanine. Full length mLYVE-1 in pRcCMV plasmid was used as a template in a PCR protocol based on the Quickchange II Site-Directed Mutagenesis Kit (Stratagene). Samples of the resulting plasmids were submitted for sequencing to confirm error-free amplification and successful mutation at the site of the target residue. Mutant or wildtype mLYVE-1 proteins were then transiently over-expressed in HEK 293T cells, prior to incubation with Fl-HA or monoclonal antibodies, appropriate secondary reagents and measurement of mean fluorescence intensity (MFI) by flow cytometry.

To permit comparison of different mLYVE-1 mutants with the wildtype receptor, it was necessary to correct for differences in expression and transfection efficiency. This was achieved by incubating cells with a saturating concentration of rabbit anti-mLYVE-1 polyclonal antibody, to measure surface expression. The use of a C-terminal GFP tag was also considered, but was discounted on the basis of previous experience with GFP-tagged LYVE-1, that had indicated a poor correlation between the GFP signal and surface expression levels (Dr. S. Banerji, personal communication). Instead, comparison of mutant and wildtype mLYVE-1 receptors was facilitated by dividing the MFI observed for Fl-HA or monoclonal antibody binding, by the MFI observed for polyclonal antibody binding, thus correcting for surface expression level. This approach assumes that polyclonal antibody binding will not be significantly affected by a single point mutation in the receptor. This assumption appeared to be valid, as surface expression levels for all 42 mutants were found to be broadly similar to the wildtype receptor, typically varying by no

more than ± 20%[1]. As further controls, data were averaged from three independent transfections, and the specificity of all antibodies was confirmed using isotype-matched control Ig and mock transfections (transfection reagent only).

3.3.3 Characterisation of the hyaluronan binding site in mouse LYVE-1

A flow cytometry screen of mouse LYVE1 mutants revealed a number of residues involved in ligand binding, many of which are conserved with human LYVE-1. A reduction in hyaluronan binding was detected for 19 out of 46 mutations, of which nine (Q50, N52, Y86, R98, R104, K107, W115, S131, and N136) showed a greater than 60% reduction in binding relative to wildtype (Figure 3.3). Two of these mutations, N52 and S131, ablate the predicted N-glycosylation sites at N52 and N129 respectively (NXS/T to NXA in the case of the latter). Similar results were seen when mutations were made in the N-glycosylation sites of human LYVE-1 (Nightingale et al., 2009). A further residue, Asn 136, is located close to S131 but remote from the putative HA-binding patch, both in primary sequence and three-dimensional space (Figure 3.4). It is unclear whether this residue has a direct role in hyaluronan binding, or whether its mutation results in a gross conformational change that disrupts binding. For example, if the N136A mutation were to disrupt formation of the nearby Cys 35 – Cys 138 disulfide, this would have a significant effect on tertiary structure. Evidence for this notion comes from reduced binding of four anti-mLYVE-1 monoclonals to the N136A mutant (section 3.3.6).

Previous site-directed mutagenesis of hLYVE-1 had revealed six candidate HA-binding residues, Y87, I97, R99, N103, K105, and K108 (Banerji et al., 2009). Of the remaining

[1] One exception, the K107A mutant, was poorly expressed and discounted from the epitope analysis.

six residues identified in this study, three are direct homologues (Y86, R98 and K107), and a fourth is semi-conserved (R104). A mutant of N102 (N103 in human) did not

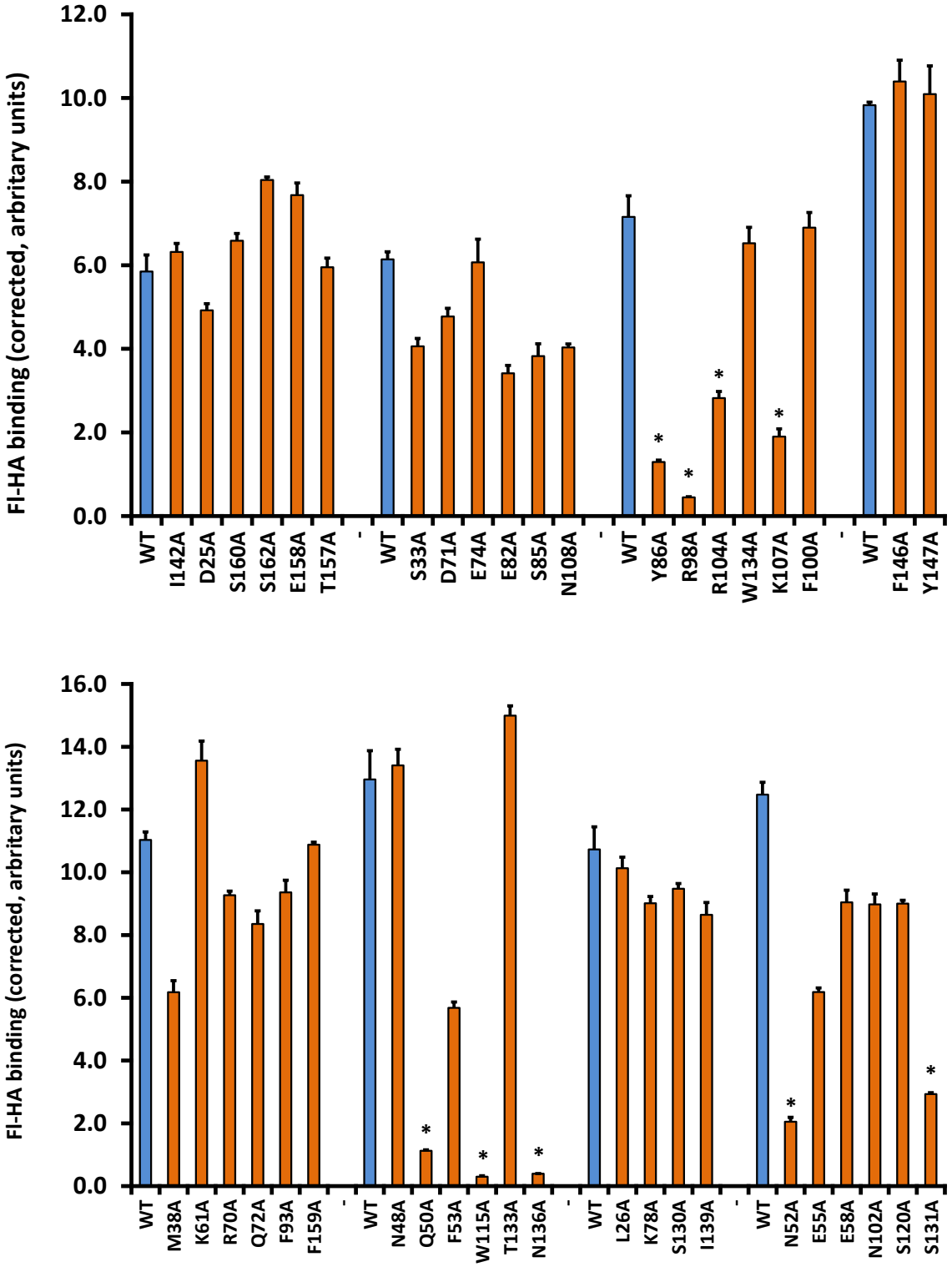


Figure 3.3. **Influence of site-directed mutagenesis on hyaluronan binding by mouse LYVE-1 transfected HEK 293T cells.** Forty-two mLYVE-1 mutants (*orange bars*) were

screened in batches for reduced binding of fluorescently-labelled hyaluronan (Fl-HA) as detected by flow cytometry. In each experiment, wildtype mLYVE-1 transfected 293T cells (*blue bars*) were used as a positive control. Surface expression level and HA-binding were measured as the mean fluorescence intensity (MFI) of cells stained independently with a polyclonal Ab or Fl-HA. The specificity of these reagents was confirmed by the lack of binding to mock-transfected cells or of rabbit IgG to transfected cells (data not shown). Fl-HA binding was corrected for differences in LYVE-1 surface expression between individual transfectants. To do this, the MFI for Fl-HA-stained cells was divided by the MFI of cells stained with polyclonal antibody. Data are the mean ± SEM (n = 3 independent transfections). HA-binding residues were defined as those whose mutation resulted in a reduction in Fl-HA binding of >60% relative to wildtype mLYVE-1. Nine residues satisfying this criterion are marked with an asterisk (*). Data are representative of three independent experiments.

appear to be an HA-contact residue, although a reduction in HA-binding of 28% was observed. A further difference between the two species came with the identification of W115 and Q50 as putative HA-contact residues in the mouse. W115 is not an HA-contact residue in human, although it forms part of the epitope of an HA-blocking antibody and is located within the HA-binding groove. In mouse LYVE-1, W115 appears to form part of a continuous binding patch centred around the Cys84 – Cys 105 disulfide, in partnership with Y86, R98, R104 and K107 (Figure 3.4).

Q50 is of particular interest because it falls within the ß1-α1 loop, a region that is critical for HA-binding in both human and mouse CD44. Conserved arginine and lysine residues (R45/Y46 in mouse) form the lower ‘jaw’ of the CD44 binding groove, but are not conserved with LYVE-1 (Figure 3.4). Extensive mutagenesis of this region in hLYVE-1 failed to find any HA-contact residues, suggesting that the binding patch is more compact than that in CD44. Involvement of Q50 in the mLYVE-1 HA-binding site could indicate a closer resemblance to CD44 than the human homologue. However, a semi-conservative mutation will be required to demonstrate that this mutation does not cause a gross-

conformational defect, as the Q50A substitution resulted in decreased monoclonal antibody binding, which may indicate that the protein is mis-folded (see section 3.3.6).

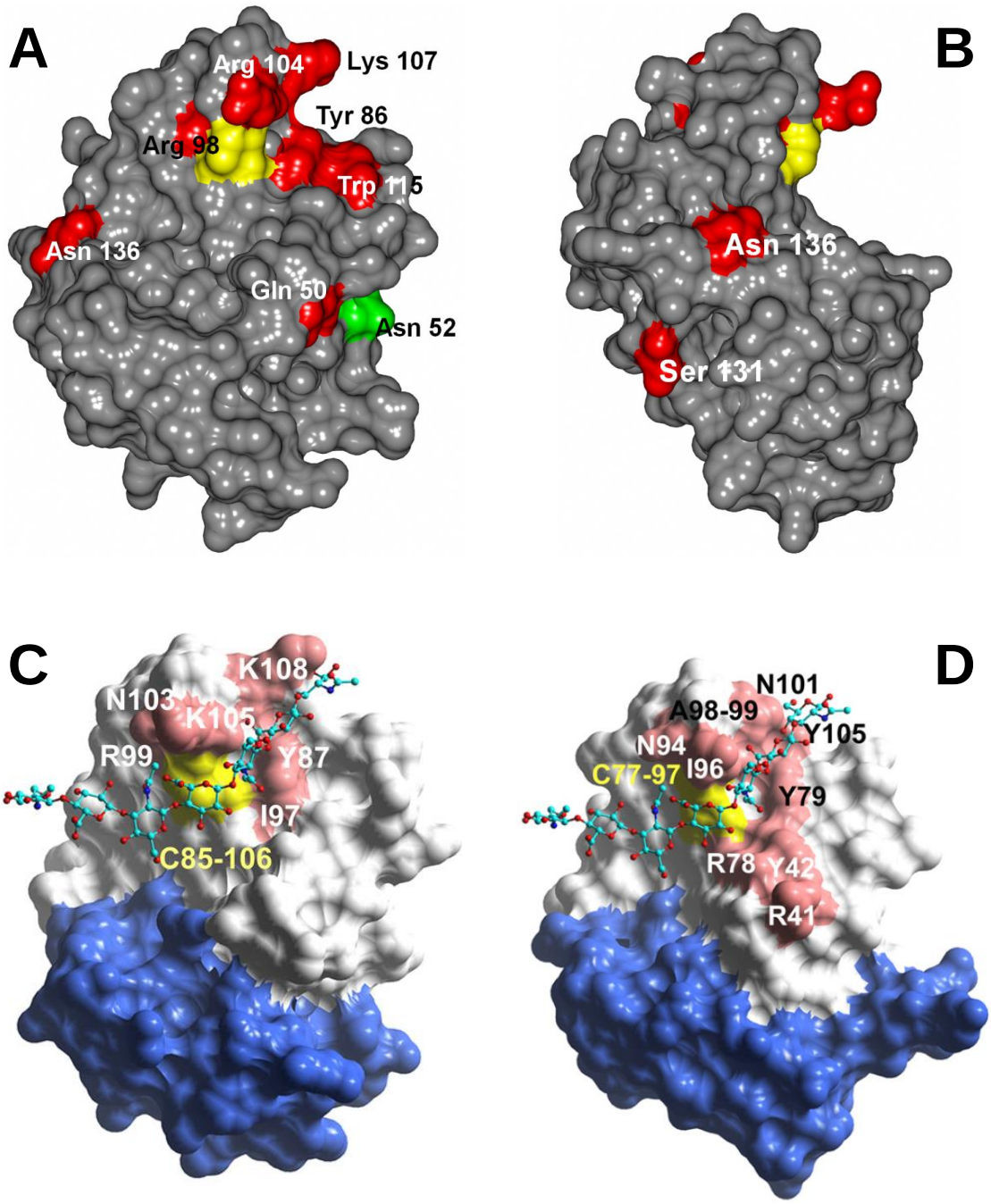


Figure 3.4. **The Hyaluronan binding site of mouse LYVE-1 shows similarities to both human LYVE-1 and human CD44.** (A) Space-filled representation of the mouse LYVE-1 HABD model. Amino acids identified by site-directed mutagenesis that may play a role in HA binding are shown plotted in *red*. Asn 52 (shown in *green*) is a predicted N-glycosylation site. (B) A 90^{o} rotation about the y-axis of the view shown in panel A, such that Ser 131 is visible. (C, D) For comparison, a model of human LYVE-1 HA-binding

domain (C) and solution structure of human CD44 HABD (D), taken *(Banerji et al., 2010).* An HA-octasaccharide is shown docked into the putative ligand-binding site, and critical HA-contact residues are shown in *pink.* The structural disulfide located in the HA binding site of all three proteins is highlighted in *yellow.*

3.3.4 Influence of mouse LYVE-1-specific monoclonal antibodies on hyaluronan binding by LYVE-1

In order to characterise the function-blocking properties of B1/10 and C1/8 a critical issue must be addressed, namely whether or not they are capable of blocking hyaluronan binding by the receptor. To answer this question, two experiments were performed to assess the influence of antibody concentration on HA binding by either soluble LYVE-1 Fc fusion protein or cell-surface expressed receptors. MAB2125 and ALY7, described by the manufacturers as HA blocking antibodies, were included as a positive control.

In the first experiment, monoclonal antibodies were pre-incubated at a range of different concentrations with immobilized mouse LYVE-1 Δ165 Fc fusion protein, prior to addition of biotinylated hyaluronan (bHA). All four monoclonals were found to be capable of blocking HA binding, however MAB2125 and ALY7 were much more potent (IC_{50} ~0.35 µg/ml and ~0.45 µg/ml respectively) compared to B1/10 and C1/8 (IC_{50} ~5 µg/ml) (Figure 3.5). Total blockade of HA binding by B1/10 or C1/8 required a concentration of some 80 µg/ml.

In a second experiment, full length mouse LYVE-1 was cloned into the lentiviral expression vector pHR-SIN[1] and used to establish a stable mLYVE-1-expressing Jurkat cell line that displays constitutive hyaluronan binding. Mouse LYVE-1 pHR Jurkat cells were incubated simultaneously with bHA and anti-mLYVE-1 monoclonals or isotype-

[1] A kind gift from the Davis laboratory, Weatherall Institute of Molecular Medicine

matched Ig controls at a range of concentrations, followed by appropriate secondary detection reagents. Binding of bHA or monoclonal antibodies was subsequently measured using flow cytometry. Using this assay it was found that B1/10 and C1/8 are capable of blocking all hyaluronan binding by LYVE-1 expressing cells, albeit at high concentration (12.5 and 30 µg/ml respectively) (Figure 3.6). The difference in blocking efficiency compared to MAB2125 and ALY7 was even greater than observed by ELISA, with a difference in IC_{50} of ~100-fold (IC_{50} for B1/10 ~ 1.5 µg/ml, C1/8 ~ 7 µg/ml, ALY7 ~ 0.035 µg/ml and MAB2125 ~ 0.025 µg/ml). Similarly, the antibody concentration required for saturating binding was markedly higher (B1/10 = 12.5 µg/ml, C1/8 = 25.0 µg/ml, ALY and MAB2125 = 0.39 µg/ml).

Taken together, these data demonstrate that mAbs B1/10 and C1/8 are capable of blocking hyaluronan binding by LYVE-1, but in a comparatively weak fashion compared to other monoclonal antibodies. This may suggest that the antibodies bind an epitope that only partially overlaps the HA binding site, or that exerts some long-range effect on HA binding. However, given the high antibody concentration required to achieve saturating binding to LYVE-1 expressing cells, the potency of HA blockade may instead be a reflection of low binding affinity.

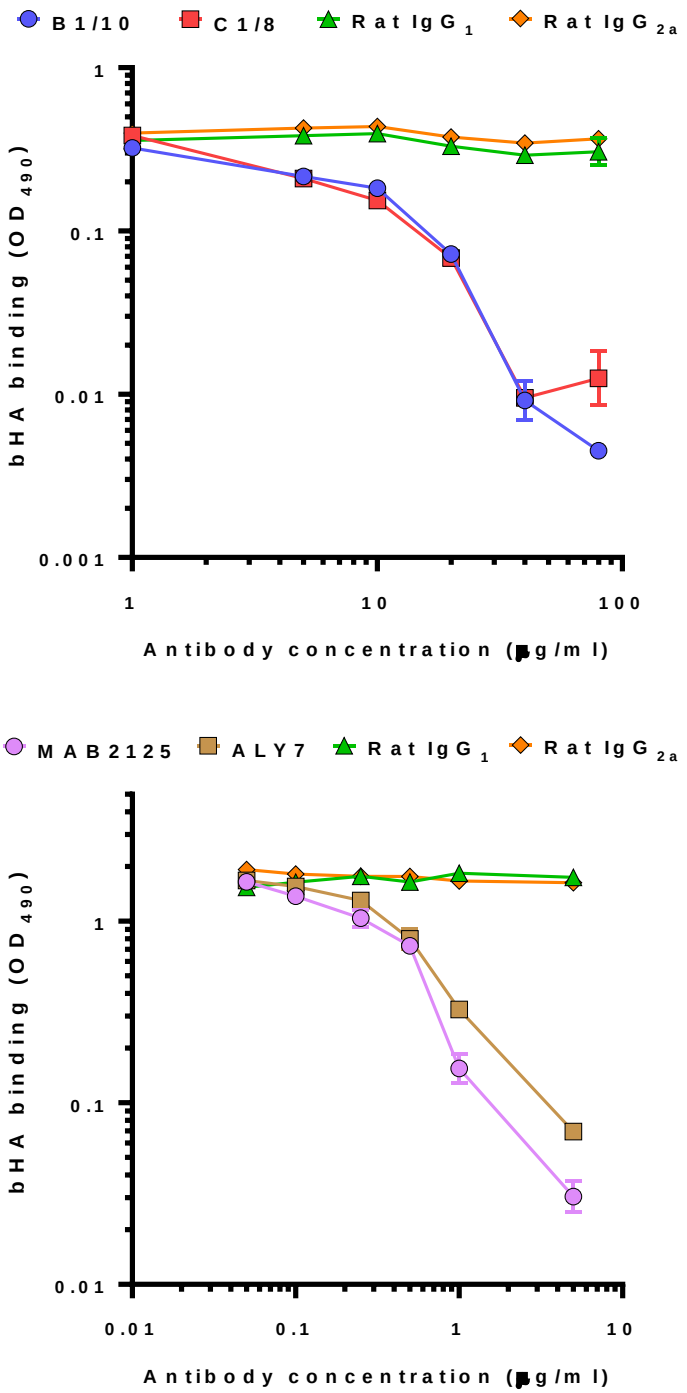


Figure 3.5. **Influence of anti-mLYVE-1 monoclonal antibodies (mAbs) on hyaluronan binding by recombinant mouse LYVE-1**. Mouse LYVE-1-specific mAbs B1/10, C1/8, MAB2125 and ALY7 and isotype controls were tested for their ability to block binding of biotinylated HA (bHA) to immobilized mLYVE-1 Δ165 Fc as detected by ELISA. Each well was incubated with mLYVE-1-specific mAbs at the concentrations indicated and subsequently with bHA at 10 µg/ml. Bound bHA was detected using a streptavidin-HRP conjugate. For estimation of IC_{50} values these data were plotted separately on linear axes, such that antibody concentration = 0 µg/ml may be displayed. Data are the mean ± SD (n = 3) less background of the assay, and representative of two independent experiments.

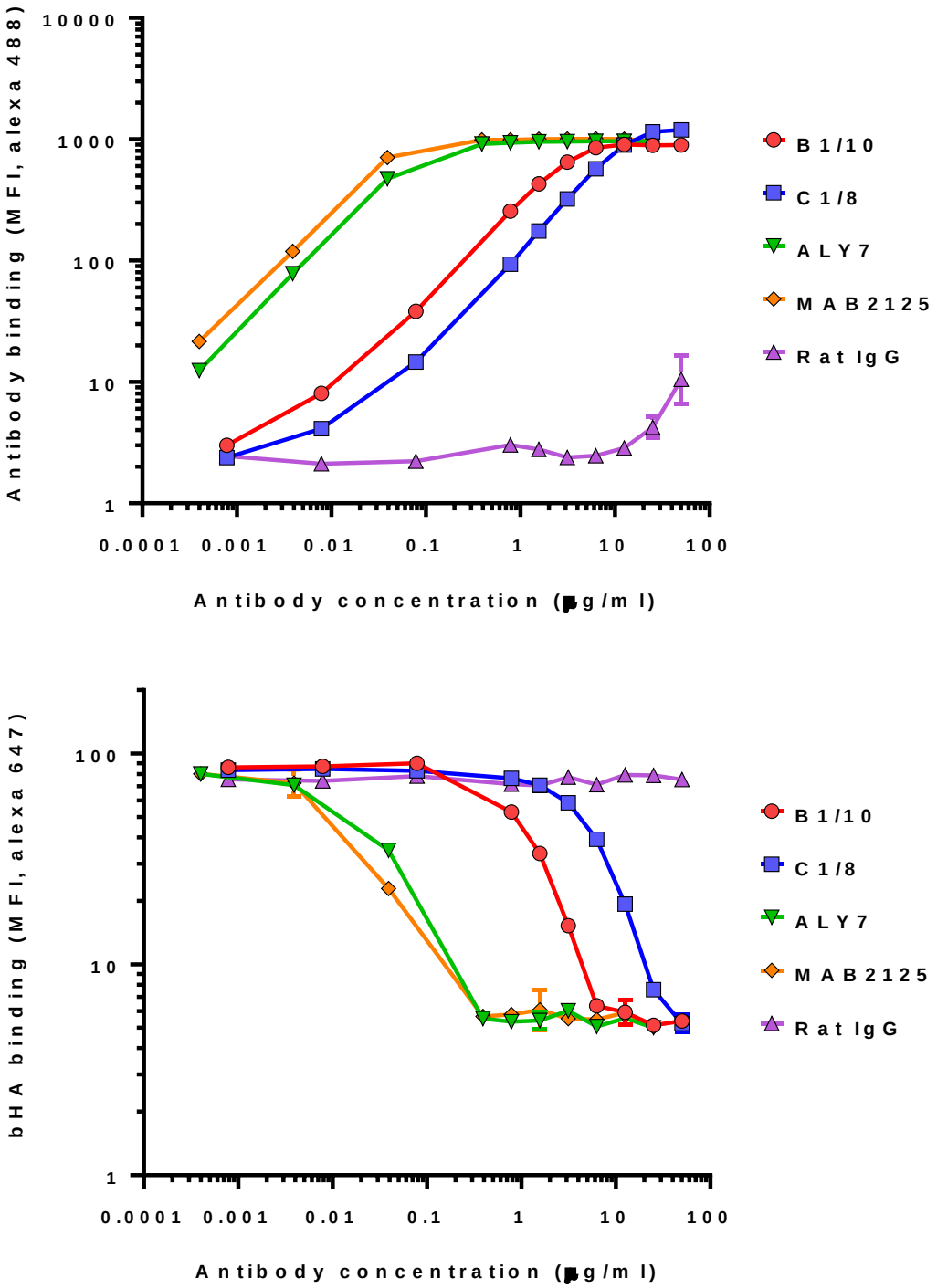


Figure 3.6. **Influence of anti-mLYVE-1 monoclonal antibodies on hyaluronan binding by mLYVE-1 transfected Jurkat cells.** Mouse LYVE-1 pHR Jurkat cells were incubated at 1.66 x 10^6 cells/ml with biotinylated HA (bHA) at 5 µg/ml either alone or in the presence of individual mLYVE-1-specific mAbs or control Ig, at increasing Ig concentration, to assess the effect on bHA binding. Bound Ig (*top panel*) or bHA (*bottom panel*) were detected with anti-rat IgG Alexa 488 and streptavidin Alexa 647 respectively. Data are the mean fluorescence intensity (MFI) ± SD (n = 3) of 20 000 cells/condition as measured by flow cytometry and are representative of two independent experiments.

3.3.5 Prediction of shared epitopes using a cross-blocking assay

One aim of this study was to answer a conundrum arising from the observation that B1/10 and C1/8 are mutually exclusive with regard their function-blocking properties. This observation could be explained if the two antibodies bound separate epitopes, resulting in different functional outcomes upon binding to the receptor. To test this hypothesis, a cross-blocking experiment was devised to detect reduced binding of two antibodies when co-incubated together with mLYVE-1 pHR Jurkats cells, compared to the binding observed when incubated singularly. This approach necessitated the production and testing of fluorescent-dye labelled antibodies, as it would not be possible to distinguish the antibodies using isotype-specific secondary antibodies in all cases.

First, B1/10 and C1/8 were conjugated with DyLight 488 and DyLight 650 respectively, according to the manufacturer's instructions (Pierce). Binding of these conjugated antibodies was tested alongside R-PE-conjugated MAB2125 (R&D Systems) and Alexa 488-conjugated ALY7 (e-biosciences) at a range of concentrations, to mLYVE-1 pHR Jurkat cells (Figure 3.7). Dye-conjugated forms of B1/10, C1/8 and MAB2125 bound efficiently, with similar concentrations required for saturated binding (B1/10 and C1/8 = 25 µg/ml, MAB2125 = 0.625 µg/ml), as were observed for the unconjugated antibody (Figure 3.6). However, Alexa 488-conjugated ALY7 did not bind mLYVE-1 pHR Jurkat cells in this experiment, nor subsequently when tested side-by-side with unconjugated ALY7. This necessitated the use of unconjugated antibody for the cross-blocking assay.

Having established the conditions required for saturating binding, the four antibodies were incubated with mLYVE-1 pHR Jurkat cells either alone, in pairs, or with isotype-matched Ig controls, with the expectation that if they shared a similar epitope, this would lead to a reduction in binding compared to that observed in the absence of a competitor.

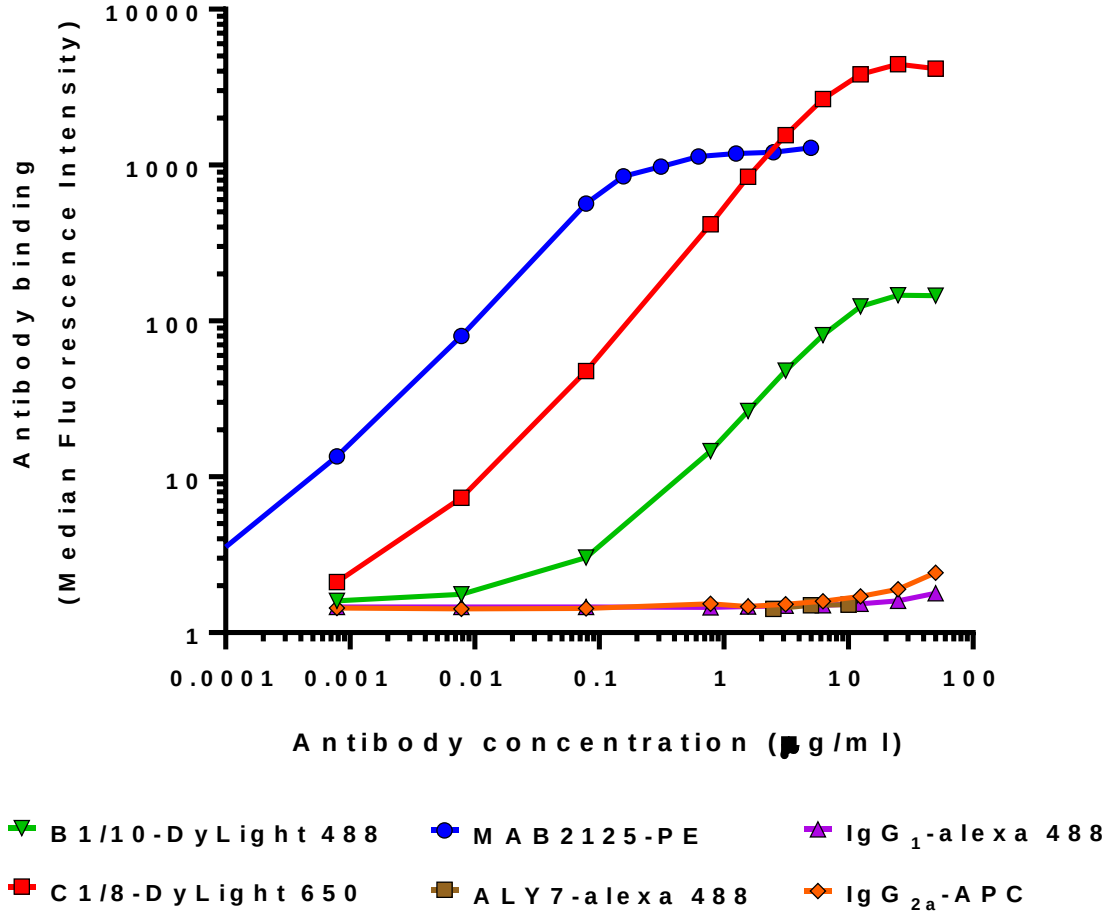


Figure 3.7. **Binding of dye-conjugated anti-mLYVE-1 monoclonal antibodies (mAbs) to mLYVE-1 expressing Jurkat cells**. Mouse LYVE-1 pHR Jurkat cells were incubated at 1.66 x 10^6 cells/ml with dye-conjugated mLYVE-1-specific mAbs or isotype-matched controls, at increasing Ig concentration, to assess binding of the mAbs following conjugation with fluorescent dyes. Data are the median fluorescence intensity of 20,000 cells/condition, as measured by flow cytometry, from a single experiment.

The results of this analysis indicated that all four antibodies cross-block, with exception of B1/10 and ALY7, where binding of the latter appears to enhance binding of the former by ~12 % (Figure 3.8). The reduction in binding resulting from co-incubation of two competing antibodies mirrored the apparent differences in binding affinity. Co-incubation of B1/10 and C1/8 led to a 50% reduction in binding of both antibodies, while co-incubation of either antibody with MAB2125 or ALY7 resulted in a 60-40 split in favour of the more potent monoclonal.

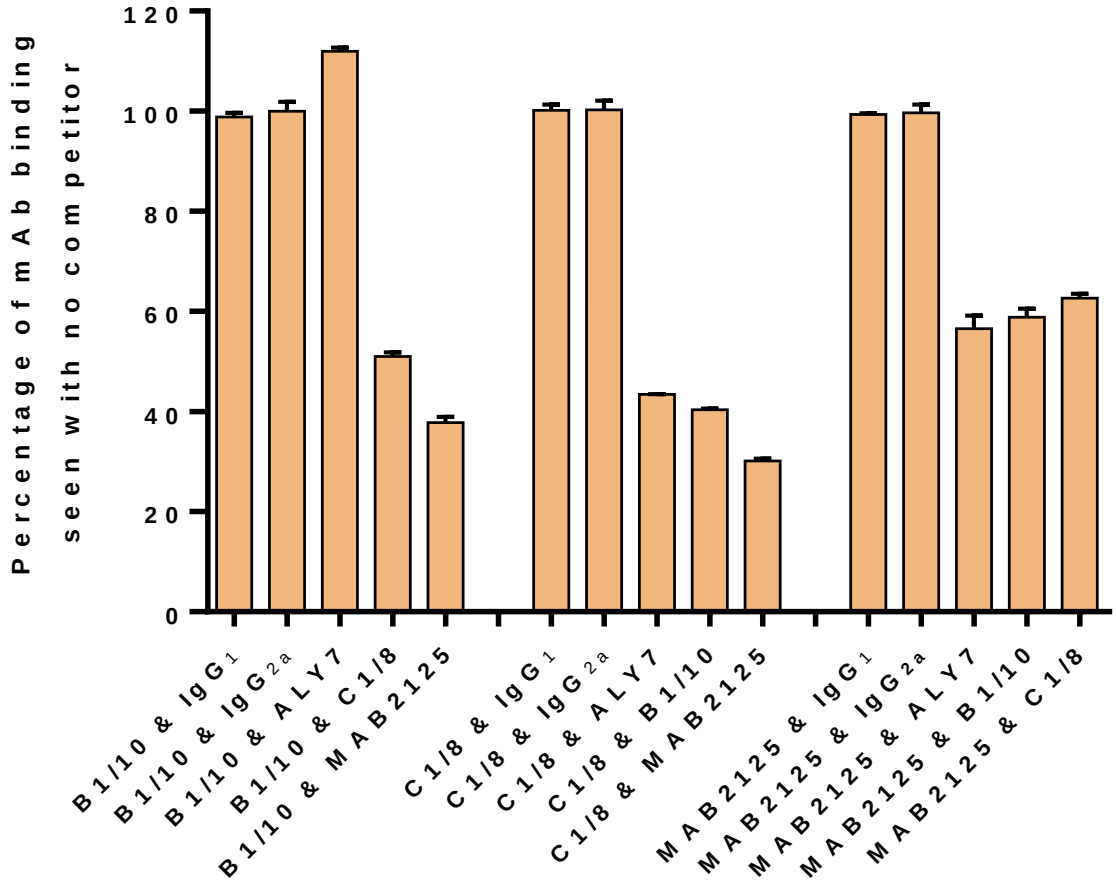


Figure 3.8. **Detection of shared epitopes for mouse LYVE-1-specific monoclonal antibodies (mAbs) by cross-blocking assay**. Mouse LYVE-1 pHR Jurkat cells were incubated at 1.66 x 10^6 cells/ml with dye-conjugated mLYVE-1-specific mAbs either alone, or simultaneously with a second mAb bearing a distinct fluorophore, or isotype-matched control IgG. A saturating concentration of Ig was used in all cases. The median fluorescence intensity (MFI) of each sample at the appropriate wavelengths was then measured using flow cytometry. Data are the percentage of the MFI observed for each mAb in the absence of competing Ig ± SD (n = 3) of 20 000 cells/condition, from a single experiment.

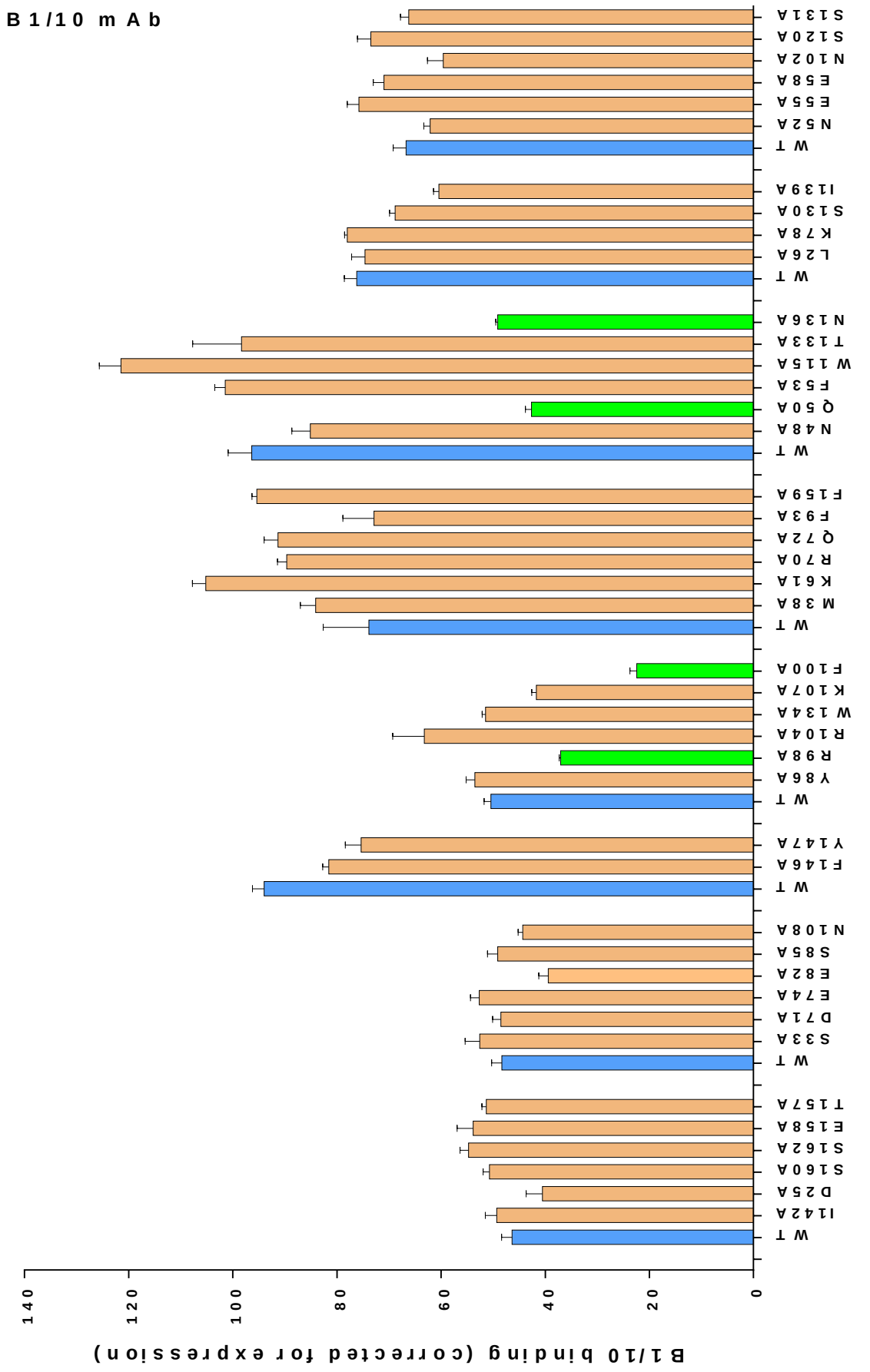
While it is possible that binding of one antibody to a protein may reduce binding of a second without the two sharing the same epitope, these data, coupled with the observation that all four antibodies block hyaluronan binding, would predict that these antibodies bind similar or overlapping epitopes, with the exception of B1/10 and ALY7. To confirm these findings it was necessary to conduct more precise epitope mapping using site-directed mutagenesis.

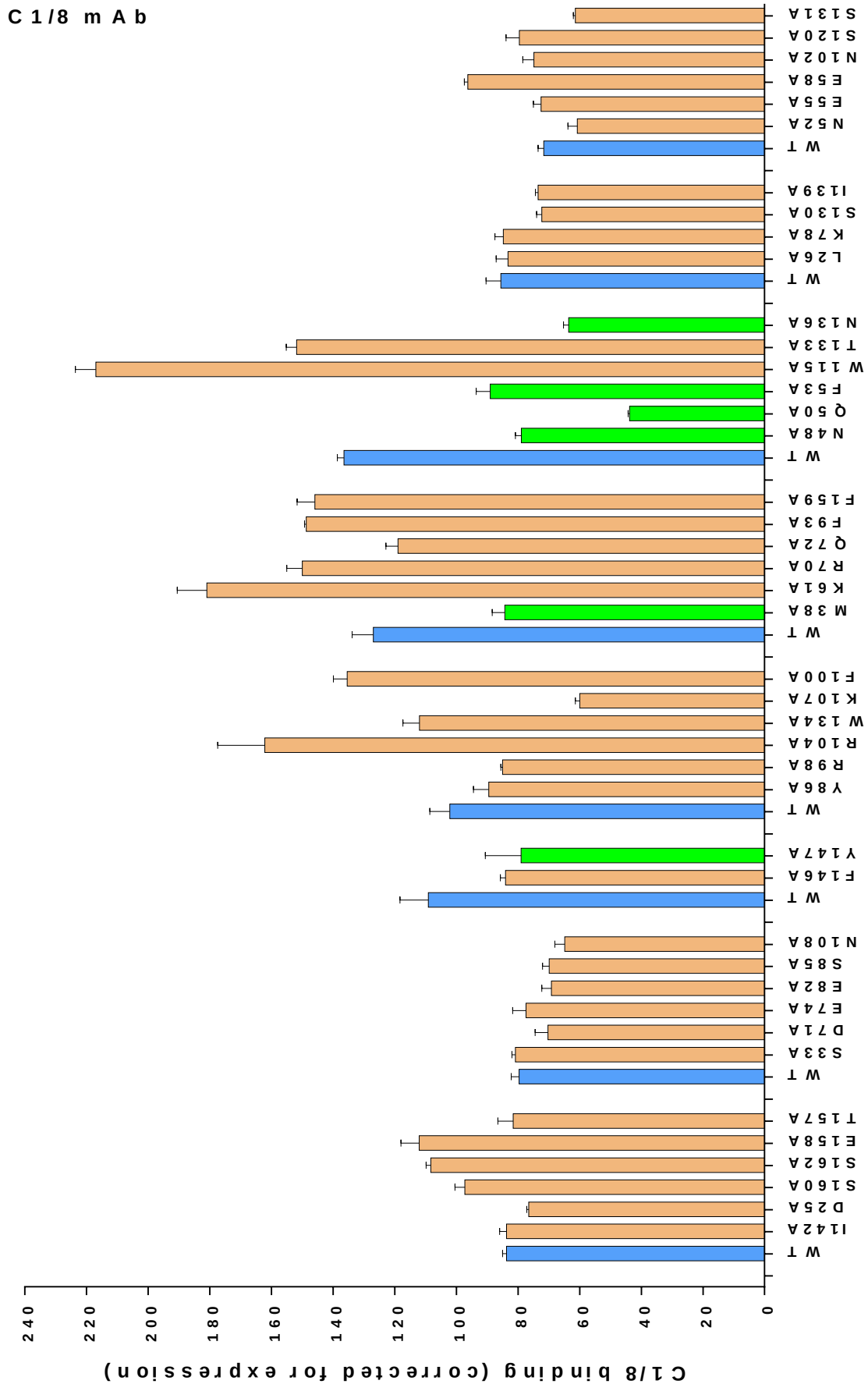
3.3.6 Mapping the epitopes of function-blocking anti-mLYVE-1 monoclonal antibodies using site-directed mutagenesis.

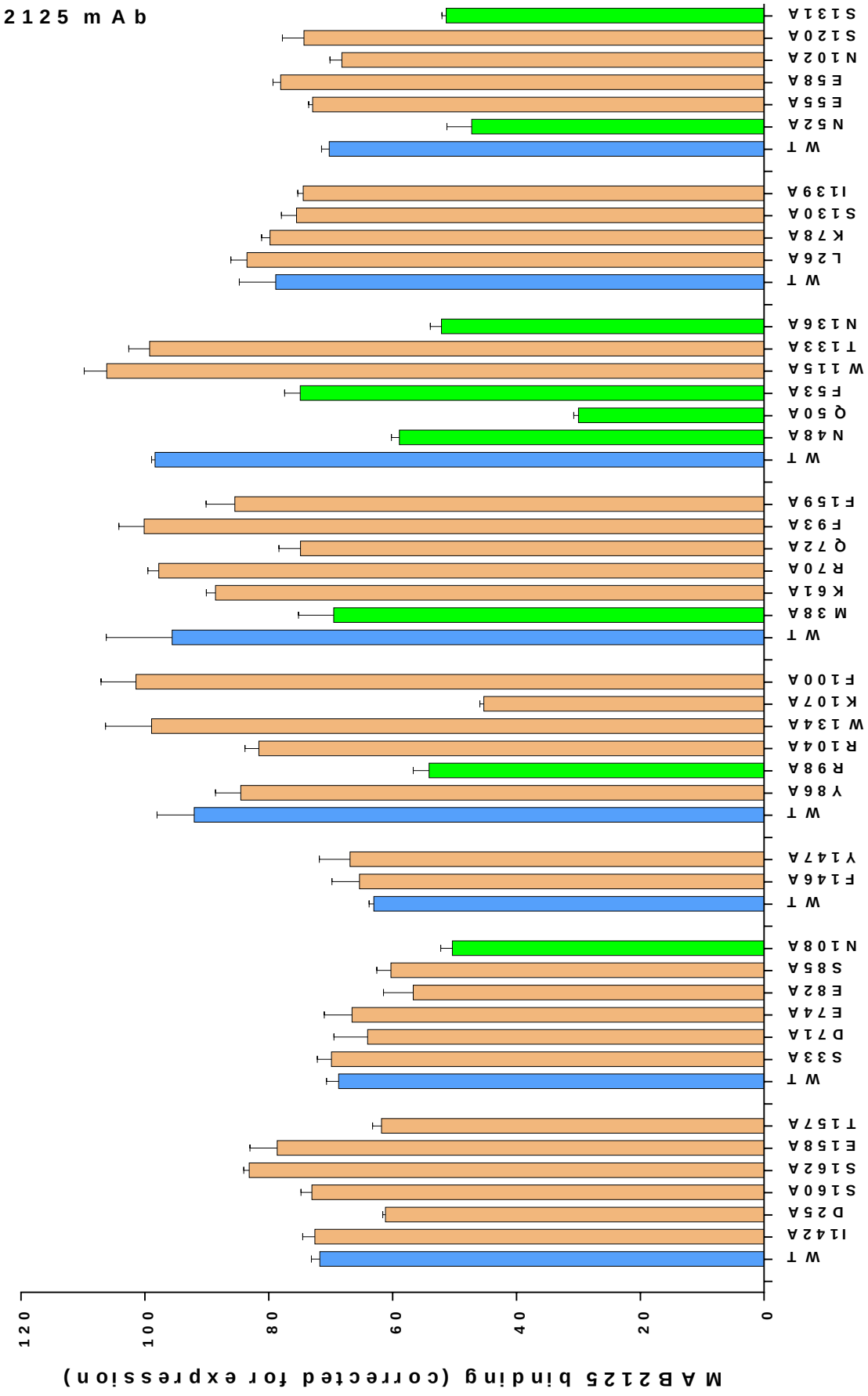
A flow cytometry screen of HEK 293T cells transiently-transfected with mLYVE-1 mutants was conducted to identify residues contributing to the epitopes of mLYVE-1 mAbs B1/10, C1/8, MAB2125 and ALY7. The antibody concentration required for saturated binding to wildtype mLYVE-1 transfected 293T cells was first established, to ensure that any decrease observed with mutant mLYVE-1 transfected cells was the result of the mutation itself. In the case of B1/10 and C1/8 the required concentration was high, some 80 µg/ml (data not shown). Mutant mLYVE-1 transfected cells were screened in batches, alongside wildtype mLYVE-1 and mock transfected (no plasmid) cells. A simple comparison of monoclonal antibody binding to mutant or wildtype mLYVE-1 transfected cells was considered, but discounted due to the likelihood of false-positives arising from differences in expression level or transfection efficiency. Instead, to standardise the analysis and accommodate for variation in expression level, the mean fluorescence intensity (MFI) measured for cells incubated with a monoclonal antibody was divided by the MFI of cells incubated with polyclonal antibody. The ratio derived for any given mAb was then compared between cells expressing mutant or wildtype mLYVE-1, to determine whether the mutation influenced binding. The rationale for this approach was that binding of the polyclonal antibody should be unaffected by a single point mutation in the receptor, whereas the same mutation, if located within the epitope of a monoclonal antibody, should lead to a significant reduction in binding.

As shown in Figure 3.9, mutation of thirteen separate residues resulted in reduced binding of one or more of the antibodies. Interestingly, seven of these (Q50, Y86, R98, R104, K107, W115, N136) had previously been identified as potential HA binding residues, a finding that had been expected on the basis that all four monoclonals block HA binding, albeit to

different extents. However, in contrast to the HA binding studies, where mutation of individual residues resulted in an 80% reduction in binding compared to wildtype, the reduction in antibody binding seen here was typically 25-50% (Table 3.1). In addition, some mutations enhanced C1/8 binding relative to wildtype. This made interpretation of the data more difficult, as it was less clear which residues are genuinely part of an antibody epitope, and which contribute to maintaining the stable conformation of the receptor. Two factors appear to have contributed to these discrepancies; firstly, transient-transfection of HEK 293T cells is efficient but does produce a population of cells with very heterogeneous LYVE-1 expression. This may skew the calculation of mean fluorescence intensity and mask some of the changes in antibody binding, although it should be pointed out that the data were highly reproducible between independent transfections. A second factor is that from a panel of forty-two mutants, no single point mutation completely ablated antibody binding, with the largest single reduction standing at 70%. This may indicate that mutating single residues in the antibody epitope to alanine was insufficient to disrupt antibody binding and that more extreme substitutions are required, for example, swapping an acidic residue for a basic one.


B1/10 mAb
WT
I142A
D25A
S160A
S162A
E158A
T157A
WT
S133A
D71A
E74A
E82A
S85A
N108A
WT
F146A
Y147A
WT
Y86A
R98A
R104A
W134A
K107A
F100A
WT
M38A
K61A
R70A
Q72A
F93A
F159A
WT
N48A
Q50A
F53A
W115A
T133A
N136A
WT
L26A
K78A
S130A
I139A
WT
N52A
E55A
E58A
N102A
S120A
S131A
B1/10 binding (corrected for expression)
0
20
40
60
80
100
120
140


C1/8 mAb
WT
I142A
D25A
S160A
S162A
E158A
T157A
WT
S333A
D71A
E74A
E82A
S85A
N108A
WT
F146A
Y147A
WT
Y86A
R98A
R104A
W134A
K107A
F100A
WT
M38A
K61A
R70A
Q72A
F93A
F159A
WT
N48A
Q50A
F53A
W115A
T133A
N136A
WT
L26A
K78A
S130A
I139A
WT
N52A
E55A
E58A
N102A
S120A
S131A
0
20
40
60
80
100
120
140
160
180
200
220
240
C1/8 binding (corrected for expression)


2125 mAb
WT
I142A
D25A
S160A
S162A
E158A
T157A
WT
S333A
D71A
E74A
E82A
S85A
N108A
WT
F146A
Y147A
WT
Y86A
R98A
R104A
W134A
K107A
F100A
WT
M38A
K61A
R70A
Q72A
F93A
F159A
WT
N48A
Q50A
F53A
W115A
T133A
N136A
WT
L26A
K78A
S130A
I139A
WT
N52A
E55A
E58A
N102A
S120A
S131A
MAB2125 binding (corrected for expression)
0
20
40
60
80
100
120

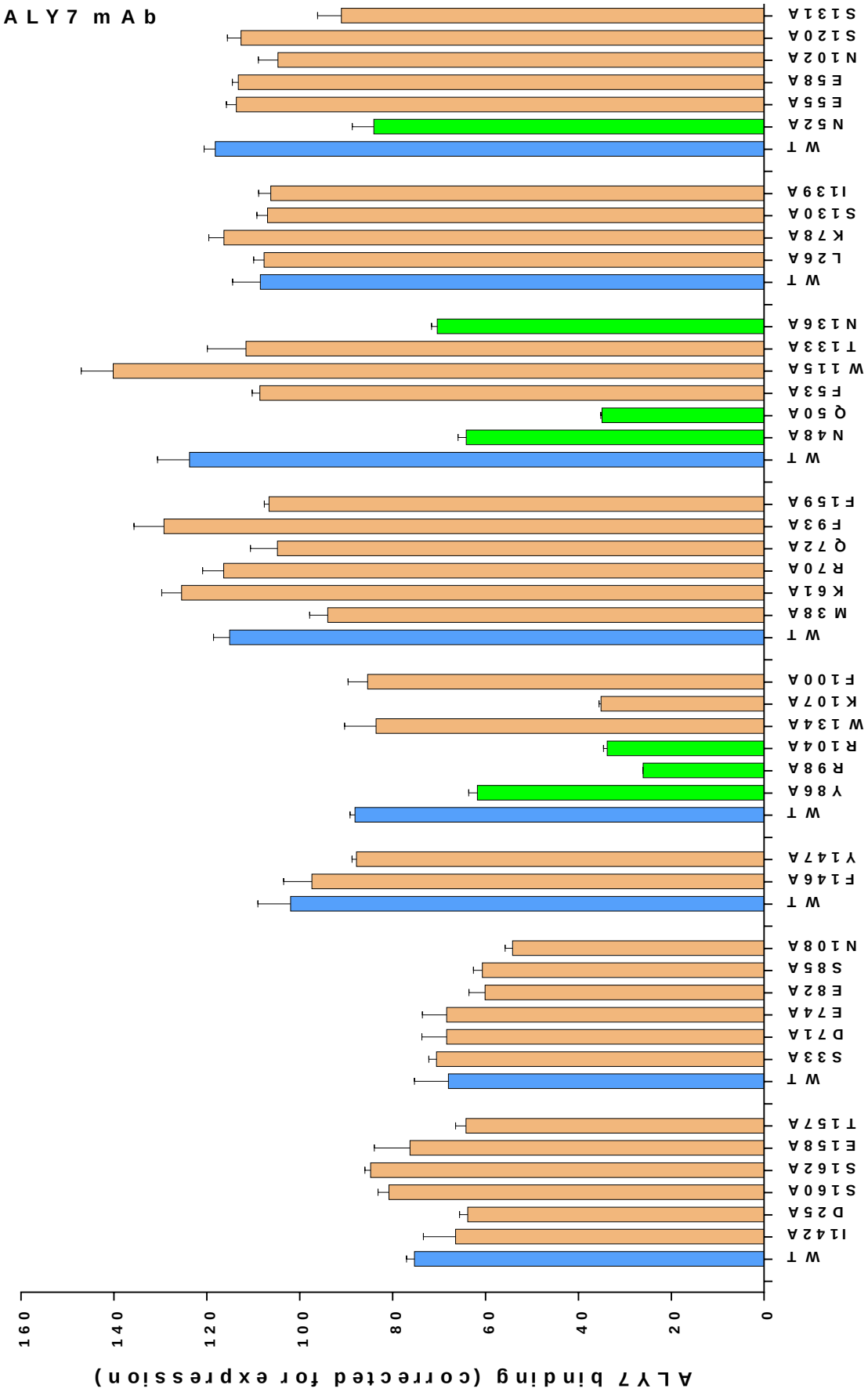

ALY7 mAb
WT
I142A
D25A
S160A
S162A
E158A
T157A
WT
S333A
D71A
E74A
E82A
S85A
N108A
WT
F146A
Y147A
WT
Y86A
R98A
R104A
W134A
K107A
F100A
WT
M38A
K61A
R70A
Q72A
F93A
F159A
WT
N48A
Q50A
F53A
W115A
T133A
N136A
WT
L26A
K78A
S130A
I139A
WT
N52A
E55A
E58A
N102A
S120A
S131A
0
20
40
60
80
100
120
140
160
ALY7 binding (corrected for expression)

Figure 3.9. **Influence of site-directed mutagenesis of mLYVE-1 on binding by anti-mLYVE-1 monoclonal antibodies (mAbs)**. Forty-two mLYVE-1 mutants were screened in batches for reduced binding of B1/10, C1/8, MAB2125 and ALY7 as detected by flow cytometry. In each experiment, wildtype (WT) mLYVE-1 transfected 293T cells were used as a positive control (*blue bars*). Protein expression was measured by calculating the mean fluorescence intensity (MFI) of cells stained independently with rabbit anti-mLYVE-1 polyclonal. The specificity of each antibody was confirmed by the lack of binding to mock-transfected cells or of isotype controls (Rab or Rat IgG) to transfected cells (see Appendix 1, Figure 7.2). Monoclonal Ab binding was corrected for protein expression in order to facilitate comparison between mutants and wildtype mLYVE-1 transfected cells. To do this, the MFI for cells incubated with mAbs was divided by the MFI of cells incubated with polyclonal Ab. Data are the mean ± SEM (n = 3 independent transfections). Candidate 'epitope residues' were identified by a reduction in mAb binding of >25%, relative to wildtype (*green bars*). Data representative of two independent experiments. A summary of these data can be found in Table 3.1.

	B1/10	C1/8	MAB2125	ALY7	HA binding (%)
Wildtype	+++	+++	+++	+++	100.0
M38A	+++	++	++	+++	56.0
N48A	+++	++	++	++	103.5
Q50A	+	+	+	+	8.7
N52A	+++	+++	++	++	16.4
F53A	+++	++	++	+++	43.8
E82A	+++	+++	+++	+++	55.6
Y86A	+++	+++	+++	++	18.1
R98A	++	+++	++	+	6.3
F100A	+	+++	+++	+++	96.4
R104A	+++	+++	+++	+	39.4
K107A					26.6
N108A	+++	+++	++	+++	65.7
W115A	+++	+++	+++	+++	2.3
S131A	+++	+++	++	+++	23.5
N136A	++	+	++	++	3.0
Y147A	+++	++	+++	+++	102.7

Monoclonal Ab binding (% of binding observed for wildtype mLYVE-1)	
0 - 25	-
25 - 50	+
50 - 75	++
> 75	+++

Table 3.1. **Summary of point mutations resulting in reduced hyaluronan binding by mLYVE-1 or reduced binding of anti-mLYVE-1 monoclonal antibodies (mAbs).**

Sixteen point mutations of mLYVE-1 resulted in reduced binding (highlighted in *red*) of one or more anti-mLYVE-1 mAbs. Binding of each antibody is shown as a percentage of binding to wildtype LYVE-1. Nine of these mutations also resulted in a reduction in HA binding (highlighted in *green*). Mutations at N52 and S131 ablate the predicted N-glycosylation sites at N52 and N129 respectively (highlighted in *orange*). Expression of K107A was markedly lower than other mutants and was excluded from epitope analysis.

Using a homology based structural model of the mLYVE-1 HABD, the position of those residues whose mutation resulted in reduced antibody binding were mapped in relation to the predicted HA binding surface (Figure 3.10). The four partial epitopes are quite similar, localising to the same 'face' of the protein, and overlap to varying degrees with the predicted HA-binding site (Figure 3.10). All of the HA binding residues identified in Figure 3.4 feature prominently, with the exception of W115, as might be expected given the capacity of these antibodies to block hyaluronan binding. The K107A mutation significantly reduced binding of C1/8, MAB2125, and ALY7, but also resulted in low surface expression, and was discounted from the analysis. Residues Asn-136 and Gln-50 appear in all four epitopes, but are separated in physical space, giving the appearance of split epitopes. Mutation of these residues also ablated HA binding, which may point to a gross conformational defect. Asn136 forms part of a β-sheet that includes the Cys-35 - Cys-138 structural disulphide, which potentially could be prevented from forming by the N136A, while Gln-50 lies adjacent to the N-glycosylation site at Asn-52. Mutation of other residues in close proximity to Asn-52, including Asn-48 and Phe-53 resulted in decreased binding of C1/8, MAB2125 and ALY7, indicating that this region of the molecule is sensitive to disruption, perhaps due to altered N-glycosylation. Semi-conservative mutation of these residues will be required to determine their involvement more conclusively.

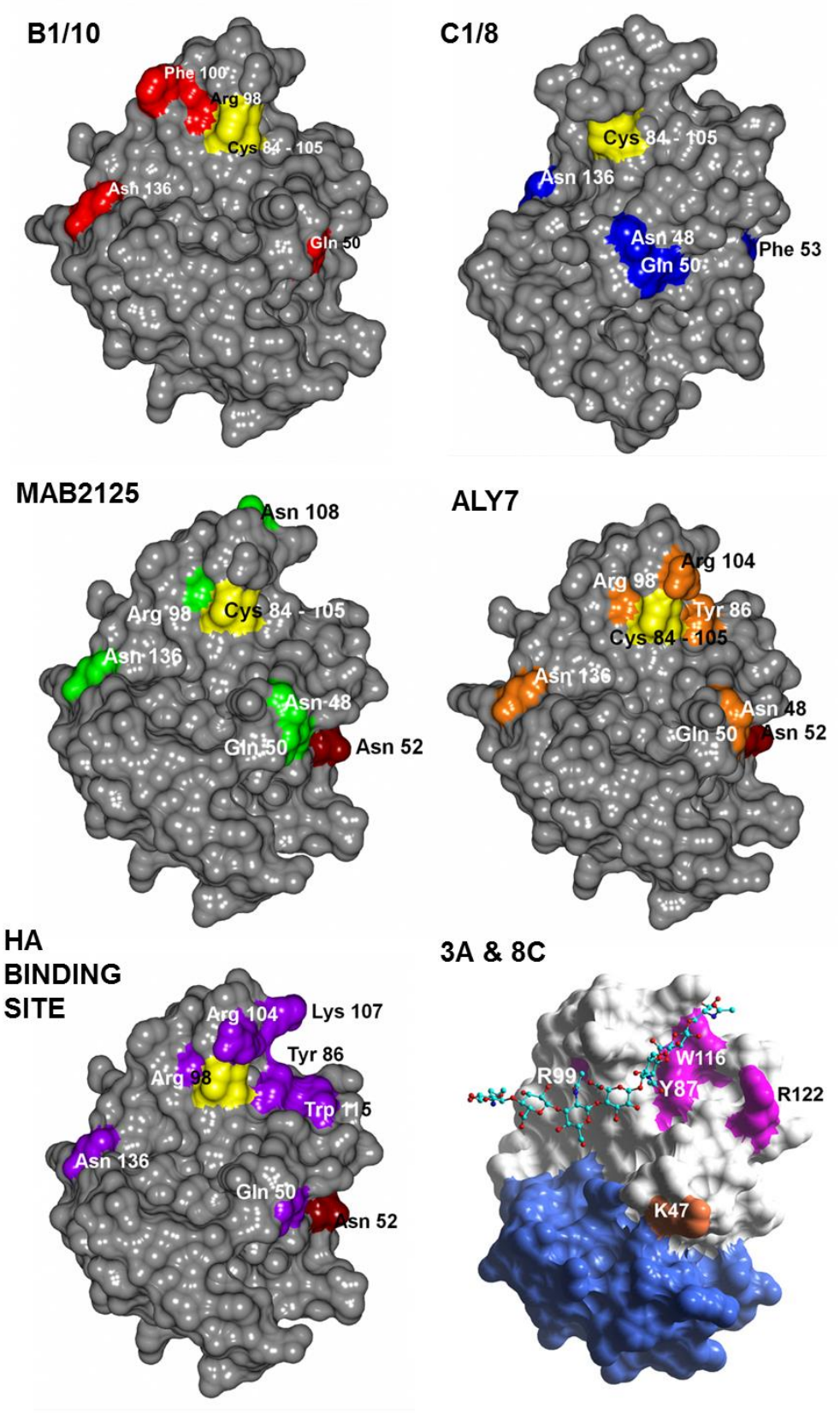


Figure 3.10. **Partial epitopes derived for anti-mLYVE-1 monoclonal antibodies (mAbs) shown in relation to the hyaluronan binding site.** Site-directed mutagenesis was used to identify residues contributing to the epitopes of anti-mLYVE-1 mAbs. Those

residues whose mutation led to a >25% decrease in binding relative to the wildtype receptor were plotted on a space-filled representation of the mLYVE-1 HABD model. Residues that may contribute to the epitopes for B1/10 are shown in *red*, for C1/8 in *blue*, for MAB2125 in *green*, and for ALY7 in *orange*. In all representations, the Cys84 – Cys105 disulfide is highlighted in *yellow*. Mutation of the predicted *N*-glycosylation site at Asn 52 reduced binding of some mAbs and is highlighted in *tan*. Residues whose mutation led to a >60% reduction in hyaluronan binding are highlighted in *purple*. For comparison, the epitope of the hyaluronan-blocking anti-hLYVE-1 mAb 3A is shown in *magenta*, on a space-filled representation of the hLYVE-1 HABD model.

Consideration of the epitope mapping data identifies a number of points that correspond with the results of the HA-blocking and cross-blocking assays, but also highlights some discrepancies (see sections 3.3.4 and 3.3.5). The close proximity of the epitopes is in agreement with the observation that the antibodies can cross-block, while the involvement of HA contact residues corresponds to the HA blocking properties observed with recombinant protein and mLYVE-1 transfected cells. The more potent HA blocking antibodies, MAB2125 and ALY7 also appear to bind more HA contact residues, while B1/10 binds one and C1/8 none (excluding Asn 136 and Gln 50). In the case of C1/8, mutation of some HA contact residues had the curious effect of enhancing antibody binding.

The cross-blocking observed between B1/10 and C1/8 would predict some overlap in their epitopes, however this proved not to be case in this analysis, although the possibility remains that binding of one antibody may induce a conformational change that disrupts binding of the other. Separation of the B1/10 and C1/8 epitopes remains an attractive hypothesis to explain the different functional outcomes mediated by binding of these antibodies. In addition, the lack of cross-blocking between B1/10 and ALY7 would predict separate epitopes, however mutagenesis of Arg 98 resulted in decreased binding of both antibodies, indicating that there is a small degree of overlap.

3.4 Discussion

In this chapter, the hyaluronan binding site in mouse LYVE-1 is identified using a combination of site-directed mutagenesis and structure-based homology modelling of the mLYVE-1 extended link domain (ELD). *N*-glycosylation at two separate sites on the ELD was shown to be obligatory for HA binding. Two monoclonal antibodies that recognise mLYVE-1, B1/10 and C1/8, were found to be capable of blocking hyaluronan binding by the receptor, albeit weakly in comparison to other more potent mAbs (ALY7 and MAB2125). This suggests that the function-blocking properties ascribed to these antibodies involves blockade of ligand binding, but fails to explain the distinct outcomes resulting from their use in animal models of inflammation and disease. Using a cross-blocking assay, it was apparent B1/10 and C1/8 block binding of one-another, suggesting that their epitopes do in fact overlap. Partial epitope mapping for all four antibodies revealed that they bind in or around the hyaluronan binding site. B1/10 and C1/8 did not contact any of the same residues from a panel of forty-two (25% coverage of HABD residues), but further analysis is required to determine whether their epitopes are discrete or feature a small degree of overlap.

The observed biological effects of these antibodies *in vivo* may be related to their relative ability to block HA-binding, and so it was first necessary to map the location of the HA-binding site. Site-directed mutagenesis identified a number of conserved HA-binding residues, as well as some novel residues that may indicate a similarity to the CD44 HA-binding patch not seen in human LYVE-1. Semi-conservative mutation of the residues involved, and their near neighbours, will be required to confirm or refute this observation. Overall, the ligand binding site in mouse LYVE-1 has the same compact shape and predominance of charged residues observed for its human homolog (Banerji et al., 2010).

A further point of similarity came with the observation that mutation of either *N*-glycosylation site resulted in very low levels of HA-binding. In human LYVE-1, *N*-glycosylation also plays a positive role in HA binding, although only the N53 site (N52 in mouse) was obligatory for binding.

Having mapped the location of a putative HA-binding patch on the surface of mLYVE-1, it was then possible to investigate the epitopes of anti-mLYVE-1 monoclonals in relation to their ability to block HA-binding. Three of the antibodies, B1/10, MAB2125 and ALY7, displayed reduced binding after disruption of residues close-by, or within the HA-binding site. Whereas the potent HA-blockers MAB2125 and ALY7 bind across the bulk of the HA-binding patch, B1/10 appears to contact a single HA-binding residue, Arg 98. Difficulties encountered with the epitope mapping have made it difficult to pin-down the epitope of C1/8, indeed mutation of some of the conserved HA contact residues led to an increase, rather than a decrease in binding. Addressing these technical issues in future would firstly involve switching to lentiviral infection of Jurkat cells, as they have the advantage of being readily infected and then sorted into populations with matched surface expression. Further site-directed mutagenesis would also be required to make semi-conservative changes to some residues, and more extreme changes to others, as it was evident from this study that single-point mutations to alanine were often insufficient to produce clear-cut reductions in mAb binding.

A role for hyaluronan in the LYVE-1 dependent transmigration of lymphatic vessels by dendritic cells, nodal dissemination of metastasizing tumour cells and alveolar egress by inflammatory macrophages now appears more likely, given the observation that both B1/10 and C1/8 are capable of blocking HA binding. However it was intriguing to note that the IC_{50} for blockade of HA binding by mLYVE-1 transfected cells was two orders of

magnitude higher for these than MAB2125 or ALY7. This may simply be a reflection of their relative binding affinity for LYVE-1, as the concentration required to saturate the available binding sites on transfected cells was also conspicuously higher. An attempt to measure the binding affinity of each antibody mLYVE-1 proved to be technically challenging due to the use of divalent mLYVE-1 Fc fusion protein as the ligand. However, a CHO-cell based expression system, described in Chapter 7, has been used with some success to produce recombinant His-tagged hLYVE-1, and could be readily adapted for production of the mouse equivalent.

One way of addressing the significance of the LYVE-1-hyaluronan interaction, would be to determine whether the greater potency of antibodies such as MAB2125 equates to an enhanced blocking effect in the various animal models described. Experiments are underway in the Jackson laboratory to answer this question, and early indications are that administration of MAB2125 does indeed lead a greater reduction in DC trafficking compared to B1/10 (L. Johnson, unpublished). However, the magnitude of the effect is not as marked as might be expected, although this may be a reflection of the fact that LYVE-1 is not the only adhesion molecule involved in DC transmigration of lymphatic endothelium.

Epitope mapping studies and analysis of the HA blocking capacity have not provided a definitive explanation for the difference in functional outcomes resulting from blockade with B1/10 or C1/8. While further epitope analysis may yet confirm discrete binding sites for the antibodies, other possibilities must now be explored. Recently, advances in the protocol for isolation and culture of primary mouse lymphatic endothelial cells have facilitated access to cells that are superior in purity to those than have previously been available. It would be intriguing to repeat some of the analyses using these cells, especially in light of the recent observation that the cells display a constitutive level of hyaluronan

binding not seen with human LEC (S. Banerji, personal communication). A number of outputs could be tested, including changes in LYVE-1 distribution following incubation with B1/10 and C1/8. Signalling changes resulting from interaction of mouse LEC with mLYVE-1 mAbs have recently been probed by post-docs Danijela Markovic and Ying-Jie Wang in the Jackson laboratory. Notably, mAb treatment leads to phosphorylation of VE-cadherin, an adherens junction component in mouse LEC, leading to re-distribution of VE-cadherin and associated changes in cellular permeability. As described in the following chapter, incubation of human LEC with certain monoclonal antibodies leads to clustering of the receptor and associated potentiation of hyaluronan binding. While mLYVE-1 mAbs B1/10 and C1/8 block, rather than enhance HA binding by mLYVE-1, the observation that LEC bind HA under certain conditions brings new focus on the role played by hyaluronan in transmigration of lymphatic endothelium, and how this process is blocked by these antibodies.

Chapter 4.
Regulation of Hyaluronan Binding in Lymphatic Endothelial Cells by LYVE-1 Surface Density

4.1 Introduction

A large body of evidence suggests that the interaction between LYVE-1 and its ligand hyaluronan is highly regulated in lymphatic endothelium. When over-expressed in cell backgrounds such as HEK 293T fibroblasts, either in full-length form or as a soluble ectodomain Fc fusion protein, LYVE-1 exhibits constitutive saturable binding to fluoresceinated (Fl-HA) or biotinylated HA (bHA), which may be blocked using LYVE-1 mAbs or an excess on unlabelled hyaluronan (Banerji et al., 1999; Prevo et al., 2001). The situation for the native receptor in lymphatic endothelial cells however is much different; cultured lymphatic endothelial cells extracted from mouse or human tissue display only residual binding to Fl-HA or bHA and lymphatic vessels when viewed in corresponding tissue sections show little if any co-localization with either endogenous or exogenously added HA (Nightingale et al., 2009). These and other findings suggest that LYVE-1 may be functionally silenced in lymphatic endothelial cells, and that mechanisms must exist to relieve this inhibition in the appropriate context *in vivo*. Cell-specific regulation is a well-documented feature of the related HA receptor CD44. Although widely expressed by a variety of cell types, most primary CD44-positive cells fail to exhibit HA receptor function (Pure and Cuff, 2001). Induction of HA binding to CD44 can be achieved using pro-inflammatory cytokines, but the underlying mechanisms are complex, including increased receptor expression, receptor clustering, and various forms of post translational modification including O- and N-glycosylation, glycosaminoglycan attachment, phosphorylation, inclusion of variant exons and receptor sulphation (see general introduction for further detail).

Prior to the start of my DPhil project, the regulation of hyaluronan binding by LYVE-1 glycosylation had been studied using a combination of mutagenesis and expression in

Chinese hamster ovary (CHO) cell lines with deficient glycosylation machinery (Nightingale et al., 2009). Mutation of the two N-glycosylation sites in hLYVE-1 had revealed that N-glycans play a positive role in HA-binding. This contrasts the situation in CD44, where N-glycan chains can play an inhibitory role (English et al., 1998), specifically when modified by terminal sialic acid residues, as evidenced by the observation that cleavage by the neuraminidase Neu1 results in activation of HA binding in T helper type 2 (Th2) cells (Katoh et al., 2010). In the case of LYVE-1, a series of elegant experiments had indicated that O-glycosylation plays an inhibitory role in HA binding through a similar sialic acid dependent mechanism. Firstly, progressive deletion of the O-glycosylated Ser/Thr-rich stalk region in a series of truncation mutants resulted in a progressive increase in HA binding. Secondly, expression of LYVE-1 in Lec 2 CHO glycosylation mutants lacking the CMP-NANA transporter essential for terminal sialylation unmasked HA binding. Lastly, treatment of wild-type CHO K1-derived sLYVE-1 ectodomains with linkage specific neuraminidases led to reactivation of HA binding, indicating that the inhibitory mechanism is reversible and is exerted by terminal sialylation, most likely through α2-3 or α2-6 linkage to O-glycans. Curiously however, the inhibitory sialyl moieties in LYVE-1 are inaccessible to cleavage by neuraminidase in intact cells, most likely due to steric hindrance (Nightingale et al., 2009).

To date, no physiological factors have been identified that promote de-sialylation and subsequent unmasking of HA binding by LYVE-1 *in vivo*. Far from activating the receptor, pro-inflammatory cytokines TNFα and TNFβ promote rapid but reversible internalisation and degradation of LYVE-1 in lysosomes, coupled with a shutdown in gene expression (Johnson et al., 2007). Crucially, LYVE-1 does not undergo activation during internalization as HA uptake proceeds almost equally in resting and TNFα -activated LEC and is unaffected by the hLYVE-1 HA blocking mAb 3A. A wider screen of cytokines,

chemokines and growth factors found no influence on LYVE-1 surface expression or HA binding. Taken together these data suggest that LYVE-1 does not engage in bulk HA clearance and catabolism, despite the active role played by the lymphatic system in this process. This being said, function blocking antibodies directed against mouse LYVE-1 have clearly implicated hyaluronan binding in LYVE-1 function, and it is likely that the form or context under which HA is presented to LYVE-1 will be critical.

While the process of sialylation/de-sialylation clearly represents one mechanism for regulation of HA binding, there are other potentially more rapidly-acting mechanisms that are also worthy of consideration. One of these is alteration of receptor surface distribution or receptor clustering – a process that can lead to enhanced binding of a polyvalent ligand through avidity effects. Measurements of the binding affinity of individual LYVE-1 monomers and dimers for HA are ongoing, but preliminary estimates of the dissociation constants (K_D) using surface plasmon resonance have yielded values in the low micro-molar range, at 107 µM and 20 µM for monomeric and dimeric LYVE-1 respectively (Dr. S. Banerji, unpublished observations). These values are not dissimilar to those reported for CD44, which are in the 10 – 100 µM range for polymeric HA (300 kDa) (Banerji et al., 2010; Banerji et al., 2007). At first glance these affinities appear rather low, however they are more than sufficient given the polyvalent nature of HA and the presence of multiple receptors at the cell surface. This is because the binding affinities of individual interactions are multiplicative with a polyvalent ligand, leading to a rapid increase in cumulative binding affinity. Based on a K_D of ~65 µM for the interaction between CD44 and high molecular weight HA, a valency of just 3 would result in sub-picomolar avidity (Wolny et al., 2010).

Analysis of CD44 interactions with HA in an artificial membrane system monitored by Quartz Crystal Microbalance with Dissipation monitoring (QCM-D) have revealed that the amount of HA binding to densely CD44-coated bilayers increases as a function of HA size (Wolny et al., 2010). Binding was reversible for smaller HA species (≤ 10 kDa) and essentially irreversible with large polymers. Furthermore, the amount of bound HA decreased with decreasing receptor surface density. These data match the findings of other authors who have observed an expression threshold for HA binding in AKR1 T-lymphoma cells (Perschl et al., 1995), and an increase in avidity with HA chain length, that defines multivalent interactions as the primary feature of HA binding by cell surface CD44 (Lesley et al., 2000). These conclusions were built on initial findings that HA binding could be induced in CD44-expressing cell lines by bivalent CD44 mAbs IRAWB14 and B26, but not by their monovalent Fab fragments (Lesley et al., 1993). Clustering of CD44 receptors by these antibodies is reported to have little effect on binding kinetics, but greatly delays dissociation of HA from the cell surface due to an increase in avidity (Lesley et al., 2000).

4.2 Aims

Much of the past effort aimed at inducing hyaluronan binding to LYVE-1 in lymphatic endothelial cells has focussed on defining conditions that stimulate removal of inhibitory sialic acid from the receptor. However, the necessary conditions remain obscure and this has prompted consideration of additional mechanisms of LYVE-1 regulation, many of which have been inspired by previous work on induction of HA binding by CD44. Recent QCM-D analysis of CD44-hyaluronan binding in an artificial membrane system have reminded how multiple weak individual interactions can tie down a large polyvalent ligand through the power of avidity (see Chapter 6). This chapter aims to determine the extent to which avidity affects the binding of HA by LYVE-1, and whether receptor clustering represents a mechanism for regulating LYVE-1 function.

1. Explore the relationship between LYVE-1 surface density and HA binding and determine whether a threshold exists for HA binding.

2. Determine whether over-expression of LYVE-1 in primary lymphatic endothelial cells can overcome inhibition of HA binding.

3. Characterize the available panel of human LYVE-1 mAbs and perform a functional screen to determine whether mAb-induced LYVE-1 clustering can influence HA binding.

4.3 Results

4.3.1 The relationship between LYVE-1 expression and hyaluronan binding

LYVE-1 is expressed abundantly in lymphatic endothelium, yet displays only weak hyaluronan binding by default. Lymphatic vessels in human or mouse tissues, when probed *in situ*, show a lack of co-localization with endogenous or exogenously-added HA. Equally, cultured monolayers of lymphatic endothelial cells (LECs) isolated from these sources display only residual levels of HA binding as detected by fluorescence microscopy or flow cytometry (Figure 4.1, A). This contrasts the situation with the majority of LYVE-1-transfected cell lines, where HA binding is efficient, and may be blocked with certain LYVE-1-specific monoclonal antibodies (mAbs) (Figure 4.1, B).

In primary LEC, inhibition appears to involve sialylation of O-linked glycans, however the mechanism by which HA binding is then activated is currently unclear (Nightingale et al., 2009). This led to consideration of whether sialylation represents a simple 'on/off' switch, that must be engaged to trigger receptor function, or rather a persistent state, that does not preclude interaction with hyaluronan under certain conditions. Given the low binding affinity of individual LYVE-1 receptors for HA (50 – 100 μM), and the polyvalent nature of the ligand, it is likely that multiple molecules are required to form a stable interaction with an HA chain, as the combined binding strength is multiplicative through avidity effects. Rather than predicting a linear relationship between LYVE-1 expression and HA binding, this model would suggest that a threshold of LYVE-1 expression or surface density must be met before stable binding may occur. However, the relationship between LYVE-1 expression and HA binding, and how this may be influenced by the degree of inhibitory sialylation, has not been explored in detail.

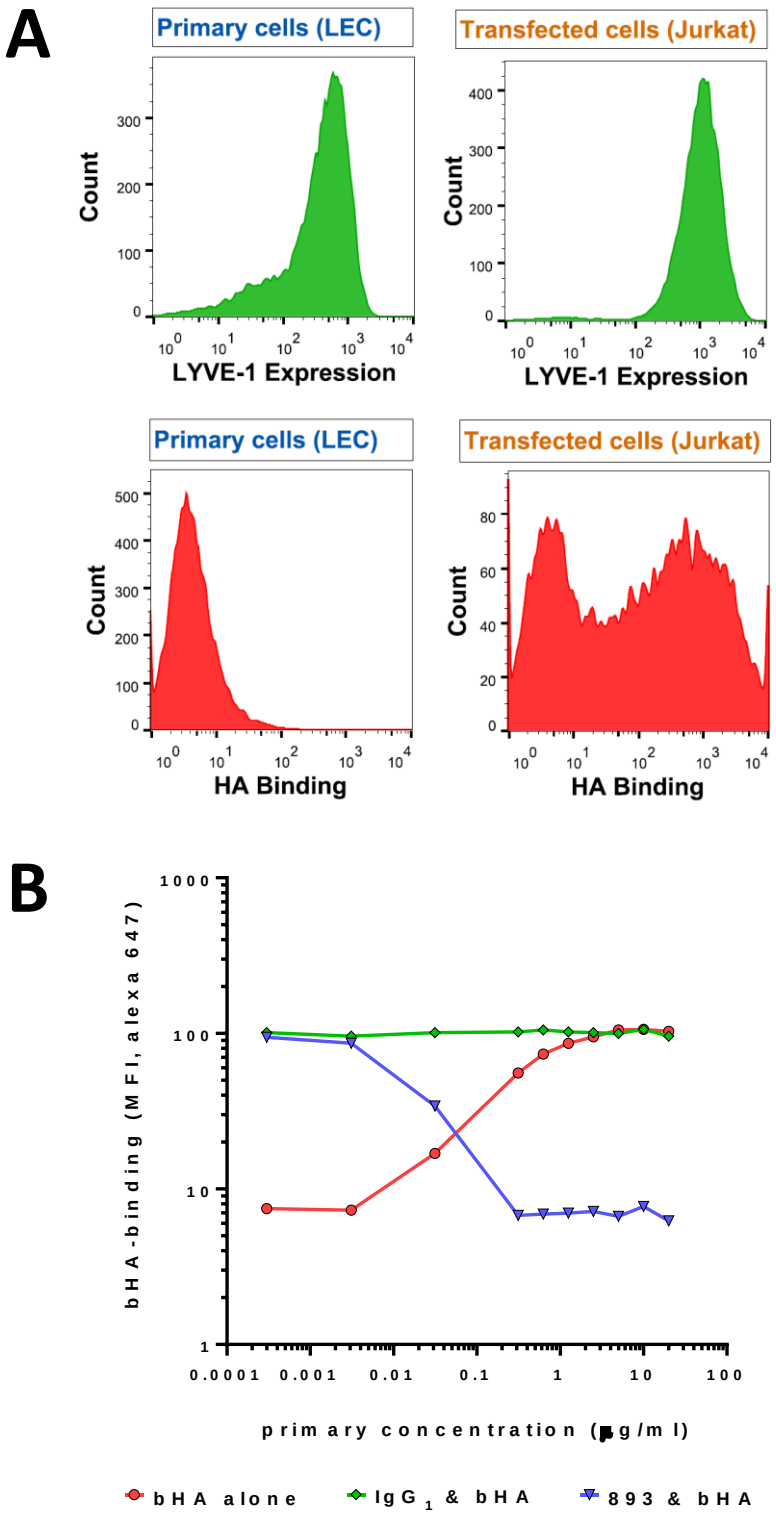


Figure 4.1. **Primary lymphatic endothelial cells (LEC) lack the constitutive hyaluronan binding observed for LYVE-1-transfected cell lines.** (A) Cultured primary LEC or LYVE-1 transfected Jurkat cells were incubated with the LYVE-1 mAb 8C or biotinylated HA (bHA) to assess LYVE-1 expression and bHA binding, as detected by flow cytometry. (B) Binding of bHA by hLYVE-1 Jurkat cells under different conditions. Cells were either incubated with bHA alone, at increasing bHA concentration (*red line*) or co-incubated with bHA (5 µg/ml) and hLYVE-1 mAb 893 (*blue line*, variable conc.) or

mouse IgG_1 isotype control (*green line*, variable conc.), to assess the effect on bHA binding. Data are the mean fluorescence intensity (MFI) of 20 000 cells/sample and are representative of multiple experiments (>3).

To enable the relationship between LYVE-1 surface density and bHA binding to be examined in more detail, separate stable cell lines were established with either high or low LYVE-1 surface expression. These were generated from the Jurkat cell line using full-length cDNAs encoding human and mouse LYVE-1, and separate lentiviral vectors capable of driving either low (pHRI) or high (pHR) levels of protein expression, by virtue of different promoters. As shown in Figure 4.2 (panels A & D), expression of LYVE-1 by human and mouse LYVE-1 pHR Jurkat cells was approximately 15-fold higher than their pHRI counterparts, as determined by flow cytometry. The level of bHA binding exhibited by both mLYVE-1 pHRI and hLYVE-1 pHRI transduced Jurkats was negligible, (Figure 4.2, B & E). By contrast, both human and mouse LYVE-1 pHR Jurkat cells displayed high levels of bHA binding, which could be fully displaced by simultaneous incubation with either the commercial LYVE-1 blocking antibody mAb 893, or an excess of unlabelled HA (Figure 4.2, G & H). While expression of LYVE-1 by pHR-transduced cells was relatively uniform, bHA binding was comparatively heterogeneous, and a large population of non HA-binding cells was evident. Further analysis using two-colour flow cytometry (Figure 4.2, C & F) revealed that a narrow threshold of LYVE-1 expression separated HA binding and non-binding cells of ~ 5-fold or less. Maximal HA binding was achieved by cells with ~10-fold higher LYVE-1 expression than non HA-binding cells. These data suggest that LYVE-1 expression, or surface density, is a critical regulator of HA binding. A minimum number of LYVE-1 molecules are required for stable or sustained binding to be detected, but above this threshold, the amount of HA bound scales rapidly with increasing LYVE-1 surface expression.

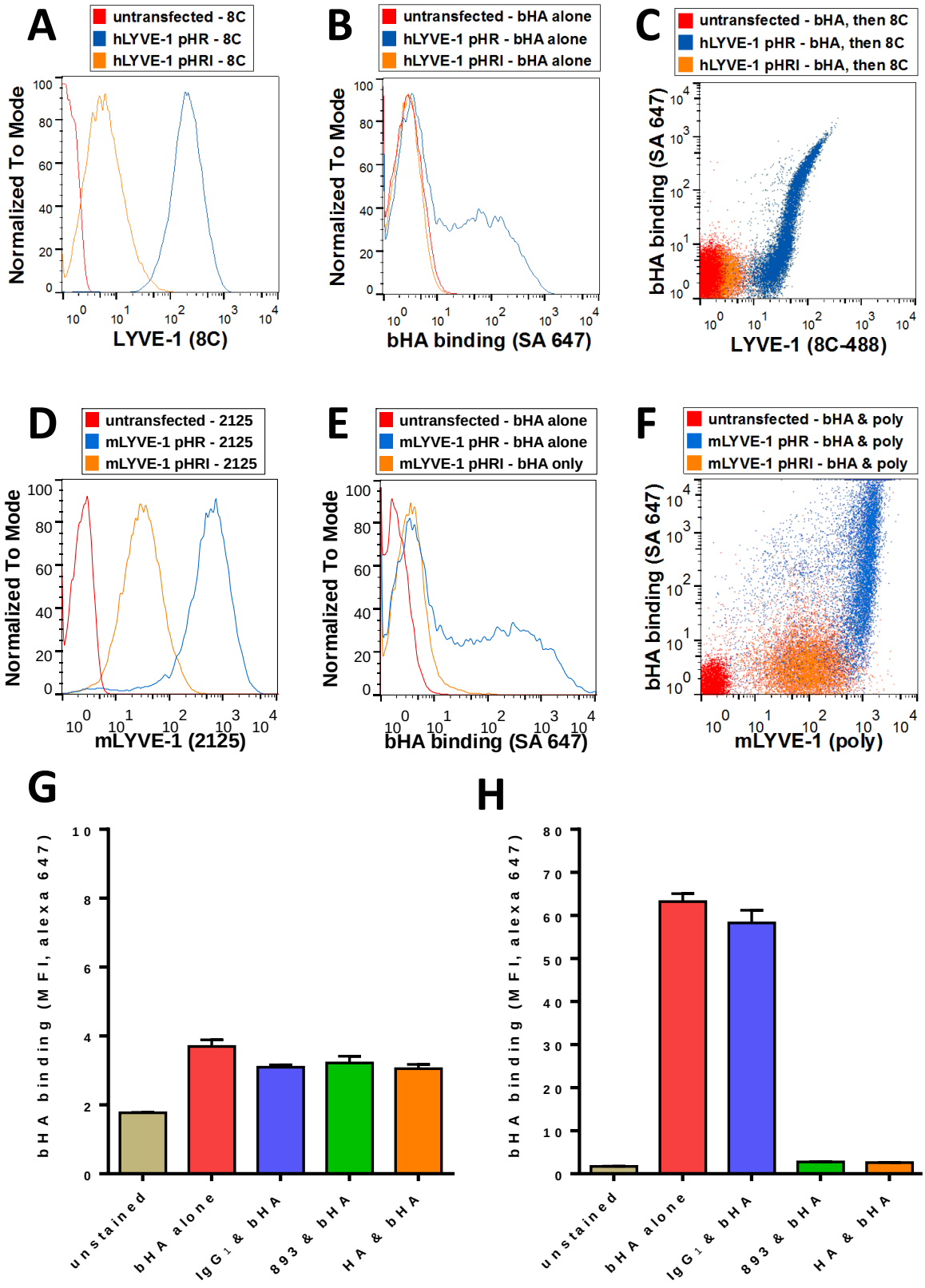


Figure 4.2. **Influence of LYVE-1 expression level on hyaluronan binding by LYVE-1 transfected Jurkat cells.** Jurkat cells were transduced with lentivirus bearing human or mouse LYVE-1 under the control of a promoter that drives high (pHR) or low levels of expression (pHRI). Cells were incubated with biotinylated hyaluronan (bHA) either alone or in combination with LYVE-1 specific antibodies or isotype-matched controls to assess

LYVE-1 expression and/or hyaluronan binding, as detected by flow cytometry. Data are the mean fluorescence intensity (MFI) of 20 000 cells/sample ± SD (n = 3). *Top row*: Comparison of hLYVE-1 expression using 8C mAb (A) and bHA binding (B) by untransfected Jurkat, hLYVE-1 pHR and pHRI Jurkat. (C) Relationship between hLYVE-1 expression and bHA binding in cells incubated first with bHA, then subsequently with Dylight 488-conjugated hLYVE-1 mAb 8C. *Middle row*: Comparison of mLYVE-1 expression using mLYVE-1 mAb 2125 (C) and bHA binding (D) by untransfected Jurkat, mLYVE-1 pHR and pHRI Jurkat. (E) Relationship between mLYVE-1 expression and bHA binding in cells co-incubated with bHA rabbit anti-mLYVE-1 polyclonal (0.5 µg/ml). bHA binding by hLYVE-1 pHRI Jurkat (G) and hLYVE-1 pHR Jurkat (H) when incubated with bHA either alone or in combination with hLYVE-1 mAb 893, isotype control or an excess on unlabelled hyaluronan (HA). Data are representative of two independent experiments.

The notion of a threshold of LYVE-1 surface density for HA binding predicts that it should be possible to reconstitute HA binding in LEC by artificially over-expressing LYVE-1 in these cells. To test this prediction, primary human dermal lymphatic endothelial cells (HDLEC) were supertransfected with hLYVE-1 using the lentiviral vector pHR and the level of bHA binding compared with that of control untransfected cells by a combination of flow cytometry and immunofluorescence microscopy. In addition, HDLEC were supertransfected with hLYVE-1 bearing a C-terminal GFP tag to enable direct detection of receptor without the use of LYVE-1-specific antibodies that may influence HA binding. As shown in Figure 4.3 A & B supertransfection led to a threefold increase in LYVE-1 surface density (MFI 721 v MFI 227) that was accompanied by high levels of bHA binding. Immunofluorescence microscopy revealed that GFP-tagged LYVE-1 co-localized with bHA staining at the cell surface, and most prominently at the borders between cells (Figure 4.4). Importantly, this binding of bHA to supertransfected HDLEC was fully displaced by competition with a 30-fold excess of unlabelled HA or co-incubation with LYVE-1 HA-blocking mAb 891. Moreover, analysis of bHA binding as a function of LYVE-1 surface level revealed a biphasic relationship, with the requirement of a minimal threshold of

LYVE-1 density (10-30 fluorescence units) for bHA binding followed by a proportional increase with LYVE-1 density (Figure 4.3, D).

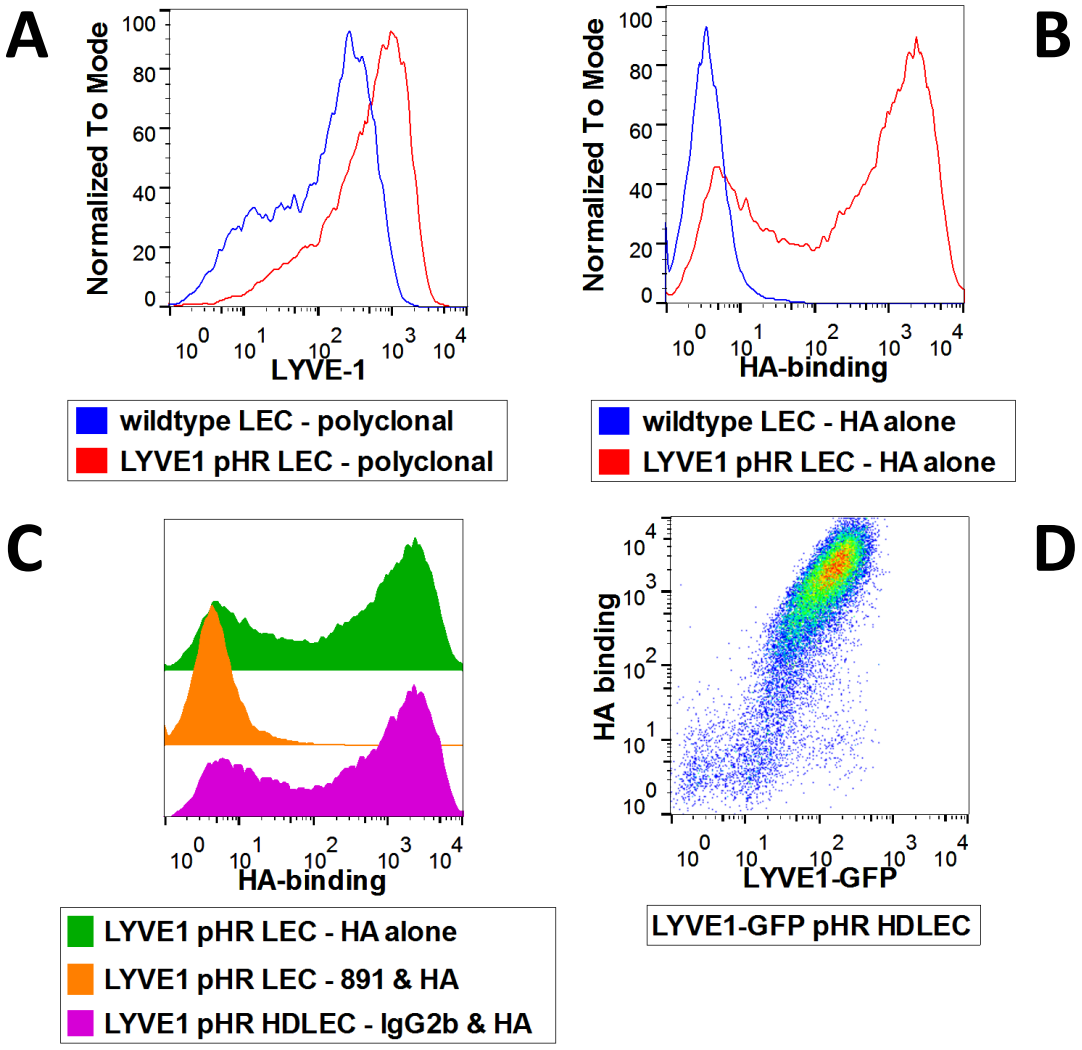
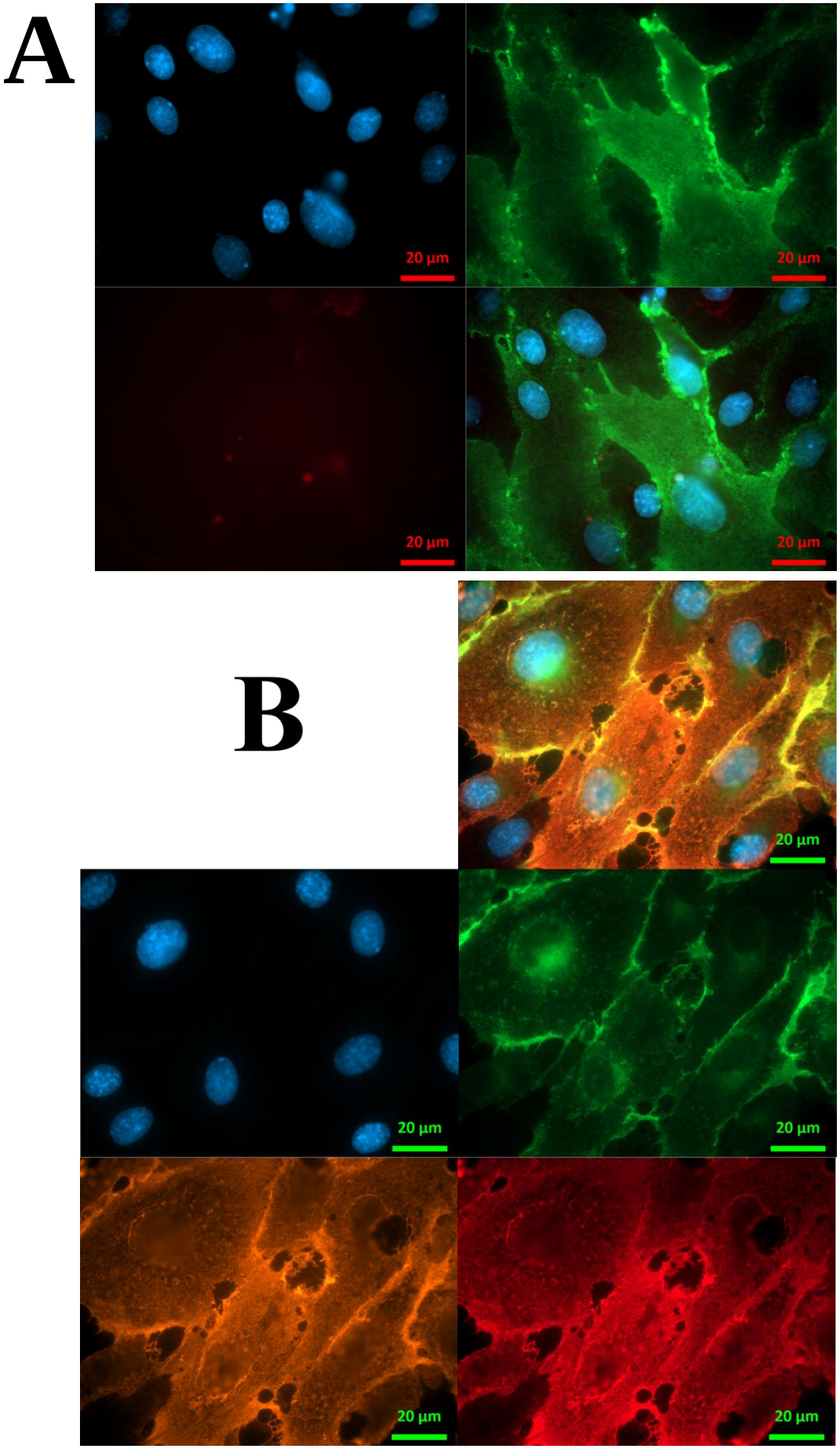


Figure 4.3. **Over-expression of human LYVE-1 in primary lymphatic endothelial cells using lentiviral infection**. Primary LEC were infected using a lentiviral vector (pHR) bearing the coding sequence of full length human LYVE-1 or LYVE-1-GFP and expanded in culture. Cells were lifted with Accutase, incubated with hLYVE-1 specific antibodies, biotinylated hyaluronan (HA) or isotype-matched controls as indicated, followed by appropriate secondary detection reagents and quantification of fluorescence using flow cytometry. (A) A polyclonal antibody was used to detect LYVE-1 expression by wildtype or hLYVE-1 pHR LEC. (B) Biotinylated hyaluronan (HA) binding by wildtype and hLYVE-1 pHR LEC. (C) HA binding by hLYVE-1 pHR LEC when incubated with HA alone, or simultaneously with hLYVE-1 mAb 893 or mouse IgG_1 isotype control. (D) HA binding by hLYVE-1-GFP pHR LEC shown in relation to LYVE-1 expression, as detected by GFP fluorescence. Data are from a single experiment.


A
20 µm
20 µm
20 µm
20 µm
B
20 µm
20 µm
20 µm
20 µm
20 µm

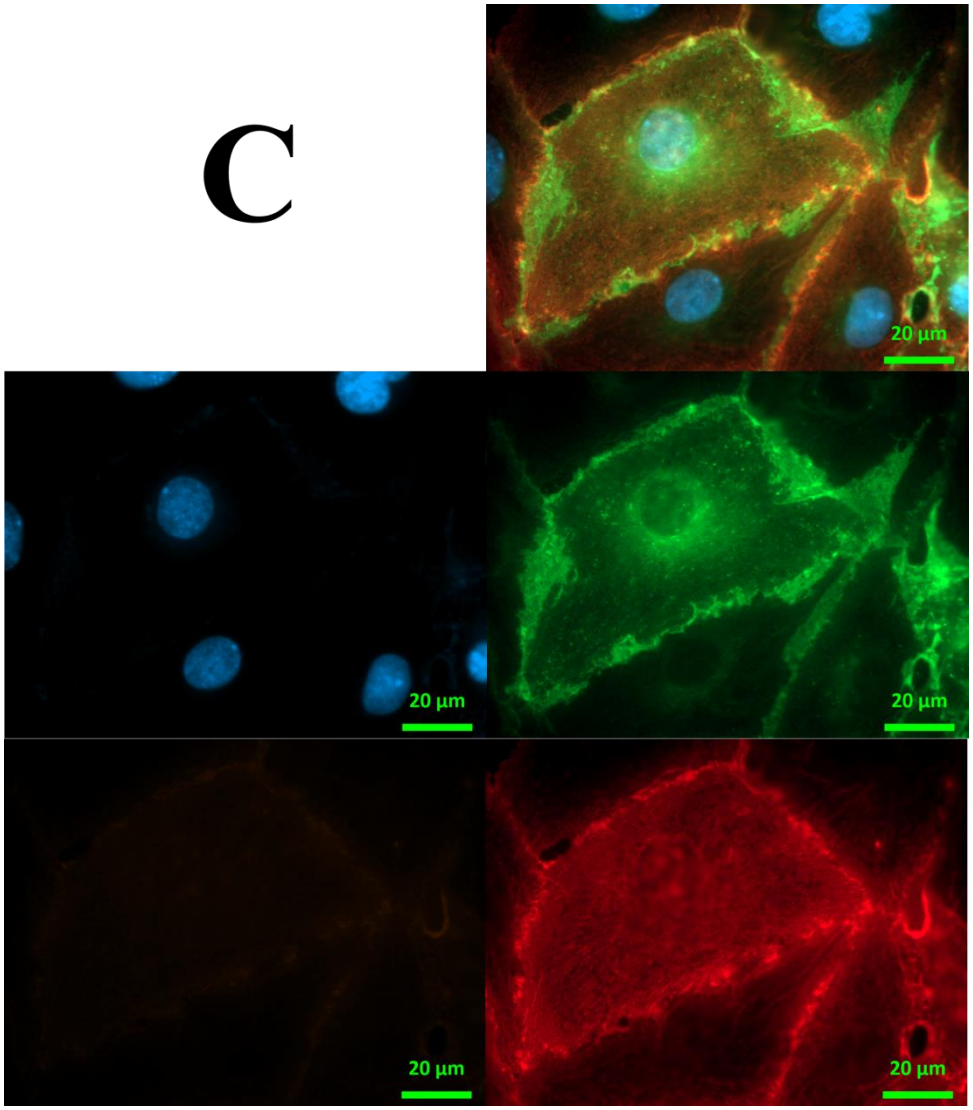


Figure 4.4. **Hyaluronan binding in adherent wildtype and hLYVE-1-GFP super-transfected HDLEC**. Primary human dermal lymphatic endothelial cells (HDLEC, **A.**) or HDLEC over-expressing GFP-tagged hLYVE-1 (hLYVE-1-GFP pHR HDLEC, **B** & **C**, *overleaf*) were cultured on gelatin-coated 8-chamber slides. Media was removed and the cells were blocked with 5% FCS, 0.05% sodium azide in PBS, prior to incubation with biotinylated HA (bHA) at 5 µg/ml either alone (**A, B**) or with hLYVE-1 mAb 891 at 20 µg/ml (**C**) in this buffer. Cells were fixed with freshly depolymerised formaldehyde, blocked once more, and incubated with goat-anti hLYVE-1 polyclonal (hLYVE-1 poly) at 1 µg/ml. Cell nuclei, bound hLYVE-1 poly, hLYVE-1-GFP and bHA were detected as follows: (**A**) Nuclei were stained with DAPI (*blue*), hLYVE-1 poly with donkey anti-goat IgG Alexa 488 (*green*) and bHA with streptavidin Alexa 647 (*red*). (**B, C**) Nuclei were stained with DAPI (*blue*), hLYVE-1-GFP by virtue of GFP fluorescence (*green*), bHA with streptavidin Alexa 594 (*orange*) and hLYVE-1 poly with donkey anti-goat IgG Alexa 647 (*red*). Images were captured using an inverted epifluorescence microscope (Zeiss Axiovert S100) fitted with a 100x oil-immersion objective and a Hammatsu digital camera. Images taken from a single experiment.

4.3.2 Triggering hyaluronan binding by lymphatic endothelial cells using monoclonal antibodies directed against human LYVE-1

Increasing the density of LYVE-1 molecules on the surface of HDLECs clearly results in induction of HA binding, however there is no evidence to suggest that a similar mechanism operates *in vivo*. However, focal increases in density arising from redistribution of LYVE-1 molecules could potentially be used to attain the threshold required for HA binding in discrete areas of the cell surface. A similar mechanism has been proposed to explain induction of HA binding following antibody-mediated cross-linking of CD44 molecules in transfected cell lines that do not constitutively bind hyaluronan (Lesley et al., 1993). A large number of LYVE-1 mAbs have been generated both commercially and within the Jackson laboratory, but to-date these antibodies have not characterised in terms of their ability to enhance HA binding.

To assess the influence of hLYVE1 mAbs on HA binding, primary HDLEC were isolated from freshly resected human skin using a combination of mechanical and enzymatic disruption, followed by immunomagnetic selection on MACS® beads using LYVE-1 mAb 8C. HDLEC were cultured on gelatin-coated tissue culture plastic until they had formed confluent monolayers, then lifted using Accutase, and incubated for thirty minutes at 4^{o}C either with biotinylated HA (bHA) alone or with a combination of bHA and 8C mAb added together, prior to analysis by two-colour flow cytometry. As shown in Figure 4.5, cells incubated with bHA alone, followed by a LYVE-1 detection antibody (bHA, then 8C mAb) displayed only residual binding. However, the combination of bHA and 8C mAb together led to a marked induction of HA binding that correlated with LYVE-1 expression level. Once again the bound bHA could be fully displaced by simultaneous incubation with the commercial HA blocking mAb 891.

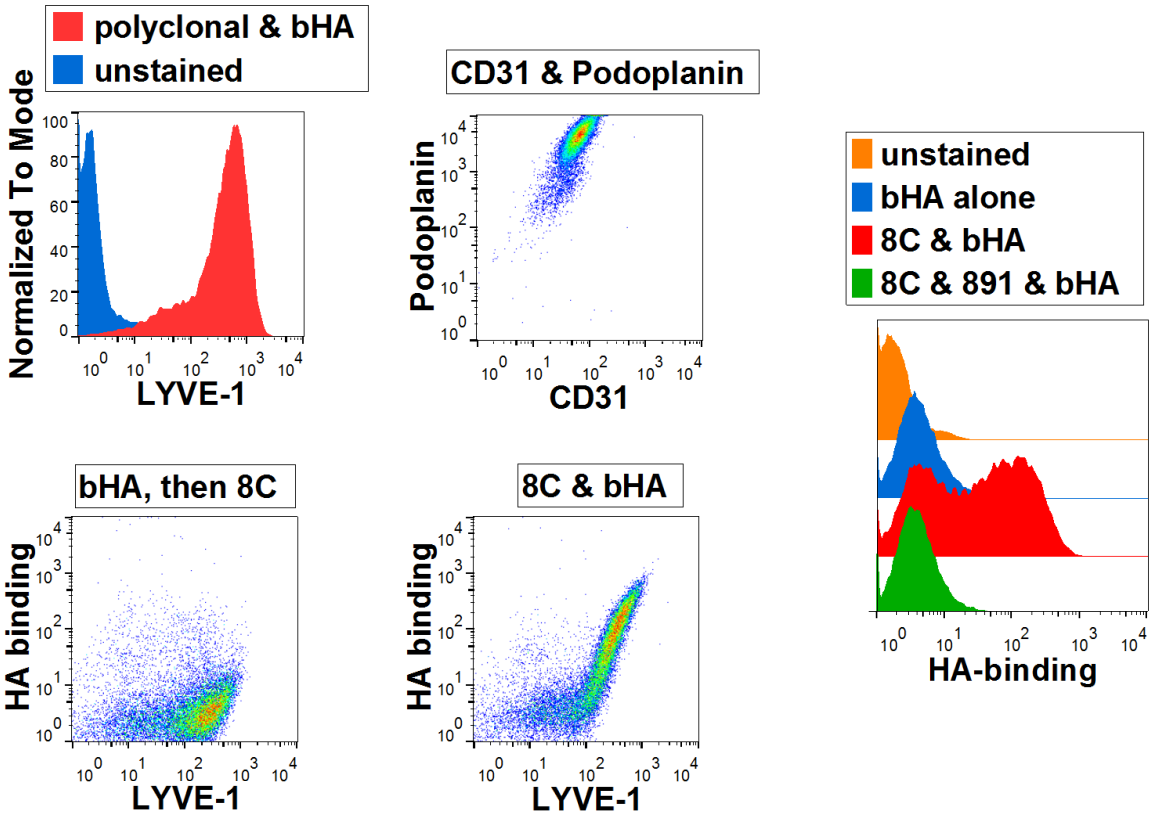
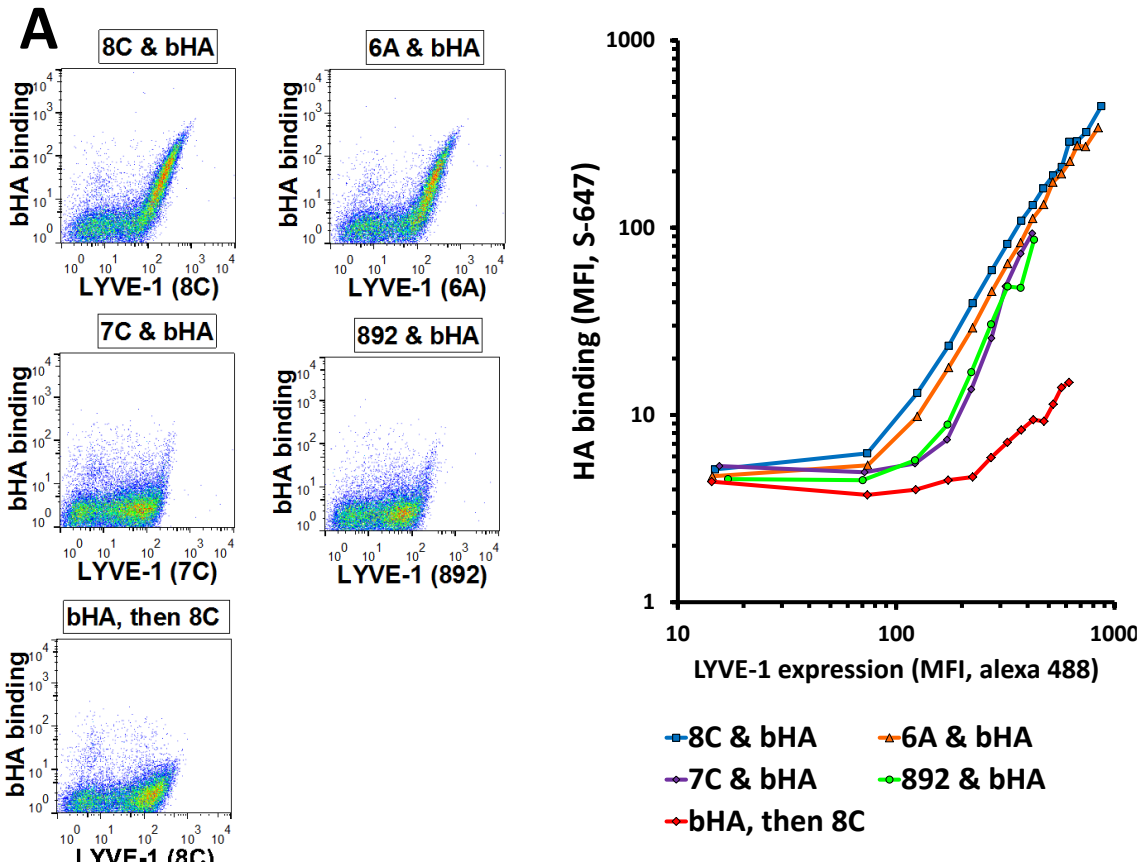
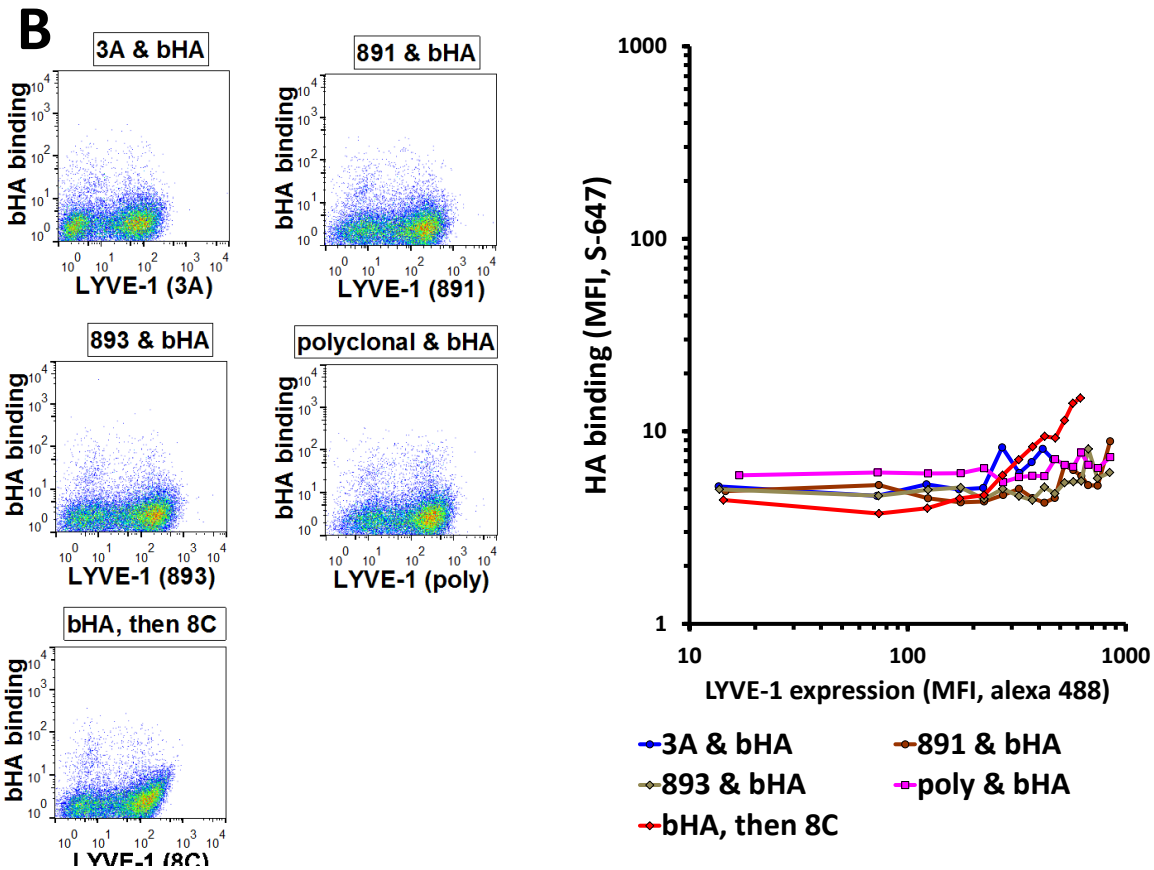


Figure 4.5. **Induction of hyaluronan binding by co-incubation of primary lymphatic endothelial cells with appropriate LYVE-1-specific monoclonal antibodies.** Primary Human Dermal Lymphatic Endothelial Cells (HDLEC) were isolated from resected human skin using manual and enzymatic disruption combined with MACS immuno-selection. Cells were expanded in culture on gelatin-coated tissue-cultureware, lifted with Accutase and phenotyped by flow cytometry using antibodies recognising the pan-endothelial marker *CD31*, the LEC-specific marker *Podoplanin* and the LEC-specific marker LYVE-1 (*polyclonal*). In addition, cells were tested for binding of biotinylated hyaluronan (*bHA*) when incubated with bHA alone, bHA followed by hLYVE-1 mAb 8C (*bHA, then 8C*), bHA combination with 8C mAb (*8C & bHA*) or bHA in combination with 8C mAb and hLYVE-1 mAb 891 (*8C & 891 & bHA*). Data are the fluorescence intensity at the relevant wavelengths of 20 000 cells/sample, and representative of multiple experiments (>3).

Following the initial observation that 8C mAb potentiates HA binding to HDLEC, a full panel of commercial and in-house generated LYVE-1 antibodies was screened for comparable effects using the same assay system described above. This panel included mAbs 6A and 7C, which bind a similar epitope to 8C, mAb 892, a non HA-blocking mAb that recognises an as yet undetermined epitope, and mAbs 3A, 891 and 893, all of which have been previously characterised as HA-blockers (Johnson et al., 2007 and R&D Systems). The results (Figure 4.6) revealed that all non HA-blocking mAbs induced bHA binding, albeit to different levels. For example, the largest induction of bHA binding was observed with mAbs 8C and 6A (60-fold increase relative to controls), whereas mAbs 892 and 7C had a more modest effect (10-fold increase). Moreover, analysis of bHA binding as a function of LYVE-1 surface levels confirmed the presence of a threshold LYVE-1 density required before induction of HA binding could be detected.

Further experiments were conducted to demonstrate the specificity of antibody-mediated potentiation of HA binding, and to determine the effect of varying the sequence of incubation with bHA or mAbs (Figure 4.7). Competition by an excess of unlabelled HA or co-incubation with blocking mAbs 3A, 891 or 893 was sufficient to block the potentiating effects of 8C mAb on HDLEC. Furthermore, induction of bHA binding was also observed when cells were pre-incubated with 8C mAb prior to addition of bHA, but not when added to cells after prior bHA incubation and subsequent washing. The size of the potentiation effect was consistently smaller when cells were pre-incubated, rather than co-incubated with 8C mAb, but this was coincident with a decrease in amount of bound antibody detected at the end of the experiment (data not shown). Finally, the magnitude of antibody-mediated potentiation of HA binding was found to decrease with time spent in culture, along with LYVE-1 expression level, and so early-passage cells (passage 2 – 5) were used in all subsequent experiments (Figure 4.8).


A
8C & bHA
6A & bHA
7C & bHA
892 & bHA
bHA, then 8C
bHA binding
LYVE-1 (8C)
LYVE-1 (6A)
LYVE-1 (7C)
LYVE-1 (892)
HA binding (MFI, S-647)
LYVE-1 expression (MFI, alexa 488)
8C & bHA
6A & bHA
7C & bHA
892 & bHA
bHA, then 8C


B
3A & bHA
891 & bHA
893 & bHA
polyclonal & bHA
bHA, then 8C
bHA binding
LYVE-1 (3A)
LYVE-1 (891)
LYVE-1 (893)
LYVE-1 (poly)
HA binding (MFI, S-647)
LYVE-1 expression (MFI, alexa 488)
3A & bHA
891 & bHA
893 & bHA
poly & bHA
bHA, then 8C

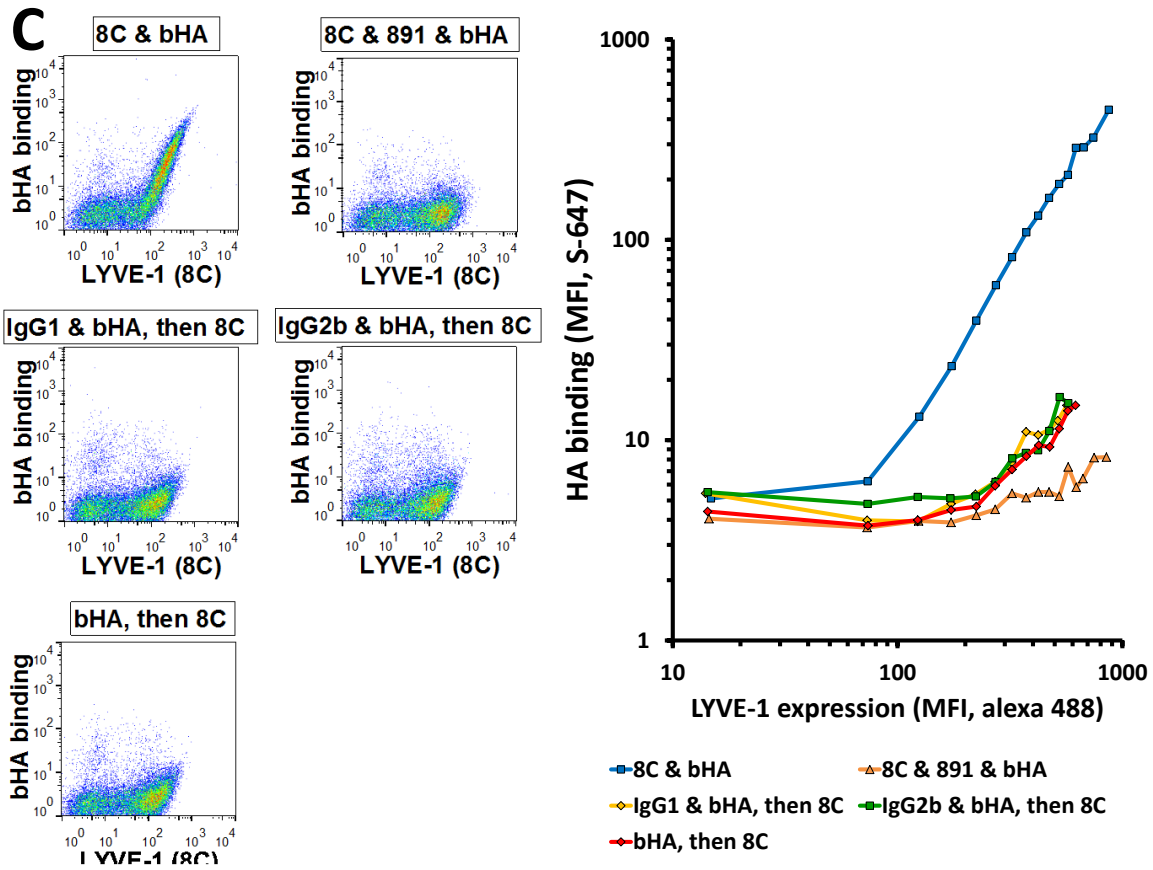


Figure 4.6. **Influence of anti-human-LYVE-1 monoclonal antibodies on hyaluronan binding by primary HDLEC and the relationship between LYVE-1 expression and antibody-mediated potentiation of HA binding.** Cultured primary HDLEC were lifted with Accutase and incubated with biotinylated HA (bHA) either alone, followed by LYVE-1 mAb 8C (to assess the constitutive level of HA binding, relative to LYVE-1 expression) or in the presence of individual LYVE-1 mAbs or control Ig, to assess the effect on bHA binding. Bound bHA and mAbs were then detected with appropriate secondary reagents and flow cytometry. For simplicity, the mAbs are separated into groups, those that potentiate HA binding (A) and those that do not (B). All mAbs in (B) have previously been shown to block hyaluronan binding by LYVE-1. Panel (C) shows the influence of isotype-matched control Ig and co-incubation of a potentiating mAb (8C) and a blocking mAb (891) on bHA binding by HDLEC. The graph in each panel shows the mean fluorescence intensity (MFI, S-647) of bHA binding at intervals of LYVE-1 expression (MFI, Alexa 488) for each of the adjacent flow cytometry plots. Data are representative of three independent experiments.

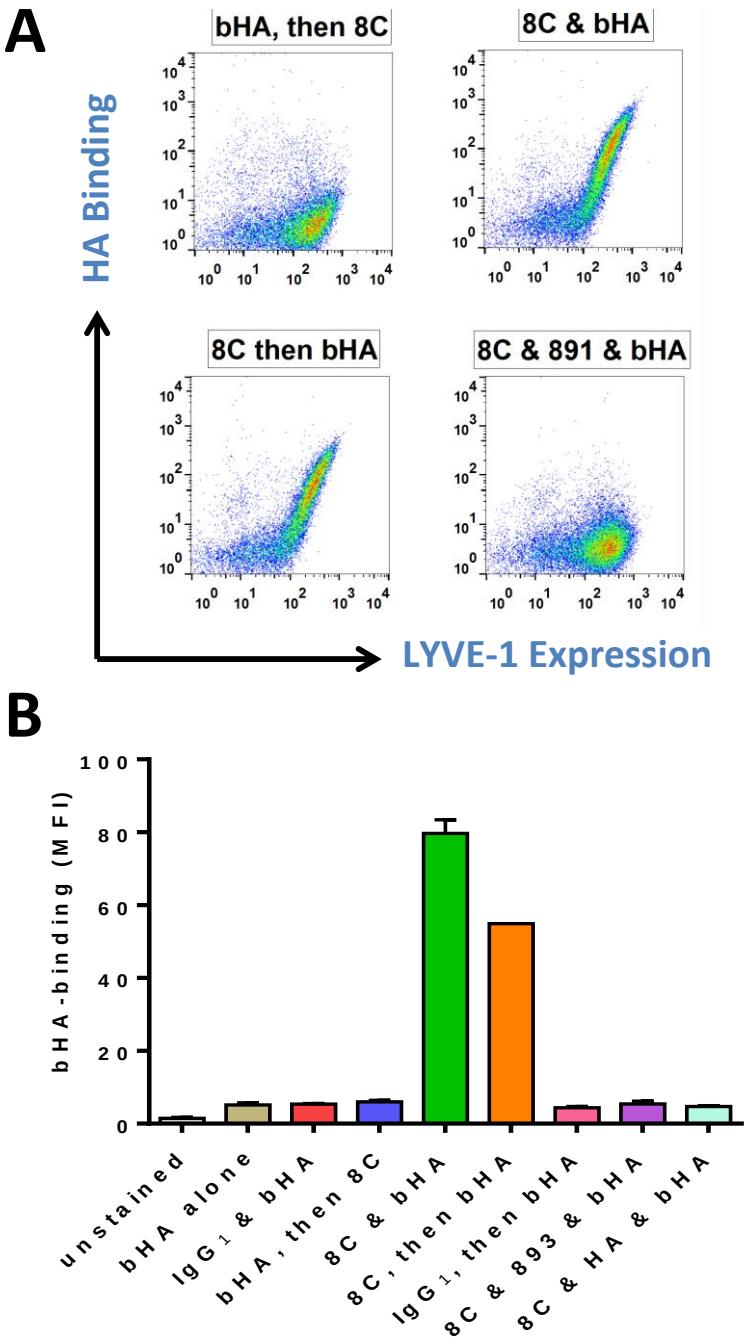


Figure 4.7. **Quantitation of mAb-mediated potentiation of HA binding to HDLEC resulting from different sequences of mAb/HA incubation.** Cultured primary HDLEC were lifted with Accutase and incubated with biotinylated HA (bHA) either alone, or in combination with individual LYVE-1 mAbs, isotype-matched control Ig, or an excess of unlabelled HA, to assess the effect on bHA binding using flow cytometry. In addition, the sequence of incubation with LYVE-1 mAbs or bHA was varied as indicated, with three washing steps between reagents. (A) Relationship between LYVE-1 expression and bHA binding in HDLEC when incubated 8C mAb, 891 mAb & bHA in the sequence indicated (B) Quantitation of bHA binding by HDLEC under the conditions described. Data are the mean fluorescence intensity (MFI) ± SD of 20 000 cells/sample (n = 3) and are representative of three independent experiments.

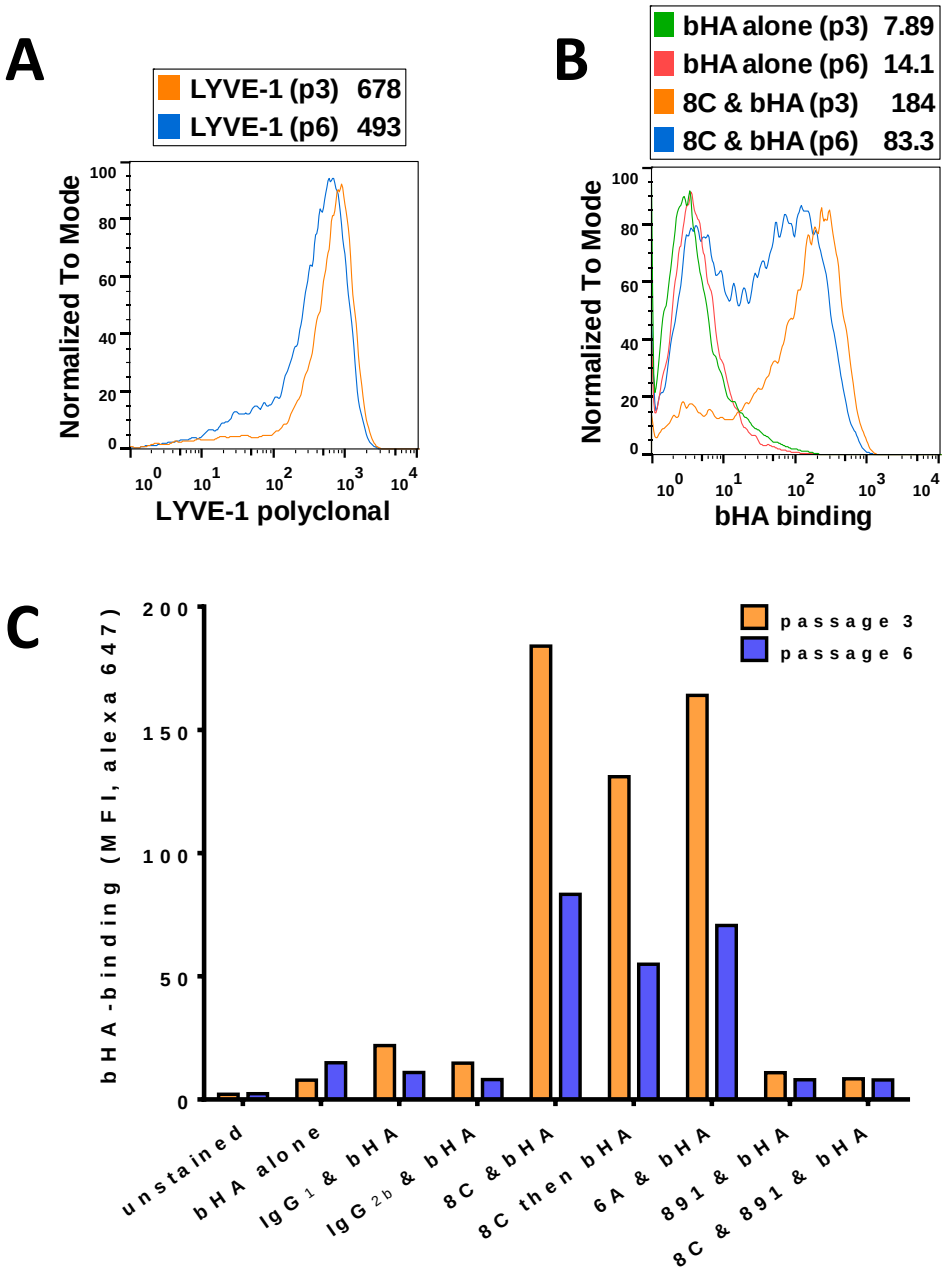


Figure 4.8 **Influence of passage on LYVE-1 expression and antibody-mediated potentiation of HA binding.** A single batch of primary HDLEC were cultured to early (p3) and late passage (p6), lifted with Accutase and incubated with biotinylated HA (bHA) either alone, or in combination with individual LYVE-1 mAbs or isotype-matched control Ig, to assess the effect on bHA binding using flow cytometry. In addition, the sequence of incubation with LYVE-1 mAbs or bHA was varied as indicated, with three washing steps between reagents. Representative flow cytometry panels showing (A) LYVE-1 expression by HDLEC as detected by a polyclonal Ab, (B) constitutive and Ab-potentiated bHA binding. (C) Quantitation of bHA binding by under the conditions described. Data are the mean fluorescence intensity (MFI) 20 000 cells/sample from a single experiment.

4.3.3 Influence of LYVE-1 mAbs on HA binding by adherent HDLEC monolayers

In the experiments described thus far, the influence of LYVE-1 mAbs on HA binding has been tested using cells lifted from cell-culture plastic using Accutase® solution. This treatment will result in a redistribution of LYVE-1 molecules on the cell surface, which may be a significant factor as the surface density of receptors is predicted to regulate HA binding. To determine the influence of potentiating mAbs on HA binding by a 'native' distribution of LYVE-1 molecules, adherent monolayers of HDLEC were incubated with bHA in combination with LYVE-1 mAbs and visualized using immunofluorescence microscopy (Figure 4.9).

Cells incubated with bHA alone did not bind bHA and had a generally even, diffuse distribution of LYVE-1 with occasional areas of higher density at the cell border, but an absence of the LYVE-1-enriched flap valves observed for lymphatic vessels *in vivo*. Incubation of the monolayer with bHA and 8C mAb for 30 minutes at room temperature resulted in a distinctive punctate distribution of LYVE-1, and induction of bHA binding in areas with enriched for LYVE-1. Binding of bHA was generally weaker compared to LYVE-1 super-transfected HDLEC, which have ~10-fold higher LYVE-1 expression and bHA binding (Figure 4.4). However, induction of bHA binding by 8C mAb could be efficiently blocked by co-incubation with HA-blocking mAb 891. The punctate distribution of LYVE-1 resulting from incubation with 8C mAb is consistent with a clustering mechanism resulting from antibody cross-linking of LYVE-1 molecules. Interestingly, no such clustering was observed following incubation with mAb 891 alone or in combination with 8C. The high density of LYVE-1 molecules within clusters is likely to promote binding of bHA by increasing the avidity of the interaction, in a manner simulating a global increase in surface density resulting from increased expression.

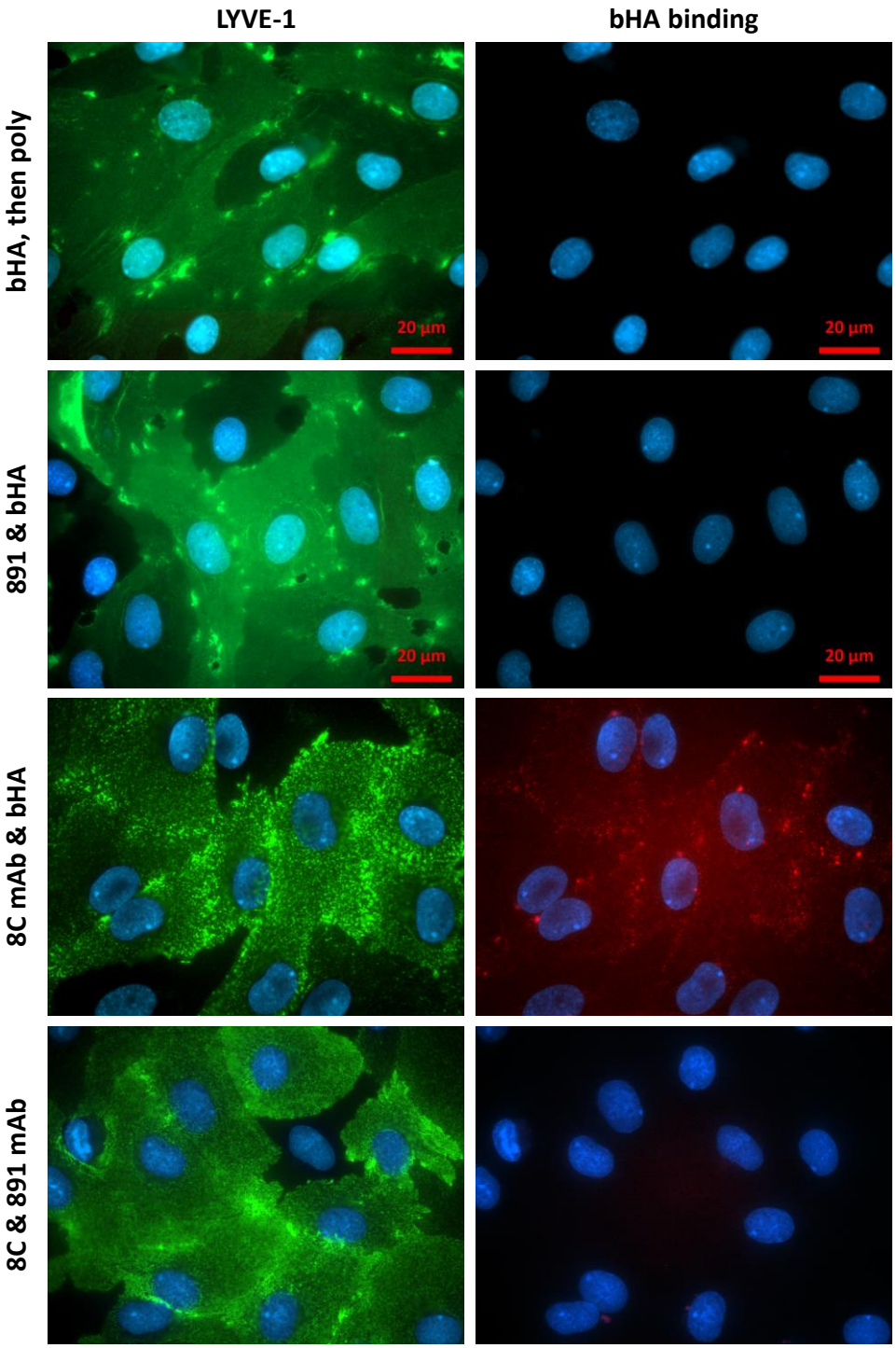


Figure 4.9. **Influence of anti-human-LYVE-1 monoclonal antibodies on hyaluronan binding by adherent primary LEC.** Primary LEC were cultured on 8-chamber slides. Cells were incubated with biotinylated HA (bHA) either alone or with hLYVE-1 mAbs 8C or 891, as indicated. Cells were fixed with freshly depolymerised formaldehyde and incubated with goat-anti hLYVE-1 polyclonal (poly). Cell nuclei were stained with DAPI (*blue*), hLYVE-1 poly with anti-goat IgG Alexa 488 (*green*) and bHA with streptavidin Alexa 647 (*red*). Images were captured using an inverted epifluorescence microscope (Zeiss Axiovert S100) fitted with a 100x oil-immersion objective and a Hammatsu digital camera. Images representative of three independent experiments.

4.3.4 Antibody-mediated potentiation of HA binding to LYVE-1 transfected cells

A variety of cell types have been transfected with LYVE-1 in order characterise the activity of the receptor, including 293T fibroblasts (Nightingale, 2004), and Jurkat, an immortalized T-cell line (see section 4.3.1). To determine whether either of these cell types are a suitable model for study of antibody-mediated potentiation of HA binding, the influence of hLYVE-1 mAbs on bHA binding was quantified using the assay described for HDLEC. The results revealed that potentiation can also occur in both transfected HEK293T and Jurkat cells, leading to a significant enhancement over the constitutive level of HA binding (Figure 4.10 & Figure 4.11). As had been observed with primary cells, the largest potentiation of bHA binding was mediated by mAbs 8C and 6A, while 892 and 7C had only a modest influence on binding (Figure 4.10). Moreover, the potentiating effect of mAbs 8C, 6A and 892 was concentration dependent (Figure 4.11). When titrated against a fixed number of hLYVE-1 pHR Jurkat cells, a concentration of 1-2 µg/ml was sufficient for both maximal binding of 8C and 6A and maximal potentiation of bHA binding. By contrast, mAb 892 was not in excess even at 20 µg/ml, suggesting that the lower potentiating capacity of this antibody is due to a low binding affinity for LYVE-1.

A comparison was also made of the influence of LYVE-1 mAbs on bHA binding by hLYVE-1 pHR and pHRI Jurkat cells, in order to determine whether LYVE-1 expression level is a limiting factor (Figure 4.12). As was the case for HDLEC, potentiating antibodies such as 8C and 6A did not induce bHA binding in cells with the lowest LYVE-1 expression (pHRI), but did significantly enhance constitutive bHA binding by cells expressing high levels of LYVE-1 (pHR). Furthermore, two-colour flow cytometry revealed that potentiation of bHA binding is seen only above a threshold LYVE-1 expression, and plateaus in cells with the highest surface density of LYVE-1 (Figure 4.12, B). Taken

together, these data suggest that both 293T and Jurkat cells are appropriate models for study of Ab-mediated potentiation of HA binding, most likely because the mechanism is a physical one and largely independent of cell-type specific factors, such as intracellular signalling or surface organisation of LYVE-1 molecules.

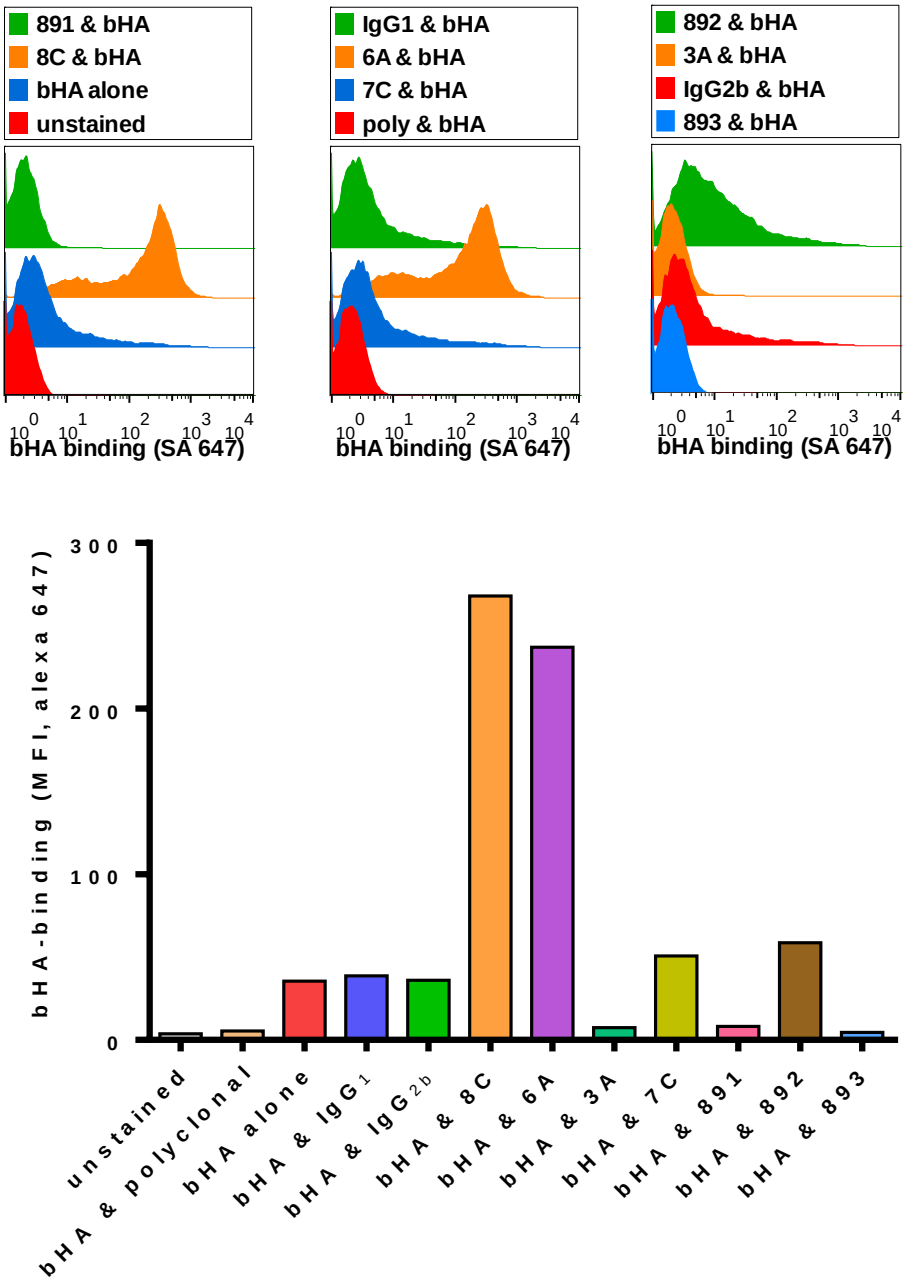


Figure 4.10. **Influence of anti-human-LYVE-1 monoclonal antibodies on hyaluronan binding by LYVE-1-expressing HEK 293T cells.** Stably-transfected hLYVE-1 HEK 293T cells were lifted using 5mM EDTA in PBS and incubated with biotinylated HA (bHA) either alone or in combination with hLYVE-1-specific antibodies or isotype-matched control Ig, to assess the effect on bHA binding using flow cytometry. Data are the mean fluorescence intensity (MFI) of 20 000 cells/sample from a single experiment.

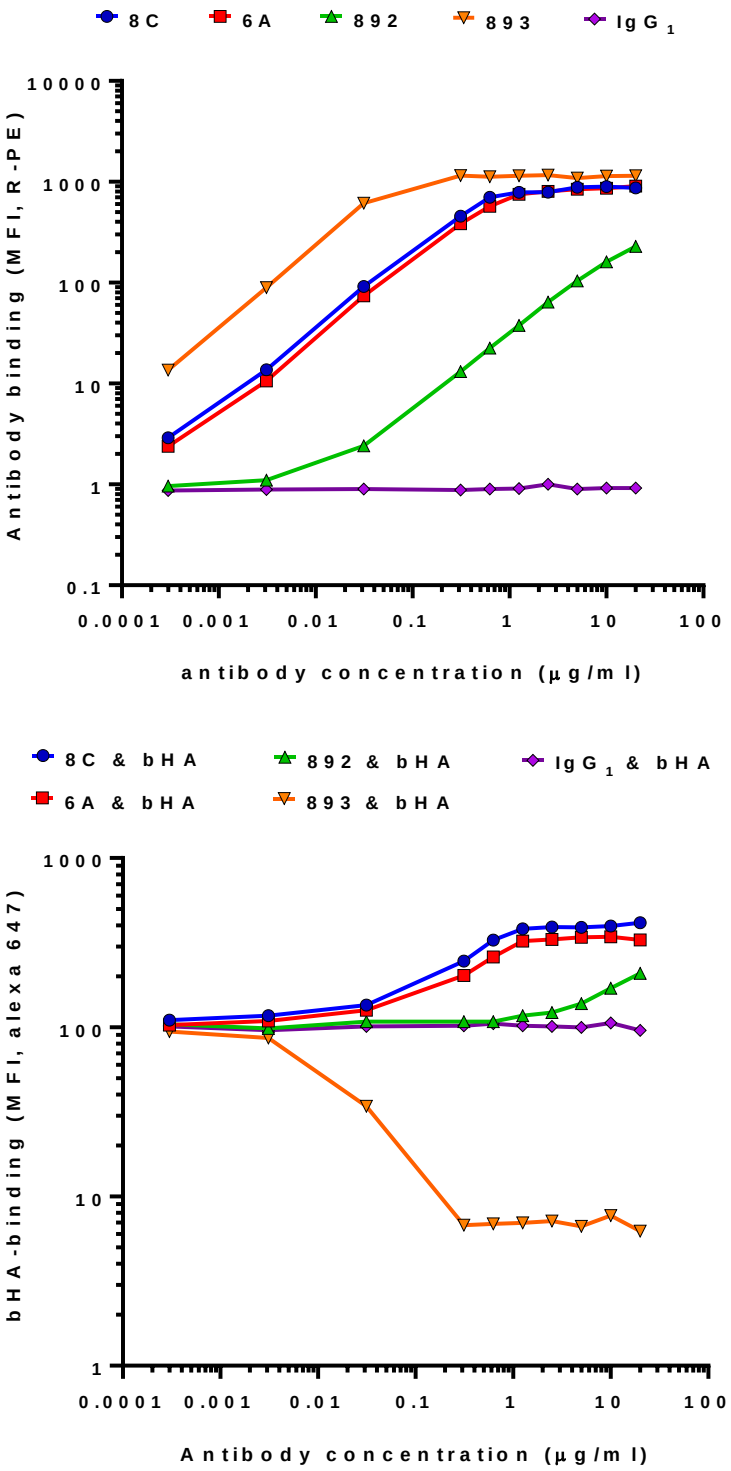


Figure 4.11. **Influence of anti-hLYVE-1 monoclonal antibodies on hyaluronan binding by hLYVE-1-GFP transfected Jurkat cells.** Human LYVE-1 pHR Jurkat cells were incubated at 1.66 x 10^6 cells/ml with biotinylated HA (bHA) either alone or in the presence of individual hLYVE-1-specific mAbs or control Ig, at increasing Ig concentration, to assess the effect on bHA binding. Bound Ig (*top panel*) or bHA (*bottom panel*) were detected with anti-mouse IgG Alexa 488 and streptavidin Alexa 647 respectively. Data are the mean fluorescence intensity (MFI) 20 000 cells/condition as measured by flow cytometry and are representative of two independent experiments.

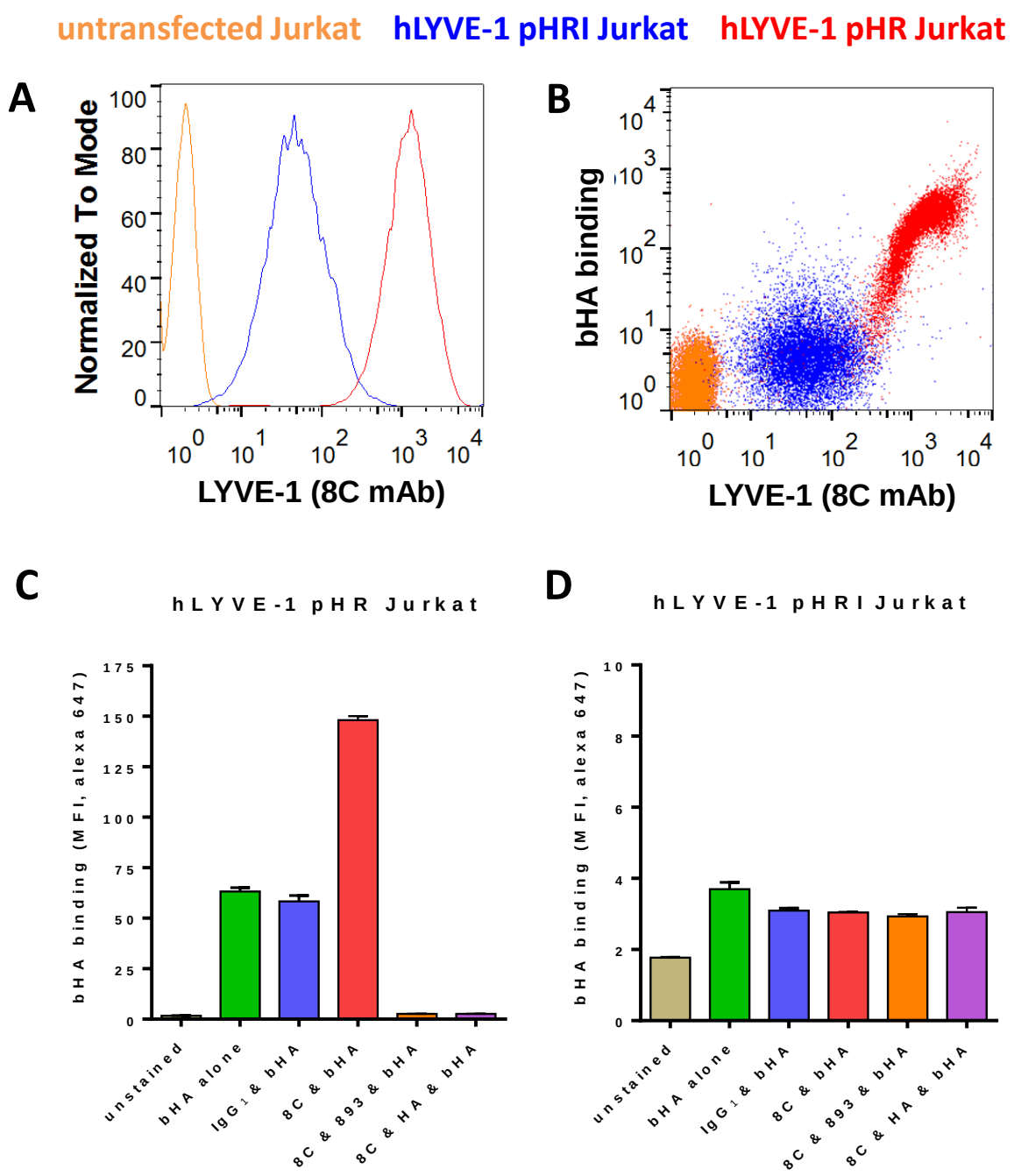


Figure 4.12. **Influence of LYVE-1 expression level on antibody-mediated potentiation of HA binding to hLYVE-1 transfected Jurkats.** Jurkat cells expressing high (pHR) or low (pHRI) levels of LYVE-1 were incubated with biotinylated hyaluronan (bHA) either alone or in combination with LYVE-1 specific antibodies, isotype-matched controls or unlabelled hyaluronan (HA) to assess LYVE-1 expression and/or bHA binding, as detected by flow cytometry. (A) Comparison of hLYVE-1 expression using 8C mAb. (B) Relationship between hLYVE-1 expression and bHA binding in cells incubated with 8C mAb and bHA simultaneously. (C, D) Quantification of bHA binding by hLYVE-1 pHR and pHRI cells respectively under the conditions described. Data are the mean fluorescence intensity (MFI) of 20 000 cells/sample ± SD (n = 3) and are representative of two independent experiments.

4.3.5 Effect of LYVE-1 antibodies on hyaluronan binding by mouse LYVE-1 transfected Jurkat cells

As described in Chapter 3, monoclonal antibodies raised against mouse LYVE-1 in the Jackson laboratory and elsewhere were found to block HA binding by the receptor, albeit to different degrees. The discovery of a potentiating antibody would provide a valuable reagent to test the functional consequences of inducing HA binding in *in vitro* assays or mouse models of inflammation and disease. To this end, samples of all commercially available anti-mLYVE-1 mAbs were tested for their influence on HA binding by mLYVE-1 pHR Jurkat cells, using MAB2125, a potent HA blocker, as a control (Figure 4.13). Unfortunately, two of the antibodies (14-4 and 4D17) were found to be potent blockers of HA binding and the third (E9VA4) could not be shown to recognise mLYVE-1 using flow cytometry.

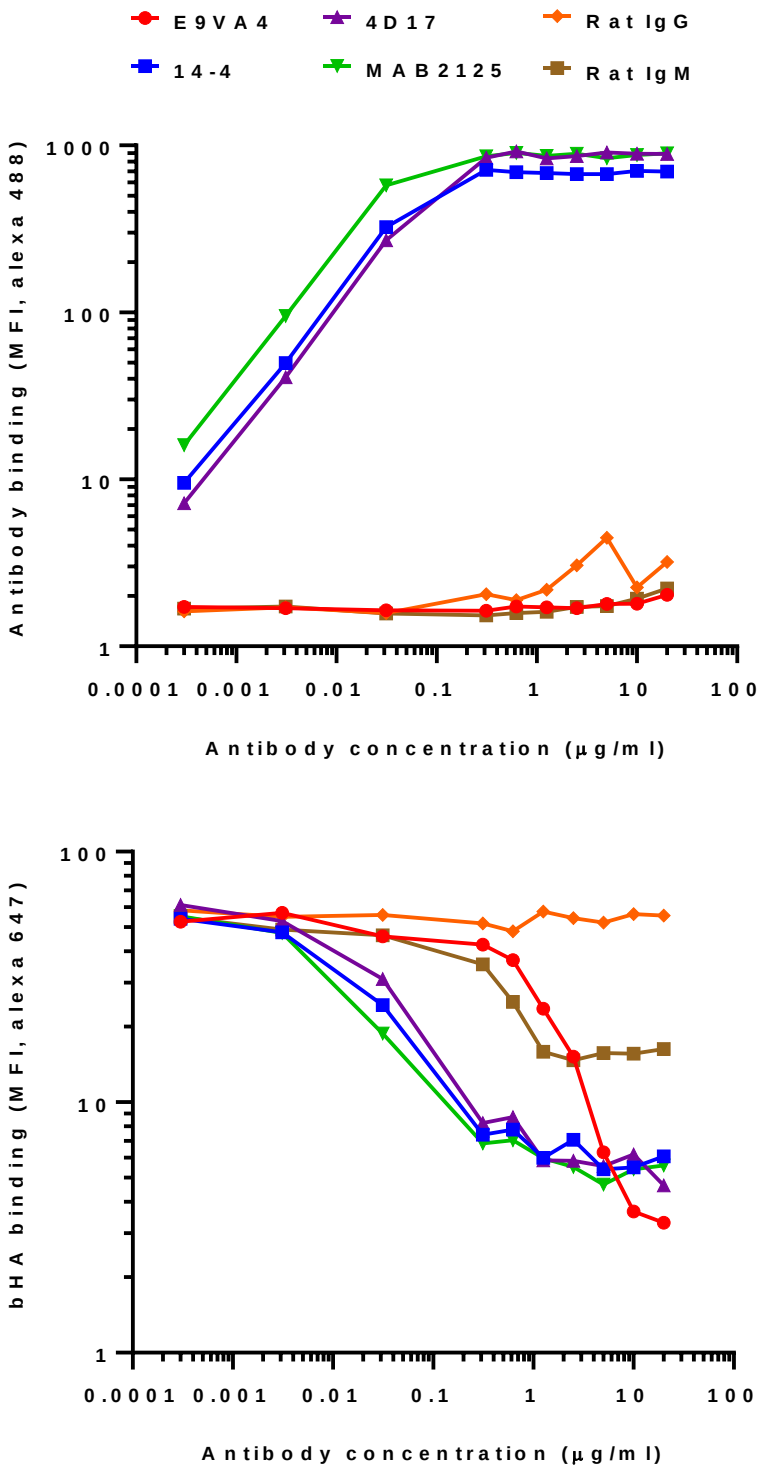


Figure 4.13. **Influence of commercially sourced anti-mouse-LYVE-1 monoclonal antibodies on hyaluronan binding by Jurkat cells expressing mouse LYVE-1.** Mouse LYVE-1 pHR Jurkat cells were incubated at 1.66 x 10^6 cells/ml with biotinylated HA (bHA) either alone or in the presence of individual mLYVE-1-specific mAbs or control Ig, at increasing Ig concentration, to assess the effect on bHA binding. Bound Ig (top panel) or bHA (bottom panel) were detected with appropriate secondary reagents. Data are the mean fluorescence intensity (MFI) of 20 000 cells/condition as measured by flow cytometry from a single experiment.

4.3.6 Mechanism of antibody-mediated potentiation of hyaluronan binding by LYVE-1

The potentiating effects of LYVE-1 mAbs on HA binding are reminiscent of mAbs IRAWB14 and IRAWB26 that are known to enhance HA binding by CD44 in a manner dependent on mAb bivalency (Lesley et al., 1993). Incubation of HDLEC monolayers with 8C or 6A mAb leads to redistribution of LYVE-1 into punctate clusters, a phenomenon that likely involves antibody cross-linking of LYVE-1 dimers (Figure 4.14). However, there are a number of other potential mechanisms that may be at play, including a conformational change in the receptor upon mAb binding that increases HA binding affinity, artificial dimerization of LYVE-1 monomers, or downstream signalling events that lead to activation of HA binding.

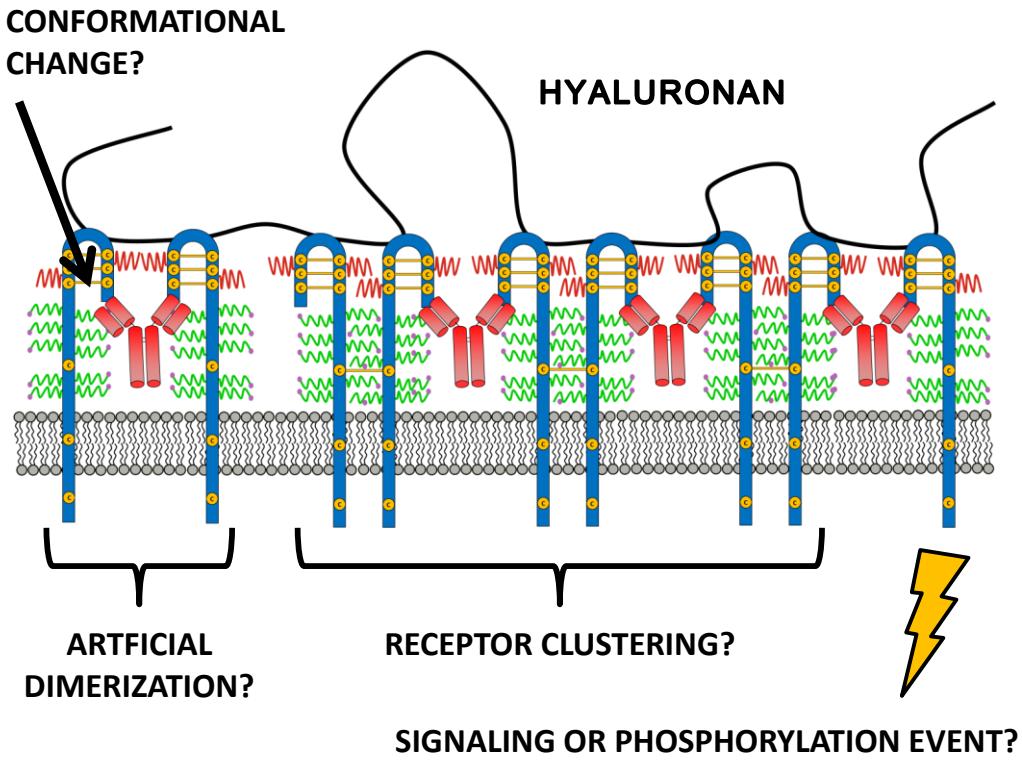


Figure 4.14. **Potential mechanisms of antibody-mediated potentiation of HA binding.** Schematic representation of hLYVE-1 mAb 8C (*red*) bound to LYVE-1 monomers and dimers (*blue*) present in the plasma membrane of a lymphatic endothelial cell (*grey*). A hyaluronan chain (*black*) is shown bound by LYVE-1 molecules.

4.3.7 Enhancement of HA binding to LYVE-1 by monoclonal antibodies – dependence on antibody bivalency

In view of the observation that LYVE-1 mAbs which induce HA binding also promote receptor clustering, it was reasonable to assume that their mode of action might involve receptor crosslinking - a process that requires antibody bivalency. As a means of exploring this possibility, the capacity of LYVE-1 mAbs to induce HA binding in HDLEC as intact Ig was compared to that of the corresponding monovalent Fab fragments. Accordingly, Fab were prepared from mAbs 8C and 6A by controlled digestion of mAb using Ficin in the presence of cysteine, according to the manufacturer's protocol (Pierce). The resulting digestion products were further separated by Superdex S200 size-exclusion chromatography to ensure effective removal of contaminating $F(ab')_2$ or aggregated Fab followed by purification of monovalent Fab on Protein A Agarose. As assessed by non-reducing LDS-PAGE (Figure 4.15), the procedure yielded Fab that migrated as a single major band at a position close to the expected molecular weight of 49 kDa.

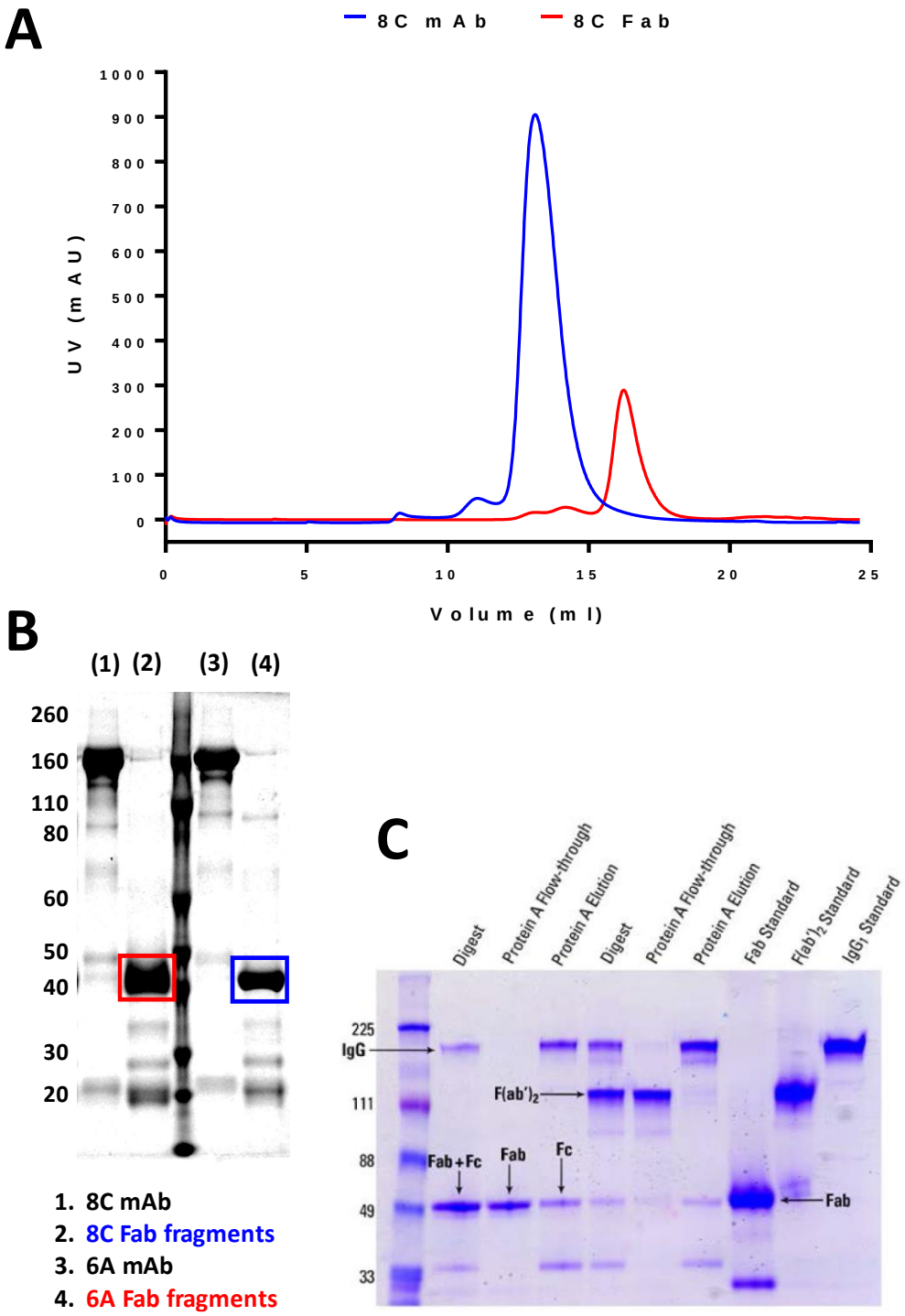


Figure 4.15. **Generating Fab fragments of anti-human-LYVE-1 monoclonal antibodies 8C and 6A.** Fab fragments of hLYVE-1 mAbs 8C and 6A were generated by Ficin digest according to the manufacturer's instructions (Pierce). Samples of intact antibody and Fab fragments were further purified by size-exclusion chromatography using a superdex S200 10/300 column (GE) (A). Fractions spanning the appropriate peaks were pooled and analysed for purity by non-reducing LDS-PAGE (B). The reference SDS-PAGE gel provided by the manufacturer is shown for comparison, note the size of the molecular weight standards in the last three lanes (C). Data are representative of three independent Fab preparations.

As a test of the integrity of the purified Fab fragments, their binding capacity for LYVE-1 was compared with that of intact Ig using flow cytometry. Both 8C and 6A Fabs exhibited a similar capacity to bind hLYVE-1 pHR Jurkat cells as their intact counterparts in terms of the molar concentration (in terms of Fab) required for saturating binding (Figure 4.16). The small decrease in mean fluorescence intensity can be attributed to the loss of the Fc epitope recognised by the polyclonal secondary antibody. Next, the capacity of the Fab fragments to induce bHA binding was assessed using intact Ig as a comparison. Conversion of both 8C and 6A to monovalent Fab fragments significantly reduced, but did not completely inhibit their capacity to induce HA binding to LYVE-1 transfected Jurkat (Figure 4.16 & 4.19). Indeed at saturating concentrations, each Fab retained approximately a quarter of the potency of intact antibody (Figure 4.18).

Similar results were obtained with three separate batches of primary HDLEC, although the influence of Fab fragments on HA binding was slightly smaller (Figure 4.17 & 4.19). These results are consistent with the conclusion that antibody-mediated potentiation of HA binding involves cross-linking of LYVE-1 molecules, but indicate that other mechanisms may also be involved. Interestingly, Fab fragments prepared from mAbs IRAWB14 and IRAWB26 were also found to induce a small increase in HA binding by CD44, which was attributed to low levels of contamination with aggregated Fab (Lesley et al., 1993). Analysis of 8C and 6A Fab preparations by LDS-PAGE and quantitation of band intensity using a Li-Cor Odyssey Imager suggested that contamination with aggregated Fab was extremely low (Figure 4.15, B and data not shown). However, it was decided to further characterize Fab fragment preparations by determining their influence on LYVE-1 distribution in adherent HDLEC monolayers, and on the HA binding capacity of recombinant LYVE-1 protein (see sections 4.3.8 & 4.3.9).

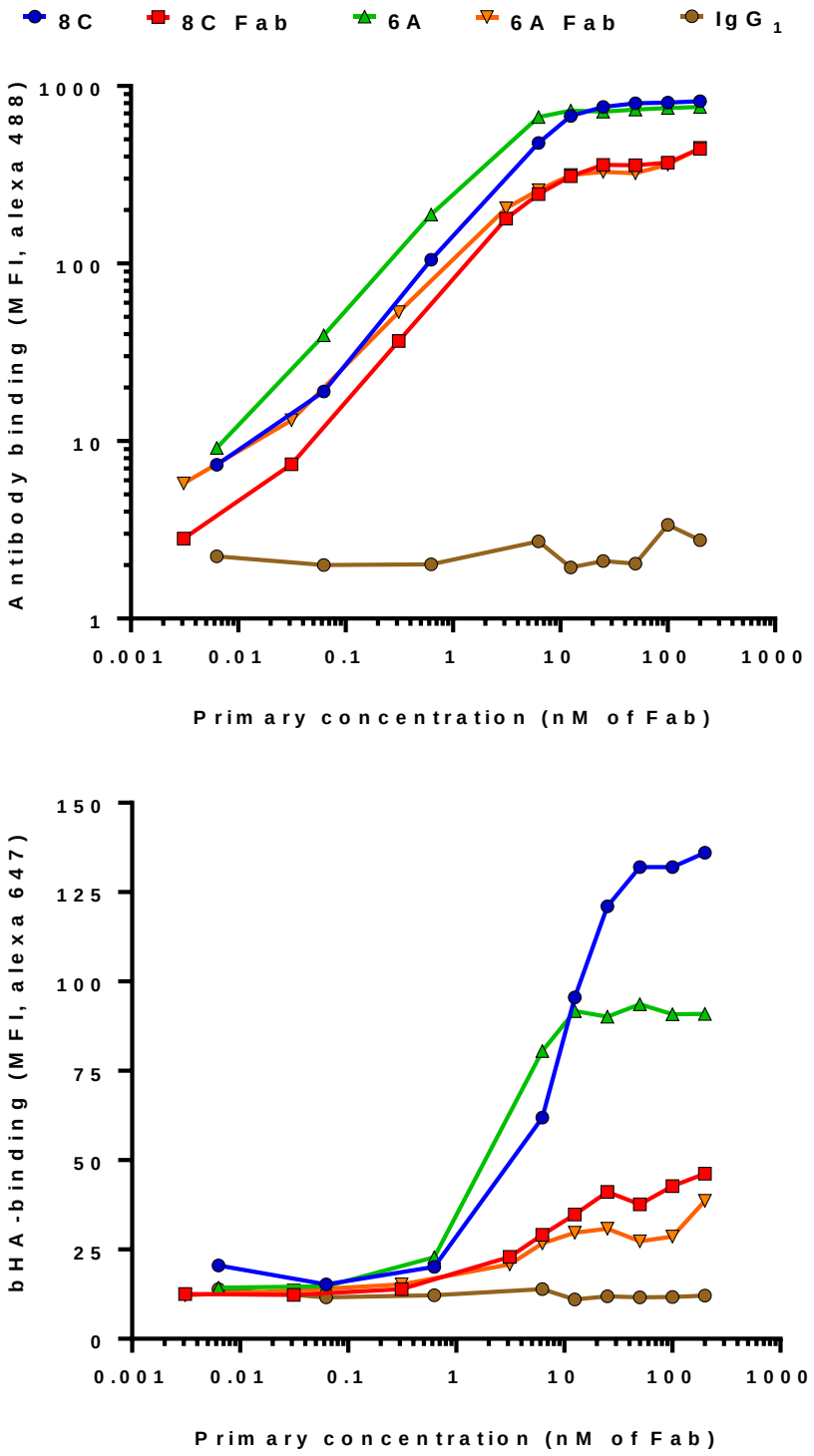


Figure 4.16. **Influence of 8C and 6A monoclonal antibodies and Fab fragments on hyaluronan binding by human LYVE-1 expressing Jurkat cells.** Human LYVE-1 pHR Jurkat cells were incubated with biotinylated HA (bHA) either alone or in the presence of either intact hLYVE-1 mAb or Fab fragments or control Ig, at increasing Ig concentration, to assess the effect on bHA binding. Bound Ig (*top panel*) or bHA (*bottom panel*) were detected with anti-mouse IgG Alexa 488 and streptavidin Alexa 647 respectively. Data are the mean fluorescence intensity (MFI) 20 000 cells/condition as measured by flow cytometry and are representative of two independent experiments.

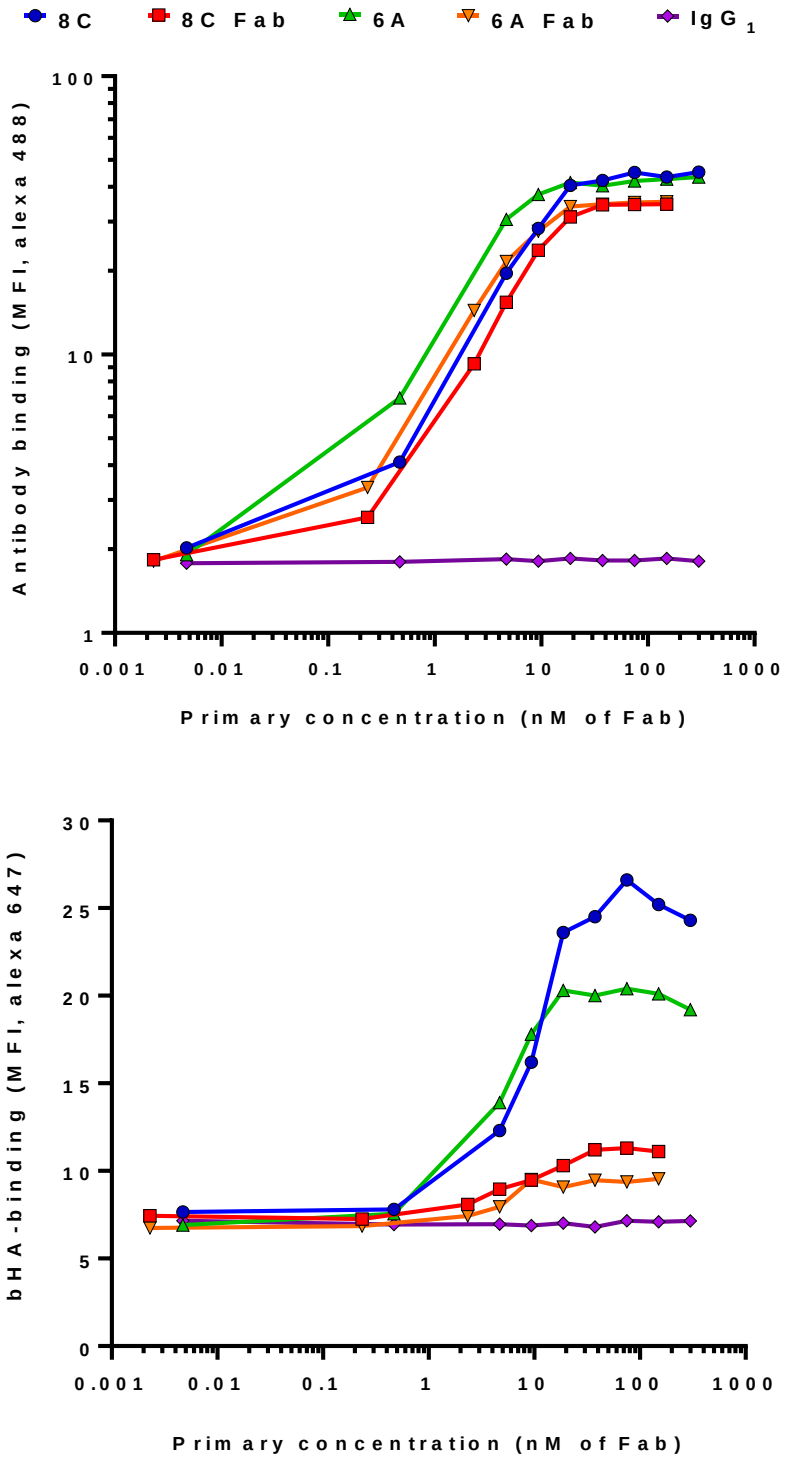


Figure 4.17. **Influence of 8C and 6A monoclonal antibodies and Fab fragments on hyaluronan binding by primary human dermal lymphatic endothelial cells.** HDLEC were lifted with Accutase and incubated with biotinylated HA (bHA) either alone or in the presence of either intact hLYVE-1 mAb or Fab fragments or control Ig, at increasing Ig concentration, to assess the effect on bHA binding. Bound Ig (*top*) or bHA (*bottom*) were detected with anti-mouse IgG Alexa 488 and streptavidin Alexa 647 respectively. Data are the mean fluorescence intensity (MFI) 20 000 cells/condition as measured by flow cytometry and are representative of three independent experiments.

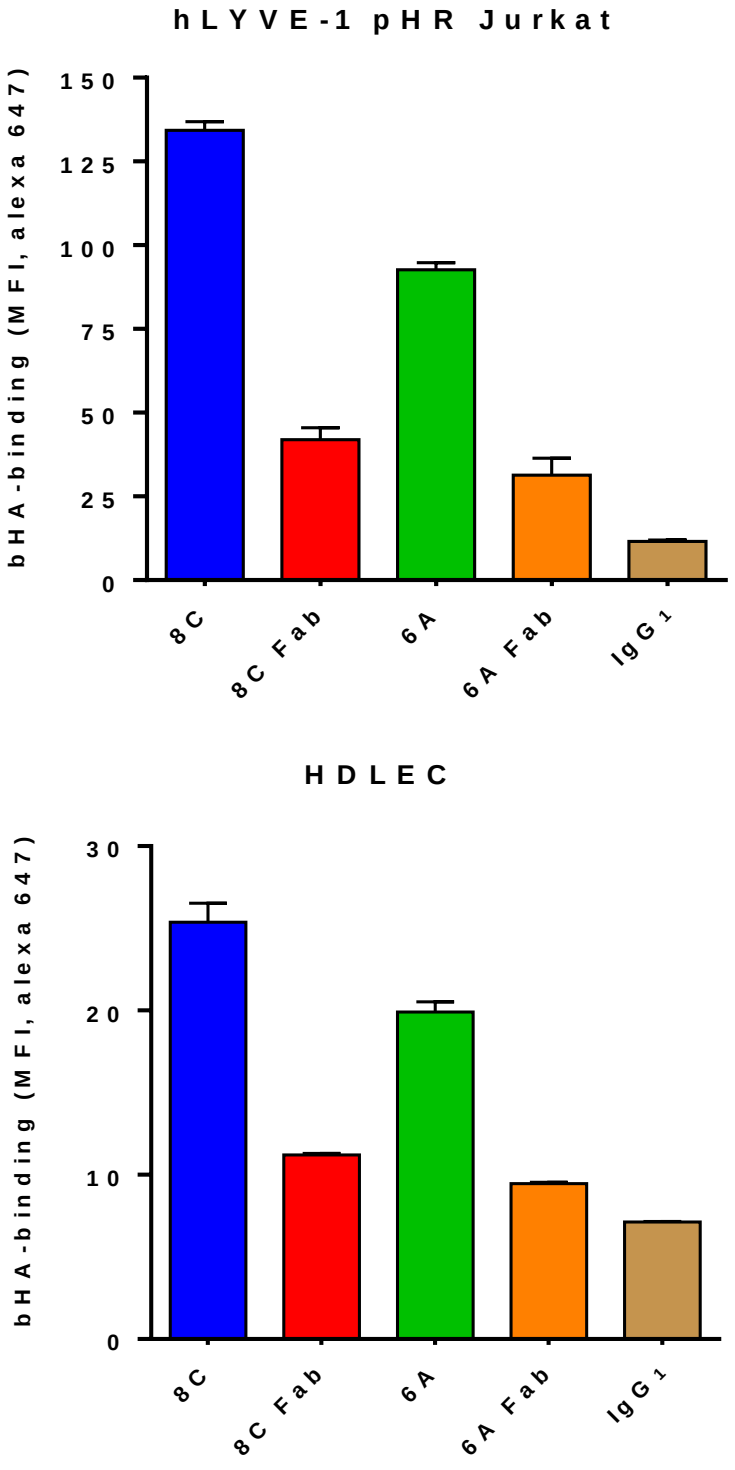


Figure 4.18. **Influence of Fab fragments on hyaluronan binding by LYVE-1 expressing cells summarised**. hLYVE-1 pHR Jurkat cells and HDLEC were incubated with biotinylated hyaluronan (bHA) in combination with intact hLYVE-1 mAbs or Fab fragments, at increasing Ig concentration, to assess the effect on bHA binding (see Figures Figure 4.16, Figure 4.17). Data are the mean fluorescence intensity (MFI) of bHA binding at saturating Ig concentration ± SD of 20 000 cells/condition (n = 3) from single experiments.

4.3.8 Influence of Fab fragments on LYVE-1 distribution in adherent HDLEC monolayers

Having established that intact mAbs have a larger potentiating effect on HA binding than Fab fragments, both species were tested for the ability to elicit redistribution of LYVE-1 on the surface of wildtype (Figure 4.19) or hLYVE-1-GFP pHR HDLEC (Figure 4.20) grown as adherent monolayers. Live cells or cells fixed with freshly depolymerised formaldehyde were incubated with LYVE-1 mAbs or Fab fragments alone or in combination with biotinylated HA. Following incubation, cells were fixed once more to prevent post-preparation clustering by the secondary detection antibody, and visualized using fluorescence microscopy. The results (Fig 4.17) show that cells incubated with intact bivalent 8C mAb alone or in the presence of bHA exhibited the same distinctive punctate LYVE-1 distribution observed in initial experiments (see Figure 4.9), while incubation with monovalent 8C Fab retained the even distribution of LYVE-1 seen in cells treated with an irrelevant control Ig. Interestingly, the punctate distribution of LYVE-1 promoted by incubation with intact 8C mAb was largely inhibited by inclusion of the blocking mAbs 891 or 893 (Figure 4.19 & 4.21). These data demonstrate that clustering of LYVE-1 molecules is dependent on antibody bivalency, underlining the importance of this process in mediating potentiation of HA binding to HDLEC.

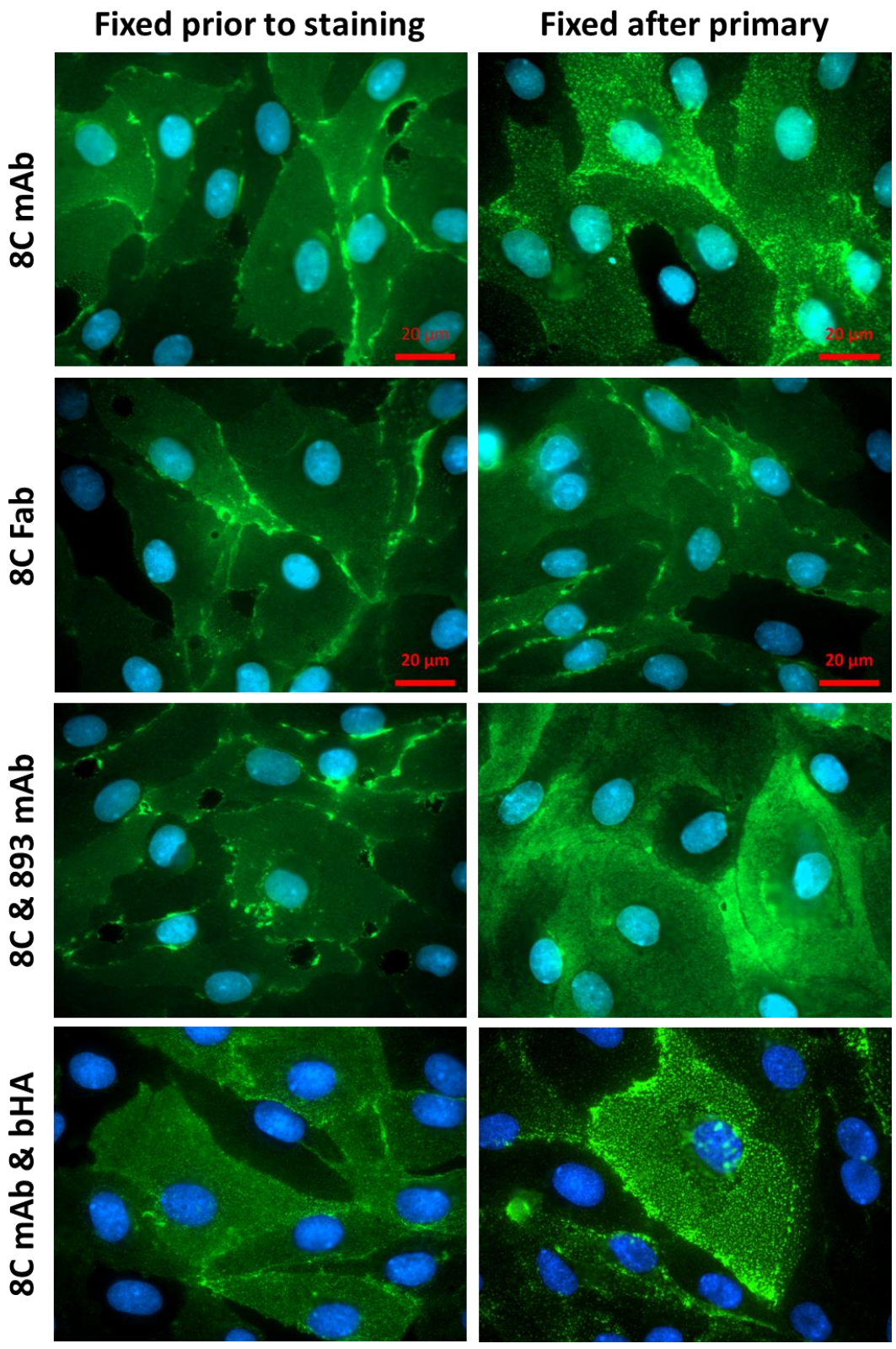


Figure 4.19. **Influence of 8C and 8C Fab fragments on LYVE-1 distribution in adherent primary LEC.** Primary HDLEC were cultured on gelatin-coated 8-chamber slides. Media was removed and the cells were either blocked with 5% FCS, 0.05% sodium azide in PBS or fixed immediately with 2% formaldehyde in PBS, prior to incubation with hLYVE-1 mAbs or Fab fragments alone, or in combination with biotinylated hyaluronan

(bHA), as indicated. Following 30 mins incubation at room temperature, cells were fixed and blocked once more. Cell nuclei were stained with DAPI (*blue*) and LYVE-1 antibodies with goat anti-mouse IgG Alexa 488 (*green*). Images were captured using an inverted epifluorescence microscope (Zeiss Axiovert S100) fitted with a 100x oil-immersion objective and a Hammatsu digital camera and are representative of three independent experiments

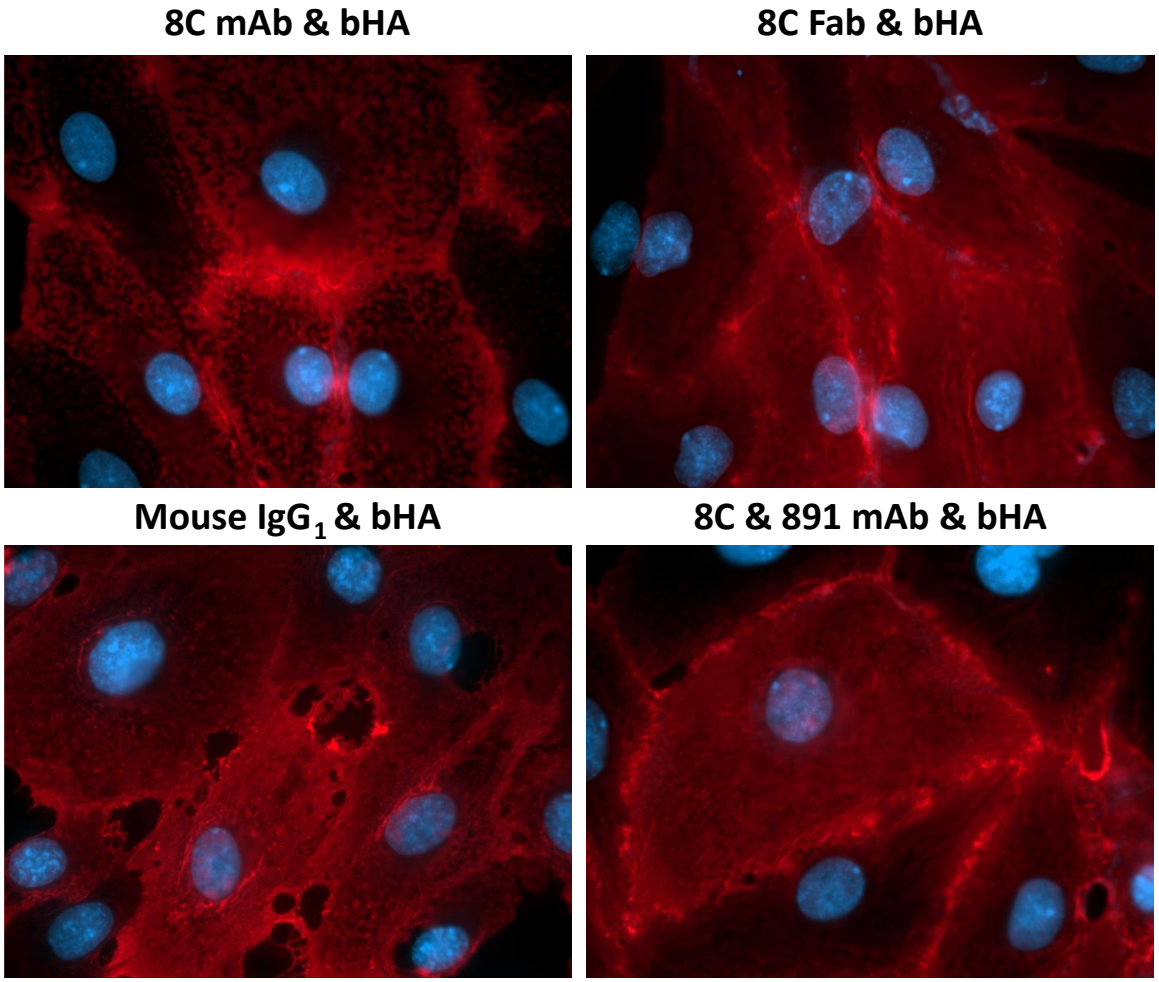


Figure 4.20. **Influence of 8C and 8C Fab fragments on LYVE-1 distribution in hLYVE-1-GFP HDLEC**. Primary HDLEC over-expressing hLYVE-1-GFP were cultured on gelatin-coated 8-chamber slides. Media was removed and the cells were blocked with 5% FCS, 0.05% sodium azide in PBS, prior to incubation with biotinylated hyaluronan (bHA) in combination with either mouse IgG_1 isotype control, 8C mAb, 8C Fab or 8C and 891 mAb, to assess the influence on LYVE-1 distribution in these cells. Cells were fixed with freshly depolymerised formaldehyde, blocked once more, and incubated with goat anti-hLYVE-1 polyclonal. Cell nuclei were stained with DAPI (*blue*) and hLYVE-1 poly with donkey anti-goat IgG Alexa 647 (*red*). Images were captured using an inverted epifluorescence microscope (Zeiss Axiovert S100) fitted with a 100x oil-immersion objective and a Hammatsu digital camera from a single experiment.

4.3.9 Influence of LYVE-1 antibodies and Fab fragments on HA binding by recombinant LYVE-1

The majority of evidence suggests that potentiation of HA binding to HDLEC is dependent on clustering of LYVE-1 molecules by bivalent antibody, a process that must be reliant on lateral mobility of LYVE-1 molecules at the cell surface. However, experiments using Fab fragments suggest that there may also be a contribution from an antibody-induced conformational change that enhances HA binding affinity. To interrogate both possibilities further, 8C mAb and 8C Fab fragments were tested for the ability to enhance HA binding by recombinant LYVE-1 in an ELISA-based system that precludes lateral mobility of the receptor, or interaction with other proteins (Figure 4.21). Recombinant human LYVE-1 extracellular domain bearing a C-terminal 10-Histidine tag was separated by size-exclusion chromatography into separate samples of monomeric and dimeric protein. Both species were serially diluted from a starting concentration of 1.25 µg/ml and immobilized by incubation with Ni-NTA coated HiSorb plates (Qiagen). Samples were incubated with biotinylated hyaluronan (bHA) either alone or in combination with 8C mAb or 8C Fab, to assess the effect on bHA binding.

As shown in Figure 4.21, there was clear relationship between LYVE-1 coating concentration and bHA binding, which made it possible to interrogate the influence of 8C mAb and 8C Fab. Neither species had a significant impact on bHA binding by hLYVE-1 monomer, however incubation of dimeric protein with 8C mAb caused a small increase in bHA binding, and 8C Fab a larger increase still. In a further experiment, hLYVE-1 monomer and dimer were immobilized side-by-side at 1 and 2 µg/ml respectively, prior to incubation with LYVE-1 mAbs, Fab fragments or unlabelled HA, to determine the effect on bHA binding (Figure 4.22). As observed in the previous experiment, both 8C mAb and 8C Fab were capable of potentiating bHA binding by hLYVE-1 dimer, however the

increase in binding was modest, and there was no effect on the monomer. Co-incubation of either species with bHA and an excess of unlabelled HA was sufficient to block bHA binding, while co-incubation with HA blocking mAb 891 gave incomplete blockade of hLYVE-1 monomer, but was effective against the dimer.

Taken together, these data give support to the notion that clustering is the most significant component of antibody-mediated potentiation of HA binding. In this system, lateral motion of LYVE-1 molecules is prevented, thus precluding cross-linking by LYVE-1 mAbs, except where molecules are immediately adjacent. The result of this restriction appears to be an inability to significantly potentiate HA binding. Fab fragments of 8C mAb did increase HA binding by recombinant hLYVE-1 dimer, indicating that an increase in HA binding affinity does occur upon Ab binding. However, the size of the potentiation was modest, and it is curious that Fab fragments influenced only dimeric, but not monomeric LYVE-1. The relevance of using recombinant LYVE-1 could be called into question given that this material was produced in a non-native cell type, and may not bear the same pattern of inhibitory glycosylation seen with primary cells. However in Chapter 6, antibody-mediated potentiation of HA binding by recombinant LYVE-1 is demonstrated using an alternative cell-free system, the Quartz Crystal Microbalance (QCM). The critical difference with a QCM system is that LYVE-1 molecules are captured by an artificial lipid bilayer, granting them free lateral movement and the potential to form clusters.

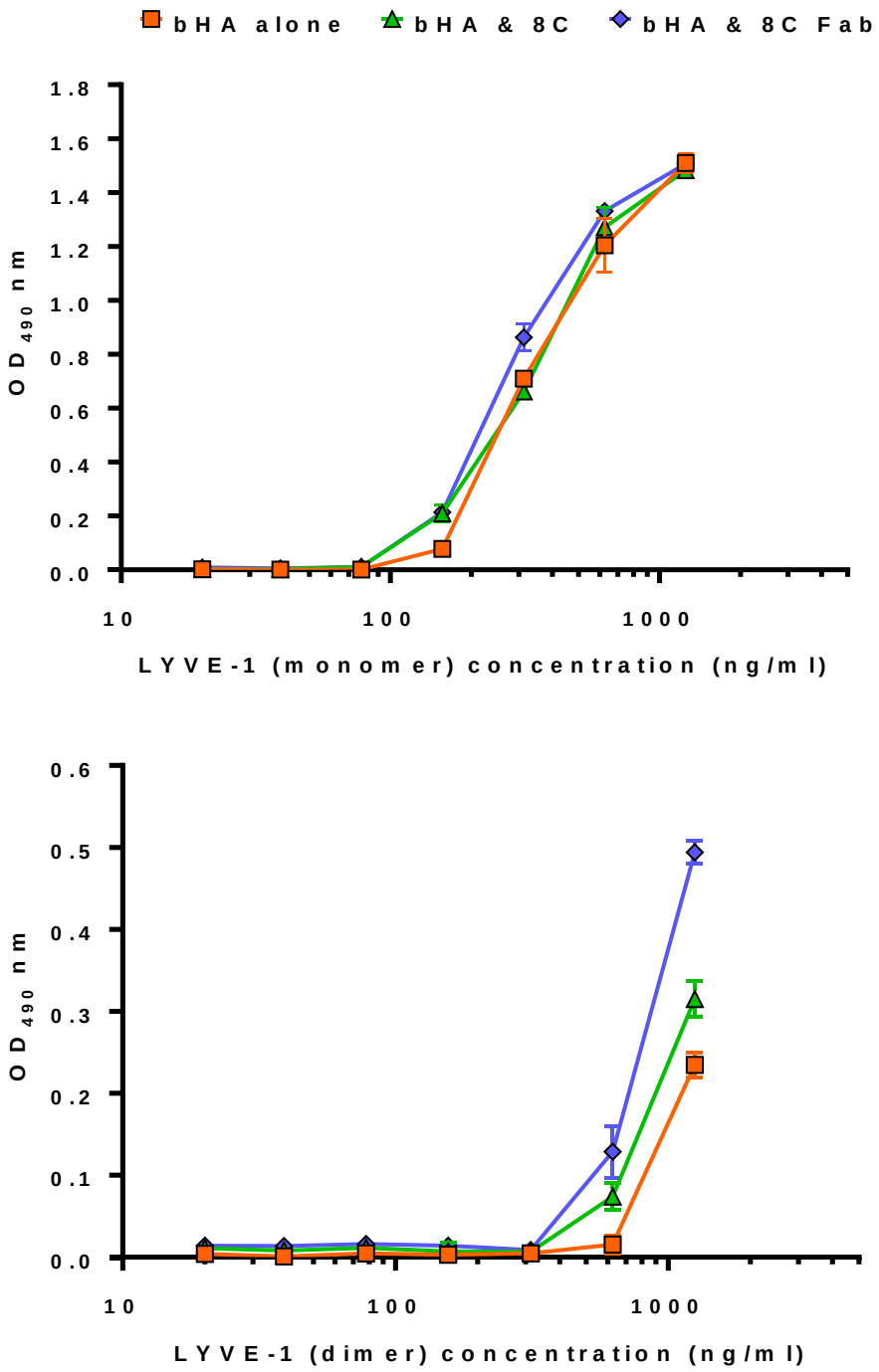


Figure 4.21. **Influence of anti-hLYVE-1 monoclonal antibodies on HA binding by recombinant hLYVE-1 monomer and dimer**. Recombinant human LYVE-1 extracellular domain bearing a C-terminal 10 His tag was separated by size-exclusion chromatography into separate samples of monomeric and dimeric protein. Both species were serially diluted from a starting concentration of 1.25 µg/ml and immobilized by incubation with Ni-NTA coated HiSorb plates (Qiagen). Samples were incubated with biotinylated hyaluronan (bHA) either alone or in combination with 8C mAb or 8C Fab, to assess the effect on bHA binding. Bound bHA was detected using streptavidin-HRP, a colorometric substrate and a plate reader capable of reading optical density at 490nm wavelength (OD_{490}). Data are the mean ± SD (n = 3) from a single experiment.

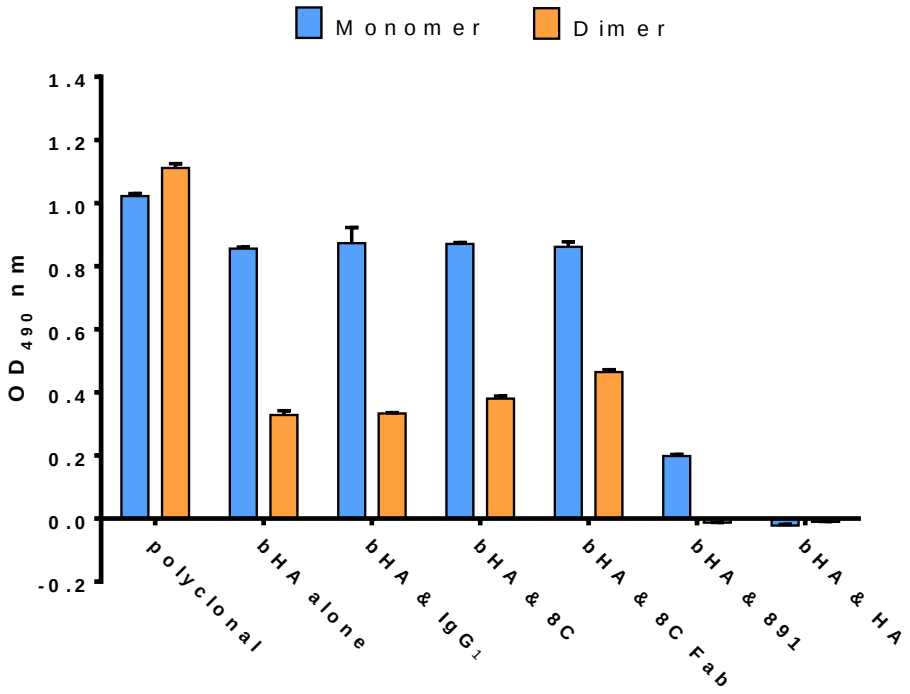


Figure 4.22. **Influence of anti-hLYVE-1 monoclonal antibodies on HA binding by recombinant hLYVE-1 monomer and dimer.** Monomer and dimeric human LYVE-1 extracellular domain bearing a C-terminal 10 His tag were immobilized by incubation with Ni-NTA coated HiSorb plates (Qiagen). Samples were incubated with biotinylated hyaluronan (bHA) either alone or in combination with either hLYVE-1-specific mAb, Fab, isotype-matched control Ig, or an excess of unlabelled HA, to assess the effect on bHA binding. Separate samples were incubated with anti-hLYVE-1 polyclonal to measure bound protein. Bound bHA or polyclonal were detected using streptavidin-HRP or anti-goat IgG-HRP, a colorometric substrate and a plate reader capable of reading optical density at 490nm wavelength (OD_{490}). Data are the mean ± SD (n = 3) from a single experiment.

4.3.10 Formation of artificial LYVE-1 dimers by potentiating antibodies

While formation of LYVE-1 clusters by potentiating mAbs is clearly a very important process, it is unlikely to be the only structure resulting from antibody cross-linking of individual receptors. Approximately 50% of LYVE-1 molecules at the cell surface are present as disulfide-linked dimers, while the remainder are monomeric. Lattice formation will be interrupted by the inclusion of a LYVE-1 monomer, due to the lack of a second binding site for the antibody. Furthermore, it would appear just as likely that an antibody would cross-link two monomers, thus forming an artificial dimer, which may have the same enhanced HA binding affinity exhibited by its disulphide-linked counterpart.

To determine whether antibody-mediated potentiation of HA binding can occur in the absence of the dimeric form of the receptor, hLYVE-1 mAbs were tested for their influence on HA binding by hLYVE-1-GFP and hLYVE-1 C201A-GFP pHR Jurkat cells (Figure 4.23). These cell lines have very closely matched LYVE-1 expression, while the C201A mutation deletes the cysteine residue required for formation of disulphide-linked dimers (for more detail, see Chapter 6). Loss of dimeric LYVE-1 resulted in an ~20% reduction in constitutive HA binding compared to wildtype hLYVE-1-GFP expressing cells. However, when co-incubated with HA and 8C or 6A mAb, HA binding by both cells types was identical. Clearly potentiation of HA binding to LYVE-1 transfected Jurkat cells can occur in the absence of dimeric LYVE-1 and the possibility of cluster formation. The mechanism of potentiation could conceivably involve an enhancement of HA binding affinity, or formation of artificial dimers from hLYVE-1 C201A-GFP monomers. One means of addressing this question would be to test the influence of 8C Fab fragments on hLYVE-1 C201A-GFP Jurkat cells, as in this situation the possibility of forming artificial dimers would be excluded.

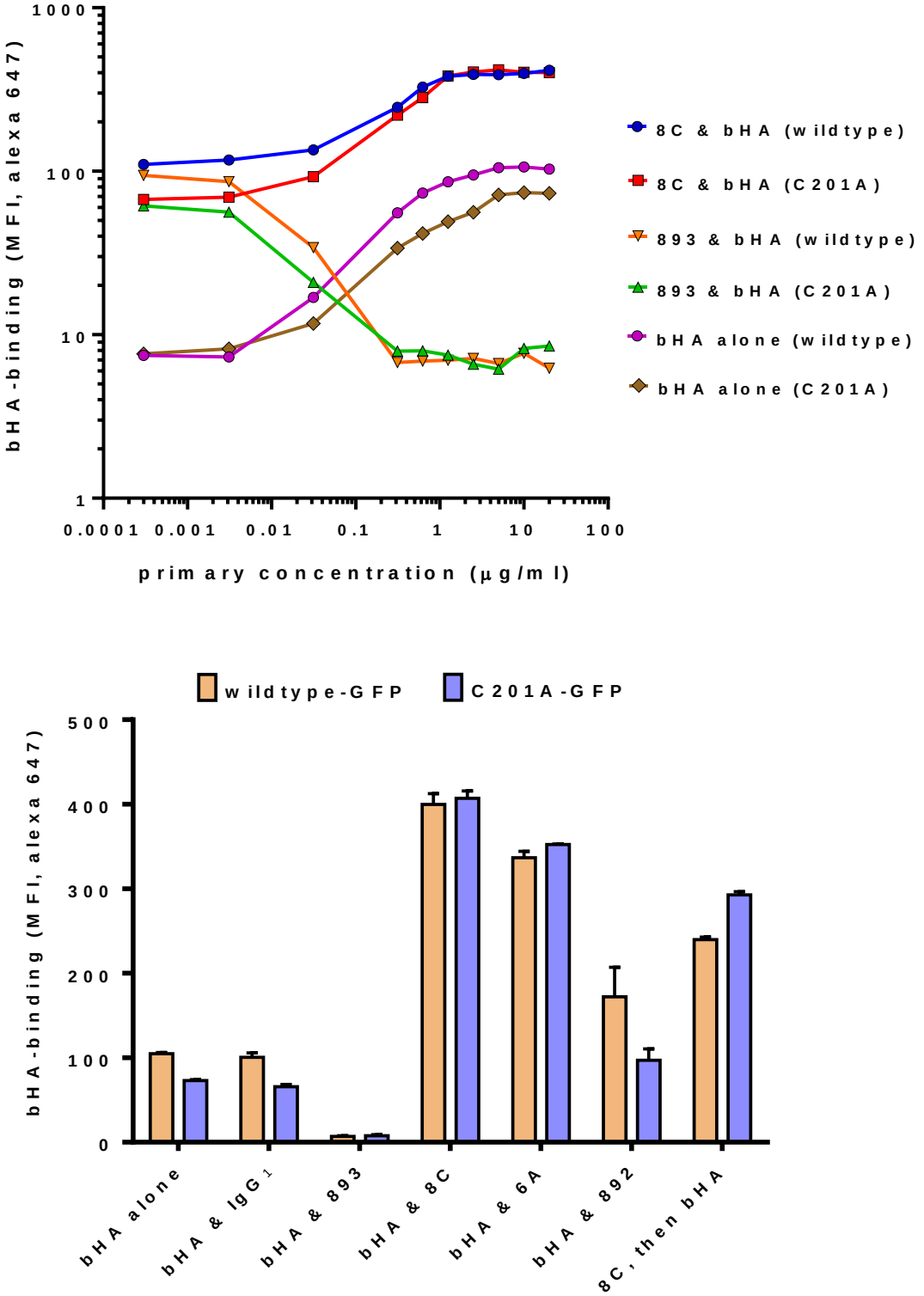


Figure 4.23. **Antibody-mediated potentiation of hyaluronan binding to Jurkat cells expressing a mutant LYVE-1 that cannot form disulfide-linked dimers.** Jurkat cells were infected with lentivirus bearing the coding sequence of hLYVE-1 with a C-terminal GFP tag or hLYVE-1 C201A-GFP, a mutant of LYVE-1 that cannot form disulphide-linked homodimers. These cells were tested for binding of biotinylated HA under different conditions, detected by streptavidin Alexa 647 and flow cytometry. Cells were either (i) incubated with bHA alone, at increasing bHA concentration (*bHA alone*), or (ii) co-

incubated with bHA (fixed at 5 µg/ml) and hLYVE-1-specific mAbs or mouse IgG_1 isotype control, at increasing Ig concentration, or (iii) pre-incubated with 8C mAb at various concentrations, prior to incubation with bHA (5 µg/ml) (*8C, then bHA*), to assess the effect on bHA binding. Data are the (MFI) of 20 000 cells/condition (*Top panel*) and the MFI ± SD of 20 000 cells/condition at saturating Ig concentration (n = 3) (*Bottom panel*). Data are representative of two independent experiments.

However, subsequent experiments involving over-expression of hLYVE-1 C201A monomer in primary HDLEC have called into question the relevance of these observations made using LYVE-1 transfected Jurkat cells. The results of these experiments, which are described in detail in Chapter 6 (Figure 6.8), indicated that over-expression of hLYVE-1 C201A monomer in HDLEC is insufficient to trigger constitutive bHA binding, whereas over-expression of wildtype LYVE-1 leads to very high levels of hyaluronan binding. Furthermore, co-incubation with bHA and 8C mAb enhances bHA binding by wildtype LYVE-1 expressing cells, but has only a minor influence on bHA binding by hLYVE-1 C201A expressing HDLEC. In the latter case, the small increase in bHA binding mediated by 8C mAb was attributed to a background of endogenous LYVE-1 expression, which produces a mixture of monomeric and dimeric LYVE-1. These data suggest that cross-linking of LYVE-1 monomers by potentiating antibodies does not significantly enhance HA binding to primary HDLEC, and that clustering of dimeric LYVE-1 is the most significant mechanism underlying antibody-mediated potentiation of bHA binding. The discrepancy between primary HDLEC and LYVE-1-transfected Jurkat may well be explained by cell-type specific glycosylation of the receptor. Primary HDLEC lack the constitutive level of HA binding observed for hLYVE-1 pHR Jurkat cells due to inhibitory sialylation of LYVE-1 molecules. While cross-linking of LYVE-1 monomers at the surface of HDLEC may well occur, this does not appear to significantly enhance HA binding.

4.4 Discussion

In this chapter, the relationship between LYVE-1 expression, surface density and hyaluronan binding is explored. The key findings were that LYVE-1 surface expression is a critical regulator of hyaluronan binding in both primary and transfected cell lines, and that this threshold may be manipulated by cross-linking LYVE-1 molecules, leading to clustering of the receptor. In transfected cells, hyaluronan binding is only seen above a narrow threshold of LYVE-1 expression; beyond this point HA binding scales rapidly with small increases in the amount of LYVE-1. The situation in primary lymphatic endothelial cells is different due to the absence of constitutive HA binding, indicating that a higher threshold of LYVE-1 surface density operates, perhaps as a result of negative charge repulsion between sialylated receptors. This can be overcome by artificial over-expression of LYVE-1 in LEC, which results in high levels of constitutive HA binding from a 4 to 5 fold increase in LYVE-1 expression. Analysis by western blot of over-expressed LYVE-1 from HDLEC indicated a similar molecular weight to the endogenous receptor, however a more comprehensive glycan analysis will be required to demonstrate that the protein is correctly modified with sialic acid.

In wildtype LEC, simple application of potentiating antibodies such as 8C and 6A induces rapid conversion to high levels of HA binding, without the need for over-expression or desialylation of LYVE-1. Antibody-mediated potentiation of HA binding is also dependent on LYVE-1 expression, and may be inhibited by LYVE-1 blocking mAbs or competition with an excess of unlabelled HA. It is also effective with LYVE-1 transfected cells, increasing HA binding beyond that seen in the absence of potentiating antibody, in a manner dependent on LYVE-1 expression and antibody concentration. Enhancement of HA binding was also observed when cells were pre-incubated 8C mAb, prior to addition

of HA, but not when this sequence is reversed. Potentiation is rapid, occurring in as little as 10 minutes, and is equally efficient at both 4^{o}C and room temperature (based on pilot experiments), suggesting that the mechanism is not dependent on an enzymatic reaction, such as an intracellular signalling event.

All non HA-blocking human LYVE-1 mAbs were found to potentiate HA binding, albeit to different degrees. 8C and 6A mAbs were by far the most potent, increasing HA binding ~15-fold when averaged across the cell population and ~60-fold for the highest LYVE-1 expressing cells. Modest levels of potentiation were recorded for mAbs 7C and 892, which appeared to be driven by low affinity for LYVE-1, rather than binding of a different epitope. On the basis that over half the hLYVE-1 mAbs tested were found to be potentiating antibodies, it had been hoped that a similar mLYVE-1 mAb could be identified amongst the five commercially available clones. Sadly all five were found to be potent HA blockers, precluding their use for testing the effect of potentiating antibodies *in vivo*.

There appear to be three processes that contribute to antibody-mediated potentiation of HA binding; an increase in the HA binding affinity of LYVE-1 dimers upon mAb binding, the formation of artificial dimers from LYVE-1 monomers, and the cross-linking of LYVE-1 dimers and monomers to form higher-order clusters. The evidence for the latter is by far the strongest and fits particularly well with a model of LYVE-1-hyaluronan binding that predicts that multivalent interactions are essential for stable binding. Incubation of live HDLEC monolayers with potentiating mAbs resulted in a punctate LYVE-1 distribution that occurs only with bivalent antibody and not Fab fragments. Furthermore, potentiating antibodies exhibited only a minor effect on HA binding by recombinant LYVE-1 in an ELISA-based experiment, where the receptor is immobilized, but did significantly enhance

HA binding in a QCM-D system, where lateral mobility is maintained using an artificial lipid bilayer (see Chapter 6).

Experiments aimed at comparing the influence of intact mAbs and Fab fragments on HA binding indicated that Fab do exhibit a modest potentiating effect on HA binding by LYVE-1 transfectants, and to a lesser extent with primary cells. Some authors have reported that Fab fragments can form multimeric complexes with cross-linking capacity, a process that can be blocked by treatment with the alkylating agent iodoacetamide, thus preventing inappropriate inter-chain disulphide bond formation (Lesley et al., 1993). The purity of 8C and 6A Fab preparations was high when assessed by SDS-PAGE, although they were not treated with iodoacetamide. However, Fab fragments did not influence the distribution of LYVE-1 in adherent HDLEC monolayers, which argues against a cross-linking artefact mediated by Fab multimerization. A direct effect of potentiating antibodies on HA binding cannot therefore be ruled out, and further experiments will be required to address this possibility. A potentially informative experiment would be to ascertain the influence of Fab fragments on HA binding by cells expressing the hLYVE-1 C201A mutant, which cannot form dimers, thus excluding the possibility of clustering.

Finally, any process of cross-linking or clustering of LYVE-1 at the cell surface will require free lateral mobility of the receptor. Therefore if potentiation of HA binding by LYVE-1 mAbs is dependent on clustering, preventing this lateral motion should in turn block any increase in HA binding. In preliminary experiments, fixation of LYVE-1 pHR Jurkat cells prior to incubation with 8C mAb was sufficient to prevent potentiation, but also resulted in significant non-specific staining with the streptavidin detection reagent, even in the absence of biotinylated HA (data not shown). To address this question via a different route, recombinant His-tagged LYVE-1 was immobilized using Ni-NTA plates, which have the

advantage of securing the protein in place without artificially dimerizing it, as would be the case with a capture antibody. In the absence of lateral mobility, 8C mAb had no influence on HA binding, although 8C Fab fragments had a modest effect on LYVE-1 dimers. However, as described later in Chapter 6, antibody-mediated potentiation of HA binding can occur when recombinant LYVE-1 is captured by an artificial lipid bilayer, where free lateral movement is permitted.

Taken together, these data suggest that native LYVE-1 is an active HA receptor, and may have evolved to engage with ligand only after appropriate surface redistribution, or presentation of HA in a form that promotes this process. Focal increases in surface density through self-association or clustering are likely through avidity effects to surpass the threshold requirement for stable binding. This predicts that the receptor may function to discriminate for certain presentations of hyaluronan. Rather than binding bulk serum or matrix HA, LYVE-1 may be adapted to bind only HA bound by certain proteins or presented on the surface of a migrating cell. Some of these possibilities are described in more detail in the next chapter.

Chapter 5.
Modifying the valency of the ligand - Enhanced binding of cross-linked hyaluronan

5.1 Introduction

Hyaluronic acid is bound by a variety of proteins that constrain its movement, alter its physical properties, influence the binding of other hyaladherins, and alter the behaviour of cells with which it interacts. The number and diversity of these HA binding proteins, each with their own or inter-connected functions, result in the capacity for HA to be involved in a wide range of cellular and disease processes, including regulation of cell motility and proliferation, cell adhesion and activation, tumour metastasis, maintenance of matrix stability and water retention (reviewed in Day and Prestwich, 2002; Jackson, 2009). In many cases, association with specific binding proteins leads to the formation of cross-linked fibrils, cable-like structures and other molecular architectures that are central to processes of inflammation, ovulation, and scaffolding (reviewed in Day and de la Motte, 2005).

One prominent hyaluronan binding protein (HABP), TNFα stimulated gene 6 protein (TSG-6) is a naturally occurring HA cross-linker (Baranova et al., 2011) that plays important roles in inflammation and ovulation (Fulop et al., 2003). Expression of TSG-6 is tightly controlled, with little or no constitutive expression in adult tissues, but the protein is synthesized by a variety of cell types in response to pro-inflammatory mediators or certain growth factors. TSG-6 has been shown to modulate the interaction between hyaluronan and CD44, enhancing or inducing binding by the HA receptor on constitutive and inducible cell backgrounds, respectively (Lesley et al., 2004). As such, TSG-6 mediated cross-linking of HA has been proposed as a functional mechanism for regulation of leukocyte adhesion (Day and de la Motte, 2005). The protein is composed mainly of two contiguous domains, a Link module, responsible for HA binding, and a C-terminal CUB

module, the function of which is unclear, but is thought to include mediating TSG-6 oligomerization.

Enhancement of HA binding to CD44 is a feature of recombinant TSG-6 both in its full length form (FL_TSG-6) and as a truncated variant comprising the Link module only (Link_TSG-6), although the former is much more potent (Lesley et al., 2004). This enhancing property is dependent on pre-complexing of TSG-6 with HA, and the mechanism is believed to involve cross-linking of HA chains, leading to an increase in binding avidity, and potential clustering of the receptor. Direct evidence of rigidification and condensation of end-grafted HA films in solution has been obtained for both FL_TSG-6 and Link_TSG-6 (Baranova et al., 2011). Full length TSG-6 was shown to bind with positive cooperativity due to HA-induced oligomerization, leading to cross-linking of HA chains and collapse in HA ultrastructure. Link_TSG-6 could also condense HA films, but was less potent and bound with lower affinity.

Cross-linking of HA chains by Link_TSG-6 oligomerization would appear unlikely on the basis that the protein lacks the C-terminal CUB domain and is solely monomeric in both the absence and presence of an HA octasaccharide (Blundell et al., 2005; Blundell et al., 2003). However, some Link_TSG-6 mutants with close-to wildtype levels of hyaluronan binding were found to have reduced or increased activity on CD44 binding of HA, suggesting that some residues outside of the HA binding site may be involved in protein self-association (Lesley et al., 2004). A dramatic condensation of end-grafted HA films by Link_TSG-6 at low ionic strength, in excess of that observed for FL_TSG-6, also suggested the involvement of some form of cross-linking (Baranova et al., 2011). However the mechanism remains obscure, and perhaps the most easily reconciled model envisages a

rigidification of HA chains and stabilization of certain conformations, akin to 'beads-on-a-string'.

In addition to its function as an HA cross-linking protein, TSG-6 catalyses the only naturally-occurring covalent modification of HA; addition of heavy chains (HCs) donated from the serum protein inter-α-inhibitor (IαI) (Fulop et al., 2003; Jessen and Odum, 2003; Mukhopadhyay et al., 2004; Rugg et al., 2005). The ensuing HA•HC complex, which has been termed serum-derived hyaluronan-associated protein (SHAP) (Yingsung et al., 2003; Zhao et al., 1995) has been found in the sera of patients with ovarian cancer (Obayashi et al., 2008) and the synovial fluid of arthritic joints (Kida et al., 1999), amongst others. Heavy-chain HA is an important component of the cumulus-cell-oocyte complex in the ovary, where it cross-links the HA matrix and is crucial for successful ovulation and fertility (Fulop et al., 2003; Mukhopadhyay et al., 2001; Zhuo and Kimata, 2001). The formation of HA•HC complex has also been shown to promote leukocyte adhesion to HA matrices (de la Motte et al., 2003) in a CD44-dependent manner (Zhuo et al., 2006). Lastly, airway smooth muscle cells produce similar HA•HC cable structures up to 200 μM in length with enhanced leukocyte binding properties in response to the viral mimic poly(I:C) (Lauer et al., 2013).

The precise nature of heavy-chain cross-linking of HA, the involvement of additional proteins, and its influence on HA structure and resulting cellular responses are complex (Baranova et al., 2013). TSG-6 mediated crosslinking of HA films was found to be impaired in the presence of IαI, and this effect suppressed TSG-6-mediated enhancement of HA binding to CD44 positive cells. In addition to the known covalent HC•TSG-6 complexes that arise during transfer of HC to HA, a number of high affinity, non-covalent species were observed, including HC-TSG-6. Furthermore, modification of HA with HCs

had only a minor condensation effect on HA films, suggesting cross-linking by HC-HC interactions is rather weak. The overall picture is of a hierarchy of protein-protein and protein-HA interactions that alters the degree of HA cross-linking and is likely regulated by temporal and localised expression of the various components.

Recent work in the Jackson laboratory has revealed that primary lymphatic endothelial cells are capable of binding the HA coat of certain strains of group A streptococci in a LYVE-1 dependent manner (Banerji, Lynskey, Sriskandan and Jackson, manuscript in preparation). Group A streptococcus are responsible for infections ranging from mild, self-limiting pharyngitis to invasive and potentially life threatening streptococcal toxic shock syndrome (STSS) and necrotizing fasciitis (Lynskey et al., 2011). Certain strains produce a hyaluronan capsule that aids immune evasion, and also correlates with the capacity of the bacterium to invade lymphatic vessels and downstream lymph nodes. The interaction of LYVE-1 with the bacterial HA coat leads to clustering of the receptor at the point of contact, suggesting that constrained arrangements of hyaluronan can alter receptor distribution and induce HA binding (Lynskey and Banerji, unpublished observations). This observation suggests that the close array of HA chains on the surface of a cell, perhaps anchored by CD44 or extruded by an HA synthase, may be sufficient to promote stable binding by LYVE-1.

5.2 Aims

As described in the introduction, there are numerous examples in the literature where association of HA with one hyaladherin can influence binding of a second, and often with consequences for the expressing cell. To date, studies of LYVE-1 interactions with HA have focussed on binding of free native HA chains, or fluorescein/biotin-labelled derivatives thereof. These forms of HA are not bound constitutively by primary lymphatic endothelial cells, but as shown in the previous chapter, altering the distribution of LYVE-1 molecules at the cell surface is sufficient to promote binding. Whether a similar mechanism of clustering operates *in vivo* is unclear, but it would be intriguing to determine whether cross-linking of the ligand has a similar effect on LYVE-1 distribution. Previous studies have shown that cross-linking of HA by proteins such as TSG-6 can enhance or even induce binding by CD44-expressing cells. Tethering several HA chains together is likely to restrain their motion and present a larger array of binding sites to a membrane-bound HA receptor. There is ample scope therefore to explore the effect of cross-linking, multimerization or close array of HA chains on binding by LYVE-1.

1. Test the hypothesis that multimerization of HA can enhance binding by LYVE-1 by comparing binding of free and streptavidin-cross-linked biotinylated HA.

2. Investigate whether multimeric complexes of TSG-6 and HA potentiate HA binding by LYVE-1 transfected cells and primary HDLEC, using the full length protein (cross-linking proficient) and recombinant TSG-6 Link module (cross-linking deficient).

3. Determine whether the close array of HA chains on a surface, such as that which may exist on the membrane of a transmigrating cell, may cluster LYVE-1 and induce stable binding.

5.3 Results

5.3.1 Cross-linking of biotinylated hyaluronan using streptavidin enhances binding by LYVE-1 transfected cells

In the previous chapter, cross-linking of LYVE-1 molecules using certain LYVE-1 mAbs was shown to result in clustering of the receptor and induction of HA binding in primary cells. While individual LYVE-1 molecules appear to redistribute in the plasma membrane when bound by potentiating mAbs, incubation with free HA chains alone does not alter LYVE-1 distribution. However, an inter-chain cross-linked macromolecular complex of hyaluronan, such as those formed *in vivo* by TSG-6 or heavy chain HA, would have a much larger footprint on the cell surface. It is reasonable to assume that binding of such a HA complex would therefore be stronger than that of free HA due to restraint on the movement of HA chains, increased valency of interaction with LYVE-1 molecules, and clustering of the receptor as the HA complex diffuses across the cell surface.

As an initial proof of principle, binding of free randomly-biotinylated HA (bHA) by LYVE-1 transfected cells was compared with that of bHA pre-incubated with streptavidin Alexa 647 to form cross-linked HA aggregates (bHA-SA647) (Figure 5.1, A). The degree of cross-linking was varied by altering the ratio (w/w) of SA647 to bHA during pre-incubation. The results showed markedly enhanced binding of bHA-S647 compared to bHA alone, indicating that crosslinking of HA, like crosslinking of LYVE-1 can indeed modulate binding. The enhancement of HA binding increased with the degree of cross-linking up to an optimal SA647:bHA ratio of 0.06:1 (w/w). Beyond this point binding decreased, mostly likely due to saturation of the available biotin moieties and a reduction in inter-chain crosslinking. Binding of the complex was confirmed as a LYVE-1/HA interaction by competition with HA-blocking mAb 891 or unlabelled HA (Figure 5.1, B).

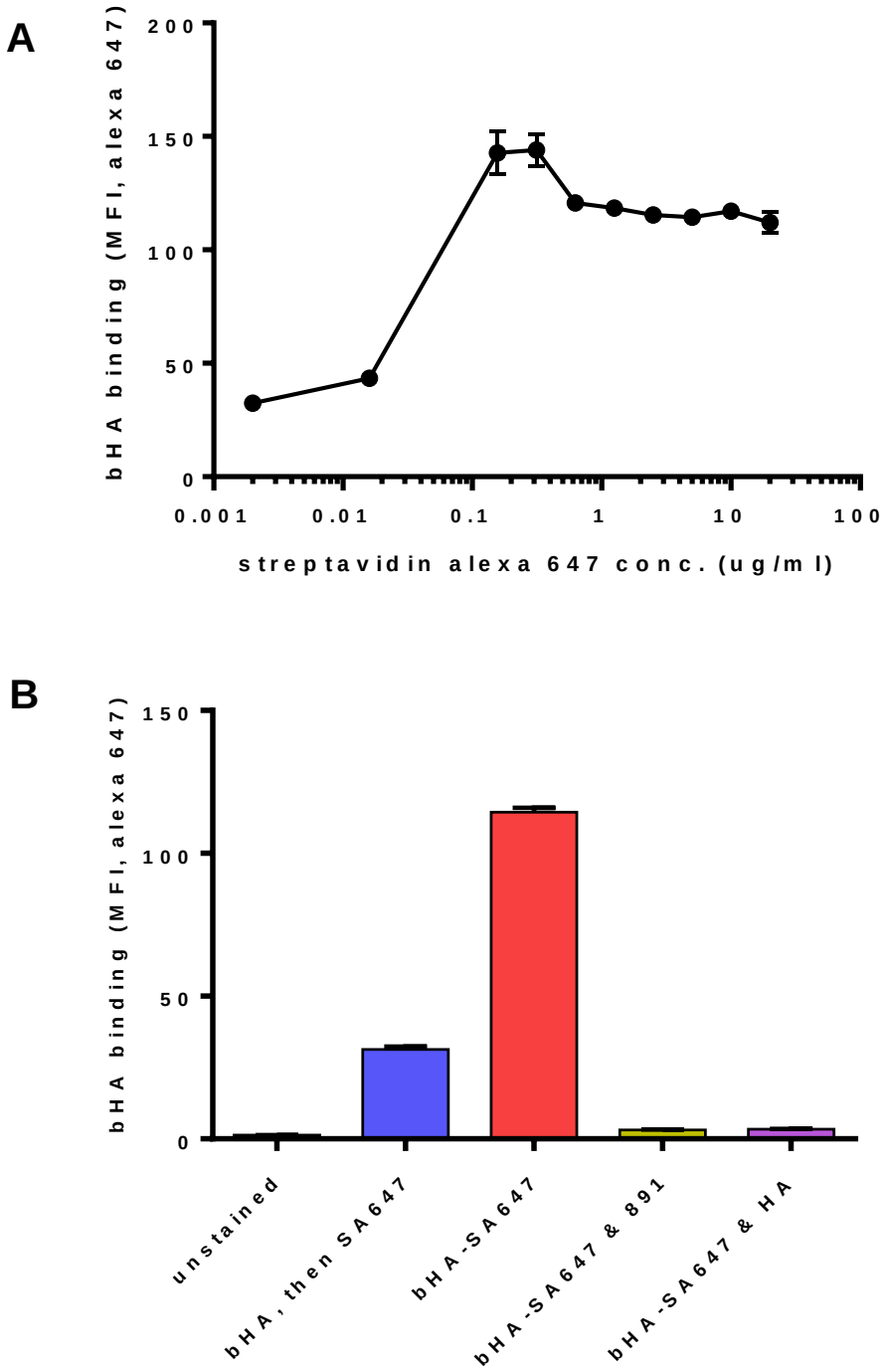


Figure 5.1. **Effect of streptavidin crosslinking of biotinylated HA on binding by human LYVE-1 expressing Jurkat cells.** Streptavidin Alexa 647-complexed biotinylated HA (bHA-S647) was formed by pre-incubation of bHA at 5 µg/ml for 30 min with streptavidin Alexa 647 (SA647) at the concentrations indicated. (A) Human LYVE-1 pHR Jurkat cells were incubated with bHA-SA647 to assess the effect on bHA binding. (B) Cells were incubated with bHA (5 µg/ml), followed by SA647 (5 µg/ml) or bHA-SA647 (5 µg/ml) either alone or in combination with HA blocking mAb 891 or an excess of unlabelled HA, to assess the effect on bHA binding. (A & B) Bound bHA was detected using SA647 at 5 µg/ml. Data are the mean fluorescence intensity (MFI) ± SD (n = 3) of 20 000 cells/condition as measured by flow cytometry from a single experiment.

5.3.2 Cross-linking of hyaluronan with the inflammation-associated protein TSG-6 activates binding by LYVE-1

TNFα stimulated gene 6 protein (TSG-6) is a HABP with an inherent hyaluronan cross-linking activity that plays important roles in inflammation and ovulation. TSG-6 has been shown to modulate the interaction between hyaluronan and CD44, enhancing or inducing binding by the HA receptor on constitutive and inducible cell backgrounds (Lesley et al., 2004). To determine whether HA binding by LYVE-1 may be similarly enhanced by TSG-6, binding of free HA by hLYVE-1 pHR Jurkat cells was compared to that of HA pre-incubated with the Link module from TSG-6 (Link_TSG-6) or the full-length protein (FL_TSG-6)[1] (Figure 5.2). Pre-complexing was performed using a protocol based on that developed for enhancement of HA binding by CD44, but with the inclusion of biotinylated HA (bHA) with subsequent detection by SA647 in addition to fluorescein-labelled HA (Fl-HA) (Lesley et al., 2004). Briefly, Link_TSG-6 or FL_TSG-6 (at 200 µg/ml) were pre-incubated for 30 minutes at room temperature with Fl-HA or bHA (at 40 µg/ml) in 50mM Na:HEPES, pH6.0, the pH at which HA binding by Link_TSG-6 is optimal (Parkar et al., 1998). Human LYVE-1 pHR Jurkat cells were titrated with free bHA and Fl-HA to determine the concentration at which HA binding is 80% of the maximum (2 µg/ml, data not shown). TSG-6:HA complexes or free HA were then serially diluted from a starting concentration of 2 µg/ml, incubated with cells for 30 minutes at room temperature, washed and analysed for HA binding using flow cytometry.

As shown in Figure 5.2, the Link_TSG-6:bHA complex displayed a modest (2-3 fold) increase in binding relative to free bHA, at the highest concentration used (2 µg/ml). No increase was seen with Link_TSG-6:Fl-HA, however this may be a product of the generally

[1] Recombinant TSG-6 was a kind gift from Professor Anthony Day, Wellcome Trust Centre for Cell Matrix Research, University of Manchester.

lower fluorescence signal recorded for Fl-HA compared to bHA and streptavidin Alexa 647. In contrast, FL_TSG-6:HA complexes prepared from both Fl-HA and bHA showed substantially higher binding that amounted to an enhancement over free HA of ~5-fold and ~35-fold respectively. At a TSG-6:HA ratio of 5:1 (w/w), FL_TSG-6 (30.1 kDa) is present at an ~3-fold molar disadvantage compared to Link_TSG-6 (10.9 kDa), but has a much greater effect on HA binding, suggesting that cross-linking of HA chains is the critical factor for enhancing binding by LYVE-1. Furthermore, FL_TSG-6:HA complexes increased not only the amount of HA bound but the percentage of HA binding cells, consistent with a clustering effect on LYVE-1 that lowers the threshold of expression required for stable HA binding. To determine whether enhancement of bHA binding may be extended to cells expressing lower, more physiologically relevant levels of LYVE-1, hLYVE-1 pHRI Jurkat cells were incubated with Link_TSG-6 or FL_TSG-6:bHA complexes at the highest HA concentration of 2 µg/ml (Figure 5.3). No substantial enhancement was detected however, indicating that a minimum LYVE-1 expression level is required for HA binding, as was observed in experiments using potentiating LYVE-1 mAbs.

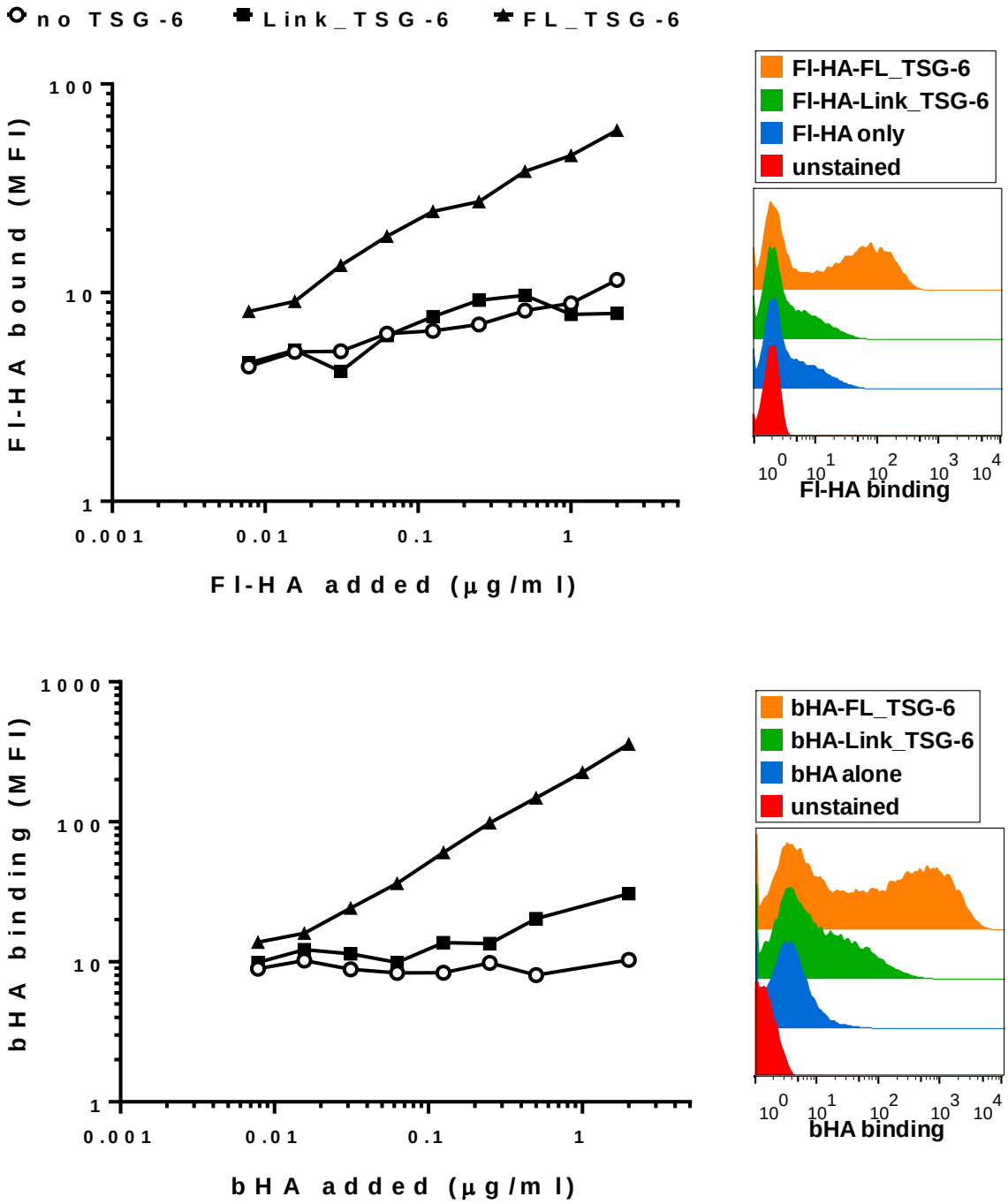


Figure 5.2. **Titration of hyaluronan bound to human LYVE-1 expressing Jurkat cells in the presence or absence of Link TSG-6 or Full Length TSG-6.** Fluoresceinated HA (Fl-HA) or biotinylated HA (bHA) was pre-incubated with the Link module from TSG-6 (Link_TSG-6) or the full length protein (FL_TSG-6) at a ratio of 5:1 (w/w) to form TSG-6:HA complexes. LYVE-1 transfected Jurkats were incubated with Fl-HA/bHA alone or Fl-HA/bHA:TSG-6 complexes at increasing HA concentration, and bound HA detected by fluorescein fluorescence or streptavidin Alexa 647 respectively. Histograms show the raw data at a HA concentration of 2 µg/ml. Data show in graph form are the mean fluorescence intensity (MFI) of 20 000 cells/condition and are representative of three independent experiments.

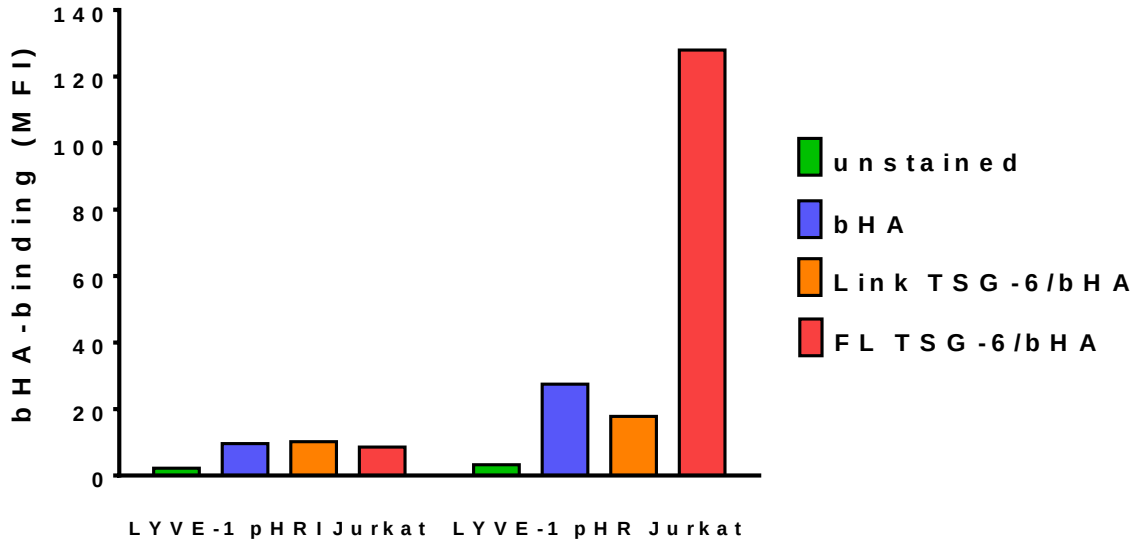


Figure 5.3. **Comparison of TSG-6:bHA binding by Jurkat transfectants expressing high or low levels of human LYVE-1.** Biotinylated HA (bHA) was pre-incubated with the Link module from TSG-6 (Link_TSG-6) or the full length protein (FL_TSG-6) at a ratio of 5:1 (w/w) to form TSG-6:HA complexes. LYVE-1 transfected Jurkats expressing low levels of LYVE-1 (pHRI) or high levels of LYVE-1 (pHR) were incubated with bHA alone or bHA:TSG-6 complexes at a bHA concentration of 2 µg/ml. Bound HA detected using streptavidin Alexa 647. Data are the mean fluorescence intensity (MFI) of 20 000 cells/condition from a single experiment.

Following the observation that TSG-6 can enhance constitutive HA binding by LYVE-1 transfected cell lines, it was important to determine whether TSG-6 could equally enhance binding by primary lymphatic endothelial cells. The results shown in Figures 5.4 – 5.6 demonstrate that this is indeed the case, which is the first indication that endogenous LYVE-1 is capable of binding a native HA format in primary cells. In an initial pilot experiment, the optimal TSG-6:bHA was determined empirically for both Link_TSG-6 and FL_TSG-6 (Figure 5.4). The rather modest effect of Link_TSG-6 on bHA binding by LYVE-1-transfectants contrasts the situation with similar CD44-expressing cells, where enhancement of HA binding was pronounced, even if reduced in comparison with FL_TSG-6 (Lesley et al., 2004). A requirement for cross-linking of HA chains would appear the most likely explanation, however it is also possible that the 5:1 (w/w) ratio of

TSG-6 to HA is unfavourable, for example if too few binding sites remain for LYVE-1 due to saturation with Link_TSG-6 molecules. To determine whether TSG-6:HA ratio is significant, primary HDLEC were cultured on gelatin-coated tissue-cultureware, lifted with Accutase and incubated for 30 minutes with Link_TSG-6 or FL_TSG-6:bHA complexes produced with varying TSG-6:bHA ratios from 10:1 - 0:1 (Figure 5.3). Enhancement of bHA binding by FL_TSG-6 increased markedly with TSG-6:bHA ratio to a peak at 5:1, but was significantly ablated at 10:1. Surprisingly, the behaviour of Link TSG-6 was opposite, with no apparent enhancement of bHA binding until pre-complexed at a ratio of 10:1. Ratios of 5:1 (FL_TSG-6) and 10:1 (Link_TSG-6) were therefore utilised in all subsequent experiments.

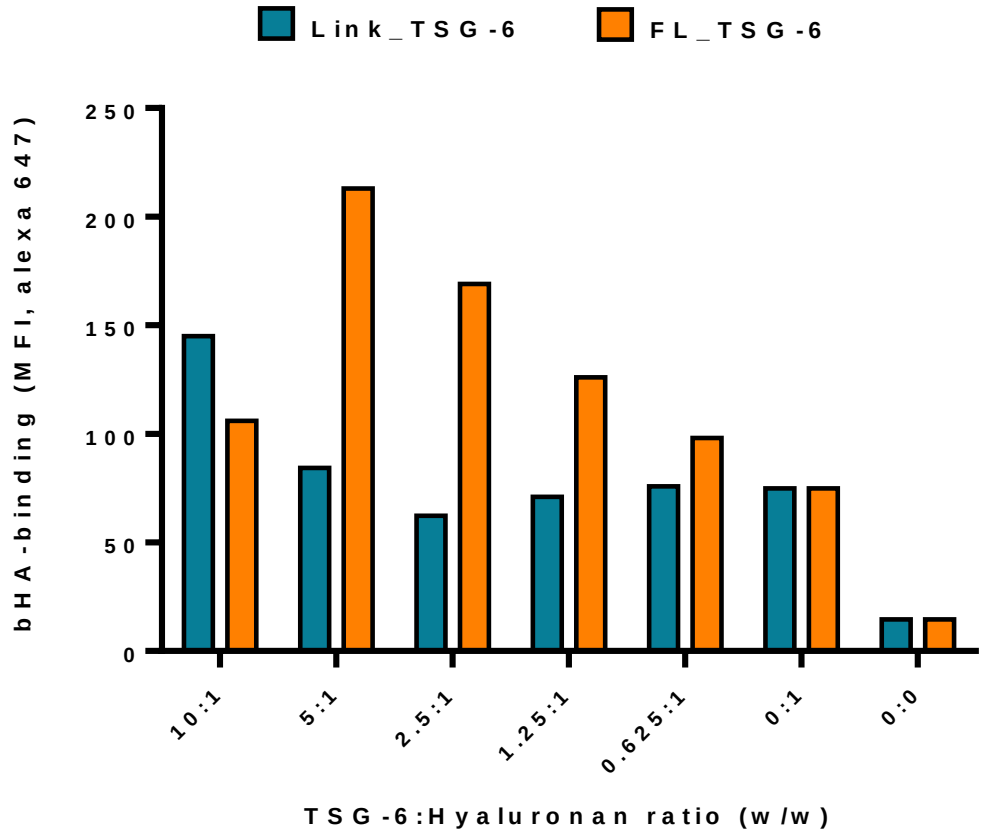


Figure 5.4. **Effect of varying TSG-6:HA ratio on hyaluronan binding by Human Dermal Lymphatic Endothelial Cells (HDLEC).** Biotinylated HA (bHA) at 5 µg/ml was pre-incubated with the Link module from TSG-6 (Link_TSG-6) or the full length protein (FL_TSG-6) at the ratios (w/w) indicated to form bHA:TSG-6 complexes. HDLEC were lifted with Accutase and incubated with bHA alone or bHA:TSG-6 complexes before

detection of bound bHA using streptavidin Alexa 647 and flow cytometry. Data are the mean fluorescence intensity (MFI) of 20 000 cells/condition from a single experiment.

Link_TSG-6 and FL_TSG-6 were tested for their ability to modify binding of bHA by native LYVE-1 on lymphatic endothelial cells in one of two ways; firstly bHA and either Link_ or FL_TSG-6 were pre-incubated for 30 minutes at the optimal ratio for each species and then diluted to 5 µg/ml bHA, prior to addition to cells and secondly, bHA and Link_ or FL_TSG-6 were diluted separately and then added together to HDLEC at the same final concentration as the pre-incubated reagents. When pre-incubated with bHA, Link_TSG-6 mediated a modest 1.6-fold enhancement of the weak residual bHA binding observed with low passage HDLEC with maximal LYVE-1 expression (Figure 5.5). Crucially, enhancement of bHA binding was seen only when bHA was pre-complexed with Link_TSG-6 and not when added separately during incubation with the cells. Binding of the Link_TSG-6:bHA complex could also be blocked effectively by co-incubation with LYVE-1 HA-blocking mAb 893 or an excess of unlabelled HA.

Pre-incubation of bHA with FL_TSG-6 also led to an enhancement of bHA binding that was stronger than that observed for Link_TSG-6, at 2.7-fold (Figure 5.6). Enhancement of bHA binding was also dependent on pre-incubation with TSG-6 and could be blocked using 893 mAb or free unlabelled HA. The greater potency of FL_TSG-6 over Link_TSG-6 was further demonstrated by comparing their effect on bHA binding by hLYVE-1 or hLYVE-1-GFP pHR HDLEC (Figure 5.7). These cells are infected with lentivirus such that they over-express wildtype or GFP-tagged hLYVE-1 and have high levels of constitutive HA binding. Pre-complexing of bHA with FL_TSG-6, but not Link_TSG-6 was found to significantly enhance bHA binding by these cells. In summary, although optimization of the TSG-6:HA ratio clearly reduced the difference in potency between Link_TSG-6 and

FL_TSG-6, these data, in combination with observations made using LYVE-1-transfected cells, demonstrate that cross-linking of hyaluronan can potently enhance HA binding by native LYVE-1 on the surface of primary HDLEC.

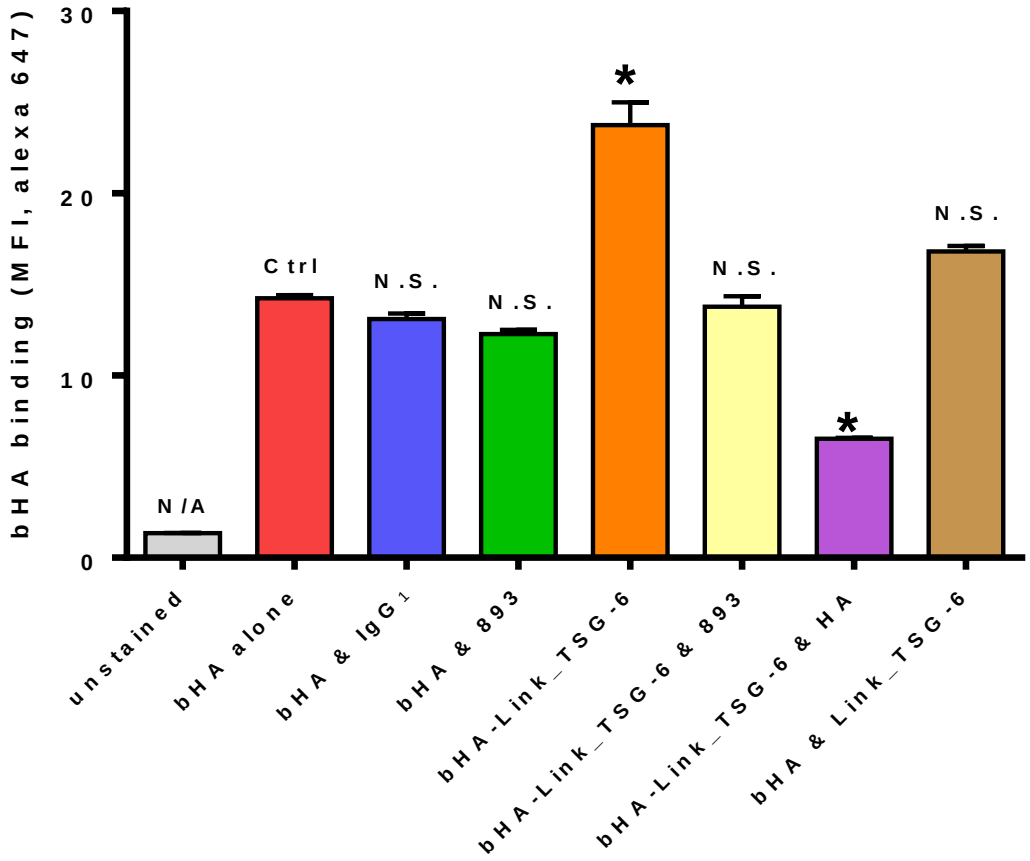


Figure 5.5. **Influence of Link_TSG-6 on hyalurona binding by primary Human Dermal Lymphatic Endothelial Cells (HDLEC).** Biotinylated HA (bHA) was pre-incubated with the Link module from TSG-6 (Link_TSG-6) at a ratio of 10:1 (w/w) TSG-6:HA to form a bHA-Link_TSG-6 complex. Cultured primary LEC were lifted with Accutase and incubated with bHA-Link_TSG-6 either alone, or in combination with HA blocking mAb 893, mouse IgG_1 isotype control or an excess on unlabelled HA. To permit comparison with the constitutive level of HA binding, cells were also incubated with bHA either alone, or in combination with 893 mAb or mouse IgG_1. To determine the significance of pre-incubation of Link_TSG-6 with bHA, both reagents were added to cells without prior pre-incubation (bHA & Link_TSG-6). In all instances, bound bHA was detected using streptavidin Alexa 647 and flow cytometry. Data are the MFI ± SEM of 20 000 cells/condition (n = 3) and are representative of two independent experiments. Statistics are a one-way ANOVA at a 99% CL using control cells (Ctrl) as the comparator. Asterisk (*****) denote a P value of <0.01, **N/S** denotes not significant, **N/A** denotes not applicable.

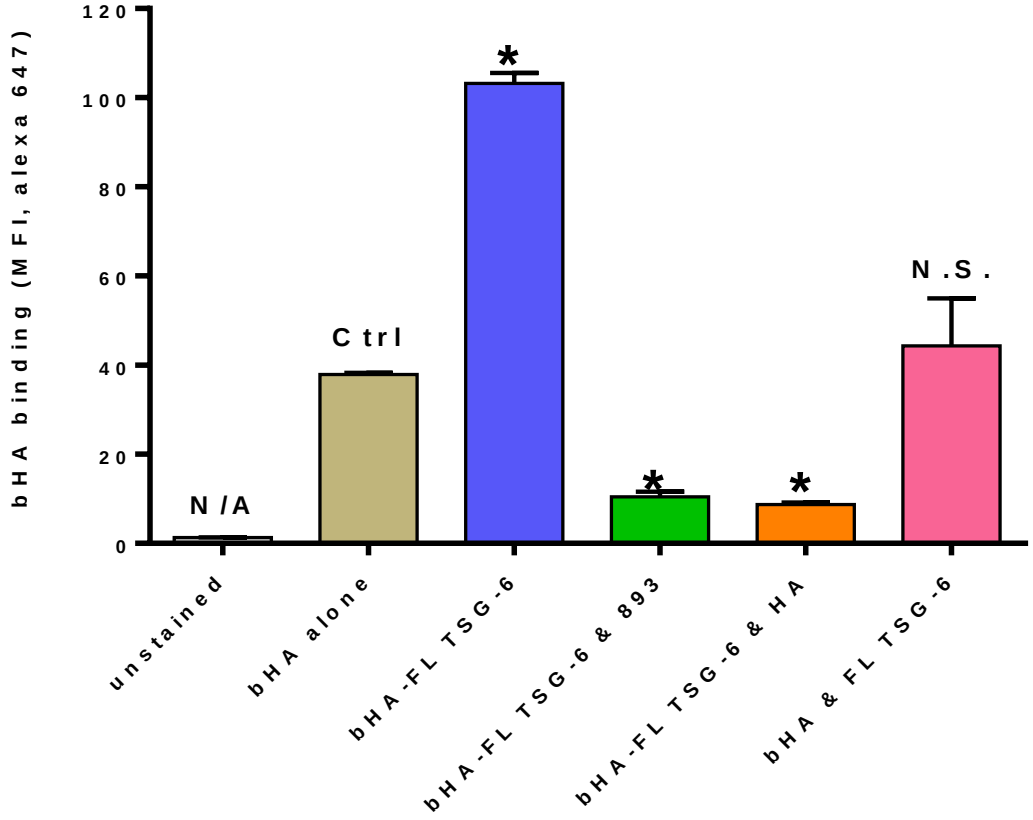


Figure 5.6. **Influence of Full Length_TSG-6 on hyaluronan binding by primary Human Dermal Lymphatic Endothelial Cells (HDLEC).** Biotinylated HA (bHA) was pre-incubated with Full length TSG-6 (FL_TSG-6) at a ratio of 5:1 (w/w) TSG-6:HA to form a bHA-FL_TSG-6 complex. Cultured primary HDLEC were lifted with Accutase and incubated with bHA-FL_TSG-6 either alone, or in combination with HA blocking mAb 893, mouse IgG_1 isotype control or an excess on unlabelled HA. To permit comparison with the constitutive level of hyaluronan binding, cells were also incubated with bHA either alone, or in combination with 893 mAb or mouse IgG_1. To determine the significance of pre-incubation of FL_TSG-6 with bHA, both reagents were added to cells without prior pre-incubation (bHA & FL_TSG-6). In all instances, bound bHA was detected using streptavidin Alexa 647 and flow cytometry. Data are the mean fluorescence intensity ± SEM of 20 000 cells/condition (n = 3) and are representative of two independent experiments. Statistics are a one-way ANOVA at a 99% CL using control cells (Ctrl) as the comparator. Asterisk (*****) denote a P value of <0.01, **N/S** denotes not significant, **N/A** denotes not applicable.

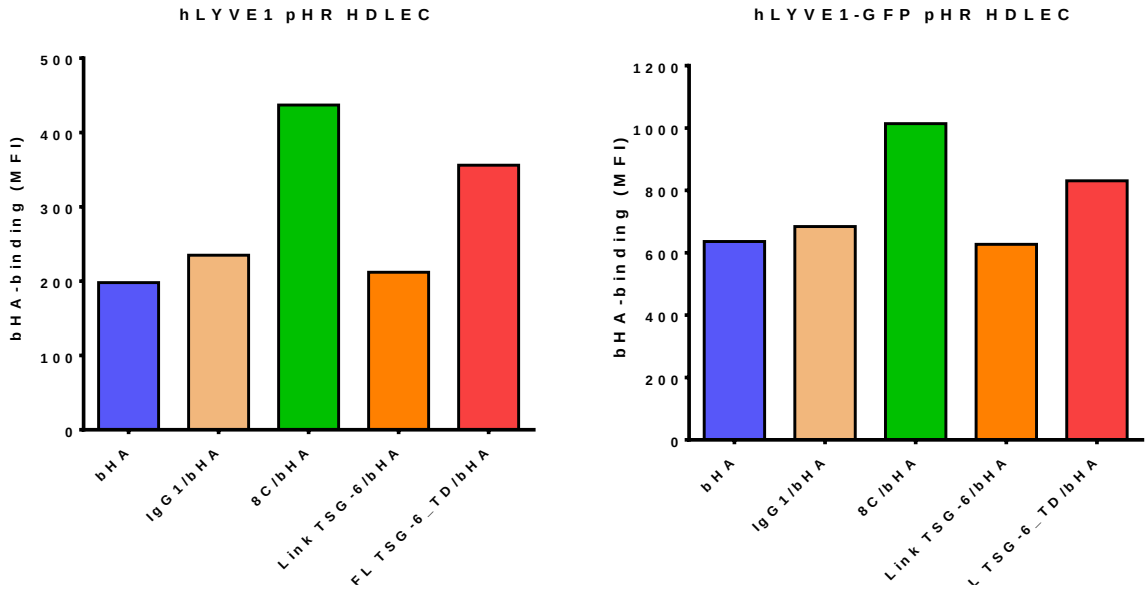


Figure 5.7. **Influence of pre-incubation of Link_TSG-6 or Full length TSG-6 with hyaluronan on binding by primary HDLEC super-transfected with wildtype human LYVE-1 or GFP-tagged human LYVE-1.** Primary HDLEC were infected using a lentiviral vector (pHR) encoding full length human LYVE-1 or LYVE-1-GFP and expanded in culture. Biotinylated HA (bHA) was pre-incubated with the Link module from TSG-6 (Link_TSG-6) or the full length protein (FL_TSG-6) at a ratio of 5:1 (w/w) to form TSG-6:HA complexes. Cells were incubated with TSG-6:bHA complexes or bHA, either alone or in combination with hLYVE-1 mAb 8C or isotype-matched control Ig (IgG_1), to assess the effect on bHA binding. In all instances, bound bHA was detected using streptavidin Alexa 647 and flow cytometry. Data are the mean fluorescence intensity of 20 000 cells/condition from a single experiment.

5.3.3 Influence of TSG-6:HA complexes on LYVE-1 surface distribution

The mechanism by which TSG-6-crosslinking enhances HA binding may involve two complementary processes; firstly, the large footprint of the TSG-6:HA complex is likely to contact a greater number of LYVE-1 molecules than a single HA chain, resulting in increased binding avidity. This increased footprint is likely to result from TSG-6-mediated intra- and inter-chain linking that concentrates HA molecules and restrains their motion. Secondly, lateral diffusion of the complex across the cell surface may ‘collect’ and cluster LYVE-1 molecules, resulting in a local increase in receptor density that in turn enhances

binding through avidity effects. To determine whether enhancement of bHA binding by TSG-6 involves a change in LYVE-1 distribution, adherent monolayers of primary HDLEC were incubated with Link_TSG-6 or FL_TSG-6:bHA complexes and resulting changes in LYVE-1 staining observed by immunofluorescence microscopy (Figure 5.8). Interestingly, no binding of free bHA or Link_TSG-6:bHA complexes was detected, however punctate staining for FL_TSG-6:bHA was clearly visible. These areas corresponded well with identical punctate areas of LYVE-1 staining, although these local increases in LYVE-1 occurred with similar frequency in cells incubated with bHA alone. Further experiments using confocal microscopy followed by quantification of LYVE-1 enriched areas on cells treated with bHA alone or FL_TSG-6:bHA complexes will be required to demonstrate conclusively that LYVE-1 is clustered by contact with the latter.

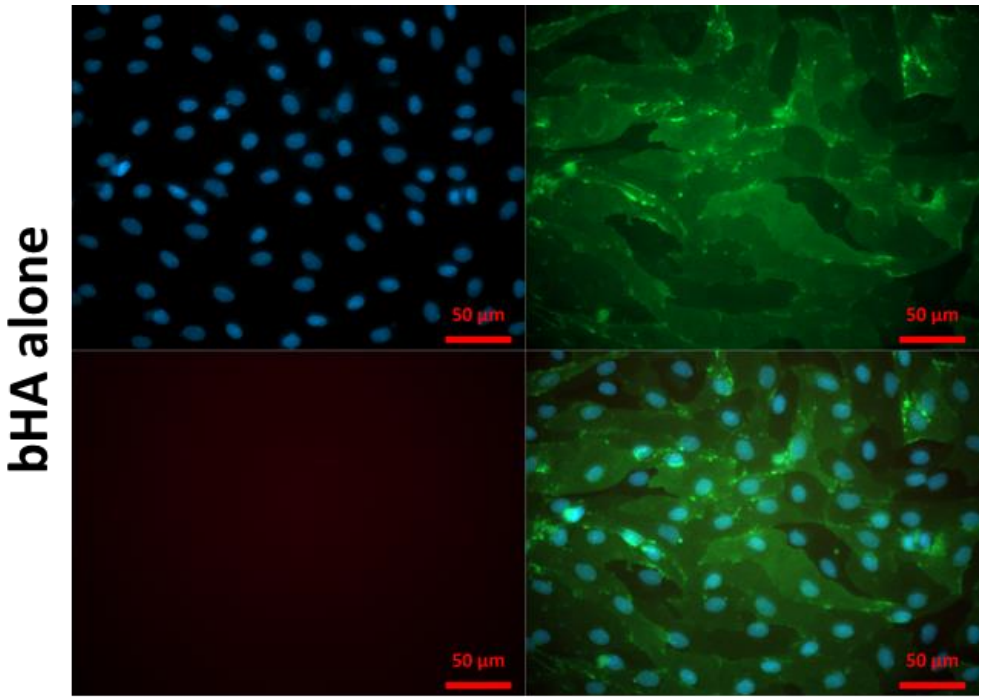
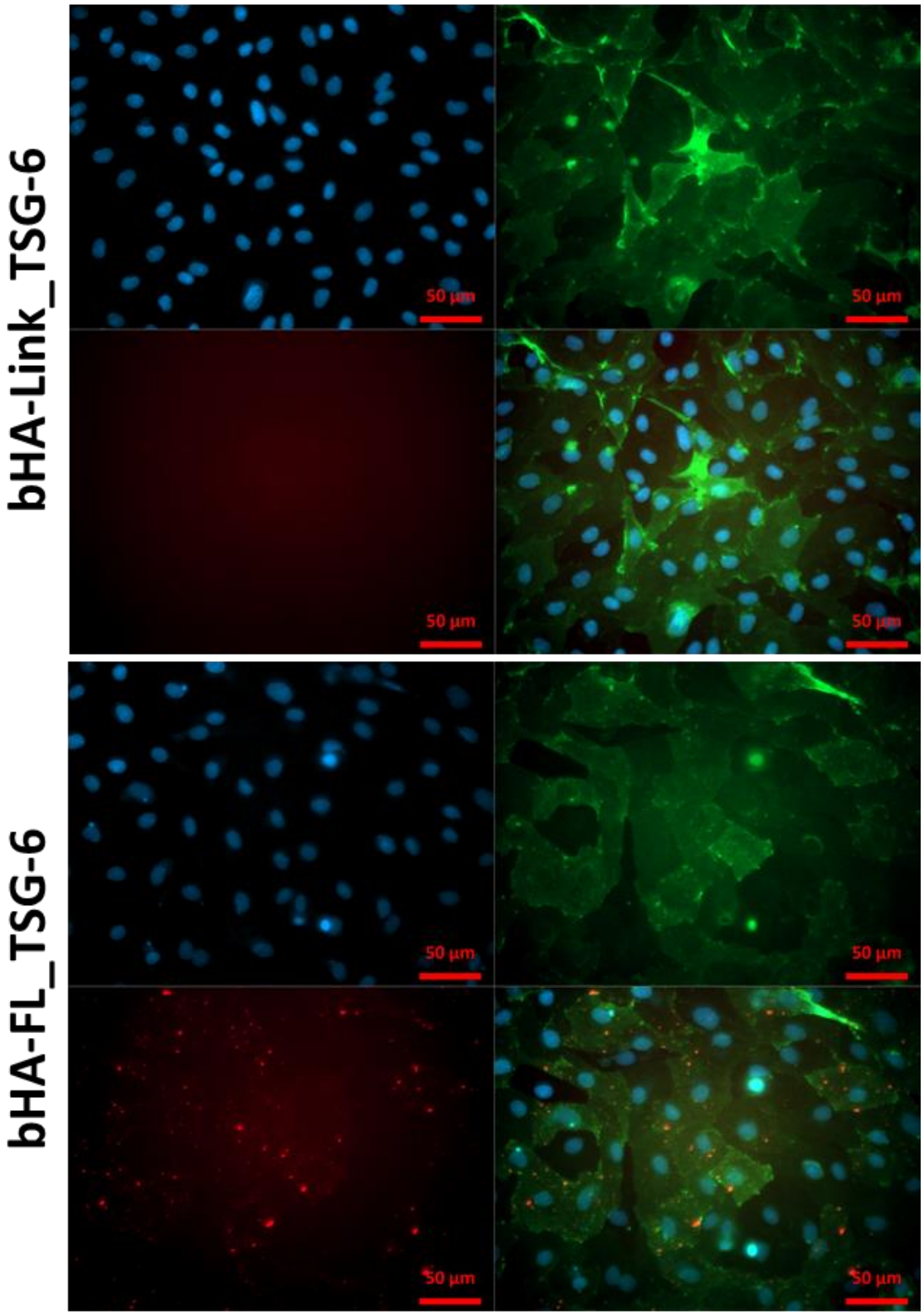


Figure 5.8. **Influence of pre-incubation of hyaluronan with Link TSG-6 or Full Length TSG-6 on binding by adherent primary Human Dermal Lymphatic Endothelial Cells**. Biotinylated HA (bHA) was pre-incubated with the Link module from TSG-6 (Link_TSG-6) or the full length protein (FL_TSG-6) at a ratio of 10:1 (Link) or 5:1 (FL) (w/w) to form TSG-6:HA complexes. Primary HDLEC were cultured on gelatin-coated 8-chamber slides (*continued overleaf*).

Cells were incubated with bHA, bHA-Link_TSG-6 or bHA-FL_TSG-6 as indicated, fixed with formaldehyde and incubated with DyLight488-conjugated 8C mAb (*green*) and streptavidin Alexa 647 (*red*). Cell nuclei were stained with DAPI (*blue*). Images were captured using an inverted epifluorescence microscope at 40x magnification and are representative of two independent experiments.



5.3.4 Modification of hyaluronan with heavy-chains from on inter-α-inhibitor and the influence on binding by LYVE-1

In addition to its function as an HA cross-linking protein, TSG-6 catalyses the only naturally-occurring covalent modification of HA; modification with heavy chains (HCs) donated from the serum protein inter-α-inhibitor (IαI) (Jessen and Odum, 2003; Mukhopadhyay et al., 2004; Rugg et al., 2005). Amongst other roles, the formation of HA•HC complex has been shown to promote leukocyte adhesion to HA matrices (de la Motte et al., 2003) in a CD44-dependent manner (Zhuo et al., 2006) and to modulate TSG-6 mediated enhancement of HA binding by CD44-expressing cells (Baranova et al., 2013). To determine whether modification of hyaluronan with heavy chains can influence HA binding by LYVE-1, it was first necessary to generate HA•HC complexes suitable for detection by flow cytometry. Accordingly, a method was chosen based on a protocol kindly shared by Dr. Mark Lauer (Lerner Research Institute, USA), with some modifications. Fl-HA or bHA were mixed with recombinant FL_TSG-6 (R&D Systems) and Human serum (Sigma) in 1x PBS to a final concentration of 40 µg/ml, 5 µg/ml and 0.04x, respectively. After incubation at room temperature for three hours, all of the heavy chains present in serum as IαI are expected to have been transferred to HA to form Fl-HA•HC or bHA•HC. Additional non-covalent TSG-6:HA complexes would also be expected, but at a ratio 0.125:1 (w/w) TSG-6:HA, which is below the minimal ratio found to enhance HA binding by LYVE-1 in Figure 5.4. To control for the contribution of such TSG-6:HA complexes, separate samples were generated in the absence of serum. To perform the binding step, free Fl-/b-HA, HA•HC, or TSG-6:HA were diluted to a final concentration of 5 µg/ml HA in 1% BSA, 5 mM EDTA, 0.05% NaN_3 in PBS and incubated with hLYVE-1 pHR Jurkat cells, to assess the influence on HA binding.

In pilot experiments, both Fl-HA•HC and bHA•HC complexes were found to bind more efficiently to hLYVE-1 pHR Jurkat cells than free Fl-HA or bHA alone (Figure 5.9). However, TSG-6 had the surprise effect of enhancing both Fl-HA and bHA binding by ~ 2-fold in the absence of serum (TSG-6:HA complex), despite the use of a sub-optimal TSG-6:HA ratio. The size of this enhancement was comparable, albeit lower than that observed with HA•HC (TSG-6 + serum + HA), at ~ 2.1-fold and ~ 2.6-fold for Fl-HA and bHA, respectively. Curiously, blockade of HA•HC binding by hLYVE-1 mAb 891 or an excess of unlabelled HA was incomplete, even at concentrations that are effective at blocking antibody-mediated potentiation of HA binding. Complexes of bHA•HC also enhanced 8C-mAb potentiation of bHA binding beyond that seen with free bHA. Taken together, these data suggested that commercial recombinant TSG-6 (R&D Systems) is capable of enhancing HA binding by LYVE-1 at lower TSG-6:HA ratios than previously observed, albeit using a different protocol for complex formation. The enhancement of HA binding was greater when HA and TSG-6 were pre-incubated in the presence of serum, consistent with heavy chain transfer to HA from IαI. The resulting HA•HC:TSG-6 complex exhibited greater binding to LYVE-1 expressing cells than TSG-6:HA complexes alone, potentially due to increased cross-linking of HA chains.

.

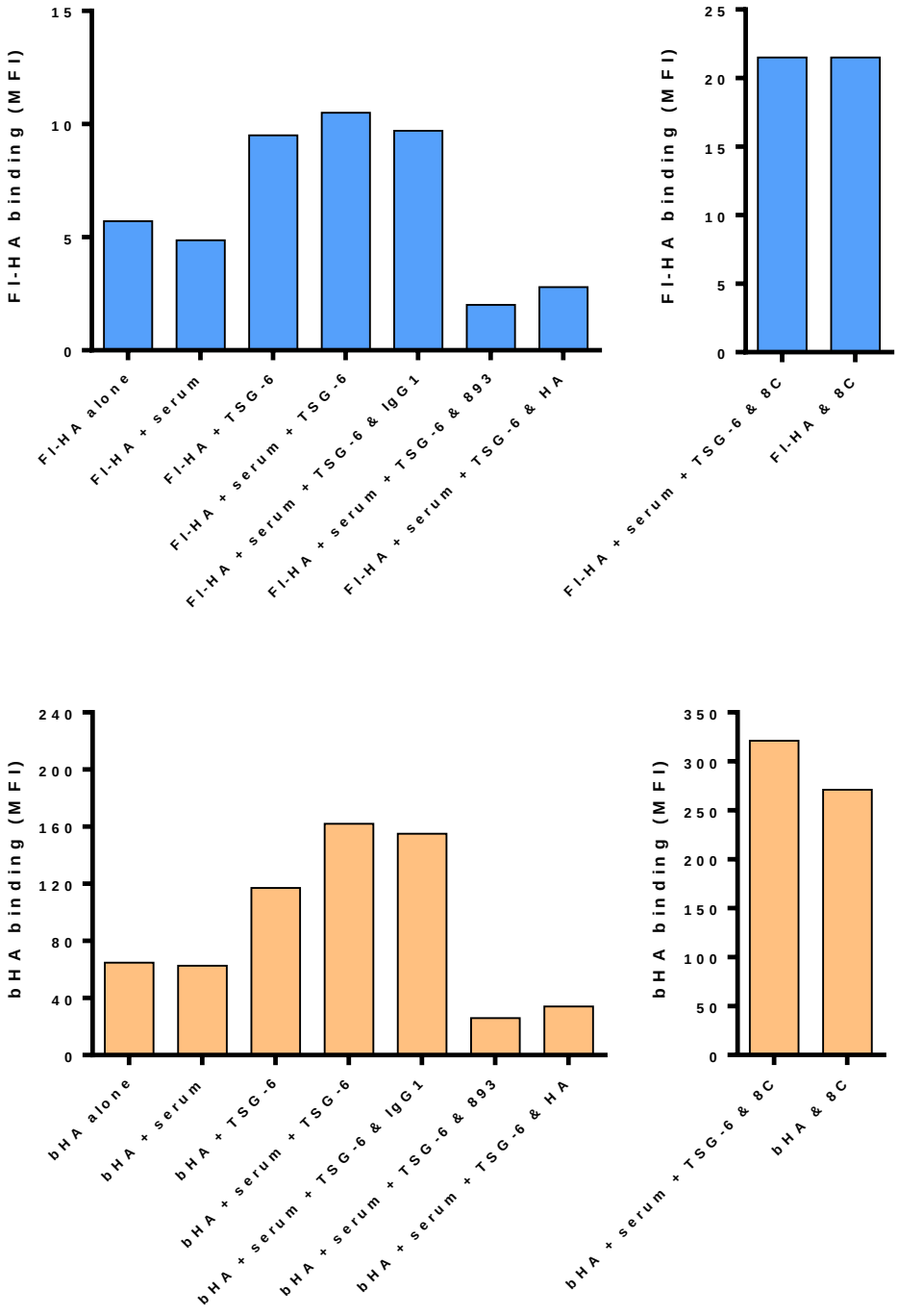


Figure 5.9. **Influence of Heavy Chain Hylauronan (HA•HC) and Full Length TSG-6 on hyaluronan binding by LYVE-1 expressing Jurkat cells.** Fluoresceinated or biotinylated HA (Fl-HA/bHA) was pre-incubated in PBS in the presence of human serum (HA + serum), recombinant full length TSG-6 (HA + TSG-6), or serum and TSG-6 (HA + serum + TSG-6). Human LYVE-1 pHR Jurkat cells were incubated at 1.66 x 10^6 cells/ml with HA alone, HA + serum, HA + TSG-6 or HA + serum + TSG-6 either alone, or in combination with individual hLYVE-1-specific mAbs, an excess of unlabelled HA or control Ig, to assess the effect on Fl-/bHA binding. Bound Fl-HA or bHA were detected with appropriate secondary detection reagents and flow cytometry. Data are the mean fluorescence intensity (MFI) 20 000 cells/condition from a single experiment.

The discrepancy in behaviour of commercial recombinant TSG-6 used here (R&D Systems; 'TSG-6_R&D') and that used for the HA cross-linking studies in the first part of this chapter (Prof. Anthony Day; 'TSG-6_TD') warranted further investigation. To evaluate the possibility that the unexpectedly large contribution from TSG-6:HA was due to the use of commercial TSG-6, a side-by-side comparison was conducted under the conditions described for formation of HA•HC, using recombinant FL_TSG-6 provided by Dr. David Mahoney, University of Oxford ('TSG-6_DM') as a further control. No enhancement of bHA binding was detected when bHA was pre-incubated with TSG-6_TD or TSG-6_DM, regardless of whether serum was present. Pre-complexing of bHA with TSG-6_R&D led to a small enhancement of binding compared to bHA alone, comparable to that observed previously (1.5-fold enhancement versus 1.9-fold). However, the inclusion of serum containing IαI in the pre-incubation mix did not result in any further enhancement of binding. Differences in the expression system, purification and storage are likely to result in a varying percentage of active protein in each sample of TSG-6, which may explain the differences observed in behaviour. However, comparison of a separate activity of TSG-6, that of osteoclast activation, suggested that the activity of TSG-6_ R&D is ~100-fold lower (Dr. D. Mahoney, personal communication). Even if modification of HA with heavy chains is inhibitory for binding by LYVE-1, this is difficult to reconcile with the lack of activity observed here. An assessment of the relative modification of HA with heavy chains by each TSG-6 sample was therefore required to determine whether the formation of HA•HC has any significance for binding by LYVE-1.

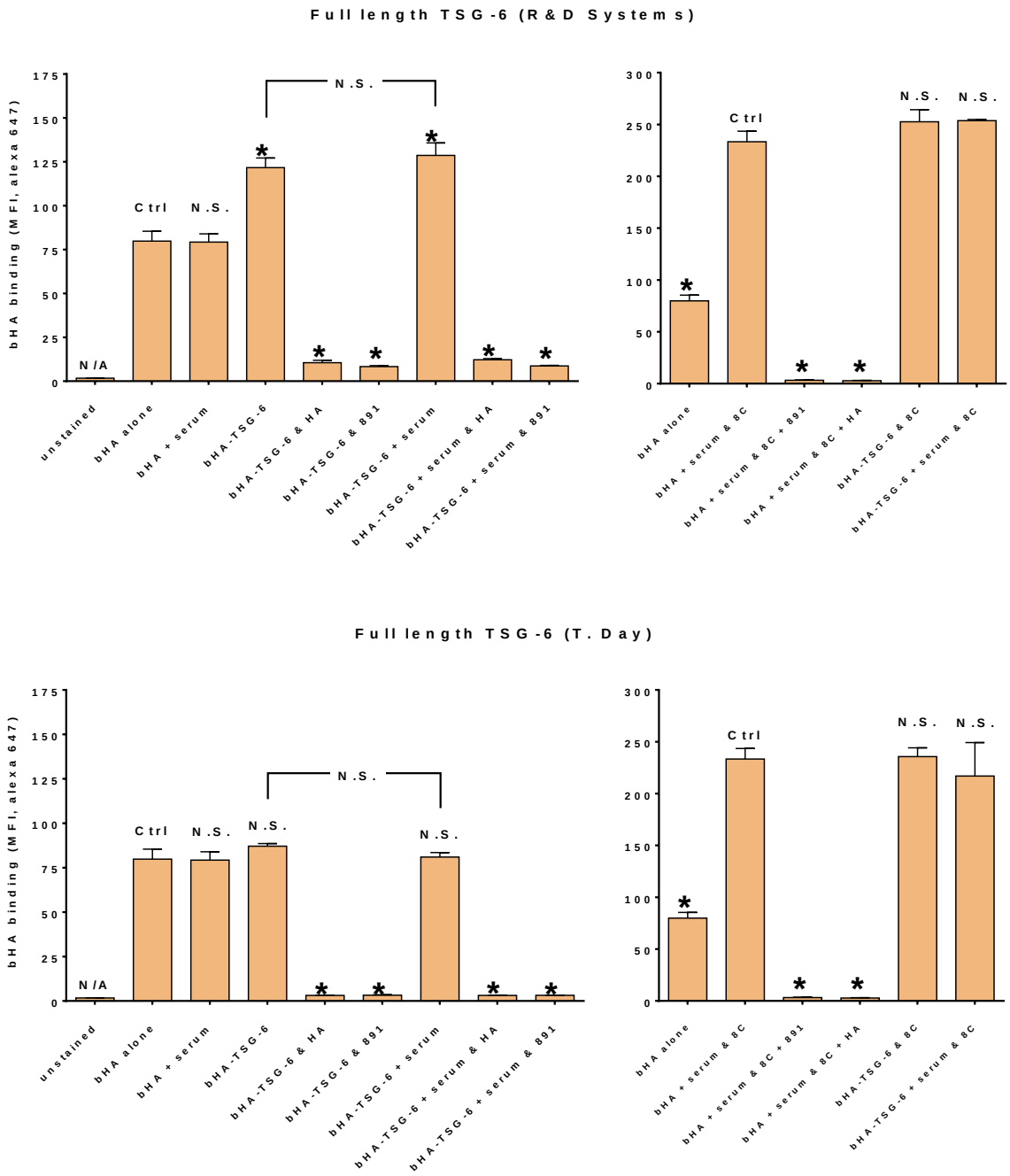


Figure 5.10 **Influence of Heavy Chain Hylauronan (HA•HC) and Full Length TSG-6 on hyaluronan binding by LYVE-1 expressing Jurkat cells – Comparison of TSG-6 from different sources.** Biotinylated HA (bHA) was pre-incubated in PBS in the presence of human serum (bHA + serum), recombinant full length TSG-6 from different sources (bHA + TSG-6), or serum and TSG-6 (bHA + serum + TSG-6). Human LYVE-1 pHR Jurkat cells were incubated with bHA alone, bHA + serum, bHA + TSG-6 or bHA + serum + TSG-6 either alone, or in combination with individual hLYVE-1-specific mAbs, an excess of unlabelled HA or control Ig, to assess the effect on bHA binding. Bound bHA were detected with streptavidin Alexa 647 and flow cytometry. Data are the mean fluorescence intensity (MFI) ± SD of 20 000 cells/condition (n = 3). *Continued overleaf.*

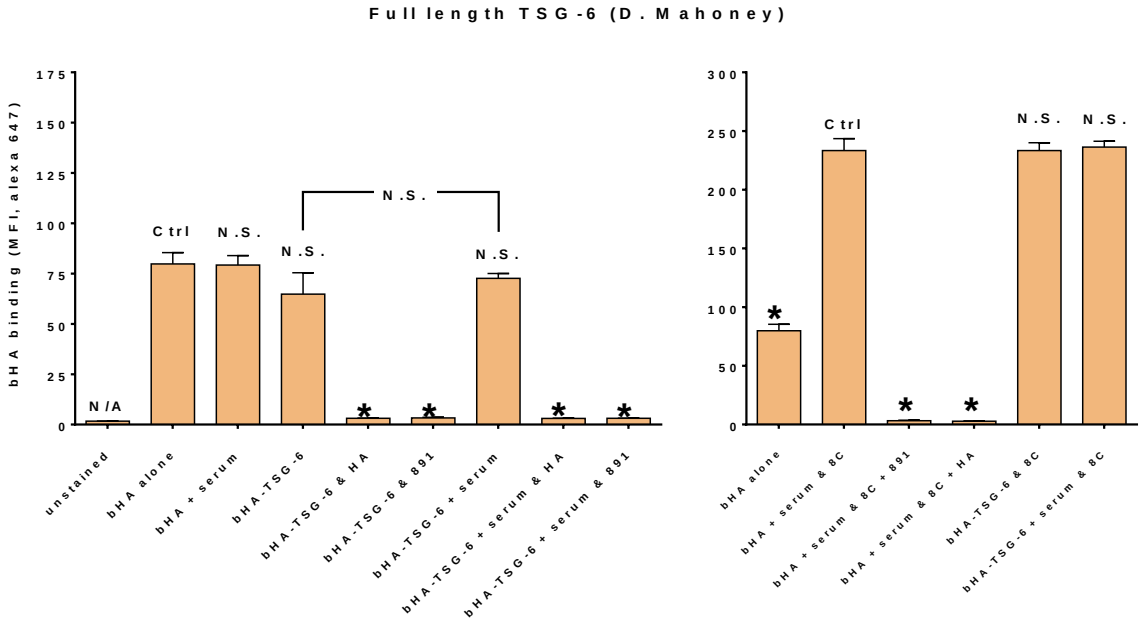


Figure 5.10 ***Continued*** Statistics are a one-way ANOVA at a 99% CL, control cells are identified by (Ctrl). Asterisk (*****) denote a P value of <0.01, **N/S** denotes not significant, **N/A** denotes not applicable. An unpaired, two-tailed t-test was used separately to compare cells incubated with bHA-TSG-6 and bHA-TSG-6 + serum at the 99% CL. **N.S.** denotes not significant (P > 0.01).

To compare the efficiency of heavy chain transfer to HA by different TSG-6 preparations, samples of HA•HC were tested for the presence of heavy chains using a protocol based on that described for the detection of HA•HC in tissues (Swaidani et al., 2013). Briefly, samples of HA•HC produced by each protein were digested with *Streptomyces* hyaluronidase for 2 hours at 37^{o}C, and probed by western blot using polyclonal anti-IαI antibody[1] (Dako) side-by-side with untreated samples. A heavy-chain gel shift from 250 kDa (i.e. IαI) to 83 kDa (HCs liberated following Hyase digestion) is evidence of HC transfer to HA. As shown in Figure 5.11, a band corresponding to heavy-chain was detected for all TSG-6 preparations, however it was present at equal intensity in both untreated and Hyase-digested samples. This is curious, as even if the serum used came from a patient

[1] Provided by Dr. M. Lauer, Lerner Research Institute, under Award Number P01HL107147 from the National Heart, Lung and Blood Institute.

experiencing inflammation, heavy chains would not be expected to be detected without Hyase-digestion. These data do suggest however, that formation of HA•HC was not effective for any of the TSG-6 preparations used, and that further experiments will be required to determine the optimal conditions for HC transfer and the effect on HA binding by LYVE-1. Unfortunately due to time constraints it was not possible to explore these observations further.

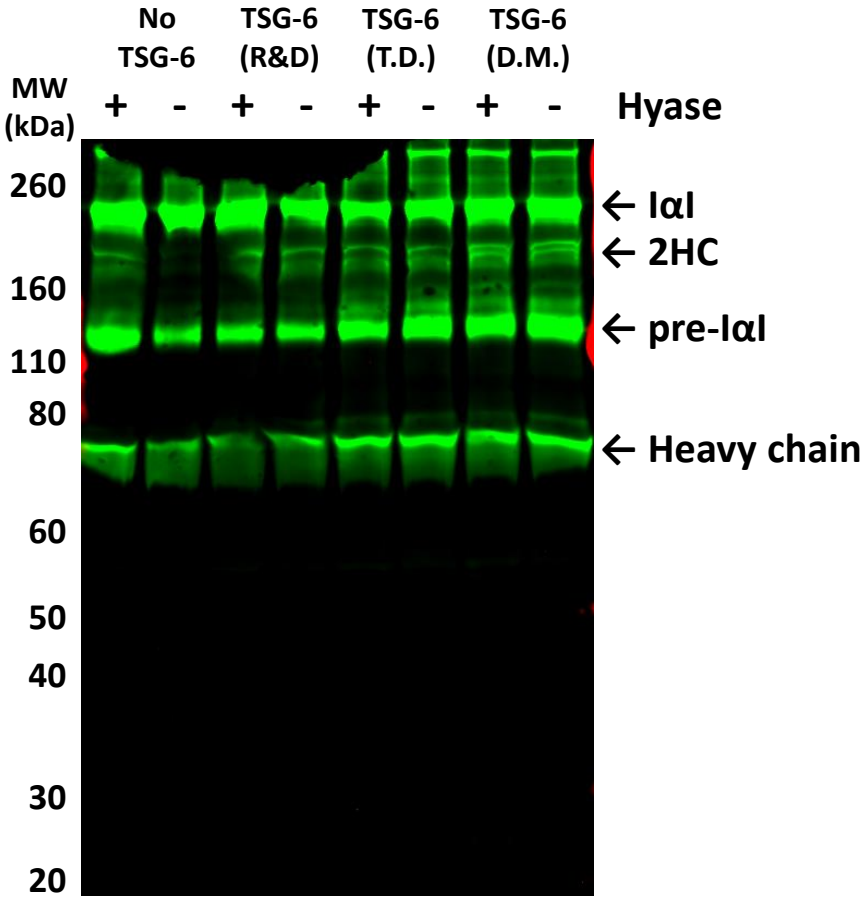


Figure 5.11. **Western blot of Heavy Chain Hylauronan (HA•HC) formation by recombinant TSG-6 samples**. Samples of HA•HC produced by different TSG-6 preparations were treated with Streptomyces Hyase for 2 hours at 37°C. Hyase-treated samples were run side-by-side with untreated samples on 4-12% LDS-PAGE gels, western blotted and probed with rabbit polyclonal anti-IαI antibody and donkey anti-rabbit IRDye 800CW secondary antibody and a Li-Cor Odyssey Classic imager. Bands corresponding to the molecular weight of IαI, biosynthetic intermediates 2HC and pre-IαI, and the digestion product heavy chain are indicated. Blot is taken from a single experiment.

5.3.5 Binding of hyaluronan-coated fluorescent microspheres to LYVE-1 in primary lymphatic endothelial cells

Recent work in the Jackson laboratory has revealed that primary lymphatic endothelial cells are capable of binding the HA coat of certain strains of group A streptococcus in a LYVE-1 dependent manner. The interaction of LYVE-1 with the bacterial HA coat leads to clustering of the receptor at the point of contact, further demonstrating that constrained arrangements of hyaluronan can alter receptor distribution and induce HA binding. This observation suggests that the close array of HA chains on the surface of a cell, perhaps anchored by CD44 or extruded by an HA synthase, may be sufficient to promote stable binding by LYVE-1. In an attempt to model this scenario *in vitro*, streptavidin-coated 1 µm-diameter fluorescent microspheres were incubated with end-biotinylated 30 kDa or 300 kDa HA[1] or randomly-biotinylated high molecular weight HA, to create artificial 'cell protusions' with a surface array of anchored HA chains. HA chains with a molecular weight of 30 or 300 kDa offer numerous potential LYVE-1 binding sites, but 30 kDa HA was found to be the approximate threshold size at which binding by CD44 became essentially irreversible (Wolny et al., 2010).

Cultured monolayers of primary HDLEC (Figure 5.12) or HDLEC over-expressing GFP-tagged hLYVE-1 (Figure 5.14) were incubated with unlabelled or hyaluronan-coated fluorescent microspheres either alone, or in combination with hLYVE-1 HA-blocking mAb 891, and visualized using epifluorescence microscopy. The results show that primary LEC are capable of binding HA coated microspheres, with no requirement for potentiation using LYVE-1-specific mAbs or HA cross-linking proteins. Microspheres coated with 30 kDa or 300 kDa HA were bound most efficiently, and in a LYVE-1 dependent manner, as

[1] 30 kDa and 300 kDa end-biointylated HA were a kind gift from Professor Paul DeAngelis, University of Oklahoma Health Sciences Centre.

demonstrated by effective blockade using 891 mAb. This was also true of LEC transduced with lentivirus that over-express LYVE-1 and bind greater numbers of microspheres than wildtype cells (Figure 5.14). Microspheres coated with randomly biotinylated HA were also bound but in much reduced numbers, which may be due to a lower surface coating of HA, while unlabelled beads did not bind (Figure 5.12). To determine whether interaction with HA-coated microspheres influenced the distribution of LYVE-1 molecules, cells were incubated with a polyclonal anti-LYVE-1 antibody and visualized at high magnification. LYVE-1 staining was most intense at the point of contact with HA-coated microspheres, including to numerous places where the sphere had dissociated during subsequent washing steps (

Figure 5.13). Interaction with the HA coat appears to cluster LYVE-1 molecules, which presumably increases the binding avidity in a similar fashion to TSG-6:HA complexes. Taken together, these data provide further evidence that close arrays of HA chains at a fixed point is sufficient to cluster LYVE-1 molecules and induce stable binding, and provide proof-of-concept of the use of hyaluronan-coated microspheres as a model system.

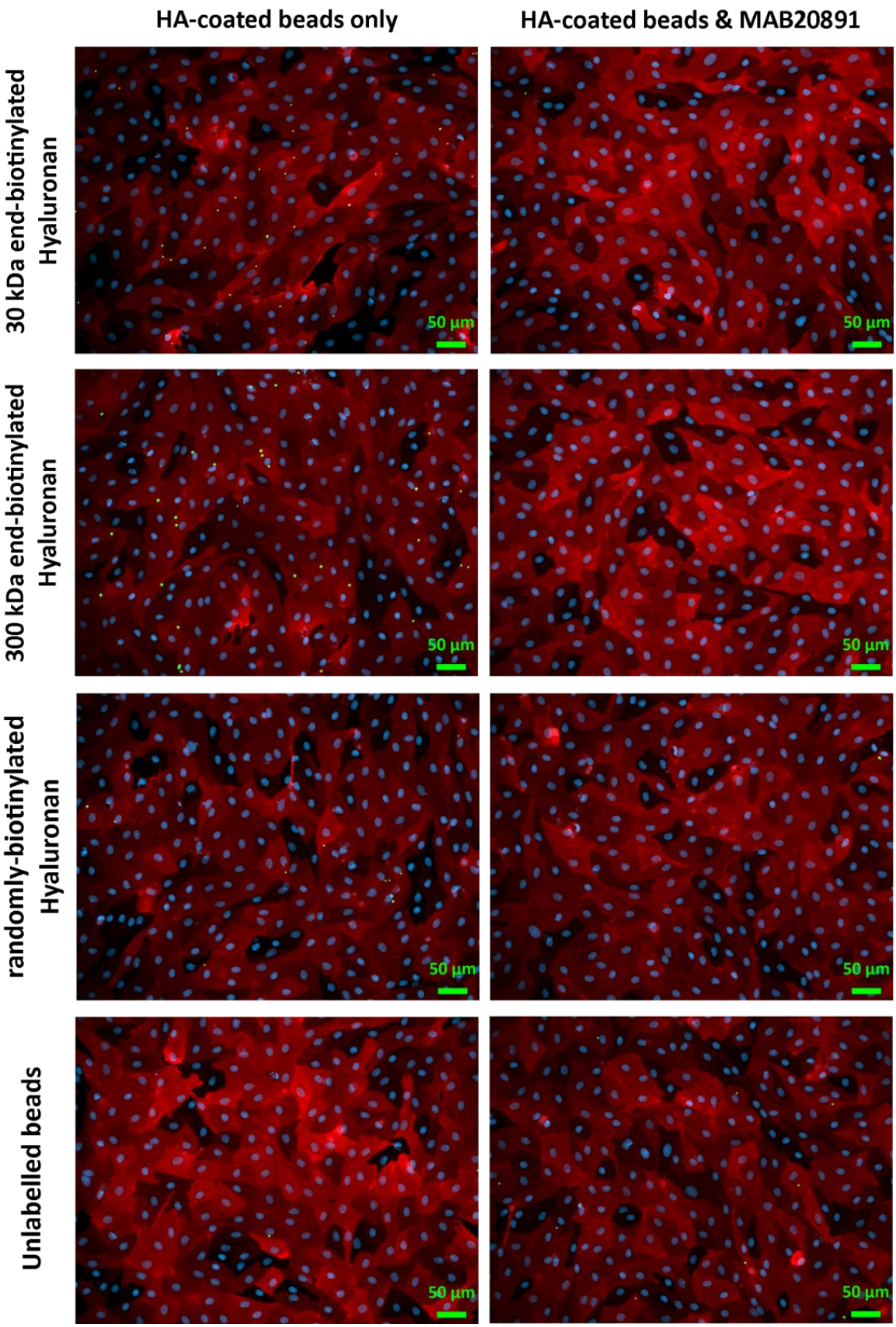


Figure 5.12. **Binding of Hyaluronan-coated fluorescent microspheres by adherent monolayers of primary HDLEC**. HDLEC were cultured on gelatin-coated 8-chamber

slides. Cells were incubated with 1 µm-diameter fluorescent polystyrene microspheres (beads, *green*) labelled with 30 kDa or 300 kDa end-biotinylated hyaluronan or randomly biotinylated HA, either alone or in combination with hLYVE-1 mAb 891. Cells were fixed with freshly depolymerised formaldehyde and incubated with goat-anti hLYVE-1 polyclonal. Cell nuclei were stained with DAPI (*blue*) and hLYVE-1 poly with anti-goat IgG Alexa 647 (*red*). Images were captured using an inverted epifluorescence microscope (Zeiss Axiovert S100) fitted with a 40x objective and a Hammatsu digital camera and are representative of two independent experiments.

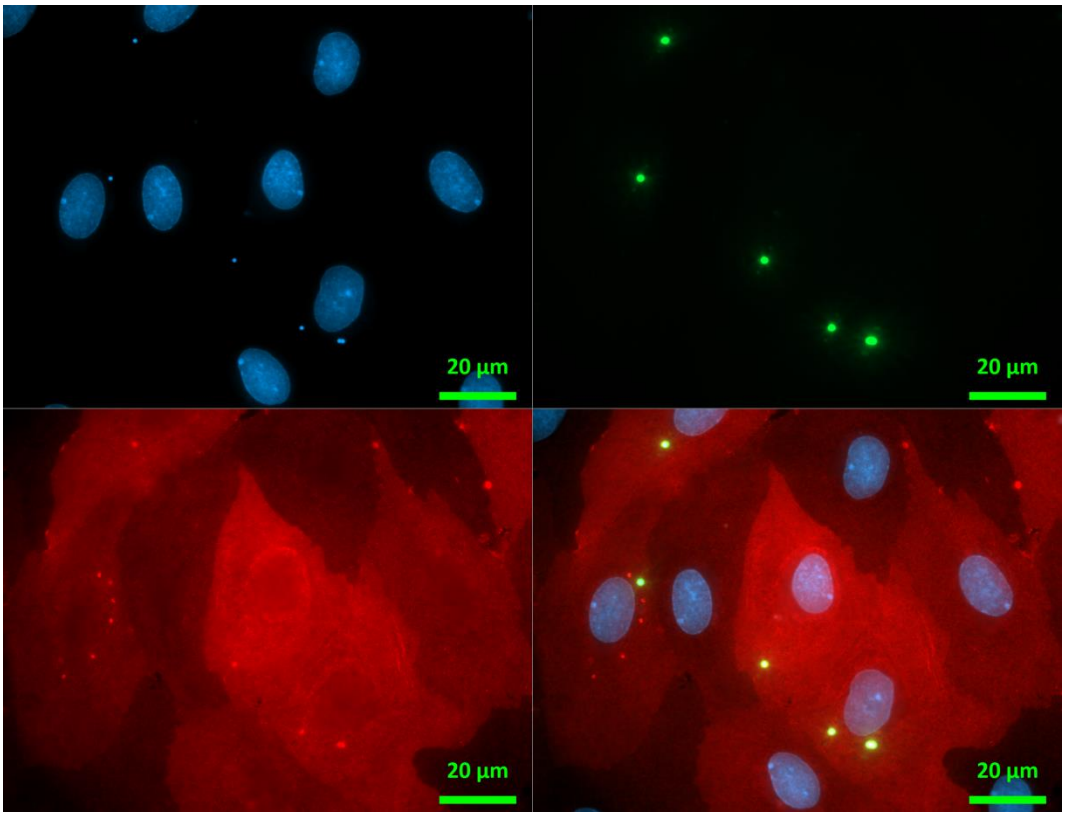


Figure 5.13. **Influence of hyaluronan-coated fluorescent microspheres on LYVE-1 distribution in adherent HDLEC monolayers.** HDLEC were cultured on gelatin-coated 8-chamber slides. Cells were incubated with 1 µm-diameter fluorescent polystyrene microspheres (*green*) labelled with 300 kDa end-biotinylated hyaluronan. Cells were fixed with freshly depolymerised formaldehyde and incubated with goat-anti hLYVE-1 polyclonal. Cell nuclei were stained with DAPI (*blue*) and hLYVE-1 poly with anti-goat IgG Alexa 647 (*red*). Images were captured from a single experiment in separate channels using an inverted epifluorescence microscope (Zeiss Axiovert S100) fitted with a 100x oil-immersion objective and a Hammatsu digital camera. A merged image is shown in the bottom right.

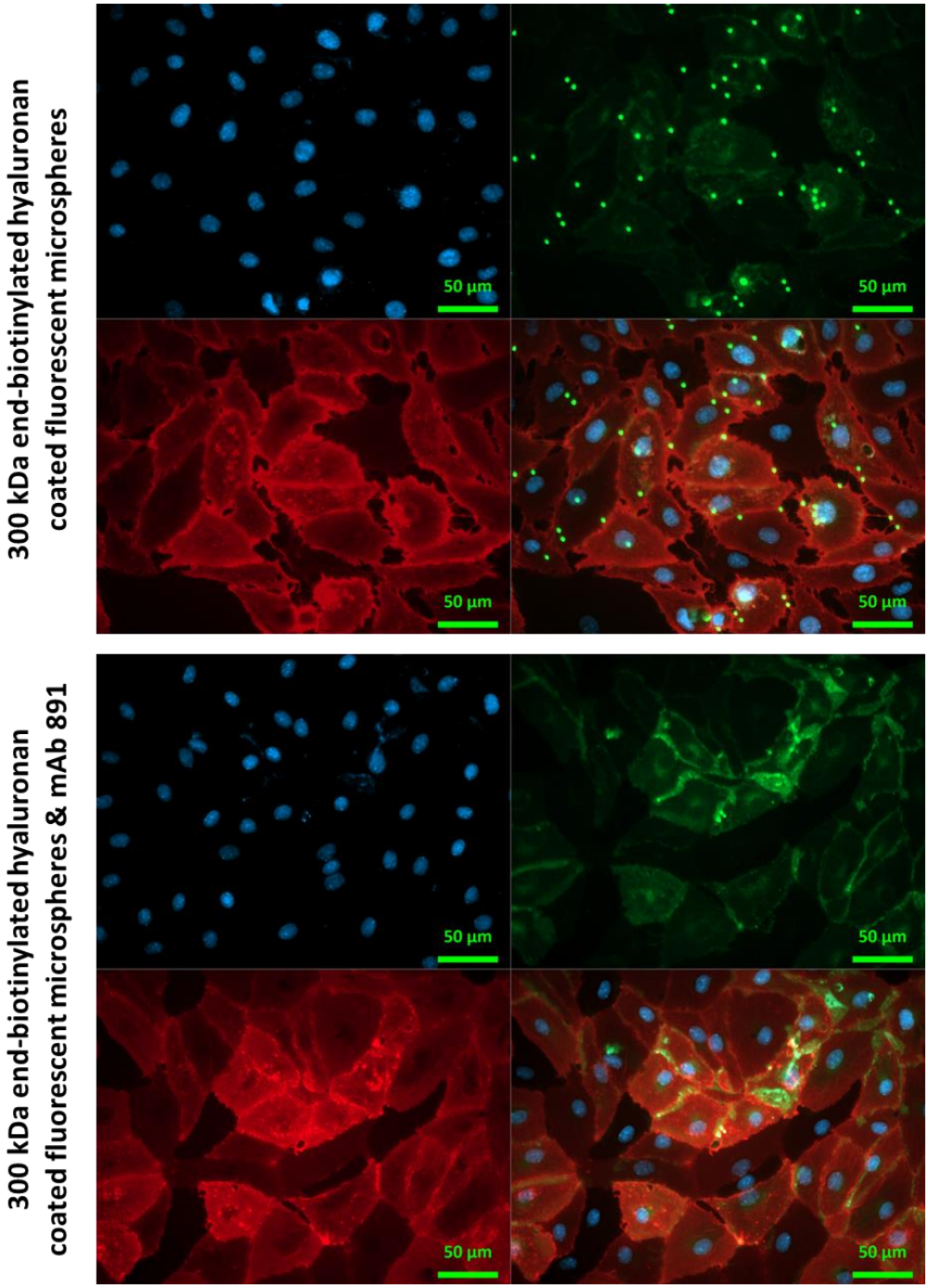


Figure 5.14. **Binding of hyaluronan-coated fluorescent microspheres by LYVE-1-GFP over-expressing adherent HDLEC monolayers.** Human LYVE-1-GFP pHR HDLEC were cultured on gelatin-coated 8-chamber slides. Cells were incubated with 1 µm-diameter fluorescent polystyrene microspheres (*green*) labelled with 300 kDa end-biotinylated hyaluronan, either alone or in combination with hLYVE-1 mAb 891. Cells were fixed with freshly depolymerised formaldehyde and incubated with goat-anti hLYVE-1 polyclonal. Cell nuclei were stained with DAPI (*blue*) and hLYVE-1 poly with anti-goat IgG Alexa 647 (*red*). Images were captured from a single experiment in separate channels using an inverted epifluorescence microscope (Zeiss Axiovert S100) fitted with a 100x oil-immersion objective. A merged image is shown in the bottom right.

5.4 Discussion

In this chapter, exposure to cross-linked hyaluronan complexes is shown to enhance constitutive binding by LYVE-1 transfected cell lines and to induce binding to LYVE-1 in primary lymphatic endothelial cells. Firstly, a proof-of-concept experiment using randomly biotinylated HA (bHA) demonstrated that cross-linking with streptavidin Alexa 647 (S647) led a to a 5-fold increase in binding compared to free bHA alone. The magnitude of the increase was related to the degree of cross-linking, with an optimal ratio of S647:bHA of 0.06:1 (w/w), above or below which the enhancement effect was lost, and binding decreased towards the constitutive level. Cross-linking of bHA increased not only the amount of bHA bound, but also the percentage of the cell population that engaged in binding. As described in Chapter 4, the difference between HA binding or not in LYVE-1 transfectants can rest on a fine threshold of LYVE-1 expression. An increase in the percentage of HA binding cells would be consistent with a lowering of this threshold, which may explained by the enlarged footprint of SA647:bHA complexes compared to individual bHA chains. This would promote stable binding in cells with lower LYVE-1 surface densities by permitting contact with a greater number of LYVE-1 receptors and restraining the motion of individual HA chains.

Cross-linking of HA by the small inflammation-induced protein TSG-6 has been reported to enhance HA binding by CD44-transfected cells and to induce binding in $CD44^+$ lines that lack constitutive binding (Baranova et al., 2013; Lesley et al., 2004). Enhancement of binding likely involves two factors; firstly an increase in the valency of HA arising from cross-linking of multiple HA chains, and second a clustering of the receptor that leads to enhanced binding through avidity effects. While direct evidence of cross-linking by full length TSG-6 (FL_TSG-6) has been found, the picture for recombinant TSG-6 Link

module (Link_TSG-6) is less clear, as it is uncertain whether the protein is capable of self-association (Baranova et al., 2011). It has been proposed however, that binding of multiple hyaladherins to an HA chain may stabilize distinct HA conformations that are more rigid than free HA (Day and Sheehan, 2001), and it is possible that Link_TSG-6 induces a conformation that enhances binding by CD44.

In this study, pre-incubation of FL_TSG-6 with HA enhanced binding by LYVE-1 transfectants and induced binding in primary LEC, while Link_TSG-6 had little or no effect. The reason for this apparent difference between LYVE-1 and CD44 is unclear, but the necessity of pre-incubation with HA for enhancement of binding and its dependence on an optimal TSG-6:HA ratio, are strongly indicative of a requirement for cross-linking. The punctate nature of both bHA and LYVE-1 distribution on the surface of LEC following incubation with bHA-FL_TSG-6, but not bHA-Link_TSG-6, also highlights the importance of HA cross-linking, and suggests TSG-6:bHA complexes are capable of clustering of the receptor. Taken together, these data demonstrate in principle that TSG-6 is capable of regulating HA binding by LYVE-1 on lymphatic endothelial cells. In terms of co-localization, TSG-6 is known to be synthesized by a variety of cell types, including dendritic cells undergoing TNFα-driven maturation (Le Naour et al., 2001), fibroblasts and vascular endothelial cells. It will be intriguing to determine whether LEC are themselves capable of producing TSG-6, or indeed whether TSG-6-crosslinked HA is encountered from the extracellular space or on the surface of a transmigrating cell. If this can be shown to be the case, it is entirely possible that TSG-6 cross-linking of HA represents a mechanism for promoting adhesion to LYVE-1 expressing lymphatic vessels during inflammation. Conceivably this would have significant impact on a variety of processes, including HA uptake and metabolism, and HA-mediated docking or transmigration of lymphatic endothelium by CD44-expressing leukocytes.

There are numerous examples in the literature where transfer of heavy chains (HC) from inter-α-inhibitor to HA by TSG-6 influences the structure of HA, with associated consequences for binding by proteins such as CD44 (Kida et al., 1999; Shen et al., 2006; Zhuo et al., 2006). The precise nature of heavy-chain cross-linking of HA, the involvement of additional proteins, and the influence on HA structure and resulting cellular responses are complex and a rapidly growing field. Most recently, HC transfer to HA has been found to partially displace bound TSG-6, leading to a reduction in TSG-6-mediated enhancement of HA binding by CD44 (Baranova et al., 2013). An attempt was made here investigate the effect of HC transfer to HA on binding by LYVE-1-transfected cells. While a pilot experiment showed initial promise, with the observation that binding of heavy-chain HA exceeded that of free HA, these data could not be repeated with other preparations of TSG-6. Furthermore, there was some doubt regarding the efficiency of HC transfer to HA, which may stem from the source of serum used, and further experiments will therefore be required to determine the influence of HC on HA binding by LYVE-1.

Recently, lymphatic endothelial cells have been shown to bind the pericellular HA coat of certain group A streptococcal strains, with the effect that LYVE-1 is densely clustered beneath the point of contact (Banerji, Lynskey, Sriskandan and Jackson, manuscript in preparation). This suggested that LYVE-1 is capable of binding native HA when densely arrayed and anchored to the cell surface. Fluorescent hyaluronan-coated microspheres were generated to model this scenario and found to bind efficiently to LEC, in a manner that could be blocked using LYVE-1 HA-blocking mAbs. Furthermore, the interaction with these microspheres led to clustering of LYVE-1, in much the same manner observed for group A streptococcus. The increased valency and clustering effect likely explain how stable binding is achieved, and has led to consideration of other situations where HA may be similarly arrayed. Dendritic cells are known to express HA synthases (HAS) and

actively synthesize HA when activated (Mummert et al., 2002). HA chains in the process of being extruded by HAS or anchored by CD44 expressed by these cells could conceivably represent a hyaluronan array that may be bound by LYVE-1, mediating DC adhesion to lymphatic vessels.

Chapter 6.
Analysis of LYVE-1-Hyaluronan Interactions using cellular assays and the Quartz Crystal Microbalance

6.1 Introduction

6.1.1 Function of LYVE-1 homodimers

The capacity of LYVE-1 to form disulphide-linked homodimers, in addition to monomers has been known for some time (Nightingale, 2004). First observed in LYVE-1-transfected cells by Western blotting, homodimers have also been identified in primary LEC from humans and mice. Multiple sequence alignments of LYVE-1 from different species (human, mouse, bovine, rat and chicken) reveal a striking region of conserved basic residues centred on an unpaired cysteine (C201 in human) within the otherwise poorly conserved stalk region of the ectodomain. Two further conserved cysteine residues are located in LYVE-1, one in the transmembrane helix (C257 in human) and a second in the cytoplasmic tail (C317 in human). Using a combination of truncation and site-directed mutagenesis, Cys 201 has been identified as the residue responsible for formation of inter-chain disulphide-linked dimers (Nightingale, 2004). The possibility that LYVE-1 monomers can self-associate in the absence of disulphide linkage has been explored using recombinant LYVE-1 and size exclusion chromatography (SEC). Monomeric LYVE-1 does not appear to self-associate, but can be separated from disulphide-linked homodimers using SEC (Dr. S. Banerji unpublished observation).

The function of LYVE-1 homodimers has not been determined categorically, but their primary role is thought to involve enhancement of HA binding through increased avidity. Early work in the Jackson laboratory hinted at an absolute requirement for disulphide-linked dimerization, on the basis that soluble LYVE-1 ectodomain-Fc fusion proteins lost the capacity to bind HA following removal of the Fc tail, unless a Cys201-Cys201 disulphide was present to maintain a dimeric organization. (Dr. S. Banerji, unpublished

observations). However, truncated LYVE-1 mutants lacking Cys201 were found to bind HA efficiently when over-expressed in HEK 293T cells, despite the absence of dimeric LYVE-1 (Nightingale et al., 2009). Furthermore, biotinylated HA pull-down of LYVE-1 expressed in 293T cells efficiently recovered both the monomer and dimer (Nightingale, 2004). Taken together, these data suggest that in transfected non-lymphoid cells LYVE-1 homodimers contribute to HA binding but are not obligatory for the process. However, recent measurements with His-tagged recombinant LYVE-1 have suggested that the dimeric protein has a higher HA binding affinity (K_D = 20 μM) compared to the monomer (K_D = 107 μM) (Dr. S. Banerji, preliminary observations). These apparently conflicting results show the functional importance of LYVE-1 homodimerization is not fully resolved. However, it remains to be determined whether LYVE-1 homodimers have a particular role to play in HA binding by primary lymphatic endothelial cells (LEC).

6.1.2 Mechanism of inhibition of hyaluronan binding by sialic acid

To date, the pattern of inhibitory sialylation added to endogenous LYVE-1 by primary LEC is the best characterised mechanism for regulation of HA binding (Nightingale et al., 2009). The native receptor is extensively sialylated, most likely through α2-3 or α2-6 linkage to O-glycans in the stalk region, with the result that HA binding is very weak or undetectable in primary LEC. Removal of sialic acid from recombinant LYVE-1 using neuraminidase enzymes has been shown to significantly enhance HA binding, however the sialyl moieties are inaccessible to cleavage by neuraminidase in intact LEC. In chapter 4, clustering of the receptor in primary LEC was shown to activate HA binding, without the requirement for removal of sialic acid. For these reasons, the significance of LYVE-1 homodimerization for HA binding may be greater in cells with a high capacity for receptor sialylation (i.e. LEC) than in those with a lower capacity (i.e. HEK 293T). Specifically, sialylation may set

the threshold for HA binding and hence the degree to which LYVE-1 homodimers are required to overcome that threshold and support stable binding.

Two models have been proposed for the mechanism by which sialylation inhibits HA binding (Figure 6.1) (Jackson, 2009). The first proposes that sialic acid residues at the termini of O-glycans may interact with the HA-binding site, blocking binding of hyaluronan. Cleavage of sialic acid by an endogenous sialidase, or *de novo* expression without sialic acid end caps, could then relieve this inhibition. In an alternative model, sialic acid blocks cooperative self-association, perhaps by charge repulsion (sialic acid bears a negative charge), or by preventing appropriate alignment of two HA binding domains. In light of recent data indicating the importance of receptor clustering, a third, alternative scenario may be envisaged in which charge repulsion maintains a low average surface density, preventing the multivalent interactions required for stable binding of an HA chain.

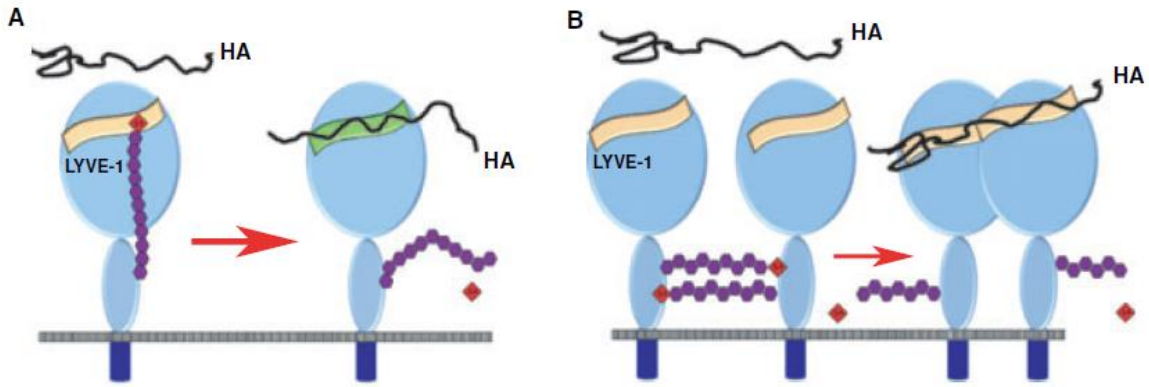


Figure 6.1. **Hypothetical models for the regulation of hyaluronan binding by sialic acid**. Evidence from truncation mutagenesis and expression in glycosylation deficient CHO cells indicates that LYVE-1 is functionally and reversibly 'silenced' by terminal sialylation of O-glycans. (A) One model of inhibition of HA-binding proposes that terminal sialic acid residues (red dots) on the O-glycans (purple) may interact with the HA-binding site, blocking HA-binding. Cleavage of sialic acid by an endogenous sialidase, or *de novo* expression without sialic acid, could then relieve this inhibition. (B) In an alternative model, sialic acid blocks cooperative self-association, perhaps by charge repulsion, or by preventing appropriate alignment of HABDs. Taken from (Jackson, 2009).

6.1.3 Use of QCM-D for the study of hyaluronan binding proteins

The Quartz Crystal Microbalance with Dissipation Monitoring (QCM-D) utilises the pizoelectric effect, whereby application of the correct electrical current deforms certain silica crystals such that an acoustic standing wave is generated across the thickness of the crystal (Figure 6.2). Two parameters are measured for 13 overtones of the standing wave; the frequency shift (Δf, Hz) that occurs as mass is deposited as a film on the surface of the crystal, effectively increasing its thickness, and dissipation (ΔD, 1E-6) of the wave through the film – which provides information on water content, the homogeneity of the bound layer and its viscoelastic properties. The interaction of biomolecules in aqueous solution with the crystal surface can be followed in real-time at high resolution. QCM-D can also be coupled with other surface sensitive techniques, such as ellipsometry and colloidal probe reflection interference contrast microscopy (RICM), which quantify adsorbed masses and allow estimation of film thickness, respectively (for a review, see: Reviakine et al., 2011).

An artificial lipid bilayer can be formed on the crystal surface that contains lipids with Tris-NTA groups attached to their headgroup (Figure 6.2, E). These lipids can effectively immobilize the 10 histidine tail of a recombinant protein via NTA while maintaining free lateral mobility throughout the bilayer. This makes QCM a powerful tool for the study of receptors like LYVE-1 that bind large polyvalent ligands such as hyaluronic acid, and represents its key advantage over other techniques, such as surface plasmon resonance, where either the protein or the ligand must be anchored in place.

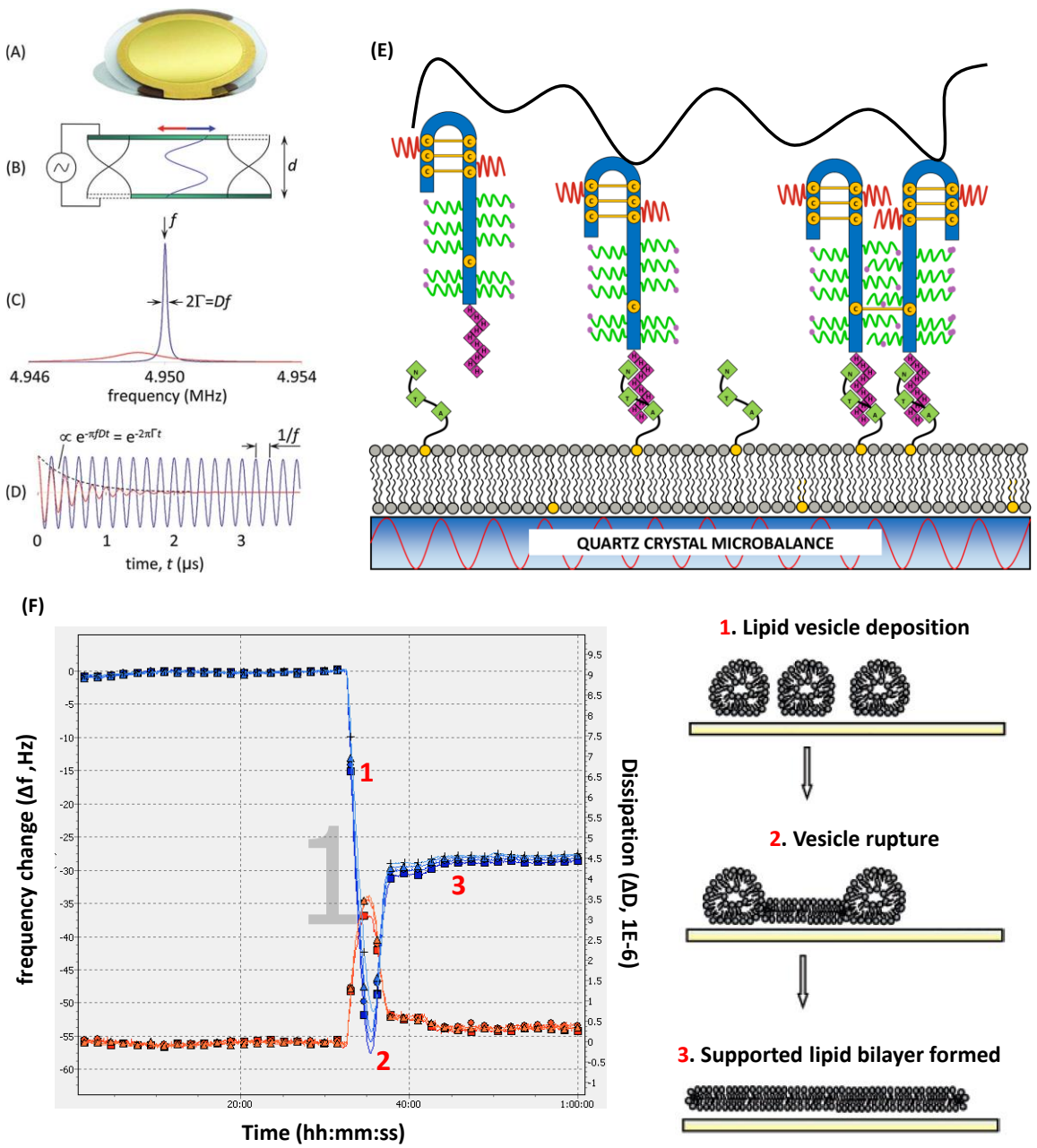


Figure 6.2. **Schematic of a QCM-D experiment, showing formation of a supported lipid bilayer**. (A) A photograph of a quartz crystal sensor (Q-Sense). (B) Side view of the crystal. Application of oscillatory voltage causes the top and bottom surfaces to move in an antiparallel fashion. The fundamental frequency (black waves at the edges of the crystal) and the third overtone (blue wave in the middle) are illustrated. (C) Resonances observed when a crystal is in air (blue) or in liquid (red). Dissipation is much greater in aqueous solution due to interaction with solvent molecules at the crystal surface (D) QCM-D uses a ring-down method, where the driving voltage is intermittently switched off and the decay in time of the oscillation is monitored. From the decay curve, the resonance frequency *f* and the energy dissipation *D* are extracted. (E) Supported lipid bilayers can be formed on

the surface of silica crystals. They share the same lipid components as biological membranes, withstand unspecific binding of most biomolecules, and can be functionalized in order to anchor recombinant proteins, such as His-tagged LYVE-1 molecules shown here bound by Tris-NTA functionalized lipids. (F) SLBs are formed by the spreading of small unilamellar vesicles (SUVs) onto the crystal surface. At sufficient density they rupture, detected as a reduction in film thickness, and merge to form a homogenous bilayer. Adapted from (Reviakine et al., 2011).

Recently, QCM-D analysis has been used to investigate fundamental aspects of CD44-hyaluronan interactions (Wolny et al., 2010). Two model systems were developed for the stable anchoring of either His-tagged CD44 Hyaluronan Binding Domain (HABD), or a dimeric Fc-fusion protein of twin CD44 HABDs, to supported lipid bilayers (SLBs). In combination with ellipsometry and RICM, it was possible to show that HA binding to SLBs densely coated with CD44 increase as a function of HA chain length, with half-maximal saturation at ~30 kDa. Furthermore, binding was irreversible for HA sizes exceeding 10 kDa, and remained so at decreasing receptor density. These data demonstrated for the first time that CD44 engages in multivalent interactions with HA, with the result that weak individual binding affinities (K_D ~65 µM) are overcome to permit long-lasting interactions with large HA chains. Similar avidity-driven processes are suspected to be critical for LYVE-1 HA binding.

6.2 Aims

The role played by LYVE-1 homodimers is currently elusive; although they clearly exhibit greater affinity for HA than monomeric LYVE-1, the latter can be sufficient for HA binding, depending on cell background and capacity for receptor sialylation. While dimeric LYVE-1 is readily detected in both primary and transfected cells, little is known about its sub-cellular location or what controls the ratio of monomeric to dimeric LYVE-1. The relatively weak HA binding affinity of individual LYVE-1 molecules suggests a requirement for multivalent interactions, particularly under conditions of heavy sialylation in lymphatic endothelium, where a dimeric receptor may well play a critical role in stabilizing HA binding.

Understanding the full functional significance of LYVE-1 homodimerization would therefore be aided by cell biological studies using both primary LEC and other transfected cell backgrounds. In addition, this would be complemented by studies with purified LYVE-1 proteins using a fully defined cell free system, where individual aspects of LYVE-1 regulation may be probed in isolation. One such system, QCM-D, is a technique readily applicable for the study of HA binding proteins and offers the possibility of probing many features of LYVE-1 regulation discussed in previous chapters. These include the relationship between surface density and HA binding, the requirement for multivalent interactions with HA, the influence of LYVE-1 mAb on HA binding, and the relative binding capacity of LYVE-1 monomers and homodimers.

1. Quantify LYVE-1 homodimer formation in primary LEC and different transfected cell types and determine the sub-cellular location of LYVE-1 homodimers.

2. Assess the comparative contribution of LYVE-1 homodimerization to HA binding in primary LEC and different transfected cell types .

3. Develop QCM-D to characterize LYVE-1 dimerization, sialylation and antibody potentiation and assess their influence on HA binding in an artificial bilayer system.

6.3 Results

6.3.1 Prevalence of LYVE-1 dimers in primary LEC and LYVE-1 transfected cells

A panel of different cells expressing LYVE-1 with varying capacity for HA binding were tested for the prevalence of LYVE-1 homodimers by western blot. These included primary lymphatic endothelial cells (HDLEC) and LYVE-1 transfected cell lines, ranked for their constitutive level of HA binding. Chinese Hamster Ovary (CHO K1) and Jurkat cells have previously been characterized as weakly permissive backgrounds for HA binding, compared to highly permissive HEK 293T fibroblasts, or CHO LEC2 cells, which lack a critical enzyme for addition of inhibitory sialylation (Nightingale et al., 2009). As shown in Figure 6.3, LYVE-1 homodimers could be detected in all cell types tested, with the exception of Jurkat cells expressing GFP-tagged hLYVE-1 C201A, a mutant receptor lacking the cysteine residue required for disulphide-linked dimerization.

Quantitation of monomer/dimer ratio revealed no obvious correlation between the prevalence of homodimers and the HA binding capacity of the cell type (Figure 6.4). For example, a similar percentage of LYVE-1 molecules were present as homodimers in two HEK 293T fibroblasts clones, one having high levels of HA binding (HA +) and the other none (HA -). There was considerable variation in monomer/dimer ratio between cell types, with the percentage of LYVE-1 molecules present as homodimers ranging between 10 and 40%. This was also true of different batches of primary LEC, suggesting that the prevalence of LYVE-1 dimers is not a fixed phenotypic attribute but is subject to change, perhaps in response to alterations in culture conditions. One obvious point of control would be in the endoplasmic reticulum, where newly synthesized proteins undergo disulphide-bond formation.

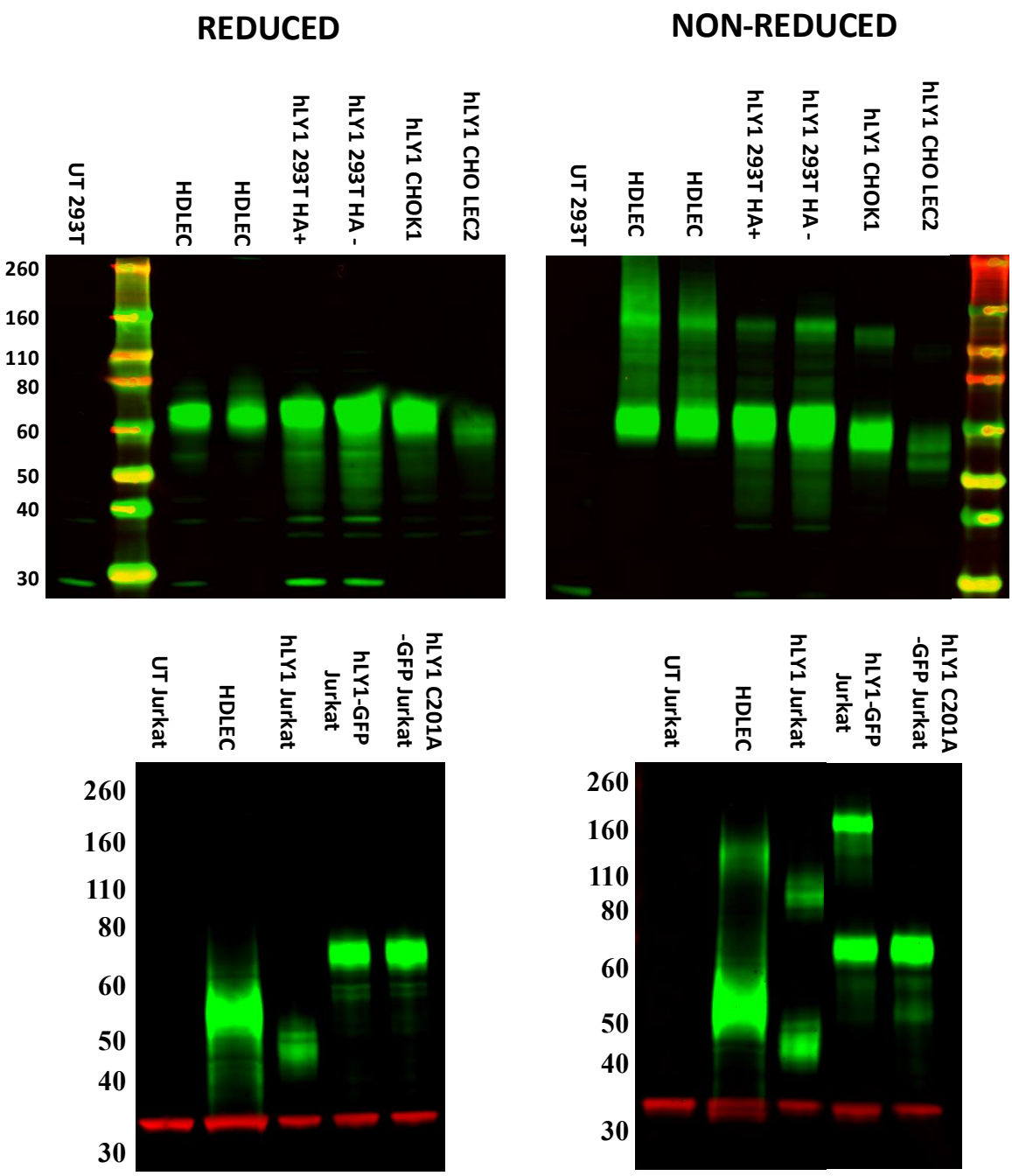


Figure 6.3. **Western blot of LYVE-1 expressed by different cell types under reducing and non-reducing conditions**. Whole-cell lysates of various untransfected (UT) or human LYVE-1 (hLY1) transfected cell lines were prepared by TCA precipitation. Samples were run on reducing and non-reducing LDS-PAGE, blotted onto PVDF membrane and probed for hLYVE-1 with goat-anti-human LYVE-1 polyclonal (R&D) or β-actin with mouse anti ß-actin mAb (Cell Sig. Tech). Bound antibody was detected with anti-goat-IgG IRDye 800CW and anti-mouse IgG IRDye 680RD secondaries and a Li-Cor Odyssey Imager. Blots are combined from two separate experiments, but represent the monomer/dimer ratio observed in a number of other experiments.

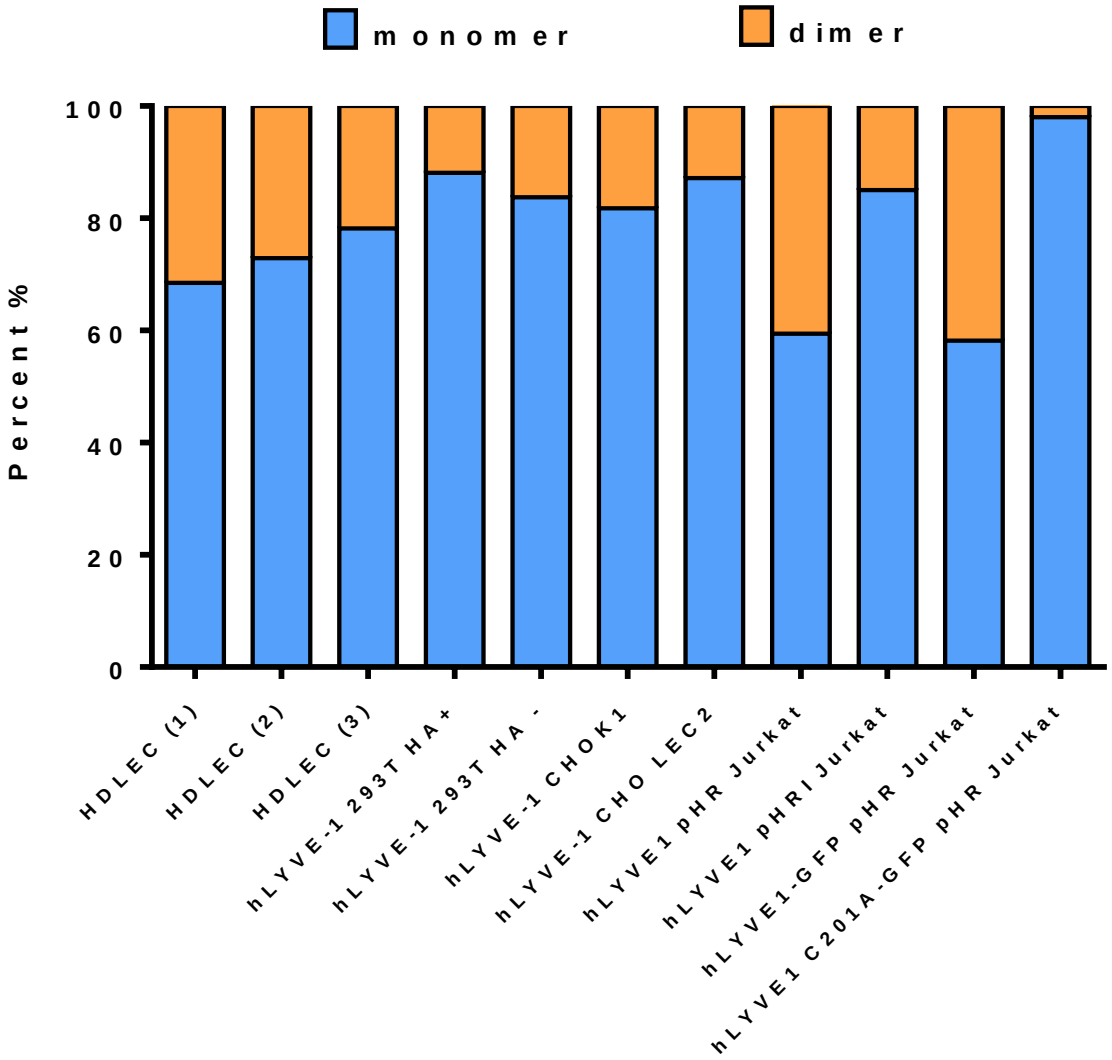


Figure 6.4 **Quantification of monomer:dimer ratio in primary Lymphatic Endothelial Cells and LYVE-1 expressing cell lines**. Image studio software (Li-Cor) was used to quantitate the fluorescence intensity of LYVE-1 monomer and dimer bands from western blots of primary lymphatic endothelial cells (HDLEC) and various LYVE-1-expressing cell lines (see Figure 6.3) Raw fluorescence intensity values were then converted to percentages by dividing by the total fluorescence intensity of monomer and dimer bands combined, and multiplying by 100.

However, disulphide interchange can also occur at the cell surface in response to changes in extracellular redox potential, for example during inflammation (Yan et al., 2009). Indeed a growing number of labile or redox-sensitive disulphide bonds have been described in cell surface receptors (Metcalfe et al., 2011). Cysteine 201, the residue responsible for inter-chain disulphide formation in LYVE-1, is located in the extended stalk region of the

extracellular domain, in proximity to a tract of basic residues. As such it is an interesting candidate for a labile disulfide, a hypothesis that is being actively pursued in the Jackson laboratory (Dr S. Banerji, manuscript in preparation).

To determine whether LYVE-1 homodimers are present at the cell surface, fractions of total, plasma membrane and intracellular protein were prepared from primary LEC and probed by western blot for LYVE-1 (Figure 6.5). A cell surface protein isolation kit that utilises a cell-impermeable biotinylation reagent (Pierce) was used to prepare the plasma membrane protein fraction, and a crude intracellular fraction was collected from the flow-through of the Neutravidin column. The purity of the plasma membrane fraction was demonstrated by total absence of the intracellular protein complex ERK1/2, which is readily detected in a whole cell lysate or intracellular protein fraction. While there was considerable variation between different batches of LEC, LYVE-1 homodimers were found to be present at the cell surface and in consistently higher proportion than observed in whole-cell lysates. A corresponding reduction in the prevalence of dimeric LYVE-1 was observed in the intracellular protein fraction. These data clearly demonstrate that LYVE-1 dimers are mostly present at the plasma membrane following biosynthesis, rather than being retained intracellularly, and may even be increasing in prevalence at the cell surface. Various mechanisms have been reported for inter-change of extracellular protein disulphides, including local changes in extracellular redox (Aichem et al., 2006) and modification by secreted protein disulphide isomerase (PDI) (Jiang et al., 1999), however it remains to be seen whether these are applicable to LYVE-1.

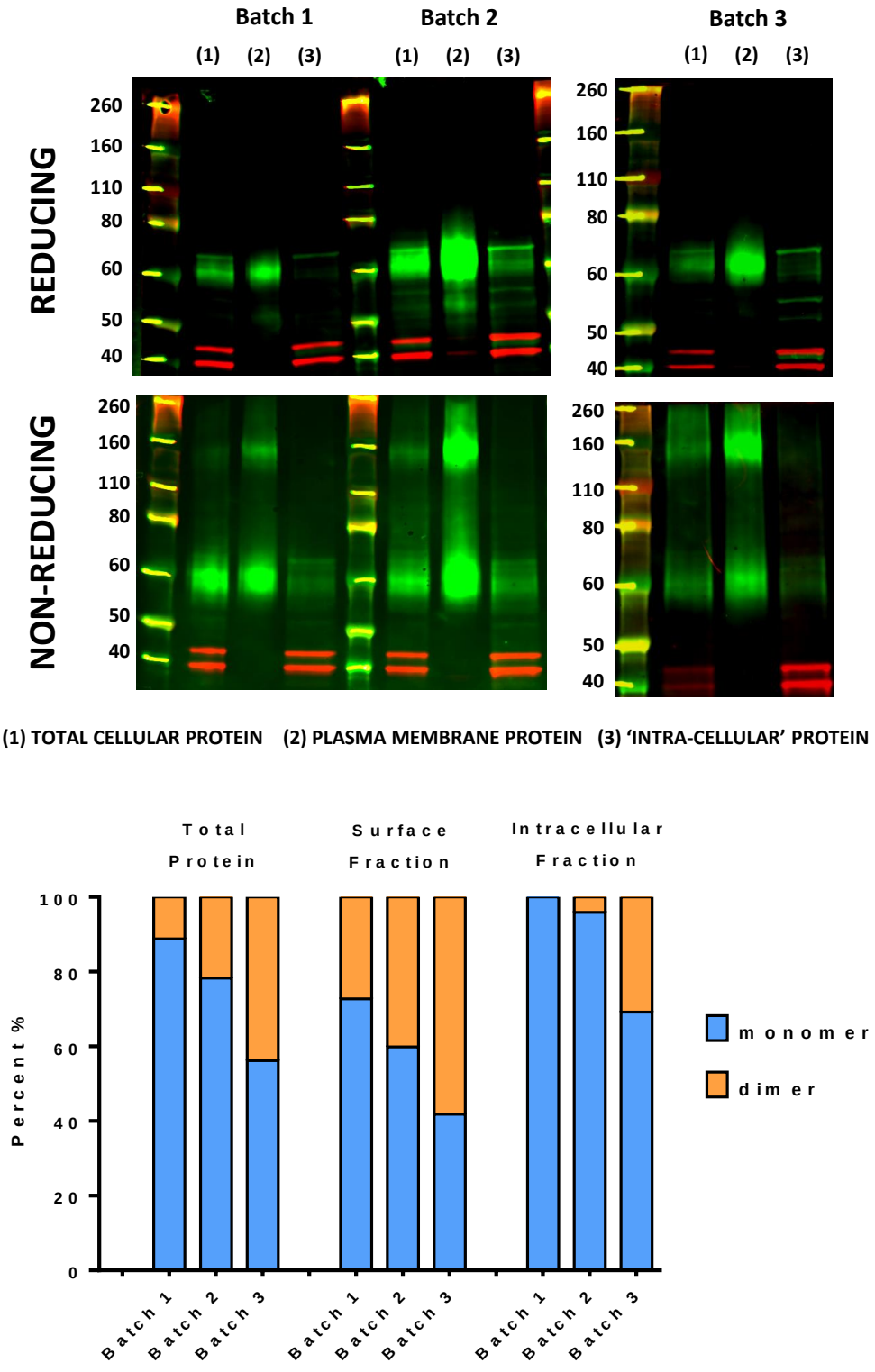


Figure 6.5. **Quantitation of LYVE-1 monomer:dimer ratio in different fractions of total cellular protein using surface biotinylation and western blot**. Three batches of primary human dermal lymphatic endothelial cells (HDLEC) were analysed for LYVE-1 monomer:dimer ratio in different fractions of cellular protein. *Total cellular protein* was prepared using a combination of cell scraping, sonication, and LDS sample buffer, with or without 50mM DTT. A *surface plasma membrane fraction* was prepared using a Cell Surface Protein Isolation Kit (Pierce) with some protocol modifications, so that a non-

reduced sample could be obtained. A crude fraction of *intracellular protein* was collected by harvesting the flow-through from the neutravidin column. Reduced and non-reduced samples were run on LDS-PAGE gels, blotted onto PVDF membrane and probed for LYVE-1 or ERK1/2 using goat-anti-hLYVE-1 polyclonal (R&D) or rabbit anti-Erk1/2 monoclonal (Sigma). Bound antibody was detected with anti-goat-IgG IRDye 800CW (*green*) and anti-rabbit-IgG IRDye 680LT (*red*) and a Li-Cor Odyssey Imager. Data are representative of two independent experiments

6.3.2 Significance of LYVE-1 homodimers for hyaluronan binding by LYVE-1 transfected cells

The effect of disrupting LYVE-1 dimerization on HA binding has been previously addressed in an indirect fashion using mutant LYVE-1 proteins with truncated extracellular domains (Nightingale et al., 2009). Graded deletion of the juxtamembrane stalk region, including cysteine 201, the residue responsible for homodimerization, had the effect of enhancing HA binding by HEK 293T. This suggested that LYVE-1 homodimers are not necessary for stable HA binding, but with the qualification that mutagenesis also deleted the O-glycosylated region to which inhibitory sialic acid is added.

To examine the role of LYVE-1 homodimers in isolation, HEK 293T cells were transiently-transfected with the eukaryotic expression vector pRcCMV bearing the coding sequence of full length wildtype hLYVE-1, or a mutant protein (C201A) that does not form homodimers[1]. As shown in Figure 6.6, hLYVE-1 and hLYVE-1 C201A HEK 293T cells had similar levels of LYVE-1 expression and binding of biotinylated hyaluronan, which could be blocked by co-incubation with an excess of unlabelled HA. This demonstrated that when over-expressed on the HEK 293T background, LYVE-1 monomers are sufficient for hyaluronan binding, even in the absence of dimeric protein.

[1] Site-directed mutagenesis was performed by Dr. S. Banerji.

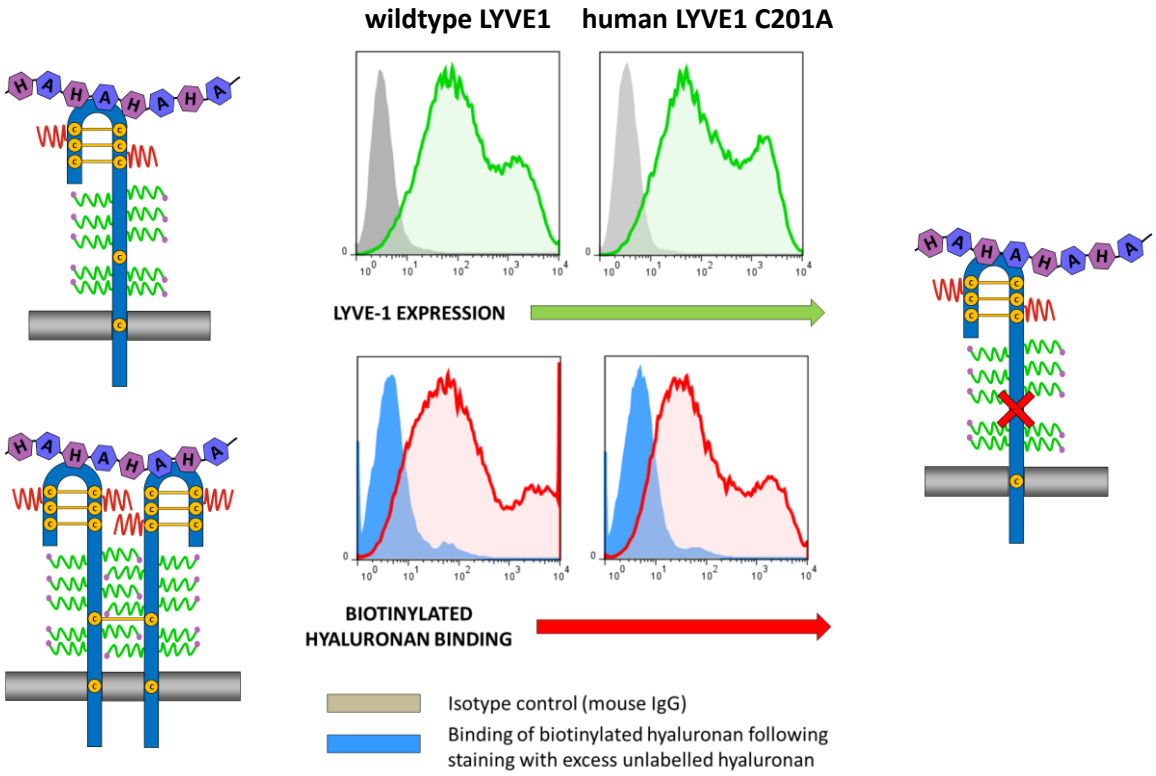


Figure 6.6. **Effect of ablating dimer formation on hyaluronan binding by LYVE-1 transfected cells.** HEK 293T fibroblasts were transiently-transfected with the eukaryotic expression vector pRcCMV bearing the coding sequence of wildtype or C201A human LYVE-1 and expanded in culture. Cells transfected with wildtype hLYVE-1 express a mixture of monomeric and dimeric LYVE-1 (cartoon, *left*) while cells transfected with hLYVE-1 C201A express monomeric LYVE-1 only (cartoon, *right*). Cells were lifted with 5mM EDTA in PBS and incubated separately with LYVE-1 mAb 8C (*green*), mouse IgG_1 isotype (*grey*) control, biotinylated HA (bHA, *red*) or bHA in combination with an excess of unlabelled HA (*blue*). Bound Ig or bHA were detected with appropriate secondary reagents and flow cytometry for 20 000 cells/condition from a single experiment.

While LYVE-1 homodimers are not required for HA binding on the HEK 293T background, it is important to recognise that this occurs in the context of over-expression. As described in Chapter 4, LYVE-1 expression level is a critical regulator of HA binding in both primary and transfected cells, most likely due to increased capacity for multivalent interactions. At very high expression level, even the lower HA binding affinity of LYVE-1 monomers is likely to be sufficient for stable binding due to avidity effects. However, a decrease in the overall amount of HA bound might be expected in the absence of high-affinity homodimers, particularly at lower expression levels.

To test this hypothesis, Jurkat cells expressing GFP-tagged wildtype or C201A hLYVE-1 were tested for hyaluronan binding, LYVE-1 expression and the proportion of receptors present as monomers or dimers. As shown in Figure 6.5, hLYVE-1-GFP Jurkat cells express a 60% monomeric, 40% dimeric LYVE-1 mix, while hLYVE-1 C201A-GFP expressing cells have monomeric LYVE-1 only. Three LYVE-1 mAbs were used to test surface expression levels, which were homogenous for both cell lines but ~15% higher for hLYVE-1 C201A-GFP Jurkats, depending on the antibody used (Figure 6.7). Despite having higher overall LYVE-1 expression, cells lacking dimeric LYVE-1 bound 32% less biotinylated HA (bHA) at saturating bHA concentration. The bHA concentration for half-maximal binding was ~0.3 µg/ml in both cases, and the concentration for half maximal blockade of bHA binding by 893 mAb was ~0.02 µg/ml. Comparison of LYVE-1 expression, using GFP-fluorescence, and bHA binding revealed an essentially linear relationship for hLYVE-1-GFP expressing cells. By contrast, there was a clear LYVE-1 expression threshold for bHA binding in hLYVE-1 C201A-GFP Jurkats. Taken together, these data demonstrate that the absence of homodimers results in a significant reduction in the HA binding capacity of LYVE-1 transfected cells, along with a shift in the expression threshold required for stable binding to be detected.

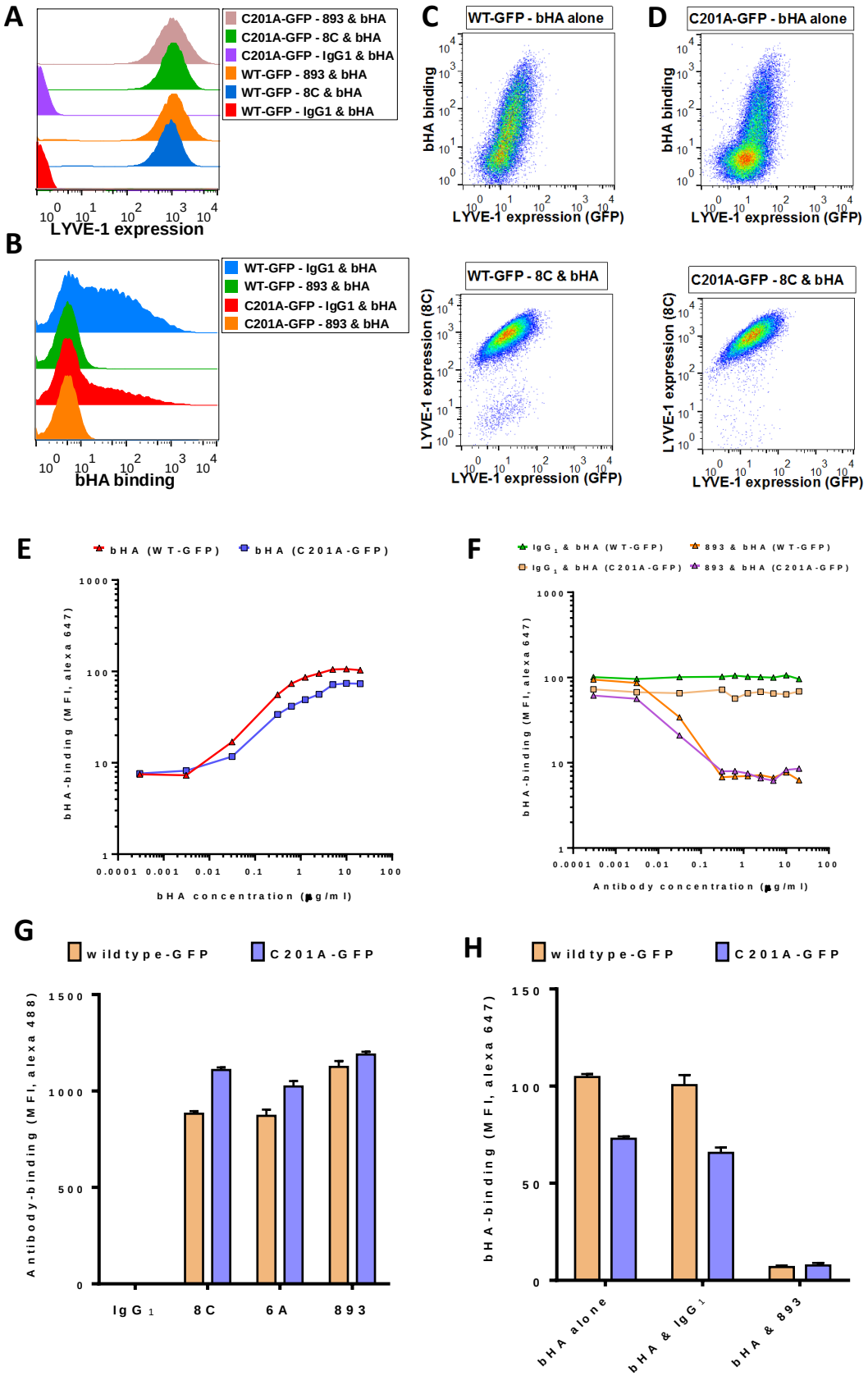


Figure 6.7. **Comparison of hyaluronan binding in Jurkat cells expressing wildtype GFP-tagged LYVE-1 or a non-dimerizing LYVE-1 C201A mutant.** Jurkat cells were infected with lentivirus bearing the coding sequence of hLYVE-1 with a C-terminal GFP

tag or hLYVE-1 C201A-GFP, a mutant of LYVE-1 that cannot form disulphide-linked homodimers. LYVE-1 expression was assessed by incubation with LYVE-1 specific mAb, appropriate secondary reagents and flow cytometry (A, G). Cells were also tested for binding of biotinylated HA (bHA) under different conditions, detected by streptavidin Alexa 647 and flow cytometry. Cells were either incubated with bHA alone, at increasing bHA concentration (E), or co-incubated with bHA (fixed at 5 µg/ml) and hLYVE-1 mAbs 893 or mouse IgG_1 isotype control, at increasing Ig concentration (F), to assess the effect on bHA binding. The relationship between bHA binding and LYVE-1 expression was assessed by comparison with GFP fluorescence (C). The relationship between GFP-fluorescence and surface expression was assessed by comparison with 8C mAb binding (D). A summary of bHA binding, either alone or in the presence of 893 mAb or IgG_1 is shown in (H). Data in histograms are the fluorescence intensity of 20 000 cells/condition. Data in graphs are the mean fluorescence intensity (MFI) of 20 000 cells/condition ± SD (n = 3) and are representative of two independent experiments.

6.3.3 Role played by LYVE-1 homodimers in primary lymphatic endothelial cells

In LYVE-1 transfected cell lines, homodimers clearly play a significant role in HA binding, but are not obligatory in the context of high surface expression. This exposes a limitation in their use as a model, as they poorly represent the LYVE-1 surface density likely to be found on lymphatic endothelial cells. In addition, most LYVE-1 transfectants have a constitutive level of HA binding that is absent in LEC, due to the specific pattern of inhibitory glycosylation in these cells.

To better understand the significance of LYVE-1 homodimerization in primary cells, LEC were transduced with lentivirus bearing hLYVE-1-GFP or hLYVE-1 C201A-GFP and assayed for HA binding using FACS (Figure 6.8). Cells expressing hLYVE-1-GFP had very high levels of constitutive HA binding (MFI = 1649) that could be efficiently blocked using mAb 891 (MFI = 22) or potentiated using mAbs 8C or 6A (MFI = 2169, 2147). Strikingly, cells expressing hLYVE-1 C201A-GFP displayed only weak levels of HA binding (MFI = 32), that could not be potentiated by 8C or 6A mAb (MFI = 37, 31).

One possible source of this discrepancy is a difference in expression level between the wild-type and C201A mutant; for example the two transfectants were closely matched in terms of GFP-fluorescence, while binding of LYVE-1 mAbs to C201A-GFP cells was 67% lower, most likely indicating a defect in export of the mutant protein to the cell surface. However, where the surface LYVE-1 expression of the two transfectants was matched in terms of 8C mAb binding, hLYVE-1 C201A-GFP expressing cells were found to exhibit little or no HA binding compared to their wildtype-GFP-expressing counterparts (Figure 6.8, B). The HA binding that is observed at the highest LYVE-1 expression is most likely a potentiation effect of 8C mAb on endogenous LYVE-1 observed in these cells using western blot (Figure 6.9).

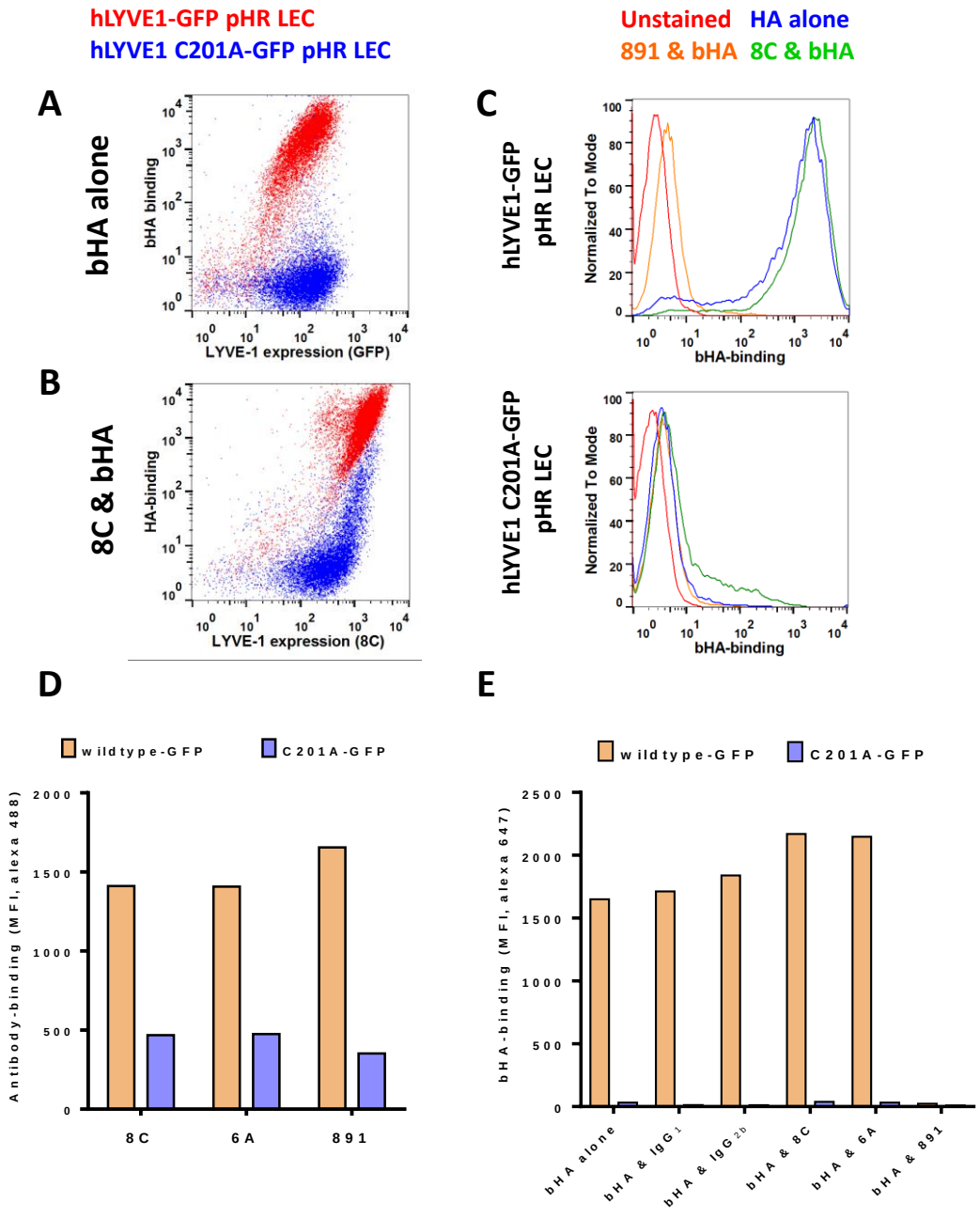


Figure 6.8. **Hyaluronan binding by primary lymphatic endothelial cells over-expressing GFP-tagged wildtype or C201A hLYVE-1.** Primary LEC were infected using a lentiviral vector (pHR) bearing the coding sequence of GFP-tagged wildtype LYVE-1, or LYVE-1 C201A, a mutant lacking the cysteine residue required for dimer formation. Cells were expanded in culture, lifted with Accutase and incubated with biotinylated hyaluronan (bHA) either alone, or in the presence of hLYVE-1 mAb or isotype-matched control Ig, followed by appropriate secondary detection reagents and quantification of fluorescence using flow cytometry. (A) Comparison of LYVE-1 expression and bHA binding using GFP-fluorescence. (B) Relationship between surface LYVE-1 levels and bHA binding for cells co-incubated with 8C mAb and bHA. (C, E) Comparison of bHA binding when cell were incubated with bHA alone or in combination with LYVE-1 mAb. (D) Comparison of surface LYVE-1 levels using LYVE-1 mAb. Data in histograms are the

fluorescence intensity of 20 000 cells/condition. Data in graphs are the mean fluorescence intensity (MFI) of 20 000 cells/condition and are representative of two independent experiments.

These results strongly suggest that the role played by LYVE-1 homodimers in HA binding by primary cells is critical. The absence of dimeric LYVE-1 has a much more profound effect than observed for LYVE-1 transfected cell lines, however this is likely due to the inhibitory effect of LEC-specific glycosylation. As a result, fully sialylated LYVE-1 monomers are unable to compensate for the lack of higher affinity dimers, even when over-expressed in LEC.

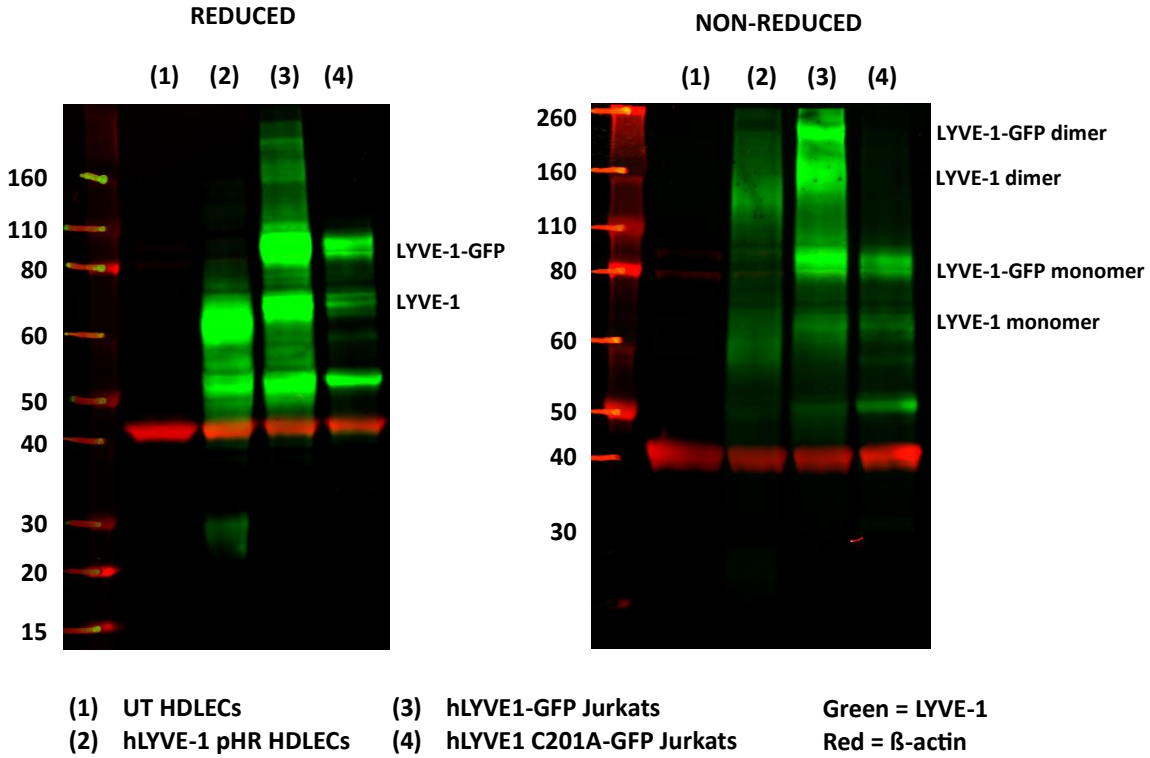


Figure 6.9. **Western blot of primary lymphatic endothelial cells over-expressing wildtype, GFP-tagged or C201A mutant human LYVE-1.** Whole-cell protein lysates were prepared by TCA precipitation of untransfected (UT), hLYVE-1 pHR, hLYVE-1-GFP pHR or hLYVE-1 C201A-GFP pHR HDLEC. Samples were run on reducing and non-reducing LDS-PAGE, blotted onto PVDF membrane and probed for hLYVE-1 with goat-anti-human LYVE-1 polyclonal (R&D) or β-actin with mouse anti ß-actin mAb (#4695, Cell Sig. Tech). Bound antibody was detected with anti-goat-IgG IRDye 800CW and anti-mouse IgG IRDye 680RD secondaries and a Li-Cor Odyssey Imager.

6.3.4 Rationale for analysis of LYVE-1-hyaluronan interactions in an artificial membrane system

Regulation of hyaluronan binding by LYVE-1 involves a number of elements, including expression level, local surface density, cell-specific glycosylation patterns and receptor dimerization. The interplay of these different factors in cellular systems poses a number of challenges for the study of any one of these aspects in isolation. For example, examining the role of LYVE-1 homodimers in transfected cells encounters issues with expression level and glycosylation pattern, while the endogenous receptor in primary cells is by default masked by inhibitory sialylation. Cell-free systems using recombinant LYVE-1 protein, such as surface plasmon resonance (SPR), avoid many of these complications, but typically can only be used to probe 1:1 interactions between LYVE-1 molecules and HA. For a low affinity receptor like LYVE-1, that relies on multiple interactions to facilitate binding of a large polyvalent ligand, this is an obvious limitation.

As described in the introduction to this chapter, QCM-D is a technique ideally suited to the study of protein interactions with large polyvalent ligands. Recombinant proteins may be anchored to an artificial membrane, termed a supported lipid bilayer (SLB), while retaining free lateral mobility. For a receptor that relies on clustering to engage its ligand, this represents the key advantage of QCM-D over related techniques such as SPR, where either the protein or the ligand must be anchored in place. QCM-D has been used previously to perform quantitative measurements of hyaluronan binding by recombinant His-tagged CD44 and determine the influence of various parameters, including surface density and HA chain length (Wolny et al., 2010). The technique is likely to be equally useful for probing these and other aspects of LYVE-1 regulation, including the relative HA binding capacity of LYVE-1 monomers and homodimers, and the influence of sialic acid on packing density and HA binding.

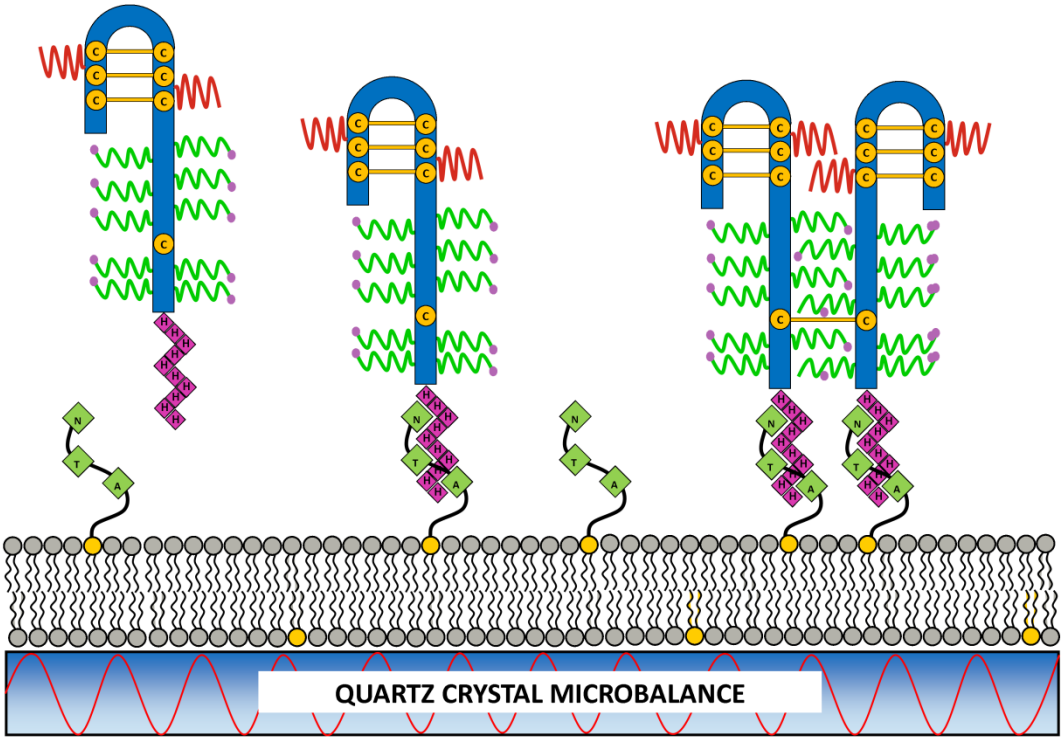


Figure 6.10. **Schematic representation of recombinant LYVE1 anchored to an artificial lipid bilayer formed on the surface of a quartz crystal microbalance.** The extracellular domain of LYVE1 (residues 1-238, *blue*) with a C-terminal 10 histidine tail (pink) is shown bound by Tris-NTA functionalized lipids (yellow head groups) that constitute ~5% of the total lipids in an artificial lipid bilayer. Lipids have free lateral mobility over the 1cm^2 surface of the silica crystal that functions as the QCM 'sensor'.

The precise mechanism by which sialic acid inhibits HA binding by LYVE-1 is currently unknown, but two competing models have been proposed. One suggests that sialic acid-capped glycans interact directly with the HA binding site, preventing access for the ligand, while the other proposes that the overall negative charge resulting from sialylation prevents clustering of individual receptors through charge repulsion. QCM-D can be used to test both of these models, particularly when used in conjunction with ellipsometry, a technique that has been used to quantify adsorbed masses on the surface of SLBs and average density the HA receptor CD44 (Wolny et al., 2010). A model system using QCM-D for the study of LYVE-1 was therefore developed in collaboration with Dr. Galina Dubacheva and Dr. Ralf Richter at the CIC biomaGUNE, Donostia, Spain.

6.3.5 Characterization of recombinant LYVE-1 samples for use in QCM-D studies

Recombinant LYVE-1 used in QCM-D studies comprised the full length extracellular domain (residues 1-238) of human LYVE-1, with a C-terminal 10x-histidine tail[1]. The protein was produced by a CHO K1 clone transfected with vector pEE14 bearing hLYVE-1 Δ238 10His and isolated for high expression using the glutamine synthetase system (Lonza). Immobilized metal ion affinity chromatography (IMAC) was used to purify recombinant LYVE-1 from CHO cell supernatant and further separated into monomeric and dimeric species by two consecutive rounds of size-exclusion chromatography (SEC) on a superdex S200 10/300 column.

SEC was found to be highly effective at separating LYVE-1 monomers (~50 kDa) and dimers (~95 kDa), however during storage and freeze-thaw a small degree of inter-conversion was observed (Figure 6.11). In addition, ~40% of dimeric LYVE-1 formed a disulphide-linked aggregate. To try and prevent this occurring, samples of monomeric protein were treated with the alkylating agent *N*-Ethylmaleimide (NEM), at room temperature for one hour, and re-purified using SEC. The degree of conversion to dimeric LYVE-1 was reduced, but not entirely eliminated (Figure 6.11). As freeze-thaw could not be avoided due to shipping requirements, it was decided to proceed while treating the samples as highly enriched rather than as pure monomer or dimer.

To investigate the influence of sialylation on HA binding, a portion of each sample was treated with Neuraminidase, at 37^{o}C for one hour, and re-purified using SEC. Removal of

[1] Dr. S. Banerji developed the hLYVE-1 Δ238 10His construct and corresponding CHO expression clone in collaboration with Janet Fennelly and Dr. S. Davis, Weatherall Institute of Molecular Medicine and assisted in purification of the protein.

sialic resulted in a small decrease in molecular weight for both monomeric and dimeric LYVE-1, as assessed by LDS-PAGE (Figure 6.11)

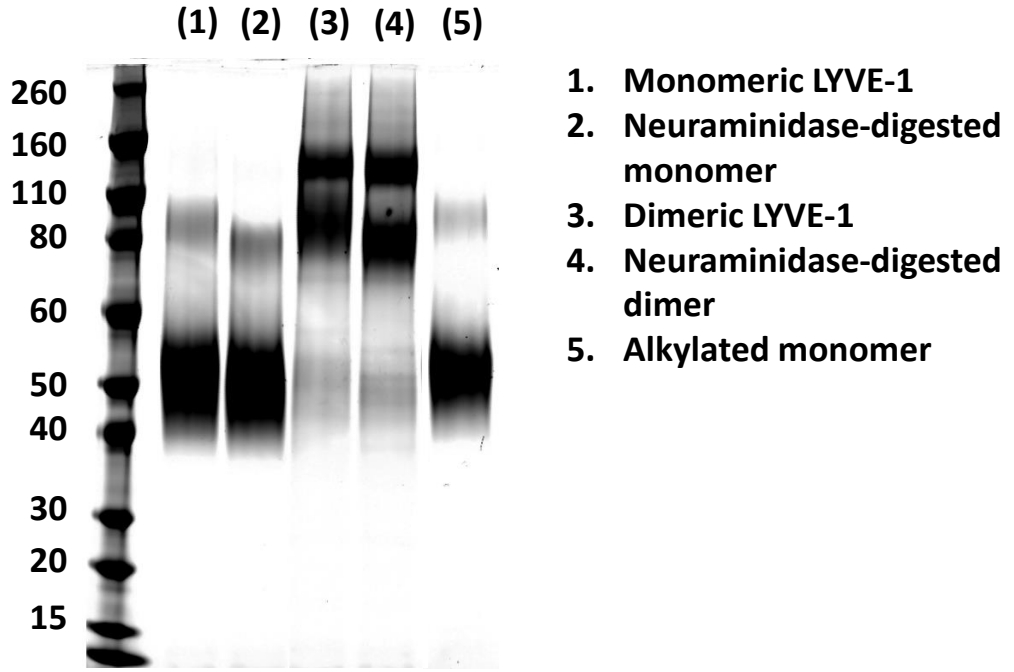


Figure 6.11. **Recombinant human LYVE-1 samples used in QCM-D studies, visualised by LDS-PAGE following storage.** Recombinant hLYVE-1 Δ238 10 His expressed by CHO GS cells was purified from supernatant using immobilized metal ion chromatography (IMAC) and separated into monomeric and dimeric species by two consecutive rounds of size-exclusion chromatography (SEC) on a superdex S200 10/300 column. A portion of each sample was treated with Neuraminidase (P0720, NEB), at 37ºC for one hour, and re-purified using SEC. An additional sample of hLYVE-1 monomer was treated with the alkylating agent *N*-Ethylmaleimide (NEM, Sigma), at room temperature for one hour, and re-purified using SEC. Samples were concentrated using a centrifugal concentrator (30 kDa size retention filter) to ~1 mg/ml concentration, divided into 50 µg aliquots and frozen at -20ºC. An aliquot of each sample was thawed, and analysed side-by-side using non-reducing LDS-PAGE. The gel was imaged using a Li-Cor Odyssey Imager, from a single experiment.

Binding of biotinylated HA was compared for all samples using a capture ELISA with mAb 8C (Figure 6.12). Samples were serially diluted from a starting concentration of 4 µg/ml prior to incubation with immobilized 8C mAb, to assess the effect on bHA binding. LYVE-1 homodimers bound approximately twice the amount of bHA detected for LYVE-

1 monomers at saturating concentration (OD_{490} = 0.987 and 0.477 respectively). Removal of sialic acid enhanced bHA binding by both species, while maintaining the hierarchy between dimers (OD_{490} = 1.417) and monomers (OD_{490} = 0.937). Alkylation of LYVE-1 monomers had the effect of ablating HA binding. The reason for this is unclear, although recently it has been observed that the structural disulphide at the centre of the HA binding site is partially sensitive to reduction in extracellular redox potential, raising the possibility that alkylation at this site may disrupt the conformation of the HABD (Dr. S. Banerji, unpublished observations). While this assay is too simplistic to draw firm conclusions about the behaviour of each sample, it does give an indication of relative HA binding capacity, which can be explored in greater detail using QCM-D.

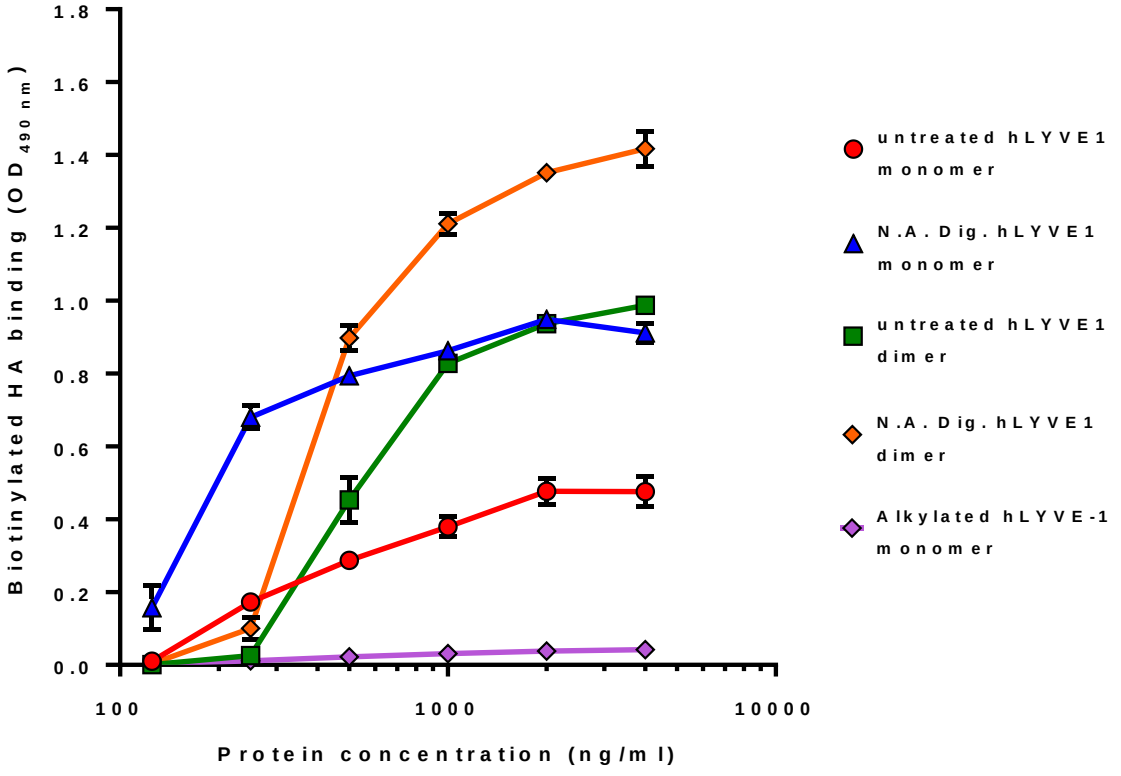


Figure 6.12. **Comparison of hyaluronan binding by recombinant hLYVE-1 samples using ELISA.** The anti-hLYVE1 mAb 8C was used in a capture ELISA to determine the relative binding of biotinylated HA (bHA) by different samples of recombinant LYVE-1 at varying concentration. A 96-well plate was coated overnight with goat anti-mouse-IgG Fc antibody, followed by incubation with 8C mAb for 1 hour. Serial dilutions of untreated, neuraminidase-digested (N.A. Dig.) or alkylated hLYVE-1 monomer and dimer were

prepared from a top concentration of 4 µg/ml, and added to the plate. Following capture, samples were incubated with bHA before washing and detection of bound ligand using streptavidin-HRP, a colorometric substrate and a plate reader capable of reading optical density at 490nm wavelength (OD_{490}). Data are the mean ± SD (n = 3).

6.3.6 Characterization of Tris-NTA functionalized lipids

His-tagged proteins may be anchored to supported lipid bilayers using bis-NTA-functionalized octadec-9-enyl-octadecyl-amine (OEOA-bis-NTA) lipids (Wolny, 2010). The divalent presentation of Ni^{2+} -loaded NTA improves the binding stability of His-tagged proteins over OEOA-NTA lipids, with dissociation constants in the low nanomolar range (Lata et al., 2005). Recently, Tris-NTA functionalized OEOA lipids have become available which offer even higher levels of stability[1]. SLBs are typically formed by the spreading of small unilamellar vesicles (SUVs) onto a planar surface, where they rupture to form a homogenous bilayer. The lipid composition of SUVs is critical, and must be determined empirically.

The major constituent lipid used in conjunction with NTA-functionalized OEOA is 1,2-dioleyl-sn-glycero-3-phopshcholine (DOPC), a zwitterionic unsaturated phospholipid with zero net charge (Wolny, 2010). To determine the correct ratio of DOPC:OEOA-tris-NTA for formation of good quality SLBs, SUV were produced comprising DOPC and different percentages of OEOA-tris-NTA (5, 7, & 9%). QCM-D was used to monitor spreading, rupture and formation of stable SLBs from these SUVs, using DOPC-only SUVs as a control (Figure 6.13). The two-phase behaviour together with the final changes in frequency and dissipation, Δf = -26 Hz and $\Delta D < 0.3 \times 10^{-6}$, upon incubation of DOPC-only SUVs are characteristic for formation of an SLB of good quality (Richter et al., 2006).

[1] Provided by Prof. Jacob Piehler (Universität Osnabrück, Germany) as part of a collaboration with Dr. Ralf Richter (CIC biomaGUNE, Spain).

SUV comprising 9% OEOA-tris-NTA failed to rupture fully, while 7% exhibited drift in F and D over time. However, 5% OEOA-tris-NTA SUV displayed typical two-phase behaviour during SLB formation, with final dissipation of < 0.3 × 10^{-6}. Change in frequency was -29 Hz, matching previous observations using OEOA-bis-NTA.

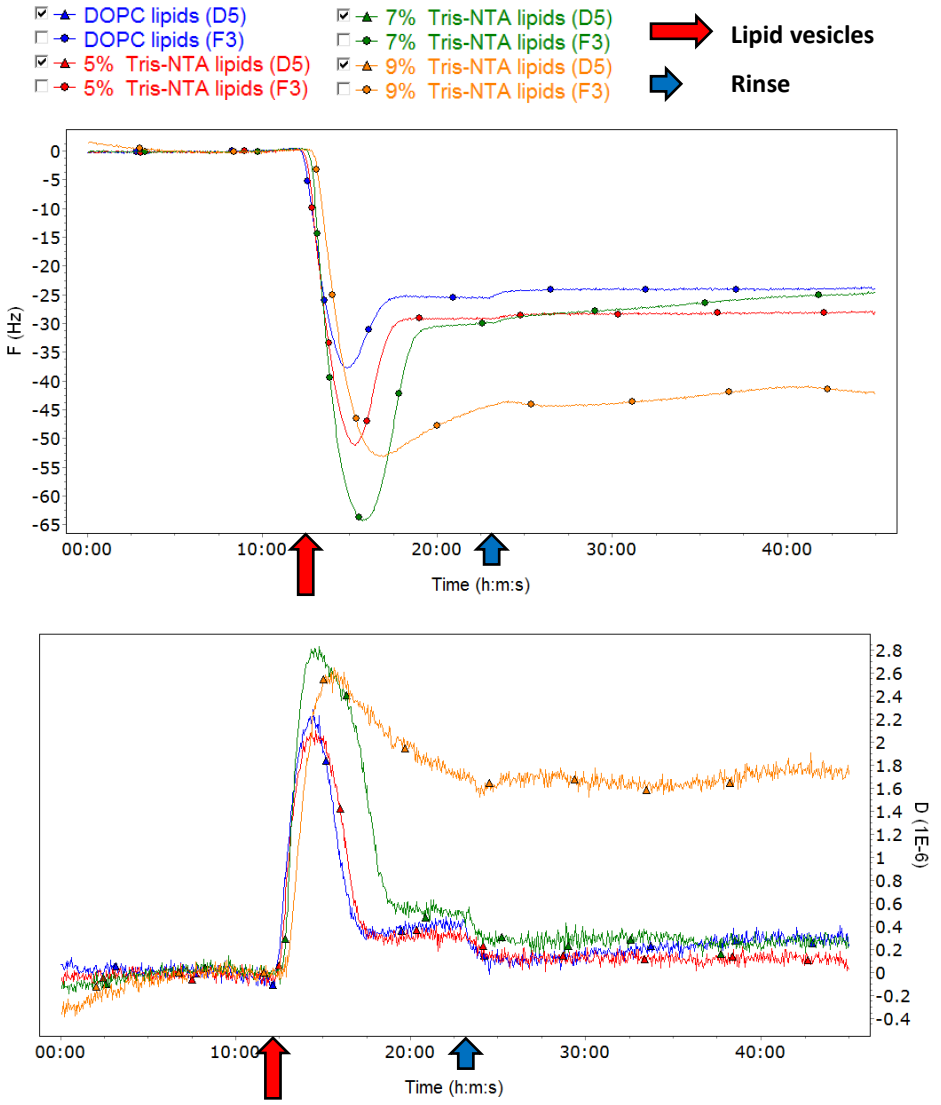


Figure 6.13. **Formation of supported lipid bilayers using lipid vesicles with different compositions.** Supported lipid bilayers (SLBs) were formed by spreading of 50 µg/ml small unilamellar vesicles (SUVs/lipid vesicles) onto silica surfaces. SUVs were comprised of DOPC lipids only, or a mixture of DOPC with 5, 7, or 9% Tris-NTA functionalized lipids. The points at which injection of lipid vesicles commenced and finished are indicated. Data are the change in frequency (F, Hz) and dissipation (D, 1 x 10^{-6}) for a single overtone, over the course of a single experiment, as measured by QCM-D.

To further characterize the behaviour of OEOA-tris-NTA lipids, adsorption of His-tagged CD44 hyaluronan binding domain (HABD) onto 5% Tris-NTA lipid bilayers was tested using QCM-D, and compared to published values derived using OEOA-bis-NTA lipids (Figure 6.14). CD44 his-HABD absorbed rapidly onto 5% Tris-NTA lipid bilayers, reaching saturation in ~30 mins, but did not interact with SLBs comprised of DOPC lipids only, which lack NTA functionality. Binding of CD44 remained very stable over prolonged periods of rinsing (>1 hour), with final frequency and dissipation shifts of Δf = -26 Hz and $\Delta D = 0.5 \pm 0.2 \times 10^{-6}$ that matched almost exactly with previous observations (Δf = -26 Hz and $\Delta D = 1.0 \pm 0.2 \times 10^{-6}$) (Wolny et al., 2010). Subsequent addition of hyaluronan (mw 250 kDa) resulted in shifts of Δf = -13 Hz and $\Delta D = 2.0 \times 10^{-6}$, which somewhat exceeded previous observations (Δf = -7 Hz and $\Delta D = 1.2 \pm 0.1 \times 10^{-6}$) but is likely explained by a higher density of CD44 his-HABD on 5% Tris-NTA lipid bilayers. Hyaluronan binding was both specific and irreversible, as it did not interact with 5% Tris-NTA SLBs lacking CD44, and was entirely stable during rinsing (1.5 hours). Taken together, these data demonstrate that SLBs comprising 5% OEOA-tris-NTA lipids are appropriate for stable anchoring of His-tagged HA binding proteins, in a native orientation that supports binding of hyaluronan.

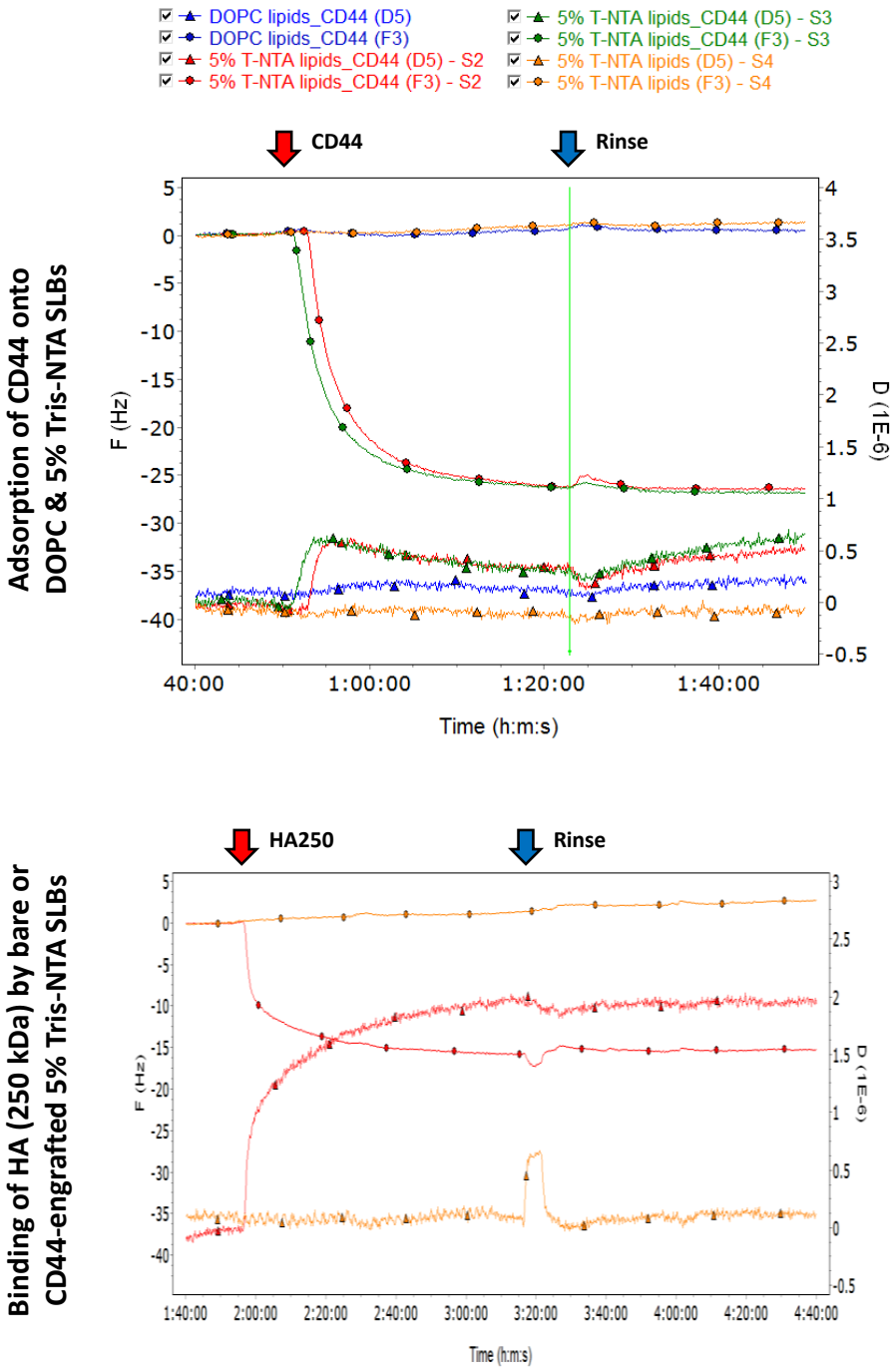


Figure 6.14. **Adsorption of His-tagged CD44 HABD onto 5% Tris-NTA functionalized SLBs and subsequent binding of 250 kDa hyaluronan.** Four SLBs were formed by the spreading of 50 µg/ml SUVs comprising DOPC lipids only (x1) or DOPC and 5% Tris-NTA functionalized lipids (x3) onto separate silica surfaces. The hyaluronan binding domain (HABD) of human CD44 with a 10His C-terminal tag was introduced onto one DOPC and one 5% Tris-NTA:DOPC SLB at 10 µg/ml until no further change in frequency (Δf) was detected. Hyaluronan (250 kDa) at 10 µg/ml was then introduced to all SLBs until (Δf) was stable. The start and finish of each injection are indicated with arrows. Δf and ΔD are shown for the 3rd and 5th overtones respectively. Data from a single experiment.

6.3.7 Analysis of LYVE-1-hylauronan interactions using an artificial membrane system monitored by QCM-D

To investigate the hyaluronan binding properties of recombinant LYVE-1, a model system was constructed based on that described for CD44. SLBs were formed by the spreading of SUVs with 5% Tris-NTA functionalized lipids onto separate quartz crystal sensors. QCM-D was used to monitor formation of good quality SLBs on the basis of characteristic biphasic behaviour, with final changes in frequency and dissipation of Δf = -29 Hz and $\Delta D < 0.3 \times 10^{-6}$ (data not shown). A comparison was then made of adsorption of different monomeric LYVE-1 samples to these bilayers (Figure 6.15). Binding of untreated, neuraminidase-digested or alkylated LYVE-1 monomer was initially rapid, before slowing to saturation point over the course of 50 minutes. The final frequency response following rinsing for all three samples was -69 Hz, and remained very stable over an extended time period. At the point of rinsing, a marked increase in dissipation (6.8 to 8.3×10^{-6}) coupled with a small negative shift in f (-65 Hz to -69Hz) was observed for untreated LYVE-1 monomer, but not for the other samples. If a process of dimerization was occurring, the opposite response would be expected, as some water would be excluded and the homogeneity of the protein film would be expected to increase, rather than decrease. Instead, a small swelling of the protein layer appears to occur, perhaps due to the removal of free, negatively-charged LYVE-1 monomers from the surrounding solvent.

While the frequency response was identical, a marked difference in dissipation through untreated or alkylated and neuraminidase-digested protein films was observed (8.3, 8.3 and 5.3×10^{-6}, respectively). The range of dissipation values occupied by different overtones was very narrow for films of neuraminidase-treated monomer, but widely spread for untreated or alkylated protein (Figure 6.16). Reduced dissipation indicates that the removal of sialic acid results in a more homogenous protein film. This may be partly explained by

a reduction in glycan complexity, but also suggests that a higher receptor density is achieved by neuraminidase-treated protein, most likely due to a reduction in charge repulsion between individual receptors. QCM-D becomes insensitive to small changes in film thickness as adsorption proceeds to saturation, but can be coupled with ellipsometry measurements to provide definitive surface densities. Such experiments will be required in future to determine whether removal of sialic acid does indeed permit closer packing of individual proteins.

Addition of hyaluronan (mw 250 kDa) revealed significant differences in HA binding by each sample of LYVE-1 monomer (Figure 6.15). Adsorption of HA onto LYVE-1-coated SLBs was rapid and very stable during rinsing (> 1 hour), following an initial loss at the end of HA injection. In a mirror image of the plate binding assay (Figure 6.12), removal of sialic acid resulted in a significant increase in HA binding (Δf = 16.8 Hz, $\Delta D = 3.0 \times 10^{-6}$) compared to wildtype protein (Δf = 9.9 Hz, $\Delta D = 2.2 \times 10^{-6}$). Interestingly, alkylated LYVE-1 monomer, which did not bind biotinylated HA when assayed by ELISA, was able to bind native HA in the QCM-D system. Such discrepancies are not uncommon when using QCM; analysis of mutant proteins that lack ligand binding using other techniques, often reveals unexpected activity due to avidity effects at the high densities achieved on SLBs (Dr. R. Richter, personal communication). In this example, HA binding by alkylated monomer was detected, but was lower than observed for the wildtype protein (Δf = 7.8 Hz and = 9.9 Hz respectively).

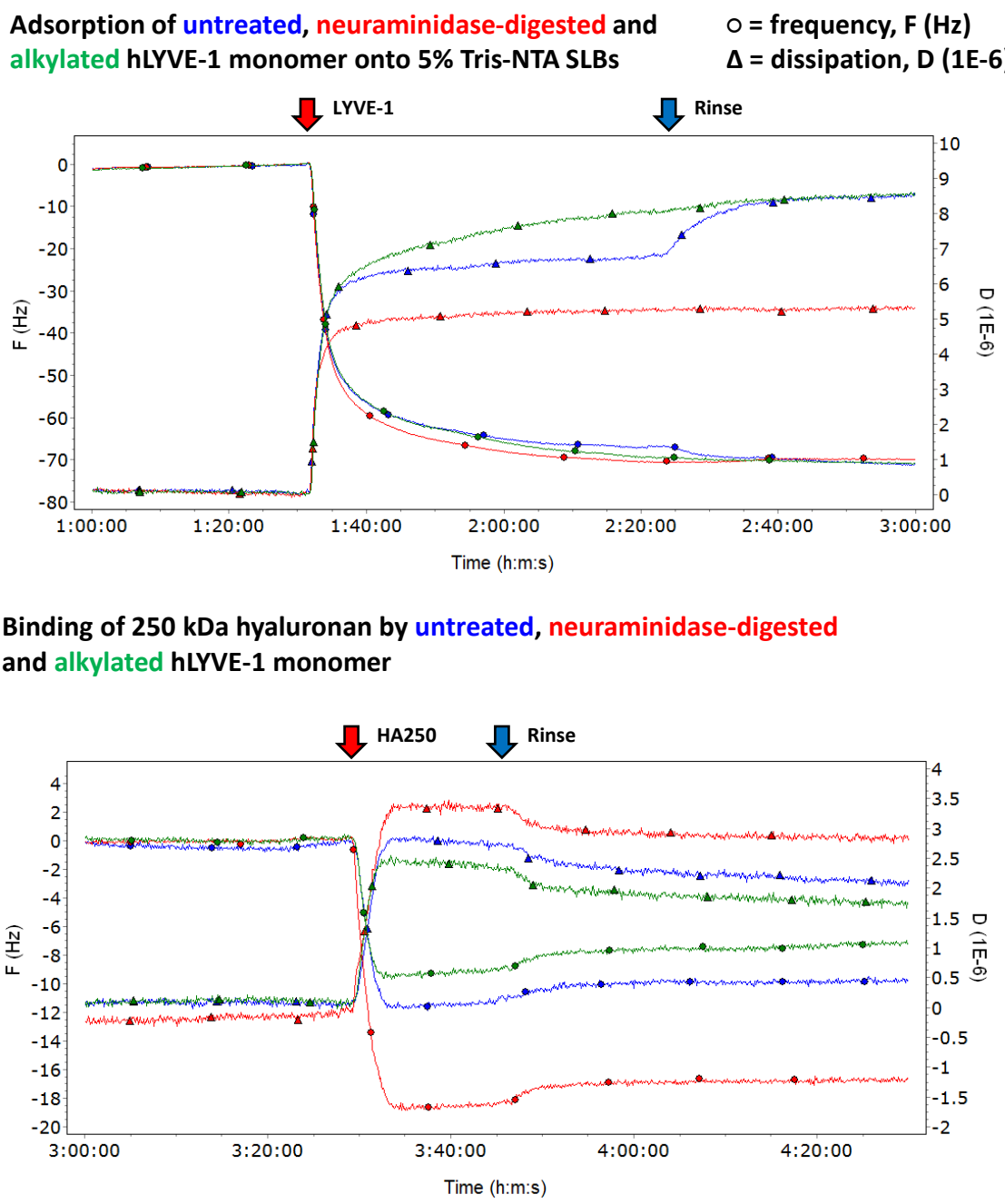


Figure 6.15. **Analysis of Hyaluronan interactions with recombinant hLYVE-1 monomer in an artificial membrane system monitored by QCM-D.** Three SLBs were formed by the spreading of 50 µg/ml SUVs comprising DOPC and 5% Tris-NTA functionalized lipids onto separate silica surfaces. Samples of His-tagged monomeric LYVE-1 were introduced onto SLBs at 10 µg/ml until no further change in frequency (Δf) was detected. LYVE-1-coated bilayers were rinsed with buffer for an extended period to observe stability of LYVE-1 binding. Hyaluronan (250 kDa) at 10 µg/ml was then introduced to all SLBs until (Δf) was stable, followed by extensive rinsing with buffer. The start and finish of each injection are indicated with arrows. Δf and ΔD are shown for the 3rd and 5th overtones respectively. Data representative of two independent experiments.

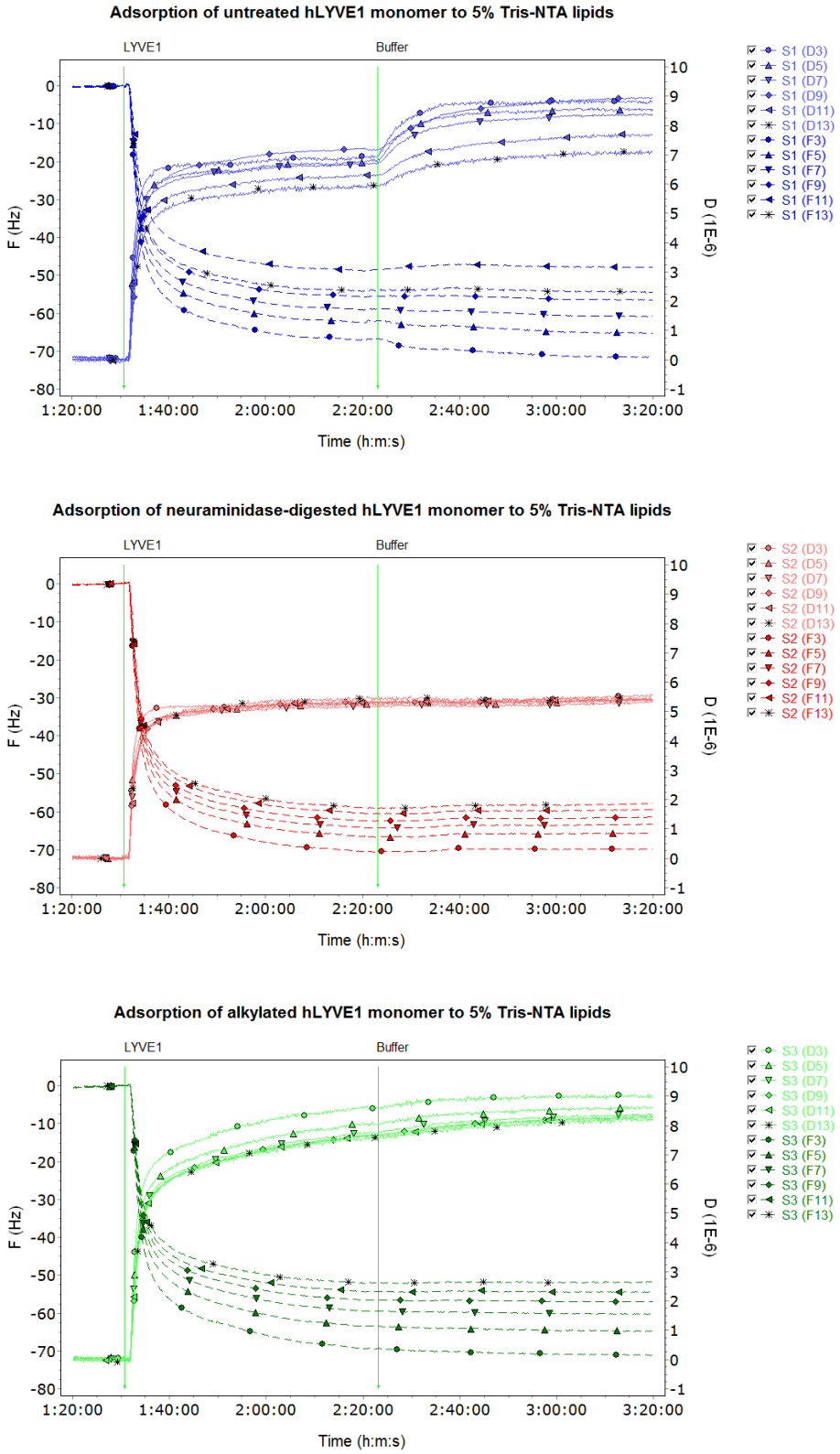


Figure 6.16. **Adsorption behaviour of recombinant hLYVE-1 monomer samples monitored by QCM-D.** Data recorded for absorption of hLYVE-1 monomer samples in Figure 6.15 shown in greater detail, with Δf and ΔD displayed for the 3rd, 5th, 7th, 9th, 11th and 13th overtones. The start and finish of LYVE-1 injection is indicated by vertical green lines.

6.3.8 Comparison of hyaluronan binding by recombinant LYVE-1 monomer and dimer

Untreated and neuraminidase-treated samples of LYVE-1 monomer and dimer were tested side-by-side using the QCM system to determine their relative HA binding capacity. All four proteins adsorbed onto 5% Tris-NTA lipid bilayers until saturation was reached after ~90 mins (Figure 6.17). Adsorption of monomeric LYVE-1 closely resembled that observed in previous experiments (untreated monomer: Δf = -70.4 Hz, $\Delta D = 8.2 \times 10^{-6}$, neuraminidase-treated monomer: Δf = -69.6 Hz, $\Delta D = 5.5 \times 10^{-6}$). The adsorption behaviour of neuraminidase-treated dimer was not dissimilar to the equivalent monomeric sample (Δf = -69.4 Hz, $\Delta D = 5.8 \times 10^{-6}$), however the final shift in f for untreated dimer was slightly lower at -64.5 Hz. This suggests that the native dimer has a less extended conformation, resulting in a slight reduction in film thickness. In both cases, dimeric LYVE-1 remained stably bound to SLBs over an extended period of rinsing. The final shift in dissipation for neuraminidase-treated dimer was lower than observed for the native protein (ΔD = 5.8 and 6.6×10^{-6} respectively), with a smaller range in dissipation values across different overtones (Figure 6.18). The difference in dissipation was not as pronounced as observed with monomeric LYVE-1 samples, but the same process appears to apply.

On the basis of the results obtained using an HA binding ELISA (Figure 6.12), it was anticipated that QCM analysis would demonstrate superior HA binding by dimeric LYVE-1 than monomeric samples, however this proved not to be the case. At saturating levels of adsorption, HA binding was very stable for both species, but greater for native monomeric (Δf = -9.0 Hz) than dimeric LYVE-1 (Δf = -6.3 Hz). The same pattern was also observed for neuraminidase-treated samples (monomer: Δf = -18.0 Hz, dimer: Δf = -9.8 Hz). This unexpected result may be explained entirely by the presence of disulphide-bonded

aggregate in samples of LYVE-1 dimer (Figure 6.11). The aggregated material is likely to bind Tris-NTA lipids and almost certainly does not bind HA, as it can only be generated by inappropriate disulphide-bond formation between Link-module cysteine residues and/or cysteine 201 in the stalk region. However, it also possible that differences between monomer and dimer are not evident such high densities due to the multivalent nature of the system, and that close packing of the dimer may even hinder its ability to bind HA.

To test this hypothesis, samples of monomeric and dimeric LYVE-1 were grafted onto 5% Tris-NTA lipid bilayers at lower density, by injecting the protein at lower concentration and halting when the frequency change equalled -25 Hz (Figure 6.19). At this level of adsorption there were a number of differences in behaviour. Final shifts in dissipation for monomeric LYVE-1 samples were identical, indicating less of an influence of neuraminidase treatment, although there was still a difference between bilayers coated with LYVE-1 dimer. Adsorption of dimeric LYVE-1 was noticeably slower than for monomeric protein, but binding of all four species remained stable during rinsing. In terms of HA binding, the hierarchy of monomeric over dimeric species was maintained (untreated monomer: Δf = -4.2 Hz, untreated dimer: Δf = -2.6 Hz). Interestingly, neuraminidase-treated samples no longer had superior HA binding compared to native protein; rather the final shifts in frequency were slightly lower (monomer: Δf = - Hz, dimer: Δf = -9.8 Hz). This suggests that removal of sialic acid does not directly enhance HA binding affinity, but instead influences adsorption of the protein onto the SLB, which is much more significant at high density. Finally, although binding of 250 kDa HA was significantly reduced at lower grafting density, it remained irreversible over extended periods of rinsing.

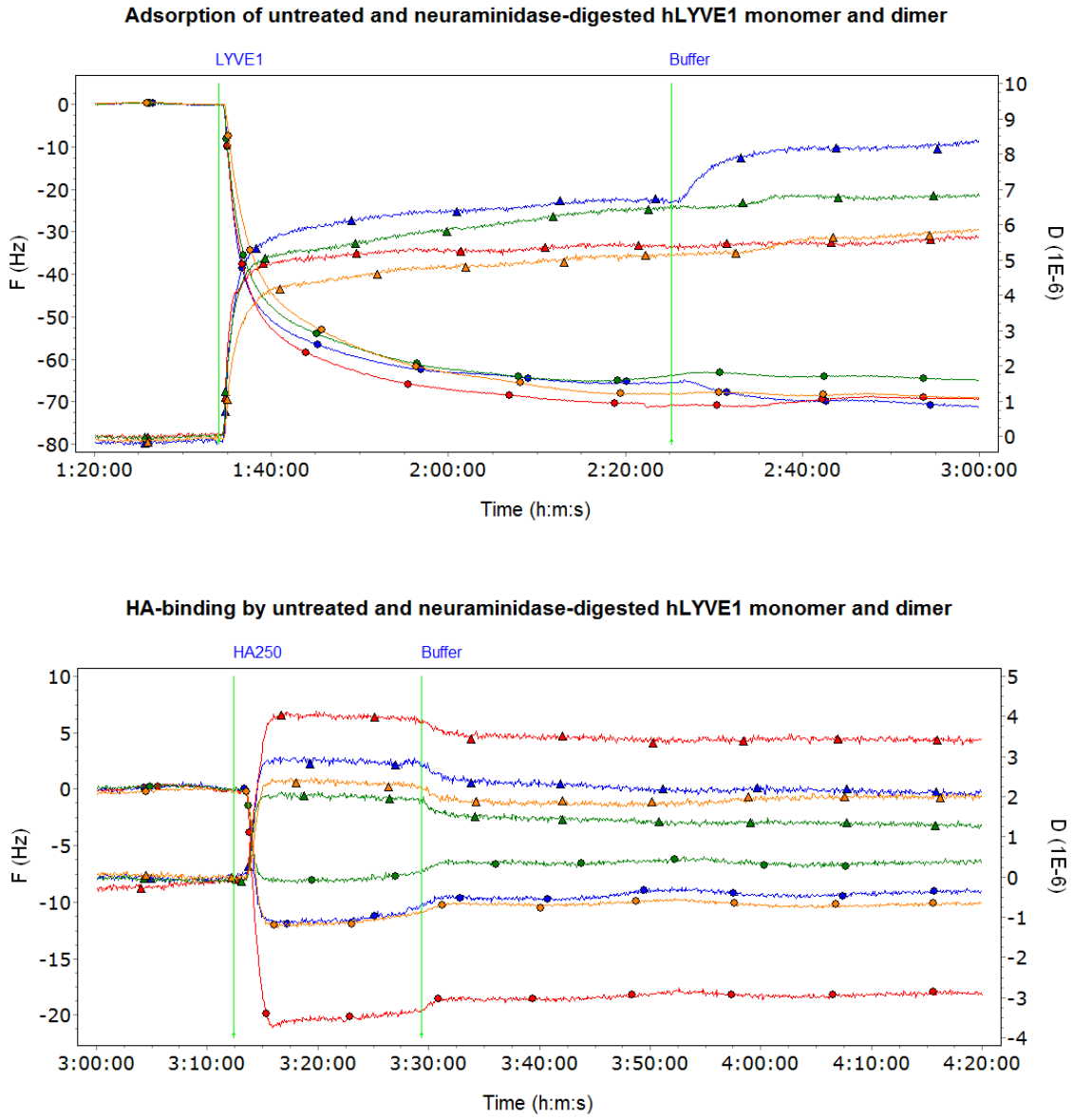


Figure 6.17. **Comparison of Hyaluronan interactions with untreated or neuraminidase-digested recombinant hLYVE-1 monomer and dimer as saturating density.** Four SLBs were formed by the spreading of 50 µg/ml SUVs comprising DOPC and 5% Tris-NTA functionalized lipids onto separate silica surfaces. Samples of untreated or neuraminidase-digested hLYVE-1 monomer or dimer were introduced separately onto SLBs at 10 µg/ml until no further change in frequency (Δf) was detected. Hyaluronan (250 kDa) at 10 µg/ml was then introduced to all SLBs until (Δf) was stable, followed by extensive rinsing with buffer. The start and finish of each injection are indicated by green lines. Δf and ΔD are shown for the 3rd and 5th overtones respectively. Data are representative of two independent experiments.

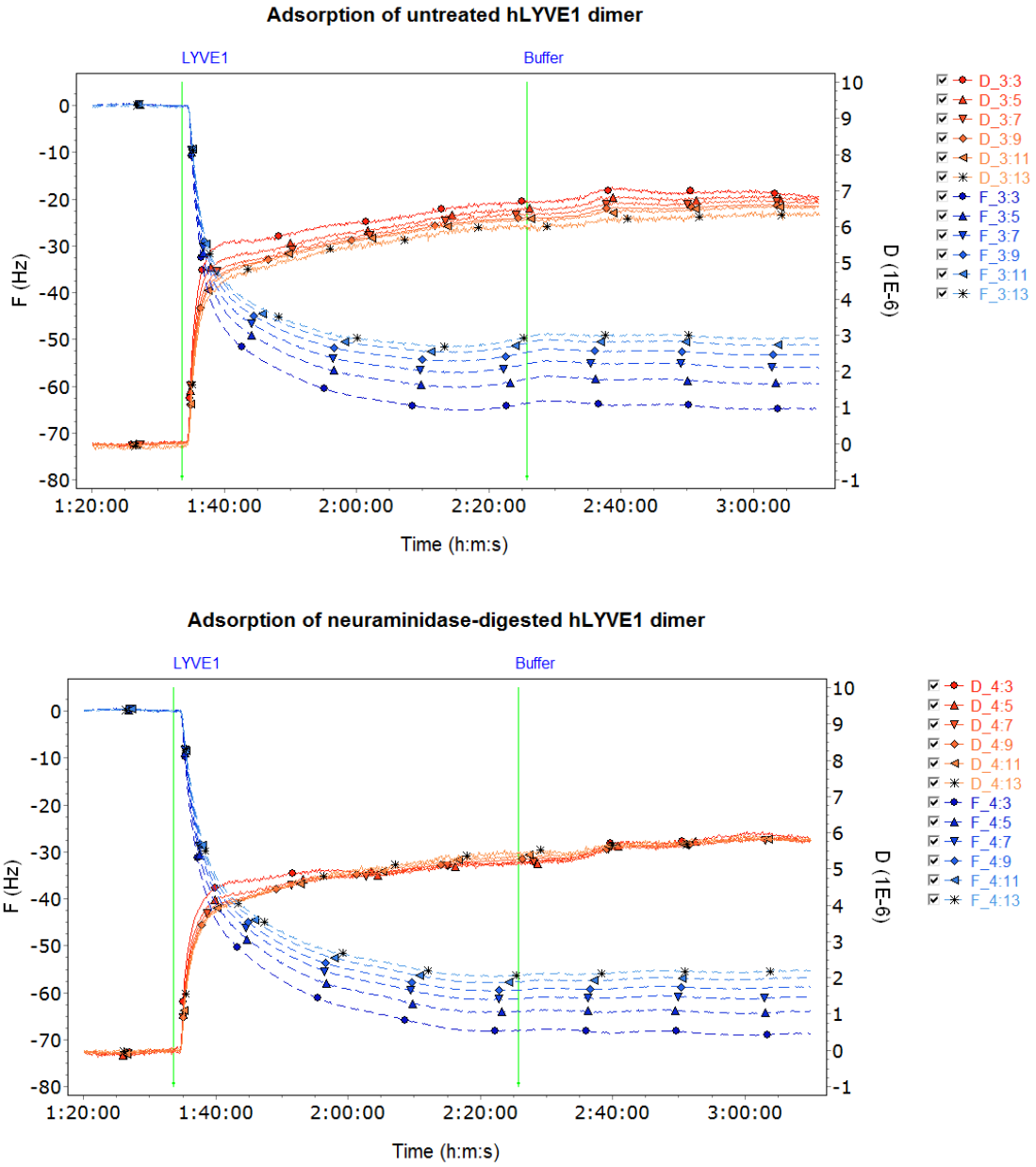


Figure 6.18. **Adsorption behaviour of recombinant hLYVE-1 monomer samples monitored by QCM-D.** Data recorded for absorption of hLYVE-1 dimer samples in Figure 6.17 shown in greater detail, with Δf and ΔD displayed for the 3rd, 5th, 7th, 9th, 11th and 13th overtones. The start and finish of LYVE-1 injection is indicated by green lines.

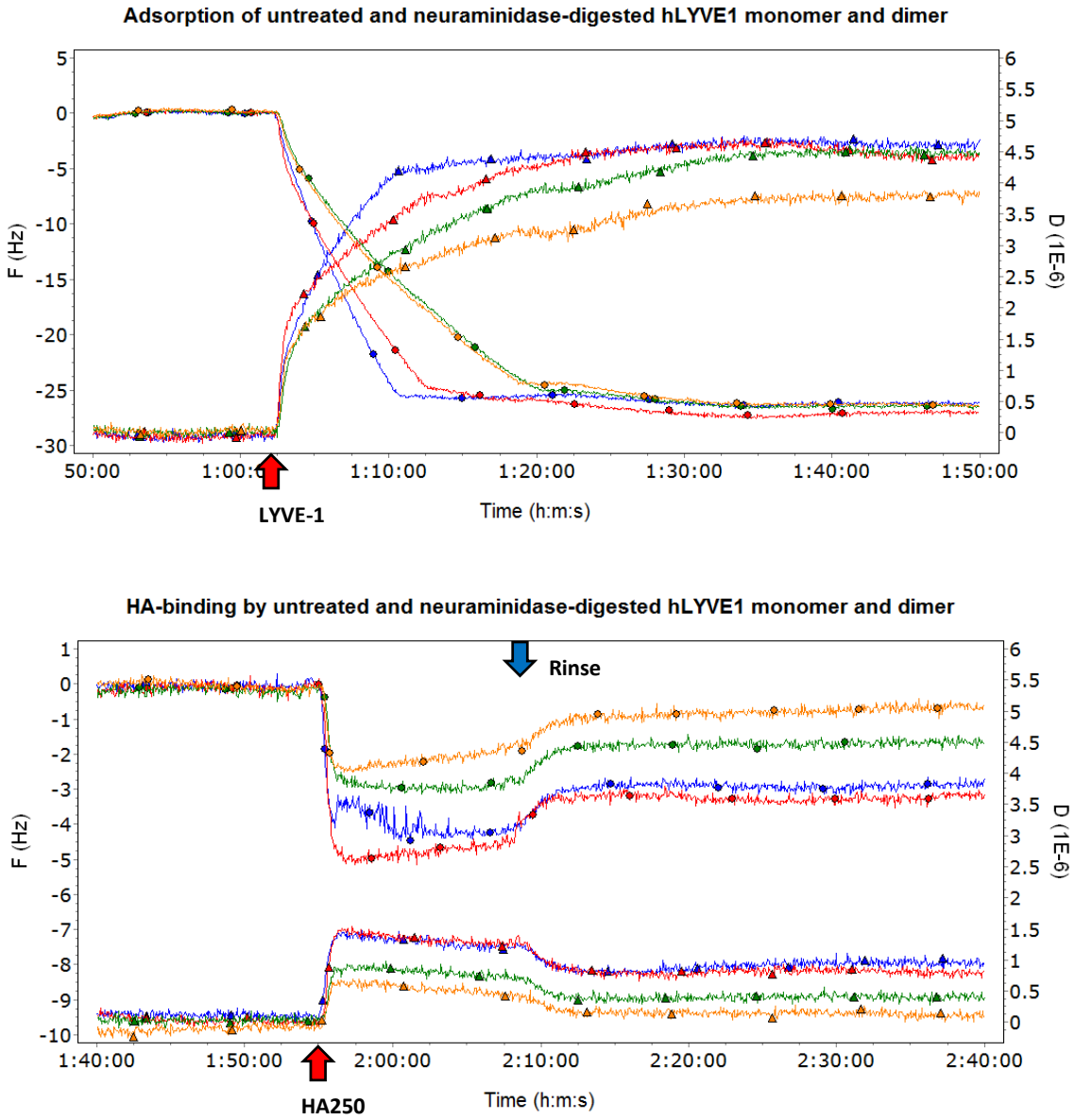


Figure 6.19. **Comparison of Hyaluronan interactions with untreated or neuraminidase-digested recombinant hLYVE-1 monomer and dimer as 'low' density.** Four SLBs were formed by the spreading of 50 µg/ml SUVs comprising DOPC and 5% Tris-NTA functionalized lipids onto separate silica surfaces. Samples of untreated or neuraminidase-digested hLYVE-1 monomer or dimer were introduced separately onto SLBs at 10 µg/ml until Δf ~ 25 Hz was detected. Hyaluronan (250 kDa) at 10 µg/ml was then introduced to all SLBs until (Δf) was stable, followed by extensive rinsing with buffer. The start and finish of each injection are indicated by green lines. Δf and ΔD are shown for the 3rd and 5th overtones respectively. Data are representative of two independent experiments.

6.3.9 Influence of LYVE-1 mAb on HA binding by recombinant LYVE-1 monitored by QCM-D

As described in chapter 4, antibody-mediated potentiation of HA binding by LYVE-1-expressing cells is driven primarily by clustering of LYVE-1 molecules. Clustering occurs both at low temperature and in the presence of sodium azide, consistent with a purely physical process independent of signalling events or active rearrangement of LYVE-1 molecules by the cell. QCM-D is a cell-free system where lateral mobility of LYVE-1 molecules is retained, and is therefore well-suited to test this assumption. Untreated LYVE-1 monomer was adsorbed onto separate SLBs and incubated with HA-blocking or potentiating mAbs, prior to addition of 250 kDa HA, to test the effect on HA binding (Figure 6.20). A low level of protein adsorption was chosen (-25 Hz), in order to avoid possible effects of steric hindrance on mAb binding exerted by close receptor packing at very high densities. One LYVE-1-engrafted SLB was left untreated, while three others were incubated separately with 6A, a mAb that potentiates HA binding by LYVE-1, 891, a mAb that blocks HA binding, or mouse IgG_{2b} isotype control. Both 6A and 891 bound rapidly and stably, with final frequency shifts of -29.0 and -28.4 Hz respectively. Mouse IgG_{2b} isotype control did not bind LYVE-1-coated SLBs.

Following addition of 250 kDa HA to all surfaces, further frequency shifts of -2.8 and -4.0 Hz were detected for untreated or IgG_{2b}-treated LYVE-1-coated bilayers, and HA binding remained stable during rinsing. Incubation with 891 mAb had the effect of blocking all HA binding (Δf = 0 Hz), while 6A mAb had a 2-fold potentiating effect (Δf = 7.9 Hz). The latter observation is particularly interesting, as potentiating mAbs were found to have no effect on HA binding by recombinant LYVE-1 when the protein was immobilized on the surface of plastic multiwall dishes in which lateral mobility is inhibited.

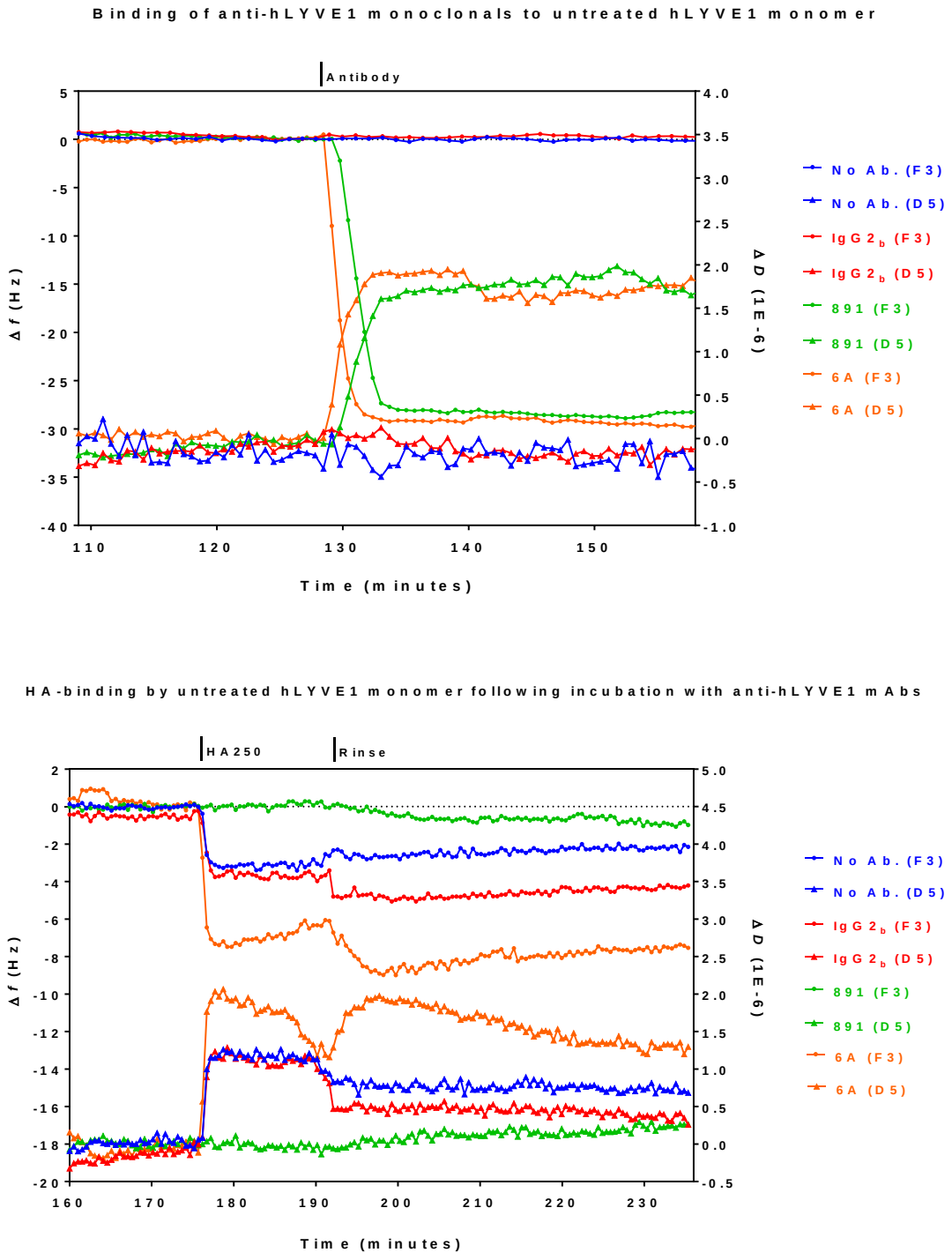


Figure 6.20. **Influence of potentiating and blocking antibodies on HA-binding by monomeric LYVE-1 in the QCM-D system.** SLBs were formed on four silica sensors and untreated hLYVE1 monomer injected at 1 µg/ml until Δf = -25Hz (data not shown). *Top panel:* Anti- hLYVE1 monoclonals 891 (*green*, an *HA-blocking* mAb) and 6A (*orange*, a *potentiating* mAb) were injected onto separate sensors, $IgG2_b$ isotype control onto a third (*red*), while a fourth was left untreated (*blue*). *Bottom panel:* Hyaluronic acid (mw 250kDa) was injected at 10 µg/ml until binding to LYVE-1 reached saturation point. The stability of binding during rinsing was monitored over time. Data are from a single experiment.

6.4 Discussion

In this chapter, the capacity of LYVE-1 to form homodimers was investigated in primary lymphatic endothelial cells and a number of different transfected cell backgrounds. The proportion of LYVE-1 homodimers relative to monomers was found to be variable, not only between cell Jurkat and 293T cells, but also between different culture isolates of primary LEC. This was also the case at the cell surface, where the monomer:dimer ratio ranged between 3:2 and 1:1 depending on the batch of cells. The prevalence of homodimers could conceivably be altered by changes in extracellular conditions affecting their stability at the cell surface, or by changes in the rate of formation during biosynthesis. There is some evidence that the percentage of homodimers is increased in both Jurkat and primary LEC transduced with lentivirus to over-express LYVE-1, particularly in cells with the highest LYVE-1 expression and HA binding (Figure 6.4 & Dr. S. Banerji, unpublished observations).

However, dimeric LYVE-1 was also found to be more prevalent at the surface of primary LEC than inside the cell, suggesting that homodimers may form or dissociate at some time following biosynthesis. The cysteine residue responsible for homodimerization, Cys 201, is located in a disordered region of the protein, and adjacent to a tract of basic residues, making it a prime candidate for a labile-disulphide. Recent experiments have shown that the Cys201-Cys201 inter-chain disulphide is sensitive to much lower levels of the reducing agent TCEP than is the case for structural disulphides in the Link domain (Dr. S. Banerji, unpublished observations). Regulation of protein function *via* redox-sensitive extracellular thiols has been described for a number of plasma membrane proteins, including CD4 (Ou and Silver, 2006), integrin α-4 (Laragione et al., 2003), and CD21 (Aichem et al., 2006). The possibility that a similar redox-sensitive mechanism controls dimer formation and

dissociation in the case of LYVE-1 is currently being investigated in the Jackson laboratory.

The influence of LYVE-1 homodimerization on hyaluronan binding was found to be dependent on both LYVE-1 expression level and cell background. Surprisingly, transfected cells over-expressing a non-dimerizing LYVE-1 C201A mutant were found to bind HA, but the level was significantly reduced compared to cells expressing a mixture of monomer and dimer. In the absence of LYVE-1 homodimers, the threshold of LYVE-1 expression required for HA binding is increased, consistent with recent observations that recombinant LYVE-1 monomer has a lower HA binding affinity (K_D = 107 µM) than the dimer (K_D = 20 µM). This disadvantage is partially overcome in the context of over-expression, most likely due to avidity effects arising from increased opportunity for multivalent interactions.

The situation in primary lymphatic endothelial cells is markedly different. Even when over-expressed in these cells, the non-dimerizing LYVE-1 C201A mutant displayed little or no HA binding, compared to very high levels for cells over-expressing wildtype LYVE-1. Although surface expression levels were not precisely matched, it was clear that the binding capacity of the monomer was drastically reduced in comparison to homodimer, and could only be increased marginally by co-incubation with the potentiating mAb 8C. This suggested that the role played by LYVE-1 homodimers in LEC is much more critical than in transfected cells. The reason for the discrepancy is almost certainly related to sialylation of the receptor in primary cells, and the failure of fully sialylated monomer to compensate for the absence of dimeric LYVE-1. Further experiments will be required to demonstrate this, but recently it has been shown that over-expression of LYVE-1 in LEC leads to an increased ratio of LYVE-1 homodimer:monomer, especially in those cells with the highest levels of HA binding (Dr. S. Banerji, manuscript in preparation). The role played by

LYVE-1 homodimers in LEC may therefore be to function as higher-affinity receptors that initiate HA binding events, to which lower affinity monomers can be recruited.

Attempts were also made to introduce wildtype or C197A mutant mouse LYVE-1 into primary human LEC, which has the advantage of permitting discrimination of the over-expressed protein and the endogenous receptor. However, it proved challenging to expand the cells sufficiently following lentiviral infection and FACS sorting. It may also be informative to repeat the biotinylated HA pull-down experiments conducted previously with LYVE-1 transfected HEK 293T cells, but using primary LEC treated with a potentiating antibody, to determine which species is most efficiently recovered.

Studying individual aspects of LYVE-1 regulation in isolation using cell-based systems is challenging, due to the interplay of factors such as surface density and cell-specific glycosylation patterns. In an attempt to overcome these hurdles, an artificial membrane system monitored by QCM-D was developed, based on a previous study of CD44 (Wolny et al., 2010). Using Tris-NTA functionalized lipid bilayers, it was possible to stably anchor recombinant His-tagged LYVE-1, while maintaining free lateral and rotational mobility of the receptor. Perhaps the most important result arising from characterization of this model system, was the observation that LYVE-1 was capable of irreversible binding of 250 kDa HA, with final frequency shifts exceeding any previously observed with CD44. Considering the low HA binding affinities of individual receptors, this provided the first direct evidence that LYVE-1 engages in multivalent interactions to secure binding of large HA chains. Furthermore, HA binding could be efficiently blocked using 891 mAb and enhanced using potentiating mAb 6A, something that did not occur when the same protein was immobilized in a plate assay.

Technical issues with purification and storage prevented direct comparison of LYVE-1 monomer and dimer, which will need to be overcome to take this work further. Separation by size exclusion chromatography prior to experiments would be one solution, as both monomer and dimer are stable at 4^{o}C for at least one week. Alkylation had the unexpected effect of ablating HA binding, but an alternative route would be to express a His-tagged hLYVE-1 C201A protein, as a potential alternative to the native monomer.

The mechanism by which sialylation inhibits HA binding remains enigmatic, but it is clear that de-sialylation enhances HA binding both in static plate binding assays and the artificial membrane system. Due to the lack of lateral mobility, the enhancement observed in the former would argue for a direct influence on HA binding affinity. Preliminary measurements using surface plasmon resonance would appear to support this (Dr. S. Banerji, unpublished observations). However, changes in dissipation observed for neuraminidase-treated LYVE-1 strongly suggested that sialic acid limits adsorption of receptors onto SLBs, suggesting that charge repulsion between molecules is significant. The lack of a difference, both in dissipation and HA binding at lower grafting density would support this argument. In future, conducting combined QCM-D and ellipsometry measurements to determine the adsorbed mass and density of both samples should settle this matter.

Chapter 7.
General Discussion

7.1 Summary

The aim of this thesis was to characterise the significance of hyaluronan as a LYVE-1 ligand, firstly by investigating whether HA is involved in the function-blocking properties of mouse LYVE-1 mAbs, and secondly by determining the conditions under which inhibition of HA binding may be overcome in lymphatic endothelium. At the outset, the role of LYVE-1 as an HA receptor was enigmatic; primary lymphatic endothelial cells (LEC) isolated from human and mouse displayed little or no constitutive HA binding, and furthermore, LYVE-1 did not appear to co-localize with endogenous or exogenously-added HA in frozen tissue sections (Nightingale et al., 2009). Further study had revealed that the native receptor is extensively sialylated, most likely through α2-3 or α2-6 linkage to O-glycans in the stalk region, with the result that HA binding is very weak or undetectable in primary LEC (Nightingale et al., 2009). However, the means by which this apparent inhibition may be alleviated were unclear. Rather than activating LYVE-1 to bind HA, pro-inflammatory stimuli had been shown to trigger both down-regulation and degradation of LYVE-1, in a manner that did not influence HA uptake (Johnson et al., 2007). Finally, function-blocking experiments with mLYVE-1 mAbs indicated a role for the receptor in transmigration of lymphatic endothelium by migratory leukocytes and tumour cells, but suggested that there may be underlying mechanisms separate from HA binding. Blockade of mLYVE-1 with mAb C1/8 invariably resulted in a different outcome to blockade with B1/10 mAb, which coupled with the apparent inhibition of HA binding in LEC, suggested that the transmigration process blocked by either antibody could be independent of HA.

The results presented in this thesis demonstrate that this is unlikely to be the case, and that disruption of the LYVE-1-hyaluronan interaction underpins the function-blocking properties of mLYVE-1 mAbs. Furthermore, they reveal for the first time that such an

interaction is possible because native LYVE-1 is competent to bind HA even when fully sialylated, and indeed may have evolved to engage with ligand only after appropriate surface redistribution, or presentation of HA in a form that promotes this process. The former observation came from detailed characterization of mLYVE-1 mAbs generated in the Jackson laboratory (B1/10 & C1/8), using potent HA-blocking antibodies from commercial sources (MAB2125 & ALY7) as a comparison. Both mAbs B1/10 and C1/8 were found to block HA binding, which raises the likelihood that HA plays a role in the LYVE-1 dependent transmigration of lymphatic vessels by dendritic cells, nodal dissemination of metastasizing tumour cells and egress of inflammatory macrophages from lung alveolae. Using a cross-blocking assay, it was apparent that B1/10 and C1/8 could displace each other's binding, suggesting that their epitopes overlap, and that differences in their behaviour are not explained by separate binding sites. These observations proved to be consistent with subsequent epitope mapping analysis which showed that the four antibody epitopes are quite similar, localising to the same 'face' of the protein, and overlap to varying degrees with the predicted HA-binding site.

Taken together, these data argue for a common mechanism of action for B1/10 and C1/8 that involves blockade of HA binding to LYVE-1. However, this hypothesis does not explain how different functional outcomes may arise when using the two antibodies in the same disease model. B1/10 and C1/8 are comparatively weak blockers of HA binding, which is most likely a reflection of their low binding affinity when compared to other mLYVE-1 mAbs such as ALY7 and MAB2125. Recent work in the Jackson laboratory has suggested that HA can induce modulation of lymphatic endothelial adherens junctions via LYVE-1 and MAPK signalling pathways in a manner that is dependent on HA size and concentration (Dr. Ying-jie Wang & Dr. Danijela Markovic, unpublished observations). It would be intriguing to determine whether B1/10 and C1/8 can modulate signalling

outcomes resulting from the interaction of LYVE-1 with different length HA chains, perhaps through partial blockade of HA binding, with resulting changes in adherens junctions and permeability of the lymphatic vessel. It is also possible that binding of either antibody may mimic binding of HA, or a particular cross-linked form of the ligand that alters distribution of the receptor. For example, all human LYVE-1 mAbs that potentiate HA binding in LEC have been found to cluster the receptor, while those that block HA binding do not alter its distribution. The influence of weak HA-blocking antibodies such as B1/10 and C1/8 on LYVE-1 organisation in mouse LEC has yet to be determined.

The conclusion that function-blocking antibodies inhibit HA binding by LYVE-1 on lymphatic endothelium raises an obvious question; how is this possible, if the receptor is maintained in a default non HA-binding state? While a process of de-sialylation clearly represents one possible mechanism for activation of HA binding it is now clear from the results in this thesis that there are other potentially more rapidly-acting mechanisms. As evidenced by the data in Chapter 4, one of these is alteration of receptor surface distribution or receptor clustering – a process that can lead to enhanced binding of a polyvalent ligand. At first glance, the individual binding affinities of HA receptors such as LYVE-1 and CD44 can appear rather low, yet are more than sufficient to support stable binding given the presence of multiple receptors at the cell surface and the repetitive structure of the HA polymer. This is because the binding affinities of individual interactions are multiplicative with a polyvalent ligand through avidity effects, leading to a rapid increase in cumulative binding affinity. An avidity-driven model of HA binding has been well documented for the CD44; various authors have described a minimal expression threshold for HA binding in AKR1 cells (Perschl et al., 1995), the relationship between receptor density and HA binding in artificial lipid membrane systems (Wolny et al., 2010) and an increase in avidity with HA chain length, that defines multivalent interactions as the primary feature of HA

binding by cell surface CD44 (Lesley et al., 2000). Various means of modulating CD44 density have also been described, including the use of potentiating antibodies to induce HA binding in T cells (Lesley and Hyman, 1992) *via* a mechanism that requires bivalent antibody (Lesley et al., 1993). HA binding to CD44-expressing cells has also been shown to be enhanced by HA cross-linking proteins such as TSG-6, which appear to increase the valency of the HA-CD44 interaction and possibly induce a similar process of receptor clustering (Lesley et al., 2004).

Hyaluronan binding to LYVE-1 is similarly dependent on the avidity of the interaction, which in conjunction with receptor sialylation and homodimerization, underpins regulation of HA binding in primary LEC. In chapters 4 and 5 of this thesis, the role of avidity was investigated using three separate approaches aimed at modifying the valency of the LYVE-1-HA interaction, including altering the global surface density of LYVE-1 molecules, clustering of the receptor into local areas of high density using monoclonal antibodies, and cross-linking individual HA chains to form higher-order architectures. An early finding was that LYVE-1 surface expression is a critical regulator of hyaluronan binding in both primary and transfected cell lines, and that the relationship between LYVE-1 expression and HA binding is not strictly linear. In transfected cells, hyaluronan binding is only seen above a narrow threshold of LYVE-1 expression; beyond this point HA binding scales rapidly with small increases in the amount of LYVE-1, and begins to plateau at the extremes of LYVE-1 surface density (Figure 7.1, A). The situation in primary lymphatic endothelial cells is different due to the absence of constitutive HA binding, indicating that a higher threshold of LYVE-1 surface density operates, perhaps as a result of negative charge repulsion between sialylated receptors (Figure 7.1, B). As shown in chapter 4, this can be overcome by artificial over-expression of LYVE-1 in LEC, which results in high levels of constitutive HA binding from a 4 to 5 fold increase in LYVE-1 expression.

Importantly, the threshold of expression required for stable HA binding may be manipulated by cross-linking of LYVE-1 molecules, leading to clustering of the receptor. In wildtype LEC, simple application of potentiating antibodies induces rapid conversion to high levels of HA binding, without the need for over-expression or desialylation of LYVE-1 (Figure 7.1, D). As such, this constitutes the first demonstration that primary lymphatic endothelial cells are capable of binding HA through LYVE-1, given appropriate rearrangement of receptor molecules. Antibody-mediated potentiation of HA binding is also dependent on LYVE-1 expression, and may be inhibited by LYVE-1 blocking mAbs or competition with an excess of unlabelled HA. It is also effective with LYVE-1 transfected cells, increasing HA binding beyond that seen in the absence of potentiating antibody, and converting cells that are below the LYVE-1 expression threshold to an HA-binding phenotype. There are two main means by which antibodies might potentiate HA binding: bivalent crosslinking of LYVE-1 monomers to form artificial dimers and crosslinking of pre-existing LYVE-1 disulphide linked homodimers into higher order lattices. The latter is concluded to have the greatest influence, given the changes in LYVE-1 distribution observed in adherent LEC monolayers following incubation with the potentiating antibodies 6A, 7C, 8C and 892 and the requirement for lateral mobility of the receptor highlighted by experiments with the QCM-D system as reported in chapters 4 and 6 of this thesis respectively. The focal increases in surface density resulting from such receptor clustering would increase the avidity of the interaction with HA, thus surpassing the threshold required for stable binding.

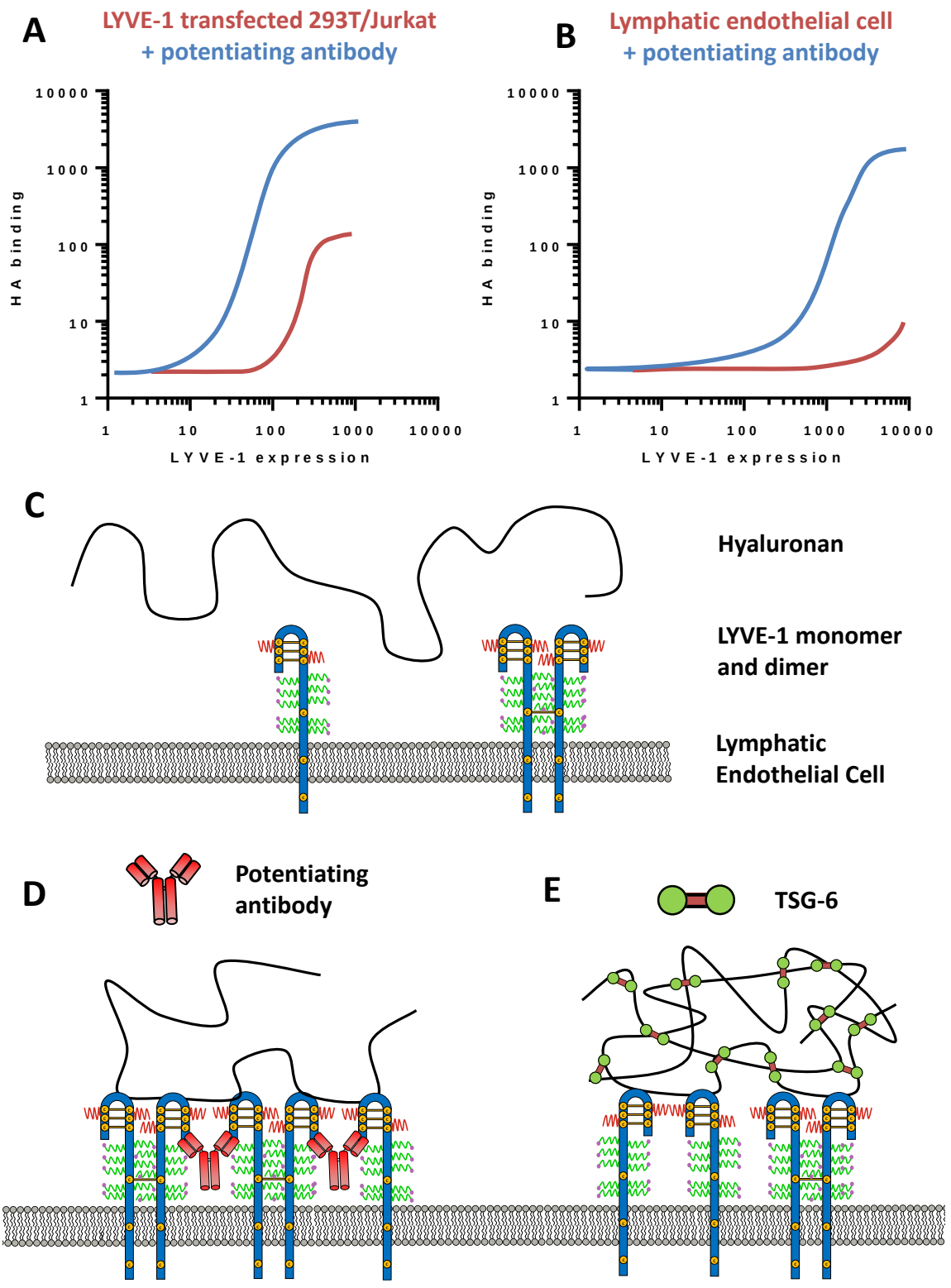


Figure 7.1 **Regulation of hyaluronan binding to LYVE-1. (C)** The native LYVE-1 receptor expressed by lymphatic endothelial cells is extensively sialylated and makes only transient interactions with HA. (**A, B**) A threshold of LYVE-1 expression is required for transfected cells to bind HA due to the multivalent nature of the interaction. In primary LEC, sialylation sets the threshold point above the typical surface density of LYVE-1 molecules. Simultaneous addition of a potentiating mAb with HA lowers this threshold in

both LEC and transfected cells, and increases the magnitude of HA binding in the former. (D) Potentiating mAbs lower the threshold by clustering LYVE-1 molecules, creating a local area of high receptor density that increases the valency of the interaction. (E) Cross-linking of HA chains using agents such as TSG-6 protein also increases the valency of the LYVE-1-HA interaction, through a combination of increased HA footprint on the cell surface and inducing clustering of LYVE-1 molecules.

Clustering of LYVE-1 molecules by specific mAbs is made possible by the capacity of receptor to form disulphide-linked homodimers, thus providing two antibody binding sites. The dimeric form of the receptor was shown to comprise ~40% of the total LYVE-1 molecules present at the surface of primary LEC as assessed by LDS-PAGE under non-reducing conditions (chapter 6), but this percentage is increased in super-transfected cells, particularly those with the highest LYVE-1 expression and HA binding (Dr. S. Banerji and Prof. D. Jackson, manuscript in preparation). The role played by LYVE-1 homodimers has in the past been elusive; although they clearly exhibit greater affinity for HA than monomeric LYVE-1, the latter can be sufficient for HA binding, depending on cell background and capacity for receptor sialylation. As shown in this thesis, HA binding to transfected Jurkat cells expressing the dimerization-deficient LYVE-1 mutant C201A was decreased, but not completely ablated when compared to their wildtype counterparts.

However, very recent measurements with recombinant LYVE-1 produced in CHO cells has revealed a far greater difference in HA binding affinity between monomer and homodimer than previously realised (monomer: K_D = 107 µM, dimer: K_D = 18.1 nM, Dr. S. Banerji and Prof. D. Jackson, manuscript in preparation), thus suggesting a much more significant role for LYVE-1 homodimerization in HA binding. These binding affinities are not dissimilar to those reported for monomeric and dimeric forms of Lox-1, the receptor for oxidized low-density lipoprotein (OxLDL), which contains a C-type lectin fold resembling the Link module, and which forms disulphide-linked dimers analogous to

LYVE-1 (Ohki et al., 2005). Accordingly, single LOX-1 homodimers bind OxLDL with an affinity in the supramicromolar range, while the monomeric protein shows only marginal binding to OxLDL. Moreover, Lox-1 has been shown to form clusters on the cell surface, and OxLDL particles have been reported to bind such cells with an apparent dissociation constant in the subnanomolar range ($K_D = 1.76 \times 10^{-10}$ M) (Ohki et al., 2011).

With a binding affinity of 18.1 nM, one might expect LYVE-1 homodimers to support constitutive binding of HA to lymphatic endothelial cells. However, the native receptor is extensively sialylated, and is likely to exhibit a much lower affinity than recombinant protein produced in a non-native cell type, with the result that HA binding is very weak or undetectable in LEC. However, the difference in binding affinity between monomeric and dimeric LYVE-1 may well be maintained, and so the role played by homodimers in LEC may therefore be to function as higher-affinity receptors that initiate HA binding events, to which lower affinity monomers can be recruited. Even when over-expressed in primary LEC, the dimerization-deficient hLYVE-1 mutant C201A was found to be incapable of inducing significant HA binding compared to cells over-expressing wildtype LYVE-1. For these reasons, the significance of LYVE-1 homodimerization for HA binding may be greater in cells with a high capacity for receptor sialylation (i.e. LEC) than in those with a lower capacity (i.e. Jurkat). Specifically, sialylation may set the threshold for HA binding and hence the degree to which LYVE-1 homodimers are required to overcome that threshold and support stable binding.

While it is possible to achieve binding of free HA chains to LEC by manipulating the distribution of LYVE-1 molecules at the cell surface, it is not known how the process might be regulated *in vivo*. Baluk and colleagues (2007) have shown by fluorescent imaging of initial lymphatic vessels in the mouse that LYVE-1 is concentrated at the tips of flap valves

– structures that act as entry point for migrating dendritic cells from the surrounding parenchyma (Pflicke and Sixt, 2009). It is generally considered that cultured monolayers of LEC do not form these same specialized flap valves, instead exhibiting a zipper-like junctional arrangement that more closely resembles the architecture of larger collecting vessels distal to the lymphatic capillaries. Clustering of LYVE-1 resulting from application of potentiating antibodies to these cells may therefore mimic areas of concentrated LYVE-1 expression seen *in vivo*. However, the density of LYVE-1 molecules on the surface of flap valves does not appear in itself to support binding of free HA, as evidenced by the failure to detect binding of endogenous HA or of exogenous Fl-HA to these structures during earlier microscopic imaging studies of mouse ear sections (Nightingale et al., 2009). Although further clustering may be required to support stable HA binding to LYVE-1 in these contexts, a more attractive hypothesis is that LYVE-1 may be poised to engage with selective forms or presentations of HA that increase the avidity of interaction through their specific architecture. Hyaluronan is bound by a variety of proteins that constrain its movement, influence the binding of other hyaladherins, and alter the behaviour of cells with which it interacts. For example, cross-linking of HA by the small inflammation-induced protein TSG-6 has been reported to enhance HA binding by CD44-transfected cells and to induce binding in $CD44^+$ lines that lack constitutive binding (Lesley et al., 2004).

In chapter 5 of this thesis, exposure to cross-linked hyaluronan complexes is shown to similarly enhance constitutive binding by LYVE-1 transfected cell lines and to induce binding to LYVE-1 in primary lymphatic endothelial cells. Pre-incubation of HA with full length recombinant TSG-6 enhanced binding by LYVE-1 transfectants and induced binding in primary LEC, in a manner that was dependent on the degree of cross-linking. However unlike CD44, a truncated version of the TSG-6 protein (Link_TSG-6) that does

not cross-link HA had little or no effect on HA binding. The reason for this apparent difference between LYVE-1 and CD44 is unclear, but the necessity of pre-incubation with HA for enhancement of binding and its dependence on an optimal TSG-6:HA ratio, are consistent with a requirement for cross-linking. The restraint placed on the motion of HA chains by TSG-6-mediated cross-linking may act to lower the entropic cost of binding by LYVE-1 molecules, or simply increase the 'footprint' of HA on the cell surface, thereby enhancing the valency of the interaction by contacting greater numbers of receptors. There was also evidence, provided by immunofluorescence microscopy, that LYVE-1 molecules are redistributed by engagement with TSG-6:HA complexes, therefore clustering the receptor in a manner that further enhances binding.

Recently, lymphatic endothelial cells have been shown to bind the HA capsule of certain pathogenic strains of group A streptococci (*S. pyogenes*), with the effect that LYVE-1 is densely clustered beneath the point of contact (Banerji, Lynskey, Sriskandan and Jackson, manuscript in preparation). Fluorescent HA-coated microspheres generated to model this scenario in chapter 5 were also found to bind efficiently to LEC, in a manner that could be blocked using LYVE-1 HA-blocking mAbs. Furthermore, the interaction with these microspheres led to clustering of LYVE-1, in much the same manner observed for group A streptococci. The effects of increased valency and clustering effect likely explain how stable binding is achieved, and have led to consideration of other situations where HA may be similarly arrayed. Dendritic cells are known to express HA synthases (HAS) and actively synthesize HA when activated (Mummert et al., 2002). It is therefore conceivable that HA chains in the process of being extruded by HAS or anchored by CD44 expressed by these cells form a hyaluronan array appropriate for binding to LYVE-1,and that such HA arrays mediate DC adhesion to lymphatic vessels.

7.2 Biological implications

The results of this thesis suggest that sialylation of LYVE-1 is not a short term regulatory modification as originally conceived, but rather a longer term mechanism that imposes a requirement for higher order receptor complex formation or HA crosslinking to achieve stable binding. This implies that native LYVE-1 is fully competent HA binding receptor even when sialylated, with implications for our understanding of the role played by the receptor in HA uptake and metabolism, and transmigration of lymphatic endothelium by migratory leukocytes. Like CD44, HA binding to LYVE-1 is dependent on multivalent interactions between receptor and ligand, that may be enhanced by processes that increase the avidity of the interaction. Understanding these processes will be key to further unravelling the physiological functions of LYVE-1 and how these are regulated.

Under resting conditions, LYVE-1 is concentrated at the tips of flap valves between individual lymphatic endothelial cells, and is thus located immediately at the entry point into the lymphatic network (Baluk et al., 2007; Pflicke and Sixt, 2009). The means by which LEC maintain this focal enrichment is currently unknown, and the receptor does not appear to be localized to lipid rafts in cultured HDLEC (Dr. D. Markovic, unpublished observations), although monolayers of these cells do not form the specialized flap valves and junctional arrangement of afferent lymphatic vessels. Attachment to the cytoskeleton *via* the cytoplasmic tail of LYVE-1 would represent one means by which LEC may actively direct the surface distribution of LYVE-1 molecules, and is an active area of research in the Jackson laboratory. In the absence of high resolution intravital-microscopy data, it is not known whether the areas of concentrated LYVE-1 expression on the surface of flap valves also contain higher order LYVE-1 clusters, but the absence of co-localization with endogenous or exogenously-added HA in mouse tissues (Nightingale et al., 2009), and the

fact that clustering triggers HA binding to cultured cells, would suggest that the receptor is normally distributed relatively diffusely. Under steady-state conditions, LYVE-1 is therefore unlikely to engage in binding of free HA chains, due to the inhibitory effect of sialylation and the absence of a process to trigger receptor clustering.

However, HA anchored to the surface of migratory leukocytes by the HA synthase or membrane-bound receptors such as CD44 in the form of a pericellular matrix may represent a closely-arrayed form of the ligand that can be bound by LYVE-1. Under homeostatic conditions, a steady migration of $CD4^+$ T-cells, particularly of the memory phenotype, and of myeloid cells such as DCs, occurs from the tissues into lymphatic vessels and on to the draining lymph nodes. Both T-cells and DCs express CD44 in an activated state in response to maturation, which supports their migration through binding to exogenous sources of HA (Lesley and Hyman, 1992; Termeer et al., 2001). Engagement of HA by CD44 is reported to trigger clustering of the receptor within lipid rafts and association with other adhesion molecules such as integrins, which presumably alters the presentation of bound HA (Lee et al., 2008). Furthermore, both T-cells and DCs actively synthesise HA and sequester it at the cell surface (Mahaffey and Mummert, 2007; Mummert et al., 2002), which has significant functional significance for both cell types. For example, hyaluronan production by DCs has been shown to promote antigen presentation and to augment T-cell activation by directly contributing to T cell-DC binding (Bollyky et al., 2010). The hyaluronan synthases, which extrude a growing HA chain into the pericellular space, are reported to be enriched in various specialized plasma-membrane regions including lipid rafts, microvilli, filopodia and lamellipodia (reviewed in Rilla et al., 2013). There is ample reason therefore to think that LYVE-1 may encounter clustered presentations of HA on the surface of migratory leukocytes, and that such presentations of HA may trigger binding and

clustering of the receptor, in a manner analogous to HA-coated microspheres and HA-encapsulated group A streptococci.

The functional significance of LYVE-1 binding to leukocyte-associated HA may be to support adhesion and transmigration of lymphatic endothelium by these cells, in a manner analogous to the role played by CD44 during leukocyte extravasation. However, whereas CD44 co-localizes with integrins and acts as a secondary adhesion molecule on blood endothelium (Nandi et al., 2004), LEC do not express the integrin counter-receptors ICAM-1 or VCAM-1 under non-inflammatory conditions, and thus DC migration into lymphatic vessels in the steady state has been shown to be integrin-independent (Lammermann et al., 2008). Instead the principle axis of guidance towards lymphatic vessels consists of the chemokine receptor CCR7, which is up-regulated by migratory DCs, T-cells and B-cells, and its ligand CCL21, which is secreted by LEC and forms an immobilized gradient radiating from the vessel (Ohl et al., 2004; Weber et al., 2013). DCs enter the lymphatic capillaries in a two-step process, first traversing 'portals' in the surrounding basement membrane, before contacting discrete 'puncta' of immobilized CCL21 on the cell surface, and entering the vessel lumen via flap-valves between individual cells (Pflicke and Sixt, 2009; Tal et al., 2011).

What is currently unclear is how, having reached the point of highest CCL21 concentration, DCs choose to no longer follow this chemotactic gradient, and instead enter the vessel lumen. Perhaps LYVE-1 functions to 'sign-post' the entrance to the vessel, and support the squeezing and probing behaviour of the DC by binding HA associated with dendrites. Recent work by Dr. D. Markovic and Dr Y-J. Wang in the Jackson lab has also suggested that ligation of LYVE-1 with cognate antibodies or HA and its fragments can trigger an increase in permeability of HDLEC monolayers, activation of MAPK signalling pathways

and remodelling of VE-cadherin adherens junctions (manuscript in preparation). With a diameter of 2 – 3 μm (Pflicke and Sixt, 2009), flap-valves between LEC are a narrow passage for a transmigrating cell, and it will be intriguing to see if this work develops into a model of LYVE-1 ligation/clustering that triggers uncoupling of adherens junctions and widening of lymphatic valves. A similar process has been reported to occur during leukocyte extravasation, following engagement of endothelial VCAM-1 with T-cell expressed VLA-4 (Vockel and Vestweber, 2013).

During inflammation, lymphatic endothelium is activated by inflammatory cytokines and strongly upregulates expression of ICAM-1, VCAM-1 and E-selectin together with a panel of chemokines (especially CCL21) that attract migratory cells (Johnson and Jackson, 2008). Ablation of DC migration to the dLNs in ICAM-$1^{-/-}$ mice (Xu et al., 2001) or by antibody blockade (Johnson et al., 2006) has demonstrated that CAMs play an important role in lymphatic entry during inflammation. Conversely, LYVE-1 expression is partially reduced in response to inflammatory cytokines (Johnson et al., 2007), which appears counterintuitive given the increase in DC transmigration seen under these conditions, and the ability of LYVE-1-specific mAbs to block this process. However, it has been reported that button junctions found in the initial lymphatics convert to a zipper formation during chronic inflammation that (Yao et al., 2012) and that lymph drainage is reduced in response to certain inflammatory stimuli (Liao and Padera, 2013). An emerging theme in lymphatic research is that entry into vessels appears to be more selective during inflammation, and so a reduction in LYVE-1 expression may form part of this strategy, particularly if ligation of the receptor is linked to uncoupling of adherens junctions.

The role played by LYVE-1 during DC transmigration may be even more significant during inflammation, not least because of increased CD44 expression and HA production by these

cells, but also due to their ability to produce TSG-6 and the long pentraxin PTX3 (Maina et al., 2009). Amongst other ligands, PTX3 binds to TSG-6 and contributes to cross-linking of HA chains and remodelling of pericellular-matrix associated HA. Neutrophil polymorphonuclear granulocytes were also reported to store TSG-6 and PTX3 in their granules, which may be significant in the lymphatic context as these cells also express CD44 and CCR7 and migrate to the draining lymph nodes in response to certain pathogens (Beauvillain et al., 2011; Maina et al., 2009). As reported elsewhere, TSG-6 mediated cross-linking of HA enhances binding to CD44-expressing cells (Lesley et al., 2004), and the results of this thesis demonstrate that the same is true of LYVE-1-expressing lymphatic endothelial cells. Preliminary experiments by Dr. S. Banerji and Dr. L. Johnson in the Jackson laboratory have focussed on imaging TNFα-treated DC in a 'crawl-in' assay of mouse ear, and have produced exciting images of cells entering the lumen of lymphatic vessels with discrete 'blobs' of HA attached to their surface. It will be intriguing to determine whether these areas of HA staining are definitely associated with DCs and whether HA is also cross-linked by TSG-6.

7.3 Future Work

An obvious starting point for future work will be to test some of the conclusions of this thesis in *in vivo* models of leukocyte and tumour cell trafficking in which the involvement of LYVE-1 has already been implicated. We are limited by the absence of a mouse LYVE-1 monoclonal that potentiates HA binding to MDLEC, but it would be entirely possible to introduce cross-linked forms of HA into mice and assess their binding to lymphatic vessels (LVs). Various experiments will also be required to ascertain whether TSG-6 forms complexes with HA on the surface of DCs under appropriate conditions *in vivo*, whether such complexes are the products of DCs themselves or are sequestered from surrounding tissues and whether such complexes contribute to LYVE-1 mediated events. It would also be interesting to extend from the flow cytometry studies that established the capacity of LYVE-1 mAbs to potentiate bHA binding to HDLECs by testing the capacity of these same mAbs to promote HA dependent adhesion and transmigration of DC and other cell types over HDLEC monolayers, and the influence of components such as TSG-6 and IαI heavy chain on either process.

Preparations are also under way to investigate LYVE-1 distribution and HA binding using a combination of live-cell imaging and techniques of super-resolution microscopy including Stimulated Emission Depletion Microscopy (STED). These techniques offer the exciting prospect of assessing the distribution of LYVE-1 receptors down to the single-molecule level, and to observe cluster formation and HA binding in real-time. Moreover they could be used to image the distribution not only of endogenous LYVE-1 in primary LEC but also transfected LYVE-1 molecules bearing appropriate C-terminal fluorescent tags for FRET analyses and mutated LYVE-1 molecules such as the dimerization defective C201A mutant for further investigating the involvement of disulphide linked homodimers

in HA binding. It will likely also be informative to observe changes in adherens junctions following ligation of LYVE-1 with antibodies or with cross-linked forms of HA. The possibility that naturally-occurring cross-linking proteins, such as sialic-acid binding members of the galectin and siglec families contribute to LYVE-1 clustering/surface distribution in LEC could also be assessed.

The Quartz Crystal Microbalance (QCM) has proved an invaluable tool for the study of CD44-HA interactions, and promises to be similarly revealing for the study of LYVE-1. Coupled with ellipsometry techniques, it should be possible to define the relationship between surface density of LYVE-1 molecules and HA binding in a controlled environment, and compare these values to those derived from microscopy experiments. It is also hoped that the QCM technique may shed further light on the unresolved question of how sialic acid inhibits HA binding to LYVE-1. Removal of sialic by digestion with neuraminidases increases the binding affinity of recombinant LYVE-1 as assessed by surface plasmon resonance, but also increases the total mass of LYVE-1 that may bind to the HA-coated sensor chip (Dr. S. Banerji, unpublished observations). Preliminary experiments presented in this thesis also suggested that de-sialylated LYVE-1 was capable of absorbing to a higher density on supported lipid bilayers than wildtype protein, and combined ellipsometry and QCM measurements should be able to determine this categorically. A direct effect of sialylated O-glycans on the HA binding domain in LYVE-1 is also being assessed using insertional mutagenesis to introduce a spacer between the HABD and stalk region of the protein.

Appendix 1

mLYVE-1 residue	hLYVE-1 equivalent	mutation	primer sequence (F)	primer sequence (R)
Y86	Y87	Y86A	ggctttgagacttgcagcgctggatgggttggag	ctccaacccatccagcgctgcaagtctcaaagcc
R98	R99	R98A	cagttctctgtcatccctgcgattttctcaaacccc	ggggtttgagaaaatcgcagggatgacagagaactg
R104	K105	R104A	gattttctcaaaccccgcgtgtgggaagaatggc	gccattcttcccacacgcggggtttgagaaaatc
N102	N103	N102A	cctcggattttctcagcccccaggtgtgggaag	cttcccacacctgggggctgagaaaatccgagg
K107	K108	K107A	ccccaggtgtggggcgaatggcaaaggtgtcc	ggacacctttgccattcgccccacacctgggg
F100	S101	F100A	gtcatccctcggattgcctcaaaccccaggtgtg	cacacctggggtttgaggcaatccgagggatgac
N108	N109	N108A	cccaggtgtgggaaggctggcaaaggtgtcctg	caggacacctttgccagccttcccacacctggg
F146	K147	F146A	ccagaaatcgttaccacagcttaccccgtgttggacac	gtgtccaacacggggtaagctgtggtaacgatttctgg
Y147	D148	Y147A	ccagaaatcgttaccacatttgcccccgtgttggacactc	gagtgtccaacacgggggcaaatgtggtaacgatttctgg
I142	I143	I142A	ctcctgcattccagaagccgttaccacattttacccc	ggggtaaaatgtggtaacggcttctggaatgcaggag
D25	L25	D25A	ccagtccaaggtgccgccctcgtgcaagacctttcc	ggaaaggtcttgcacgagggcggcaccttggactgg
S160	I163	S160A	cccgcaacagagtttgctgtcagcagcagcgcc	ggcgctgctgctgacagcaaactctgttgcggg
S162	S165	S162A	gcaacagagttttctgtcgccagcagcgcctacttgg	ccaagtaggcgctgctggcgacagaaaactctgttgc
L26	R26	L26A	gtccaaggtgccgacgccgtgcaagacctttcc	ggaaaggtcttgcacggcgtcggcaccttggac
E158	E161	E158A	caaacacccgcaacagcgttttctgtcagcagc	gctgctgacagaaaacgctgttgcgggtgtttg
T157	T160	T157A	gacactcaaacacccgcagcagagttttctgtcagc	gctgacagaaaactctgctgcgggtgtttgagtgtc
F159	F162	F159A	caaacacccgcaacagaggcttctgtcagcagcagc	gctgctgctgacagaagcctctgttgcgggtgtttg
S33	Q33	S33A	gcaagacctttccattgctacatgcagaatcatgggc	gcccatgattctgcatgtagcaatggaaaggtcttgc
E82	E83	E82A	cagaaatctggctttgcgacttgcagctatggatgg	ccatccatagctgcaagtcgcaaagccagatttctg
S85	S86	S85A	ctggctttgagacttgcgcctatggatgggttggag	ctccaacccatccataggcgcaagtctcaaagccag
E74	E75	E74A	cagcagggaccaggtagcgtcagcgcagaaatctg	cagatttctgcgctgacgctacctggtccctgctg
D71	D72	D71A	gactctggccagcagggcccaggtagagtcagcg	cgctgactctacctgggccctgctggccagagtc
F93	F94	F93A	ggatgggttggagaacaggcctctgtcatccctcgg	ccgagggatgacagaggcctgttctccaacccatcc
R70	K71	R70A	ctgactctggccagcgcggaccaggtagagtcag	ctgactctacctggtccgcgctggccagagtcag
M38	M39	M38A	ctacatgcagaatcgcgggcgttgcccttgtgggc	gcccacaagggcaacgcccgcgattctgcatgtag
S130	S131	S130A	gcctattgccacaacgcatccgacacctgggttaac	gttaacccaggtgtcggatgcgttgtggcaataggc
K61	R62	K61A	gccaacgaggcctgtgcgatgctgggactgactc	gagtcagtcccagcatcgcacaggcctcgttggc
Q72	Q73	Q72A	ctggccagcagggacgcggtagagtcagcgcag	ctgcgctgactctaccgcgtccctgctggccag
F53	F54	F53A	cccacagatgaatgccacagaagccaacgaggcc	ggcctcgttggcttctgtggcattcatctgtggg
W134	W135	W134A	caactcatccgacaccgcggttaactcctgcattcc	ggaatgcaggagttaaccgcggtgtcggatgagttg
N136	N137	N136A	ccgacacctgggttgcctcctgcattccagaaatcg	cgatttctggaatgcaggaggcaacccaggtgtcgg
K78	K79	K78A	ggtagagtcagcgcaggcatctggctttgagacttgc	gcaagtctcaaagccagatgcctgcgctgactctacc
I139	I140	I139A	cacctgggttaactcctgcgctccagaaatcgttacc	ggtaacgatttctggagcgcaggagttaacccaggtg
T133	T134	T133A	cacaactcatccgacgcctgggttaactcctgc	gcaggagttaacccaggcgtcggatgagttgtg
S131	S132	S131A	ctattgccacaactcagccgacacctgggttaac	gttaacccaggtgtcggctgagttgtggcaatag
N48	N49	N48A	gcccttgtgggcagaaacaaagccccacagatgaatttc	gaaattcatctgtggggctttgtttctgcccacaagggc
Q50	Q51	Q50A	gtgggcagaaacaaaaacccagcgatgaatttcacagaagcc	ggcttctgtgaaattcatcgctgggtttttgtttctgcccac
S120	S121	S120A	gatttggaatgctccctccgcccaaaagttcaaagcc	ggctttgaacttttgggcggagggagcattccaaatc
W115	W116	W115A	ggcaaaggtgtcctgattgcgaatgctccctccagc	gctggagggagcattcgcaatcaggacacctttgcc
N52	N53	N52A	ggcagaaacaaaaacccacagatggctttcacagaagccaac g	cgttggcttctgtgaaagccatctgtgggtttttgtttctgc c
E55	E56	E55A	cagatgaatttcacagcagccaacgaggcctg	caggcctcgttggctgctgtgaaattcatctg
E58	E59	E58A	cacagaagccaacgcggcctgtaagatgctggg	cccagcatcttacaggccgcgttggcttctgtg

Table 7.1 **List of mutations generated in mouse LYVE-1**

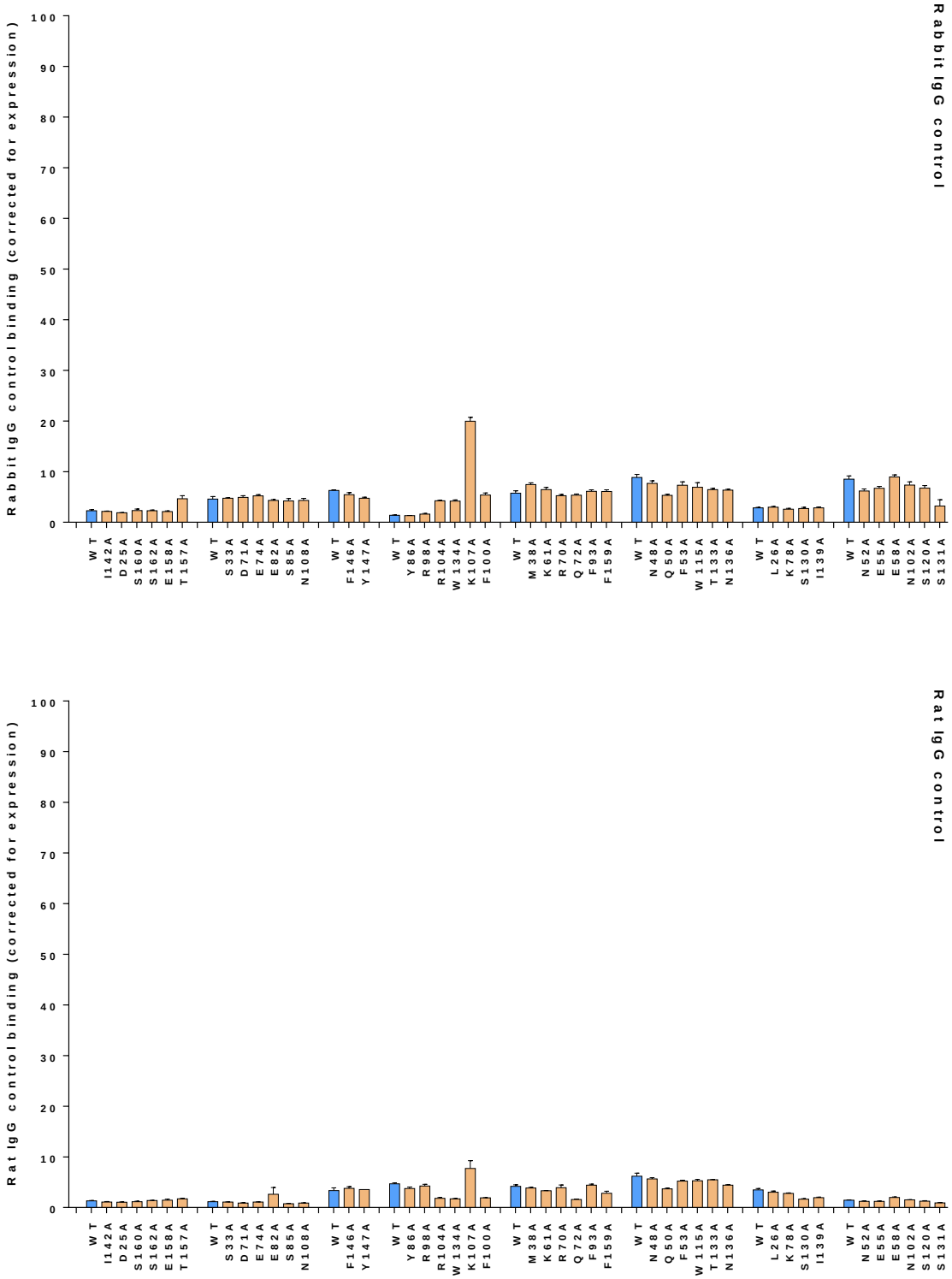


Figure 7.2 **Influence of site-directed mutagenesis of mLYVE-1 on binding by anti-mLYVE-1 monoclonal antibodies (mAbs)**. Data for isotype controls from Figure 3.9.

References

Agren, U.M., Tammi, R.H., and Tammi, M.I. (1997). Reactive oxygen species contribute to epidermal hyaluronan catabolism in human skin organ culture. Free radical biology & medicine *23*, 996-1001.

Aichem, A., Masilamani, M., and Illges, H. (2006). Redox regulation of CD21 shedding involves signaling via PKC and indicates the formation of a juxtamembrane stalk. J Cell Sci *119*, 2892-2902.

Alders, M., Hogan, B.M., Gjini, E., Salehi, F., Al-Gazali, L., Hennekam, E.A., Holmberg, E.E., Mannens, M.M., Mulder, M.F., Offerhaus, G.J., *et al.* (2009). Mutations in CCBE1 cause generalized lymph vessel dysplasia in humans. Nature genetics *41*, 1272-1274.

Alitalo, K. (2011). The lymphatic vasculature in disease. Nature medicine *17*, 1371-1380.

Almond, A., Brass, A., and Sheehan, J.K. (1998). Deducing polymeric structure from aqueous molecular dynamics simulations of oligosaccharides: predictions from simulations of hyaluronan tetrasaccharides compared with hydrodynamic and X-ray fibre diffraction data. Journal of molecular biology *284*, 1425-1437.

Almond, A., Deangelis, P.L., and Blundell, C.D. (2006). Hyaluronan: the local solution conformation determined by NMR and computer modeling is close to a contracted left-handed 4-fold helix. Journal of molecular biology *358*, 1256-1269.

Armstrong, S.E., and Bell, D.R. (2002). Relationship between lymph and tissue hyaluronan in skin and skeletal muscle. American journal of physiology Heart and circulatory physiology *283*, H2485-2494.

Aspberg, A. (2012). The different roles of aggrecan interaction domains. The journal of histochemistry and cytochemistry : official journal of the Histochemistry Society *60*, 987-996.

Bajenoff, M., Glaichenhaus, N., and Germain, R.N. (2008). Fibroblastic reticular cells guide T lymphocyte entry into and migration within the splenic T cell zone. J Immunol *181*, 3947-3954.

Baluk, P., Fuxe, J., Hashizume, H., Romano, T., Lashnits, E., Butz, S., Vestweber, D., Corada, M., Molendini, C., Dejana, E., *et al.* (2007). Functionally specialized junctions between endothelial cells of lymphatic vessels. J Exp Med *204*, 2349-2362.

Banerji, S., Day, A.J., Kahmann, J.D., and Jackson, D.G. (1998). Characterization of a functional hyaluronan-binding domain from the human CD44 molecule expressed in Escherichia coli. Protein Expr Purif *14*, 371-381.

Banerji, S., Hide, B.R., James, J.R., Noble, M.E., and Jackson, D.G. (2010). Distinctive properties of the hyaluronan-binding domain in the lymphatic endothelial receptor Lyve-1 and their implications for receptor function. J Biol Chem *285*, 10724-10735.

Banerji, S., Ni, J., Wang, S.X., Clasper, S., Su, J., Tammi, R., Jones, M., and Jackson, D.G. (1999). LYVE-1, a new homologue of the CD44 glycoprotein, is a lymph-specific receptor for hyaluronan. Journal of Cell Biology *144*, 789-801.

Banerji, S., Wright, A.J., Noble, M., Mahoney, D.J., Campbell, I.D., Day, A.J., and Jackson, D.G. (2007). Structures of the Cd44-hyaluronan complex provide insight into a fundamental carbohydrate-protein interaction. Nat Struct Mol Biol *14*, 234-239.

Bao, X., Moseman, E.A., Saito, H., Petryniak, B., Thiriot, A., Hatakeyama, S., Ito, Y., Kawashima, H., Yamaguchi, Y., Lowe, J.B., *et al.* (2010). Endothelial heparan sulfate controls chemokine presentation in recruitment of lymphocytes and dendritic cells to lymph nodes. Immunity *33*, 817-829.

Baranova, N.S., Foulcer, S.J., Briggs, D.C., Tilakaratna, V., Enghild, J.J., Milner, C.M., Day, A.J., and Richter, R.P. (2013). Inter-alpha-inhibitor impairs TSG-6-induced hyaluronan cross-linking. J Biol Chem *288*, 29642-29653.

Baranova, N.S., Nileback, E., Haller, F.M., Briggs, D.C., Svedhem, S., Day, A.J., and Richter, R.P. (2011). The inflammation-associated protein TSG-6 cross-links hyaluronan via hyaluronan-induced TSG-6 oligomers. J Biol Chem *286*, 25675-25686.

Beauvillain, C., Cunin, P., Doni, A., Scotet, M., Jaillon, S., Loiry, M.L., Magistrelli, G., Masternak, K., Chevailler, A., Delneste, Y., *et al.* (2011). CCR7 is involved in the migration of neutrophils to lymph nodes. Blood *117*, 1196-1204.

Bekku, Y., Saito, M., Moser, M., Fuchigami, M., Maehara, A., Nakayama, M., Kusachi, S., Ninomiya, Y., and Oohashi, T. (2012). Bral2 is indispensable for the proper localization of brevican and the structural integrity of the perineuronal net in the brainstem and cerebellum. The Journal of comparative neurology *520*, 1721-1736.

Bekku, Y., Su, W.D., Hirakawa, S., Fassler, R., Ohtsuka, A., Kang, J.S., Sanders, J., Murakami, T., Ninomiya, Y., and Oohashi, T. (2003). Molecular cloning of Bral2, a novel brain-specific link protein, and immunohistochemical colocalization with brevican in perineuronal nets. Molecular and cellular neurosciences *24*, 148-159.

Bekku, Y., Vargova, L., Goto, Y., Vorisek, I., Dmytrenko, L., Narasaki, M., Ohtsuka, A., Fassler, R., Ninomiya, Y., Sykova, E., *et al.* (2010). Bral1: its role in diffusion barrier formation and conduction velocity in the CNS. The Journal of neuroscience : the official journal of the Society for Neuroscience *30*, 3113-3123.

Blundell, C.D., Almond, A., Mahoney, D.J., DeAngelis, P.L., Campbell, I.D., and Day, A.J. (2005). Towards a structure for a TSG-6.hyaluronan complex by modeling and NMR spectroscopy: insights into other members of the link module superfamily. J Biol Chem *280*, 18189-18201.

Blundell, C.D., Mahoney, D.J., Almond, A., DeAngelis, P.L., Kahmann, J.D., Teriete, P., Pickford, A.R., Campbell, I.D., and Day, A.J. (2003). The link module from ovulation- and inflammation-associated protein TSG-6 changes conformation on hyaluronan binding. J Biol Chem *278*, 49261-49270.

Bode-Lesniewska, B., Dours-Zimmermann, M.T., Odermatt, B.F., Briner, J., Heitz, P.U., and Zimmermann, D.R. (1996). Distribution of the large aggregating proteoglycan versican in adult human tissues. The journal of histochemistry and cytochemistry : official journal of the Histochemistry Society *44*, 303-312.

Boensch, C., Huang, S.S., Connolly, D.T., and Huang, J.S. (1999). Cell surface retention sequence binding protein-1 interacts with the v-sis gene product and platelet-derived growth factor beta-type receptor in simian sarcoma virus-transformed cells. J Biol Chem *274*, 10582-10589.

Boensch, C., Kuo, M.D., Connolly, D.T., Huang, S.S., and Huang, J.S. (1995). Identification, purification, and characterization of cell-surface retention sequence-binding proteins from human SK-Hep cells and bovine liver plasma membranes. J Biol Chem *270*, 1807-1816.

Bollyky, P.L., Evanko, S.P., Wu, R.P., Potter-Perigo, S., Long, S.A., Kinsella, B., Reijonen, H., Guebtner, K., Teng, B., Chan, C.K., *et al.* (2010). Th1 cytokines promote T-cell binding to antigen-presenting cells via enhanced hyaluronan production and accumulation at the immune synapse. Cell Mol Immunol *7*, 211-220.

Bollyky, P.L., Falk, B.A., Wu, R.P., Buckner, J.H., Wight, T.N., and Nepom, G.T. (2009). Intact extracellular matrix and the maintenance of immune tolerance: high molecular weight hyaluronan promotes persistence of induced CD4+CD25+ regulatory T cells. J Leukoc Biol *86*, 567-572.

Bouyain, S., Rushton, S., and Drickamer, K. (2001). Minimal requirements for the binding of selectin ligands to a C-type carbohydrate-recognition domain. Glycobiology *11*, 989-996.

Brakebusch, C., Seidenbecher, C.I., Asztely, F., Rauch, U., Matthies, H., Meyer, H., Krug, M., Bockers, T.M., Zhou, X., Kreutz, M.R., *et al.* (2002). Brevican-deficient mice display impaired hippocampal CA1 long-term potentiation but show no obvious deficits in learning and memory. Mol Cell Biol *22*, 7417-7427.

Brissett, N.C., and Perkins, S.J. (1996). The protein fold of the hyaluronate-binding proteoglycan tandem repeat domain of link protein, aggrecan and CD44 is similar to that of the C-type lectin superfamily. FEBS Lett *388*, 211-216.

Brown, H.M., Dunning, K.R., Robker, R.L., Boerboom, D., Pritchard, M., Lane, M., and Russell, D.L. (2010). ADAMTS1 cleavage of versican mediates essential structural remodeling of the ovarian follicle and cumulus-oocyte matrix during ovulation in mice. Biology of reproduction *83*, 549-557.

Camenisch, T.D., Spicer, A.P., Brehm-Gibson, T., Biesterfeldt, J., Augustine, M.L., Calabro, A., Jr., Kubalak, S., Klewer, S.E., and McDonald, J.A. (2000). Disruption of hyaluronan synthase-2 abrogates normal cardiac morphogenesis and hyaluronan-mediated transformation of epithelium to mesenchyme. The Journal of clinical investigation *106*, 349-360.

Cao, R., Ji, H., Feng, N., Zhang, Y., Yang, X., Andersson, P., Sun, Y., Tritsaris, K., Hansen, A.J., Dissing, S., *et al.* (2012). Collaborative interplay between FGF-2 and VEGF-C promotes lymphangiogenesis and metastasis. Proc Natl Acad Sci U S A *109*, 15894-15899.

Cardoso, L.E., Little, P.J., Ballinger, M.L., Chan, C.K., Braun, K.R., Potter-Perigo, S., Bornfeldt, K.E., Kinsella, M.G., and Wight, T.N. (2010). Platelet-derived growth factor differentially regulates the expression and post-translational modification of versican by arterial smooth muscle cells through distinct protein kinase C and extracellular signal-regulated kinase pathways. J Biol Chem *285*, 6987-6995.

Carulli, D., Rhodes, K.E., Brown, D.J., Bonnert, T.P., Pollack, S.J., Oliver, K., Strata, P., and Fawcett, J.W. (2006). Composition of perineuronal nets in the adult rat cerebellum and the cellular origin of their components. The Journal of comparative neurology *494*, 559-577.

Chang, L.K., Garcia-Cardena, G., Farnebo, F., Fannon, M., Chen, E.J., Butterfield, C., Moses, M.A., Mulligan, R.C., Folkman, J., and Kaipainen, A. (2004). Dose-dependent response of FGF-2 for lymphangiogenesis. Proc Natl Acad Sci U S A *101*, 11658-11663.

Cherr, G.N., Yudin, A.I., and Overstreet, J.W. (2001). The dual functions of GPI-anchored PH-20: hyaluronidase and intracellular signaling. Matrix biology : journal of the International Society for Matrix Biology *20*, 515-525.

Cho, C.H., Koh, Y.J., Han, J., Sung, H.K., Jong Lee, H., Morisada, T., Schwendener, R.A., Brekken, R.A., Kang, G., Oike, Y., *et al.* (2007). Angiogenic role of LYVE-1-positive macrophages in adipose tissue. Circulation research *100*, e47-57.

Chockalingam, P.S., Zeng, W., Morris, E.A., and Flannery, C.R. (2004). Release of hyaluronan and hyaladherins (aggrecan G1 domain and link proteins) from articular cartilage exposed to ADAMTS-4 (aggrecanase 1) or ADAMTS-5 (aggrecanase 2). Arthritis Rheum *50*, 2839-2848.

Cole, C., Barber, J.D., and Barton, G.J. (2008). The Jpred 3 secondary structure prediction server. Nucleic Acids Res *36*, W197-201.

Csoka, A.B., Frost, G.I., and Stern, R. (2001). The six hyaluronidase-like genes in the human and mouse genomes. Matrix biology : journal of the International Society for Matrix Biology *20*, 499-508.

Csoka, A.B., Scherer, S.W., and Stern, R. (1999). Expression analysis of six paralogous human hyaluronidase genes clustered on chromosomes 3p21 and 7q31. Genomics *60*, 356-361.

Czeloth, N., Bernhardt, G., Hofmann, F., Genth, H., and Forster, R. (2005). Sphingosine-1-phosphate mediates migration of mature dendritic cells. J Immunol *175*, 2960-2967.

Day, A.J., and de la Motte, C.A. (2005). Hyaluronan cross-linking: a protective mechanism in inflammation? Trends Immunol *26*, 637-643.

Day, A.J., and Prestwich, G.D. (2002). Hyaluronan-binding proteins: tying up the giant. J Biol Chem *277*, 4585-4588.

Day, A.J., and Sheehan, J.K. (2001). Hyaluronan: polysaccharide chaos to protein organisation. Current opinion in structural biology *11*, 617-622.

de Belder, A.N., and Wik, K.O. (1975). Preparation and properties of fluorescein-labelled hyaluronate. Carbohydrate research *44*, 251-257.

de La Motte, C.A., Hascall, V.C., Calabro, A., Yen-Lieberman, B., and Strong, S.A. (1999). Mononuclear leukocytes preferentially bind via CD44 to hyaluronan on human intestinal mucosal smooth muscle cells after virus infection or treatment with poly(I.C). J Biol Chem *274*, 30747-30755.

de la Motte, C.A., Hascall, V.C., Drazba, J., Bandyopadhyay, S.K., and Strong, S.A. (2003). Mononuclear leukocytes bind to specific hyaluronan structures on colon mucosal smooth muscle cells treated with polyinosinic acid:polycytidylic acid: inter-alpha-trypsin inhibitor is crucial to structure and function. The American journal of pathology *163*, 121-133.

DeAngelis, P.L., Jing, W., Drake, R.R., and Achyuthan, A.M. (1998). Identification and molecular cloning of a unique hyaluronan synthase from Pasteurella multocida. J Biol Chem *273*, 8454-8458.

DeAngelis, P.L., Jing, W., Graves, M.V., Burbank, D.E., and Van Etten, J.L. (1997). Hyaluronan synthase of chlorella virus PBCV-1. Science *278*, 1800-1803.

DeAngelis, P.L., Papaconstantinou, J., and Weigel, P.H. (1993). Molecular cloning, identification, and sequence of the hyaluronan synthase gene from group A Streptococcus pyogenes. J Biol Chem *268*, 19181-19184.

Deed, R., Rooney, P., Kumar, P., Norton, J.D., Smith, J., Freemont, A.J., and Kumar, S. (1997). Early-response gene signalling is induced by angiogenic oligosaccharides of hyaluronan in endothelial cells. Inhibition by non-angiogenic, high-molecular-weight hyaluronan. International journal of cancer Journal international du cancer *71*, 251-256.

Delmage, J.M., Powars, D.R., Jaynes, P.K., and Allerton, S.E. (1986). The selective suppression of immunogenicity by hyaluronic acid. Annals of clinical and laboratory science *16*, 303-310.

Eisele, N.B., Frey, S., Piehler, J., Gorlich, D., and Richter, R.P. (2010). Ultrathin nucleoporin phenylalanine-glycine repeat films and their interaction with nuclear transport receptors. EMBO Rep *11*, 366-372.

English, N.M., Lesley, J.F., and Hyman, R. (1998). Site-specific de-N-glycosylation of CD44 can activate hyaluronan binding, and CD44 activation states show distinct threshold densities for hyaluronan binding. Cancer Res *58*, 3736-3742.

Falkowski, M., Schledzewski, K., Hansen, B., and Goerdt, S. (2003). Expression of stabilin-2, a novel fasciclin-like hyaluronan receptor protein, in murine sinusoidal endothelia, avascular tissues, and at solid/liquid interfaces. Histochem Cell Biol *120*, 361-369.

Fang, J., Dagenais, S.L., Erickson, R.P., Arlt, M.F., Glynn, M.W., Gorski, J.L., Seaver, L.H., and Glover, T.W. (2000). Mutations in FOXC2 (MFH-1), a forkhead family transcription factor, are responsible for the hereditary lymphedema-distichiasis syndrome. American journal of human genetics *67*, 1382-1388.

Forrester, J.V., and Balazs, E.A. (1980). Inhibition of phagocytosis by high molecular weight hyaluronate. Immunology *40*, 435-446.

Forster, R., Braun, A., and Worbs, T. (2012). Lymph node homing of T cells and dendritic cells via afferent lymphatics. Trends Immunol *33*, 271-280.

Forster, R., Schubel, A., Breitfeld, D., Kremmer, E., Renner-Muller, I., Wolf, E., and Lipp, M. (1999). CCR7 coordinates the primary immune response by establishing functional microenvironments in secondary lymphoid organs. Cell *99*, 23-33.

Fosang, A.J., and Hardingham, T.E. (1989). Isolation of the N-terminal globular protein domains from cartilage proteoglycans. Identification of G2 domain and its lack of interaction with hyaluronate and link protein. The Biochemical journal *261*, 801-809.

Foulcer, S.J. (2012). Structural and Functional Studies on the G1 Domain of Human Versican. In Faculty of Life Sciences (University of Manchester).

Francois, M., Caprini, A., Hosking, B., Orsenigo, F., Wilhelm, D., Browne, C., Paavonen, K., Karnezis, T., Shayan, R., Downes, M., *et al.* (2008). Sox18 induces development of the lymphatic vasculature in mice. Nature *456*, 643-647.

Fraser, J.R., Laurent, T.C., and Laurent, U.B. (1997). Hyaluronan: its nature, distribution, functions and turnover. Journal of internal medicine *242*, 27-33.

Fritz-Six, K.L., Dunworth, W.P., Li, M., and Caron, K.M. (2008). Adrenomedullin signaling is necessary for murine lymphatic vascular development. The Journal of clinical investigation *118*, 40-50.

Fu, J., Gerhardt, H., McDaniel, J.M., Xia, B., Liu, X., Ivanciu, L., Ny, A., Hermans, K., Silasi-Mansat, R., McGee, S., *et al.* (2008). Endothelial cell O-glycan deficiency causes blood/lymphatic misconnections and consequent fatty liver disease in mice. The Journal of clinical investigation *118*, 3725-3737.

Fulop, C., Szanto, S., Mukhopadhyay, D., Bardos, T., Kamath, R.V., Rugg, M.S., Day, A.J., Salustri, A., Hascall, V.C., Glant, T.T., *et al.* (2003). Impaired cumulus mucification and female sterility in tumor necrosis factor-induced protein-6 deficient mice. Development *130*, 2253-2261.

Gale, N.W., Prevo, R., Espinosa, J., Ferguson, D.J., Dominguez, M.G., Yancopoulos, G.D., Thurston, G., and Jackson, D.G. (2007). Normal lymphatic development and function in mice deficient for the lymphatic hyaluronan receptor LYVE-1. Mol Cell Biol *27*, 595-604.

Gale, N.W., Thurston, G., Hackett, S.F., Renard, R., Wang, Q., McClain, J., Martin, C., Witte, C., Witte, M.H., Jackson, D., *et al.* (2002). Angiopoietin-2 is required for postnatal angiogenesis and lymphatic patterning, and only the latter role is rescued by Angiopoietin-1. Developmental cell *3*, 411-423.

Gerli, R., Ibba, L., and Fruschelli, C. (1990). A fibrillar elastic apparatus around human lymph capillaries. Anatomy and embryology *181*, 281-286.

Getting, S.J., Mahoney, D.J., Cao, T., Rugg, M.S., Fries, E., Milner, C.M., Perretti, M., and Day, A.J. (2002). The link module from human TSG-6 inhibits neutrophil migration in a hyaluronan- and inter-alpha -inhibitor-independent manner. J Biol Chem *277*, 51068-51076.

Ghosh, P. (1994). The role of hyaluronic acid (hyaluronan) in health and disease: interactions with cells, cartilage and components of synovial fluid. Clinical and experimental rheumatology *12*, 75-82.

Girard, J.P., Moussion, C., and Forster, R. (2012). HEVs, lymphatics and homeostatic immune cell trafficking in lymph nodes. Nature reviews Immunology *12*, 762-773.

Giuliano, A.E., Hawes, D., Ballman, K.V., Whitworth, P.W., Blumencranz, P.W., Reintgen, D.S., Morrow, M., Leitch, A.M., Hunt, K.K., McCall, L.M., *et al.* (2011). Association of occult metastases in sentinel lymph nodes and bone marrow with survival among women with early-stage invasive breast cancer. JAMA : the journal of the American Medical Association *306*, 385-393.

Goncharova, V., Serobyan, N., Iizuka, S., Schraufstatter, I., de Ridder, A., Povaliy, T., Wacker, V., Itano, N., Kimata, K., Orlovskaja, I.A., *et al.* (2012). Hyaluronan expressed by the hematopoietic microenvironment is required for bone marrow hematopoiesis. J Biol Chem *287*, 25419-25433.

Greenwald, R.A., and Moak, S.A. (1986). Degradation of hyaluronic acid by polymorphonuclear leukocytes. Inflammation *10*, 15-30.

Gribbon, P., and Hardingham, T.E. (1998). Macromolecular diffusion of biological polymers measured by confocal fluorescence recovery after photobleaching. Biophysical journal *75*, 1032-1039.

Gribbon, P., Heng, B.C., and Hardingham, T.E. (2000). The analysis of intermolecular interactions in concentrated hyaluronan solutions suggest no evidence for chain-chain association. The Biochemical journal *350 Pt 1*, 329-335.

Harada, H., and Takahashi, M. (2007). CD44-dependent intracellular and extracellular catabolism of hyaluronic acid by hyaluronidase-1 and -2. J Biol Chem *282*, 5597-5607.

Harris, E.N., Kyosseva, S.V., Weigel, J.A., and Weigel, P.H. (2007). Expression, processing, and glycosaminoglycan binding activity of the recombinant human 315-kDa hyaluronic acid receptor for endocytosis (HARE). J Biol Chem *282*, 2785-2797.

Hascall, V.C., and Heinegard, D. (1974a). Aggregation of cartilage proteoglycans. I. The role of hyaluronic acid. J Biol Chem *249*, 4232-4241.

Hascall, V.C., and Heinegard, D. (1974b). Aggregation of cartilage proteoglycans. II. Oligosaccharide competitors of the proteoglycan-hyaluronic acid interaction. J Biol Chem *249*, 4242-4249.

Heinegard, D., and Hascall, V.C. (1974). Aggregation of cartilage proteoglycans. 3. Characteristics of the proteins isolated from trypsin digests of aggregates. J Biol Chem *249*, 4250-4256.

Higman, V.A., Blundell, C.D., Mahoney, D.J., Redfield, C., Noble, M.E., and Day, A.J. (2007). Plasticity of the TSG-6 HA-binding loop and mobility in the TSG-6-HA complex revealed by NMR and X-ray crystallography. Journal of molecular biology *371*, 669-684.

Hirakawa, S., Oohashi, T., Su, W.D., Yoshioka, H., Murakami, T., Arata, J., and Ninomiya, Y. (2000). The brain link protein-1 (BRAL1): cDNA cloning, genomic structure, and characterization as a novel link protein expressed in adult brain. Biochemical and biophysical research communications *276*, 982-989.

Hirose, J., Kawashima, H., Swope Willis, M., Springer, T.A., Hasegawa, H., Yoshie, O., and Miyasaka, M. (2002). Chondroitin sulfate B exerts its inhibitory effect on secondary lymphoid tissue chemokine (SLC) by binding to the C-terminus of SLC. Biochimica et biophysica acta *1571*, 219-224.

Hogan, B.M., Bos, F.L., Bussmann, J., Witte, M., Chi, N.C., Duckers, H.J., and Schulte-Merker, S. (2009). Ccbe1 is required for embryonic lymphangiogenesis and venous sprouting. Nature genetics *41*, 396-398.

Hou, W.H., Liu, I.H., Tsai, C.C., Johnson, F.E., Huang, S.S., and Huang, J.S. (2011). CRSBP-1/LYVE-1 ligands disrupt lymphatic intercellular adhesion by inducing tyrosine phosphorylation and internalization of VE-cadherin. J Cell Sci *124*, 1231-1244.

Hou, W.H., Liua, I.H., Huang, S.S., and Huang, J.S. (2012). CRSBP-1/LYVE-1 ligands stimulate contraction of the CRSBP-1-associated ER network in lymphatic endothelial cells. FEBS Lett *586*, 1480-1487.

Huang, S.S., Tang, F.M., Huang, Y.H., Liu, I.H., Hsu, S.C., Chen, S.T., and Huang, J.S. (2003). Cloning, expression, characterization, and role in autocrine cell growth of cell surface retention sequence binding protein-1. J Biol Chem *278*, 43855-43869.

Hubbard, C., McNamara, J.T., Azumaya, C., Patel, M.S., and Zimmer, J. (2012). The hyaluronan synthase catalyzes the synthesis and membrane translocation of hyaluronan. Journal of molecular biology *418*, 21-31.

Itano, N., and Kimata, K. (1996). Expression cloning and molecular characterization of HAS protein, a eukaryotic hyaluronan synthase. J Biol Chem *271*, 9875-9878.

Itano, N., Sawai, T., Atsumi, F., Miyaishi, O., Taniguchi, S., Kannagi, R., Hamaguchi, M., and Kimata, K. (2004). Selective expression and functional characteristics of three mammalian hyaluronan synthases in oncogenic malignant transformation. J Biol Chem *279*, 18679-18687.

Itano, N., Sawai, T., Yoshida, M., Lenas, P., Yamada, Y., Imagawa, M., Shinomura, T., Hamaguchi, M., Yoshida, Y., Ohnuki, Y., *et al.* (1999). Three isoforms of mammalian hyaluronan synthases have distinct enzymatic properties. J Biol Chem *274*, 25085-25092.

Jackson, D.G. (2009). Immunological functions of hyaluronan and its receptors in the lymphatics. Immunol Rev *230*, 216-231.

Jessen, T.E., and Odum, L. (2003). Role of tumour necrosis factor stimulated gene 6 (TSG-6) in the coupling of inter-alpha-trypsin inhibitor to hyaluronan in human follicular fluid. Reproduction *125*, 27-31.

Jiang, D., Liang, J., Fan, J., Yu, S., Chen, S., Luo, Y., Prestwich, G.D., Mascarenhas, M.M., Garg, H.G., Quinn, D.A., *et al.* (2005). Regulation of lung injury and repair by Toll-like receptors and hyaluronan. Nature medicine *11*, 1173-1179.

Jiang, X.M., Fitzgerald, M., Grant, C.M., and Hogg, P.J. (1999). Redox control of exofacial protein thiols/disulfides by protein disulfide isomerase. J Biol Chem *274*, 2416-2423.

Johnson, L.A., Clasper, S., Holt, A.P., Lalor, P.F., Baban, D., and Jackson, D.G. (2006). An inflammation-induced mechanism for leukocyte transmigration across lymphatic vessel endothelium. J Exp Med *203*, 2763-2777.

Johnson, L.A., and Jackson, D.G. (2008). Cell traffic and the lymphatic endothelium. Ann N Y Acad Sci *1131*, 119-133.

Johnson, L.A., and Jackson, D.G. (2010). Inflammation-induced secretion of CCL21 in lymphatic endothelium is a key regulator of integrin-mediated dendritic cell transmigration. International immunology *22*, 839-849.

Johnson, L.A., and Jackson, D.G. (2013). The chemokine CX3CL1 promotes trafficking of dendritic cells through inflamed lymphatics. J Cell Sci *126*, 5259-5270.

Johnson, L.A., Prevo, R., Clasper, S., and Jackson, D.G. (2007). Inflammation-induced uptake and degradation of the lymphatic endothelial hyaluronan receptor LYVE-1. J Biol Chem *282*, 33671-33680.

Kabashima, K., Shiraishi, N., Sugita, K., Mori, T., Onoue, A., Kobayashi, M., Sakabe, J., Yoshiki, R., Tamamura, H., Fujii, N., *et al.* (2007). CXCL12-CXCR4 engagement is required for migration of cutaneous dendritic cells. The American journal of pathology *171*, 1249-1257.

Karjalainen, J.M., Tammi, R.H., Tammi, M.I., Eskelinen, M.J., Agren, U.M., Parkkinen, J.J., Alhava, E.M., and Kosma, V.M. (2000). Reduced level of CD44 and hyaluronan associated with unfavorable prognosis in clinical stage I cutaneous melanoma. The American journal of pathology *157*, 957-965.

Karkkainen, M.J., Ferrell, R.E., Lawrence, E.C., Kimak, M.A., Levinson, K.L., McTigue, M.A., Alitalo, K., and Finegold, D.N. (2000). Missense mutations interfere with VEGFR-3 signalling in primary lymphoedema. Nature genetics *25*, 153-159.

Karkkainen, M.J., Haiko, P., Sainio, K., Partanen, J., Taipale, J., Petrova, T.V., Jeltsch, M., Jackson, D.G., Talikka, M., Rauvala, H., *et al.* (2004). Vascular endothelial growth factor C is required for sprouting of the first lymphatic vessels from embryonic veins. Nat Immunol *5*, 74-80.

Kass, E.H., and Seastone, C.V. (1944). The Role of the Mucoid Polysaccharide (Hyaluronic Acid) in the Virulence of Group a Hemolytic Streptococci. J Exp Med *79*, 319-330.

Katoh, S., Maeda, S., Fukuoka, H., Wada, T., Moriya, S., Mori, A., Yamaguchi, K., Senda, S., and Miyagi, T. (2010). A crucial role of sialidase Neu1 in hyaluronan receptor function of CD44 in T helper type 2-mediated airway inflammation of murine acute asthmatic model. Clinical and experimental immunology *161*, 233-241.

Kessler, S., Rho, H., West, G., Fiocchi, C., Drazba, J., and de la Motte, C. (2008). Hyaluronan (HA) deposition precedes and promotes leukocyte recruitment in intestinal inflammation. Clinical and translational science *1*, 57-61.

Kida, D., Yoneda, M., Miyaura, S., Ishimaru, T., Yoshida, Y., Ito, T., Ishiguro, N., Iwata, H., and Kimata, K. (1999). The SHAP-HA complex in sera from patients with rheumatoid arthritis and osteoarthritis. The Journal of rheumatology *26*, 1230-1238.

Kim, M., Koh, Y.J., Kim, K.E., Koh, B.I., Nam, D.H., Alitalo, K., Kim, I., and Koh, G.Y. (2010). CXCR4 signaling regulates metastasis of chemoresistant melanoma cells by a lymphatic metastatic niche. Cancer Res *70*, 10411-10421.

Knudson, W., Biswas, C., Li, X.Q., Nemec, R.E., and Toole, B.P. (1989). The role and regulation of tumour-associated hyaluronan. Ciba Foundation symposium *143*, 150-159; discussion 159-169, 281-155.

Kogan, G., Soltes, L., Stern, R., and Gemeiner, P. (2007). Hyaluronic acid: a natural biopolymer with a broad range of biomedical and industrial applications. Biotechnology letters *29*, 17-25.

Kohda, D., Morton, C.J., Parkar, A.A., Hatanaka, H., Inagaki, F.M., Campbell, I.D., and Day, A.J. (1996). Solution structure of the link module: a hyaluronan-binding domain involved in extracellular matrix stability and cell migration. Cell *86*, 767-775.

Koltowska, K., Betterman, K.L., Harvey, N.L., and Hogan, B.M. (2013). Getting out and about: the emergence and morphogenesis of the vertebrate lymphatic vasculature. Development *140*, 1857-1870.

Kosunen, A., Ropponen, K., Kellokoski, J., Pukkila, M., Virtaniemi, J., Valtonen, H., Kumpulainen, E., Johansson, R., Tammi, R., Tammi, M., *et al.* (2004). Reduced expression of hyaluronan is a strong indicator of poor survival in oral squamous cell carcinoma. Oral oncology *40*, 257-263.

Kuznetsova, S.A., Mahoney, D.J., Martin-Manso, G., Ali, T., Nentwich, H.A., Sipes, J.M., Zeng, B., Vogel, T., Day, A.J., and Roberts, D.D. (2008). TSG-6 binds via its CUB_C domain to the cell-binding domain of fibronectin and increases fibronectin matrix assembly. Matrix biology : journal of the International Society for Matrix Biology *27*, 201-210.

Lammermann, T., Bader, B.L., Monkley, S.J., Worbs, T., Wedlich-Soldner, R., Hirsch, K., Keller, M., Forster, R., Critchley, D.R., Fassler, R., *et al.* (2008). Rapid leukocyte migration by integrin-independent flowing and squeezing. Nature *453*, 51-55.

Lapcik, L., Jr., Lapcik, L., De Smedt, S., Demeester, J., and Chabrecek, P. (1998). Hyaluronan: Preparation, Structure, Properties, and Applications. Chemical reviews *98*, 2663-2684.

Laragione, T., Bonetto, V., Casoni, F., Massignan, T., Bianchi, G., Gianazza, E., and Ghezzi, P. (2003). Redox regulation of surface protein thiols: identification of integrin alpha-4 as a molecular target by using redox proteomics. Proc Natl Acad Sci U S A *100*, 14737-14741.

Larkin, M.A., Blackshields, G., Brown, N.P., Chenna, R., McGettigan, P.A., McWilliam, H., Valentin, F., Wallace, I.M., Wilm, A., Lopez, R., *et al.* (2007). Clustal W and Clustal X version 2.0. Bioinformatics *23*, 2947-2948.

LaRochelle, W.J., May-Siroff, M., Robbins, K.C., and Aaronson, S.A. (1991). A novel mechanism regulating growth factor association with the cell surface: identification of a PDGF retention domain. Genes & development *5*, 1191-1199.

Lata, S., Reichel, A., Brock, R., Tampe, R., and Piehler, J. (2005). High-affinity adaptors for switchable recognition of histidine-tagged proteins. Journal of the American Chemical Society *127*, 10205-10215.

Lauer, M.E., Cheng, G., Swaidani, S., Aronica, M.A., Weigel, P.H., and Hascall, V.C. (2013). Tumor necrosis factor-stimulated gene-6 (TSG-6) amplifies hyaluronan synthesis by airway smooth muscle cells. J Biol Chem *288*, 423-431.

Laurent, T.C., and Fraser, J.R. (1992). Hyaluronan. FASEB journal : official publication of the Federation of American Societies for Experimental Biology *6*, 2397-2404.

Laurent, T.C., Laurent, U.B., and Fraser, J.R. (1996). Serum hyaluronan as a disease marker. Ann Med *28*, 241-253.

Lauweryns, J.M., and Boussauw, L. (1973). The ultrastructure of lymphatic valves in the adult rabbit lung. Zeitschrift fur Zellforschung und mikroskopische Anatomie *143*, 149-168.

Le Naour, F., Hohenkirk, L., Grolleau, A., Misek, D.E., Lescure, P., Geiger, J.D., Hanash, S., and Beretta, L. (2001). Profiling changes in gene expression during differentiation and maturation of monocyte-derived dendritic cells using both oligonucleotide microarrays and proteomics. J Biol Chem *276*, 17920-17931.

Leak, L.V., and Burke, J.F. (1968). Ultrastructural studies on the lymphatic anchoring filaments. J Cell Biol *36*, 129-149.

Lee, J.L., Wang, M.J., Sudhir, P.R., and Chen, J.Y. (2008). CD44 engagement promotes matrix-derived survival through the CD44-SRC-integrin axis in lipid rafts. Mol Cell Biol *28*, 5710-5723.

Lee, J.Y., and Spicer, A.P. (2000). Hyaluronan: a multifunctional, megaDalton, stealth molecule. Curr Opin Cell Biol *12*, 581-586.

Lesley, J., Gal, I., Mahoney, D.J., Cordell, M.R., Rugg, M.S., Hyman, R., Day, A.J., and Mikecz, K. (2004). TSG-6 modulates the interaction between hyaluronan and cell surface CD44. J Biol Chem *279*, 25745-25754.

Lesley, J., Hascall, V.C., Tammi, M., and Hyman, R. (2000). Hyaluronan binding by cell surface CD44. J Biol Chem *275*, 26967-26975.

Lesley, J., and Hyman, R. (1992). CD44 can be activated to function as an hyaluronic acid receptor in normal murine T cells. Eur J Immunol *22*, 2719-2723.

Lesley, J., Hyman, R., English, N., Catterall, J.B., and Turner, G.A. (1997). CD44 in inflammation and metastasis. Glycoconjugate journal *14*, 611-622.

Lesley, J., Kincade, P.W., and Hyman, R. (1993). Antibody-induced activation of the hyaluronan receptor function of CD44 requires multivalent binding by antibody. Eur J Immunol *23*, 1902-1909.

Liao, S., Cheng, G., Conner, D.A., Huang, Y., Kucherlapati, R.S., Munn, L.L., Ruddle, N.H., Jain, R.K., Fukumura, D., and Padera, T.P. (2011). Impaired lymphatic contraction associated with immunosuppression. Proc Natl Acad Sci U S A *108*, 18784-18789.

Liao, S., and Padera, T.P. (2013). Lymphatic function and immune regulation in health and disease. Lymphat Res Biol *11*, 136-143.

Lodish, H., ed. (2004). Molecular Cell Biology, Third edn (New York: W. H. Freeman).

Lokeshwar, V.B., Cerwinka, W.H., Isoyama, T., and Lokeshwar, B.L. (2005). HYAL1 hyaluronidase in prostate cancer: a tumor promoter and suppressor. Cancer Res *65*, 7782-7789.

Louis-Sylvestre, C., Clough, K., Asselain, B., Vilcoq, J.R., Salmon, R.J., Campana, F., and Fourquet, A. (2004). Axillary treatment in conservative management of operable breast cancer: dissection or radiotherapy?

Results of a randomized study with 15 years of follow-up. Journal of clinical oncology : official journal of the American Society of Clinical Oncology *22*, 97-101.

Lundell, A., Olin, A.I., Morgelin, M., al-Karadaghi, S., Aspberg, A., and Logan, D.T. (2004). Structural basis for interactions between tenascins and lectican C-type lectin domains: evidence for a crosslinking role for tenascins. Structure *12*, 1495-1506.

Luther, S.A., Tang, H.L., Hyman, P.L., Farr, A.G., and Cyster, J.G. (2000). Coexpression of the chemokines ELC and SLC by T zone stromal cells and deletion of the ELC gene in the plt/plt mouse. Proc Natl Acad Sci U S A *97*, 12694-12699.

Lynskey, N.N., Lawrenson, R.A., and Sriskandan, S. (2011). New understandings in Streptococcus pyogenes. Current opinion in infectious diseases *24*, 196-202.

Lyons, O.T.A., and Modarai, B. (2013). Lymphoedema. Surgery *31*, 218-223.

Mahaffey, C.L., and Mummert, M.E. (2007). Hyaluronan Synthesis Is Required for IL-2-Mediated T Cell Proliferation. The Journal of Immunology *179*, 8191-8199.

Maharjan, A.S., Pilling, D., and Gomer, R.H. (2011). High and low molecular weight hyaluronic acid differentially regulate human fibrocyte differentiation. PloS one *6*, e26078.

Maina, V., Cotena, A., Doni, A., Nebuloni, M., Pasqualini, F., Milner, C.M., Day, A.J., Mantovani, A., and Garlanda, C. (2009). Coregulation in human leukocytes of the long pentraxin PTX3 and TSG-6. J Leukoc Biol *86*, 123-132.

Makinen, T., Adams, R.H., Bailey, J., Lu, Q., Ziemiecki, A., Alitalo, K., Klein, R., and Wilkinson, G.A. (2005). PDZ interaction site in ephrinB2 is required for the remodeling of lymphatic vasculature. Genes & development *19*, 397-410.

Matsumoto, K., Shionyu, M., Go, M., Shimizu, K., Shinomura, T., Kimata, K., and Watanabe, H. (2003). Distinct interaction of versican/PG-M with hyaluronan and link protein. J Biol Chem *278*, 41205-41212.

McCulloch, D.R., Nelson, C.M., Dixon, L.J., Silver, D.L., Wylie, J.D., Lindner, V., Sasaki, T., Cooley, M.A., Argraves, W.S., and Apte, S.S. (2009). ADAMTS metalloproteases generate active versican fragments that regulate interdigital web regression. Developmental cell *17*, 687-698.

McKee, C.M., Penno, M.B., Cowman, M., Burdick, M.D., Strieter, R.M., Bao, C., and Noble, P.W. (1996). Hyaluronan (HA) fragments induce chemokine gene expression in alveolar macrophages. The role of HA size and CD44. The Journal of clinical investigation *98*, 2403-2413.

Medina, A.P., Lin, J., and Weigel, P.H. (2012). Hyaluronan synthase mediates dye translocation across liposomal membranes. BMC biochemistry *13*, 2.

Mendoza, E., and Schmid-Schonbein, G.W. (2003). A model for mechanics of primary lymphatic valves. Journal of biomechanical engineering *125*, 407-414.

Metcalfe, C., Cresswell, P., Ciaccia, L., Thomas, B., and Barclay, A.N. (2011). Labile disulfide bonds are common at the leucocyte cell surface. Open biology *1*, 110010.

Meyer, K., and Palmer, J.W. (1934). The Polysaccharide Of The Vitreous Humor. Journal of Biological Chemistry *107*, 629-634.

Misra, S., Heldin, P., Hascall, V.C., Karamanos, N.K., Skandalis, S.S., Markwald, R.R., and Ghatak, S. (2011). Hyaluronan-CD44 interactions as potential targets for cancer therapy. FEBS J *278*, 1429-1443.

Mjaatvedt, C.H., Yamamura, H., Capehart, A.A., Turner, D., and Markwald, R.R. (1998). The Cspg2 gene, disrupted in the hdf mutant, is required for right cardiac chamber and endocardial cushion formation. Dev Biol *202*, 56-66.

Mohamadzadeh, M., DeGrendele, H., Arizpe, H., Estess, P., and Siegelman, M. (1998). Proinflammatory stimuli regulate endothelial hyaluronan expression and CD44/HA-dependent primary adhesion. The Journal of clinical investigation *101*, 97-108.

Mouta Carreira, C., Nasser, S.M., di Tomaso, E., Padera, T.P., Boucher, Y., Tomarev, S.I., and Jain, R.K. (2001). LYVE-1 is not restricted to the lymph vessels: expression in normal liver blood sinusoids and down-regulation in human liver cancer and cirrhosis. Cancer Res *61*, 8079-8084.

Mukhopadhyay, D., Asari, A., Rugg, M.S., Day, A.J., and Fulop, C. (2004). Specificity of the tumor necrosis factor-induced protein 6-mediated heavy chain transfer from inter-alpha-trypsin inhibitor to hyaluronan: implications for the assembly of the cumulus extracellular matrix. J Biol Chem *279*, 11119-11128.

Mukhopadhyay, D., Hascall, V.C., Day, A.J., Salustri, A., and Fulop, C. (2001). Two distinct populations of tumor necrosis factor-stimulated gene-6 protein in the extracellular matrix of expanded mouse cumulus cell-oocyte complexes. Archives of biochemistry and biophysics *394*, 173-181.

Mummert, M.E., Mummert, D., Edelbaum, D., Hui, F., Matsue, H., and Takashima, A. (2002). Synthesis and surface expression of hyaluronan by dendritic cells and its potential role in antigen presentation. J Immunol *169*, 4322-4331.

Nandi, A., Estess, P., and Siegelman, M. (2004). Bimolecular Complex between Rolling and Firm Adhesion Receptors Required for Cell Arrest. Immunity *20*, 455-465.

Neame, P.J., Christner, J.E., and Baker, J.R. (1986). The primary structure of link protein from rat chondrosarcoma proteoglycan aggregate. J Biol Chem *261*, 3519-3535.

Nightingale, T. (2004). Regulated Ligand Binding of LYVE-1: A Lymphatic Endothelium Specific Hyaluronan Receptor. In Nuffield Department of Clinical Medicine (Oxford: University of Oxford).

Nightingale, T.D., Frayne, M.E., Clasper, S., Banerji, S., and Jackson, D.G. (2009). A mechanism of sialylation functionally silences the hyaluronan receptor LYVE-1 in lymphatic endothelium. J Biol Chem *284*, 3935-3945.

Nitschke, M., Aebischer, D., Abadier, M., Haener, S., Lucic, M., Vigl, B., Luche, H., Fehling, H.J., Biehlmaier, O., Lyck, R., *et al.* (2012). Differential requirement for ROCK in dendritic cell migration within lymphatic capillaries in steady-state and inflammation. Blood *120*, 2249-2258.

Norrmen, C., Ivanov, K.I., Cheng, J., Zangger, N., Delorenzi, M., Jaquet, M., Miura, N., Puolakkainen, P., Horsley, V., Hu, J., *et al.* (2009). FOXC2 controls formation and maturation of lymphatic collecting vessels through cooperation with NFATc1. J Cell Biol *185*, 439-457.

Obayashi, Y., Yabushita, H., Kanyama, K., Noguchi, M., Zhuo, L., Kimata, K., and Wakatsuki, A. (2008). Role of serum-derived hyaluronan-associated protein-hyaluronan complex in ovarian cancer. Oncology reports *19*, 1245-1251.

Ohki, I., Amida, H., Yamada, R., Sugihara, M., Ishigaki, T., and Tate, S. (2011). Surface plasmon resonance study on functional significance of clustered organization of lectin-like oxidized LDL receptor (LOX-1). Biochimica et biophysica acta *1814*, 345-354.

Ohki, I., Ishigaki, T., Oyama, T., Matsunaga, S., Xie, Q., Ohnishi-Kameyama, M., Murata, T., Tsuchiya, D., Machida, S., Morikawa, K., *et al.* (2005). Crystal structure of human lectin-like, oxidized low-density lipoprotein receptor 1 ligand binding domain and its ligand recognition mode to OxLDL. Structure *13*, 905-917.

Ohl, L., Mohaupt, M., Czeloth, N., Hintzen, G., Kiafard, Z., Zwirner, J., Blankenstein, T., Henning, G., and Forster, R. (2004). CCR7 governs skin dendritic cell migration under inflammatory and steady-state conditions. Immunity *21*, 279-288.

Okuda, H., Kobayashi, A., Xia, B., Watabe, M., Pai, S.K., Hirota, S., Xing, F., Liu, W., Pandey, P.R., Fukuda, K., *et al.* (2012). Hyaluronan synthase HAS2 promotes tumor progression in bone by stimulating the interaction of breast cancer stem-like cells with macrophages and stromal cells. Cancer Res *72*, 537-547.

Olin, A.I., Morgelin, M., Sasaki, T., Timpl, R., Heinegard, D., and Aspberg, A. (2001). The proteoglycans aggrecan and Versican form networks with fibulin-2 through their lectin domain binding. J Biol Chem *276*, 1253-1261.

Oohashi, T., Hirakawa, S., Bekku, Y., Rauch, U., Zimmermann, D.R., Su, W.D., Ohtsuka, A., Murakami, T., and Ninomiya, Y. (2002). Bral1, a brain-specific link protein, colocalizing with the versican V2 isoform at the nodes of Ranvier in developing and adult mouse central nervous systems. Molecular and cellular neurosciences *19*, 43-57.

Ou, W., and Silver, J. (2006). Role of protein disulfide isomerase and other thiol-reactive proteins in HIV-1 envelope protein-mediated fusion. Virology *350*, 406-417.

Ouskova, G., Spellerberg, B., and Prehm, P. (2004). Hyaluronan release from Streptococcus pyogenes: export by an ABC transporter. Glycobiology *14*, 931-938.

Parkar, A.A., Kahmann, J.D., Howat, S.L., Bayliss, M.T., and Day, A.J. (1998). TSG-6 interacts with hyaluronan and aggrecan in a pH-dependent manner via a common functional element: implications for its regulation in inflamed cartilage. FEBS Lett *428*, 171-176.

Peach, R.J., Hollenbaugh, D., Stamenkovic, I., and Aruffo, A. (1993). Identification of hyaluronic acid binding sites in the extracellular domain of CD44. J Cell Biol *122*, 257-264.

Perschl, A., Lesley, J., English, N., Trowbridge, I., and Hyman, R. (1995). Role of CD44 cytoplasmic domain in hyaluronan binding. Eur J Immunol *25*, 495-501.

Petrova, T.V., Karpanen, T., Norrmen, C., Mellor, R., Tamakoshi, T., Finegold, D., Ferrell, R., Kerjaschki, D., Mortimer, P., Yla-Herttuala, S., *et al.* (2004). Defective valves and abnormal mural cell recruitment underlie lymphatic vascular failure in lymphedema distichiasis. Nature medicine *10*, 974-981.

Pflicke, H., and Sixt, M. (2009). Preformed portals facilitate dendritic cell entry into afferent lymphatic vessels. J Exp Med *206*, 2925-2935.

Pham, T.H., Baluk, P., Xu, Y., Grigorova, I., Bankovich, A.J., Pappu, R., Coughlin, S.R., McDonald, D.M., Schwab, S.R., and Cyster, J.G. (2010). Lymphatic endothelial cell sphingosine kinase activity is required for lymphocyte egress and lymphatic patterning. J Exp Med *207*, 17-27.

Pieper, U., Eswar, N., Webb, B.M., Eramian, D., Kelly, L., Barkan, D.T., Carter, H., Mankoo, P., Karchin, R., Marti-Renom, M.A., *et al.* (2009). MODBASE, a database of annotated comparative protein structure models and associated resources. Nucleic Acids Res *37*, D347-354.

Planas-Paz, L., Strilic, B., Goedecke, A., Breier, G., Fassler, R., and Lammert, E. (2012). Mechanoinduction of lymph vessel expansion. EMBO J *31*, 788-804.

Platonova, N., Miquel, G., Regenfuss, B., Taouji, S., Cursiefen, C., Chevet, E., and Bikfalvi, A. (2013). Evidence for the interaction of fibroblast growth factor-2 with the lymphatic endothelial cell marker LYVE-1. Blood *121*, 1229-1237.

Ponta, H., Sherman, L., and Herrlich, P.A. (2003). CD44: from adhesion molecules to signalling regulators. Nat Rev Mol Cell Biol *4*, 33-45.

Prange, C.K., Pennacchio, L.A., Lieuallen, K., Fan, W., and Lennon, G.G. (1998). Characterization of the human neurocan gene, CSPG3. Gene *221*, 199-205.

Prehm, P. (1984). Hyaluronate is synthesized at plasma membranes. The Biochemical journal *220*, 597-600.

Prehm, P., and Schumacher, U. (2004). Inhibition of hyaluronan export from human fibroblasts by inhibitors of multidrug resistance transporters. Biochem Pharmacol *68*, 1401-1410.

Prevo, R., Banerji, S., Ferguson, D.J., Clasper, S., and Jackson, D.G. (2001). Mouse LYVE-1 is an endocytic receptor for hyaluronan in lymphatic endothelium. J Biol Chem *276*, 19420-19430.

Protin, U., Schweighoffer, T., Jochum, W., and Hilberg, F. (1999). CD44-deficient mice develop normally with changes in subpopulations and recirculation of lymphocyte subsets. J Immunol *163*, 4917-4923.

Pure, E., and Cuff, C.A. (2001). A crucial role for CD44 in inflammation. Trends Mol Med *7*, 213-221.

Qu, X., Tompkins, K., Batts, L.E., Puri, M., and Baldwin, H.S. (2010). Abnormal embryonic lymphatic vessel development in Tie1 hypomorphic mice. Development *137*, 1285-1295.

Reed, R.K., Laurent, U.B., Fraser, J.R., and Laurent, T.C. (1990). Removal rate of [3H]hyaluronan injected subcutaneously in rabbits. The American journal of physiology *259*, H532-535.

Reviakine, I., Johannsmann, D., and Richter, R.P. (2011). Hearing what you cannot see and visualizing what you hear: interpreting quartz crystal microbalance data from solvated interfaces. Analytical chemistry *83*, 8838-8848.

Ricciardelli, C., Sakko, A.J., Ween, M.P., Russell, D.L., and Horsfall, D.J. (2009). The biological role and regulation of versican levels in cancer. Cancer metastasis reviews *28*, 233-245.

Richter, R., Mukhopadhyay, A., and Brisson, A. (2003). Pathways of lipid vesicle deposition on solid surfaces: a combined QCM-D and AFM study. Biophysical journal *85*, 3035-3047.

Richter, R.P., Berat, R., and Brisson, A.R. (2006). Formation of solid-supported lipid bilayers: an integrated view. Langmuir : the ACS journal of surfaces and colloids *22*, 3497-3505.

Rilla, K., Pasonen-Seppanen, S., Deen, A.J., Koistinen, V.V., Wojciechowski, S., Oikari, S., Karna, R., Bart, G., Torronen, K., Tammi, R.H., *et al.* (2013). Hyaluronan production enhances shedding of plasma membrane-derived microvesicles. Experimental cell research *319*, 2006-2018.

Roghani, M., and Moscatelli, D. (1992). Basic fibroblast growth factor is internalized through both receptor-mediated and heparan sulfate-mediated mechanisms. J Biol Chem *267*, 22156-22162.

Rooney, P., and Kumar, S. (1993). Inverse relationship between hyaluronan and collagens in development and angiogenesis. Differentiation; research in biological diversity *54*, 1-9.

Rooney, P., Kumar, S., Ponting, J., and Wang, M. (1995). The role of hyaluronan in tumour neovascularization (review). International journal of cancer Journal international du cancer *60*, 632-636.

Royston, D.J. (2011). The Role of LYVE-1 in Tumour Metastasis and Inflammation. In Nuffield Department of Clinical Medicine (Oxford, United Kingdom: University of Oxford).

Rugg, M.S., Willis, A.C., Mukhopadhyay, D., Hascall, V.C., Fries, E., Fulop, C., Milner, C.M., and Day, A.J. (2005). Characterization of complexes formed between TSG-6 and inter-alpha-inhibitor that act as intermediates in the covalent transfer of heavy chains onto hyaluronan. J Biol Chem *280*, 25674-25686.

Russell, D.L., Doyle, K.M., Ochsner, S.A., Sandy, J.D., and Richards, J.S. (2003). Processing and localization of ADAMTS-1 and proteolytic cleavage of versican during cumulus matrix expansion and ovulation. J Biol Chem *278*, 42330-42339.

Russo, E., Nitschke, M., and Halin, C. (2013). Dendritic cell interactions with lymphatic endothelium. Lymphat Res Biol *11*, 172-182.

Sabin, F.R. (1902). On the origin of the lymphatic system from the veins and the development of the lymph hearts and thoracic duct in the pig. American Journal of Anatomy *1*, 367-389.

Sabine, A., Agalarov, Y., Maby-El Hajjami, H., Jaquet, M., Hagerling, R., Pollmann, C., Bebber, D., Pfenniger, A., Miura, N., Dormond, O., *et al.* (2012). Mechanotransduction, PROX1, and FOXC2 cooperate to control connexin37 and calcineurin during lymphatic-valve formation. Developmental cell *22*, 430-445.

Schledzewski, K., Falkowski, M., Moldenhauer, G., Metharom, P., Kzhyshkowska, J., Ganss, R., Demory, A., Falkowska-Hansen, B., Kurzen, H., Ugurel, S., *et al.* (2006). Lymphatic endothelium-specific hyaluronan receptor LYVE-1 is expressed by stabilin-1+, F4/80+, CD11b+ macrophages in malignant tumours and wound healing tissue in vivo and in bone marrow cultures in vitro: implications for the assessment of lymphangiogenesis. J Pathol *209*, 67-77.

Schmidt, T.A., Gastelum, N.S., Nguyen, Q.T., Schumacher, B.L., and Sah, R.L. (2007). Boundary lubrication of articular cartilage: role of synovial fluid constituents. Arthritis Rheum *56*, 882-891.

Schmits, R., Filmus, J., Gerwin, N., Senaldi, G., Kiefer, F., Kundig, T., Wakeham, A., Shahinian, A., Catzavelos, C., Rak, J., *et al.* (1997). CD44 regulates hematopoietic progenitor distribution, granuloma formation, and tumorigenicity. Blood *90*, 2217-2233.

Schulte-Merker, S., Sabine, A., and Petrova, T.V. (2011). Lymphatic vascular morphogenesis in development, physiology, and disease. J Cell Biol *193*, 607-618.

Schumann, K., Lammermann, T., Bruckner, M., Legler, D.F., Polleux, J., Spatz, J.P., Schuler, G., Forster, R., Lutz, M.B., Sorokin, L., *et al.* (2010). Immobilized chemokine fields and soluble chemokine gradients cooperatively shape migration patterns of dendritic cells. Immunity *32*, 703-713.

Sen, D., Forrest, L., Kepler, T.B., Parker, I., and Cahalan, M.D. (2010). Selective and site-specific mobilization of dermal dendritic cells and Langerhans cells by Th1- and Th2-polarizing adjuvants. Proc Natl Acad Sci U S A *107*, 8334-8339.

Seyama, K., Kumasaka, T., Kurihara, M., Mitani, K., and Sato, T. (2010). Lymphangioleiomyomatosis: a disease involving the lymphatic system. Lymphat Res Biol *8*, 21-31.

Shen, L., Zhuo, L., Okumura, A., Ishikawa, T., Miyachi, M., Owa, Y., Ishizawa, T., Sugiura, N., Nagata, Y., Nonami, T., *et al.* (2006). The SHAP-hyaluronan complex in serum from patients with chronic liver diseases caused by hepatitis virus infection. Hepatology research : the official journal of the Japan Society of Hepatology *34*, 178-186.

Shields, J.D., Kourtis, I.C., Tomei, A.A., Roberts, J.M., and Swartz, M.A. (2010). Induction of lymphoidlike stroma and immune escape by tumors that express the chemokine CCL21. Science *328*, 749-752.

Shin, J.W., Min, M., Larrieu-Lahargue, F., Canron, X., Kunstfeld, R., Nguyen, L., Henderson, J.E., Bikfalvi, A., Detmar, M., and Hong, Y.K. (2006). Prox1 promotes lineage-specific expression of fibroblast growth factor (FGF) receptor-3 in lymphatic endothelium: a role for FGF signaling in lymphangiogenesis. Molecular biology of the cell *17*, 576-584.

Shyjan, A.M., Heldin, P., Butcher, E.C., Yoshino, T., and Briskin, M.J. (1996). Functional cloning of the cDNA for a human hyaluronan synthase. J Biol Chem *271*, 23395-23399.

Skelton, T.P., Zeng, C., Nocks, A., and Stamenkovic, I. (1998). Glycosylation provides both stimulatory and inhibitory effects on cell surface and soluble CD44 binding to hyaluronan. J Cell Biol *140*, 431-446.

Sleeman, J.P., and Thiele, W. (2009). Tumor metastasis and the lymphatic vasculature. International journal of cancer Journal international du cancer *125*, 2747-2756.

Slevin, M., Krupinski, J., Kumar, S., and Gaffney, J. (1998). Angiogenic oligosaccharides of hyaluronan induce protein tyrosine kinase activity in endothelial cells and activate a cytoplasmic signal transduction pathway resulting in proliferation. Laboratory investigation; a journal of technical methods and pathology *78*, 987-1003.

Slevin, M., Kumar, S., and Gaffney, J. (2002). Angiogenic oligosaccharides of hyaluronan induce multiple signaling pathways affecting vascular endothelial cell mitogenic and wound healing responses. J Biol Chem *277*, 41046-41059.

Solito, R., Alessandrini, C., Fruschelli, M., Pucci, A.M., and Gerli, R. (1997). An immunological correlation between the anchoring filaments of initial lymph vessels and the neighboring elastic fibers: a unified morphofunctional concept. Lymphology *30*, 194-202.

Soltes, L., Mendichi, R., Kogan, G., Schiller, J., Stankovska, M., and Arnhold, J. (2006). Degradative action of reactive oxygen species on hyaluronan. Biomacromolecules *7*, 659-668.

Spicer, A.P., Augustine, M.L., and McDonald, J.A. (1996). Molecular cloning and characterization of a putative mouse hyaluronan synthase. J Biol Chem *271*, 23400-23406.

Spicer, A.P., Joo, A., and Bowling, R.A., Jr. (2003). A hyaluronan binding link protein gene family whose members are physically linked adjacent to chondroitin sulfate proteoglycan core protein genes: the missing links. J Biol Chem *278*, 21083-21091.

Spicer, A.P., and McDonald, J.A. (1998). Characterization and molecular evolution of a vertebrate hyaluronan synthase gene family. J Biol Chem *273*, 1923-1932.

Spicer, A.P., Olson, J.S., and McDonald, J.A. (1997). Molecular cloning and characterization of a cDNA encoding the third putative mammalian hyaluronan synthase. J Biol Chem *272*, 8957-8961.

Srinivasan, R.S., Dillard, M.E., Lagutin, O.V., Lin, F.J., Tsai, S., Tsai, M.J., Samokhvalov, I.M., and Oliver, G. (2007). Lineage tracing demonstrates the venous origin of the mammalian lymphatic vasculature. Genes & development *21*, 2422-2432.

Srinivasan, R.S., Geng, X., Yang, Y., Wang, Y., Mukatira, S., Studer, M., Porto, M.P., Lagutin, O., and Oliver, G. (2010). The nuclear hormone receptor Coup-TFII is required for the initiation and early maintenance of Prox1 expression in lymphatic endothelial cells. Genes & development *24*, 696-707.

Stern, R. (2003). Devising a pathway for hyaluronan catabolism: are we there yet? Glycobiology *13*, 105R-115R.

Stern, R. (2004). Hyaluronan catabolism: a new metabolic pathway. Eur J Cell Biol *83*, 317-325.

Stoitzner, P., Pfaller, K., Stossel, H., and Romani, N. (2002). A close-up view of migrating Langerhans cells in the skin. The Journal of investigative dermatology *118*, 117-125.

Sugahara, K.N., Murai, T., Nishinakamura, H., Kawashima, H., Saya, H., and Miyasaka, M. (2003). Hyaluronan oligosaccharides induce CD44 cleavage and promote cell migration in CD44-expressing tumor cells. J Biol Chem *278*, 32259-32265.

Swaidani, S., Cheng, G., Lauer, M.E., Sharma, M., Mikecz, K., Hascall, V.C., and Aronica, M.A. (2013). TSG-6 protein is crucial for the development of pulmonary hyaluronan deposition, eosinophilia, and airway hyperresponsiveness in a murine model of asthma. J Biol Chem *288*, 412-422.

Swartz, M.A. (2001). The physiology of the lymphatic system. Adv Drug Deliv Rev *50*, 3-20.

Swartz, M.A., and Lund, A.W. (2012). Lymphatic and interstitial flow in the tumour microenvironment: linking mechanobiology with immunity. Nature reviews Cancer *12*, 210-219.

Tal, O., Lim, H.Y., Gurevich, I., Milo, I., Shipony, Z., Ng, L.G., Angeli, V., and Shakhar, G. (2011). DC mobilization from the skin requires docking to immobilized CCL21 on lymphatic endothelium and intralymphatic crawling. J Exp Med *208*, 2141-2153.

Tammi, R.H., Kultti, A., Kosma, V.M., Pirinen, R., Auvinen, P., and Tammi, M.I. (2008). Hyaluronan in human tumors: pathobiological and prognostic messages from cell-associated and stromal hyaluronan. Seminars in cancer biology *18*, 288-295.

Taylor, K.R., Trowbridge, J.M., Rudisill, J.A., Termeer, C.C., Simon, J.C., and Gallo, R.L. (2004). Hyaluronan fragments stimulate endothelial recognition of injury through TLR4. J Biol Chem *279*, 17079-17084.

Teriete, P., Banerji, S., Noble, M., Blundell, C.D., Wright, A.J., Pickford, A.R., Lowe, E., Mahoney, D.J., Tammi, M.I., Kahmann, J.D., *et al.* (2004). Structure of the regulatory hyaluronan binding domain in the inflammatory leukocyte homing receptor CD44. Mol Cell *13*, 483-496.

Termeer, C., Benedix, F., Sleeman, J., Fieber, C., Voith, U., Ahrens, T., Miyake, K., Freudenberg, M., Galanos, C., and Simon, J.C. (2002). Oligosaccharides of Hyaluronan activate dendritic cells via toll-like receptor 4. J Exp Med *195*, 99-111.

Termeer, C., Johannsen, H., Braun, T., Renkl, A., Ahrens, T., Denfeld, R.W., Lappin, M.B., Weiss, J.M., and Simon, J.C. (2001). The role of CD44 during CD40 ligand-induced dendritic cell clustering and maturation. J Leukoc Biol *70*, 715-722.

Termeer, C.C., Hennies, J., Voith, U., Ahrens, T., Weiss, J.M., Prehm, P., and Simon, J.C. (2000). Oligosaccharides of hyaluronan are potent activators of dendritic cells. J Immunol *165*, 1863-1870.

Thomas, N.K., and Brown, T.J. (2010). ABC transporters do not contribute to extracellular translocation of hyaluronan in human breast cancer in vitro. Experimental cell research *316*, 1241-1253.

Tian, X., Azpurua, J., Hine, C., Vaidya, A., Myakishev-Rempel, M., Ablaeva, J., Mao, Z., Nevo, E., Gorbunova, V., and Seluanov, A. (2013). High-molecular-mass hyaluronan mediates the cancer resistance of the naked mole rat. Nature *499*, 346-349.

Tlapak-Simmons, V.L., Baggenstoss, B.A., Clyne, T., and Weigel, P.H. (1999). Purification and lipid dependence of the recombinant hyaluronan synthases from Streptococcus pyogenes and Streptococcus equisimilis. J Biol Chem *274*, 4239-4245.

Tlapak-Simmons, V.L., Kempner, E.S., Baggenstoss, B.A., and Weigel, P.H. (1998). The active streptococcal hyaluronan synthases (HASs) contain a single HAS monomer and multiple cardiolipin molecules. J Biol Chem *273*, 26100-26109.

Toole, B.P. (2002). Hyaluronan promotes the malignant phenotype. Glycobiology *12*, 37R-42R.

Toole, B.P. (2004). Hyaluronan: from extracellular glue to pericellular cue. Nature reviews Cancer *4*, 528-539.

Toole, B.P. (2009). Hyaluronan-CD44 Interactions in Cancer: Paradoxes and Possibilities. Clin Cancer Res *15*, 7462-7468.

Trzewik, J., Mallipattu, S.K., Artmann, G.M., Delano, F.A., and Schmid-Schonbein, G.W. (2001). Evidence for a second valve system in lymphatics: endothelial microvalves. FASEB journal : official publication of the Federation of American Societies for Experimental Biology *15*, 1711-1717.

Tvorogov, D., Anisimov, A., Zheng, W., Leppanen, V.M., Tammela, T., Laurinavicius, S., Holnthoner, W., Helotera, H., Holopainen, T., Jeltsch, M., *et al.* (2010). Effective suppression of vascular network formation by combination of antibodies blocking VEGFR ligand binding and receptor dimerization. Cancer Cell *18*, 630-640.

Uhrin, P., Zaujec, J., Breuss, J.M., Olcaydu, D., Chrenek, P., Stockinger, H., Fuertbauer, E., Moser, M., Haiko, P., Fassler, R., *et al.* (2010). Novel function for blood platelets and podoplanin in developmental separation of blood and lymphatic circulation. Blood *115*, 3997-4005.

Vassileva, G., Soto, H., Zlotnik, A., Nakano, H., Kakiuchi, T., Hedrick, J.A., and Lira, S.A. (1999). The reduced expression of 6Ckine in the plt mouse results from the deletion of one of two 6Ckine genes. J Exp Med *190*, 1183-1188.

Vigl, B., Aebischer, D., Nitschke, M., Iolyeva, M., Rothlin, T., Antsiferova, O., and Halin, C. (2011). Tissue inflammation modulates gene expression of lymphatic endothelial cells and dendritic cell migration in a stimulus-dependent manner. Blood *118*, 205-215.

Vockel, M., and Vestweber, D. (2013). How T cells trigger the dissociation of the endothelial receptor phosphatase VE-PTP from VE-cadherin. Blood *122*, 2512-2522.

Vuorio, E., Einola, S., Hakkarainen, S., and Penttinen, R. (1982). Synthesis of underpolymerized hyaluronic acid by fibroblasts cultured from rheumatoid and non-rheumatoid synovitis. Rheumatology international *2*, 97-102.

Wang, H.W., Trotter, M.W., Lagos, D., Bourboulia, D., Henderson, S., Makinen, T., Elliman, S., Flanagan, A.M., Alitalo, K., and Boshoff, C. (2004). Kaposi sarcoma herpesvirus-induced cellular reprogramming contributes to the lymphatic endothelial gene expression in Kaposi sarcoma. Nature genetics *36*, 687-693.

Watanabe, H., Cheung, S.C., Itano, N., Kimata, K., and Yamada, Y. (1997). Identification of hyaluronan-binding domains of aggrecan. J Biol Chem *272*, 28057-28065.

Watanabe, K., and Yamaguchi, Y. (1996). Molecular identification of a putative human hyaluronan synthase. J Biol Chem *271*, 22945-22948.

Weber, M., Hauschild, R., Schwarz, J., Moussion, C., de Vries, I., Legler, D.F., Luther, S.A., Bollenbach, T., and Sixt, M. (2013). Interstitial dendritic cell guidance by haptotactic chemokine gradients. Science *339*, 328-332.

Weigel, P.H., and DeAngelis, P.L. (2007). Hyaluronan synthases: a decade-plus of novel glycosyltransferases. J Biol Chem *282*, 36777-36781.

Weissmann, B., and Meyer, K. (1954). The Structure of Hyalobiuronic Acid and of Hyaluronic Acid from Umbilical Cord1,2. Journal of the American Chemical Society *76*, 1753-1757.

West, D.C., Hampson, I.N., Arnold, F., and Kumar, S. (1985). Angiogenesis induced by degradation products of hyaluronic acid. Science *228*, 1324-1326.

Wight, T.N. (2002). Versican: a versatile extracellular matrix proteoglycan in cell biology. Curr Opin Cell Biol *14*, 617-623.

Wigle, J.T., and Oliver, G. (1999). Prox1 function is required for the development of the murine lymphatic system. Cell *98*, 769-778.

Witte, M.H., Jones, K., Wilting, J., Dictor, M., Selg, M., McHale, N., Gershenwald, J.E., and Jackson, D.G. (2006). Structure function relationships in the lymphatic system and implications for cancer biology. Cancer metastasis reviews *25*, 159-184.

Wolny, P.M. (2010). Novel model systems for the investigation of polyvalent protein-hyaluronan interactions on the cell surface (Universität Heidelberg).

Wolny, P.M., Banerji, S., Gounou, C., Brisson, A.R., Day, A.J., Jackson, D.G., and Richter, R.P. (2010). Analysis of CD44-hyaluronan interactions in an artificial membrane system: insights into the distinct binding properties of high and low molecular weight hyaluronan. J Biol Chem *285*, 30170-30180.

Xu, H., Guan, H., Zu, G., Bullard, D., Hanson, J., Slater, M., and Elmets, C.A. (2001). The role of ICAM-1 molecule in the migration of Langerhans cells in the skin and regional lymph node. Eur J Immunol *31*, 3085-3093.

Yamada, H., Watanabe, K., Shimonaka, M., and Yamaguchi, Y. (1994). Molecular cloning of brevican, a novel brain proteoglycan of the aggrecan/versican family. J Biol Chem *269*, 10119-10126.

Yamaguchi, Y. (2000). Lecticans: organizers of the brain extracellular matrix. Cellular and molecular life sciences : CMLS *57*, 276-289.

Yan, Z., Garg, S.K., Kipnis, J., and Banerjee, R. (2009). Extracellular redox modulation by regulatory T cells. Nature chemical biology *5*, 721-723.

Yao, L.C., Baluk, P., Srinivasan, R.S., Oliver, G., and McDonald, D.M. (2012). Plasticity of button-like junctions in the endothelium of airway lymphatics in development and inflammation. The American journal of pathology *180*, 2561-2575.

Yingsung, W., Zhuo, L., Morgelin, M., Yoneda, M., Kida, D., Watanabe, H., Ishiguro, N., Iwata, H., and Kimata, K. (2003). Molecular heterogeneity of the SHAP-hyaluronan complex. Isolation and characterization of the complex in synovial fluid from patients with rheumatoid arthritis. J Biol Chem *278*, 32710-32718.

Yoshida, H., Nagaoka, A., Kusaka-Kikushima, A., Tobiishi, M., Kawabata, K., Sayo, T., Sakai, S., Sugiyama, Y., Enomoto, H., Okada, Y., *et al.* (2013). KIAA1199, a deafness gene of unknown function, is a new hyaluronan binding protein involved in hyaluronan depolymerization. Proc Natl Acad Sci U S A *110*, 5612-5617.

Yuan, L., Moyon, D., Pardanaud, L., Breant, C., Karkkainen, M.J., Alitalo, K., and Eichmann, A. (2002). Abnormal lymphatic vessel development in neuropilin 2 mutant mice. Development *129*, 4797-4806.

Zawieja, D.C. (2009). Contractile physiology of lymphatics. Lymphat Res Biol *7*, 87-96.

Zhang, X., Wang, J.F., Chandran, B., Persaud, K., Pytowski, B., Fingeroth, J., and Groopman, J.E. (2005). Kaposi's sarcoma-associated herpesvirus activation of vascular endothelial growth factor receptor 3 alters endothelial function and enhances infection. J Biol Chem *280*, 26216-26224.

Zhao, M., Yoneda, M., Ohashi, Y., Kurono, S., Iwata, H., Ohnuki, Y., and Kimata, K. (1995). Evidence for the covalent binding of SHAP, heavy chains of inter-alpha-trypsin inhibitor, to hyaluronan. J Biol Chem *270*, 26657-26663.

Zhuo, L., Kanamori, A., Kannagi, R., Itano, N., Wu, J., Hamaguchi, M., Ishiguro, N., and Kimata, K. (2006). SHAP potentiates the CD44-mediated leukocyte adhesion to the hyaluronan substratum. J Biol Chem *281*, 20303-20314.

Zhuo, L., and Kimata, K. (2001). Cumulus oophorus extracellular matrix: its construction and regulation. Cell structure and function *26*, 189-196.

Zimmermann, D.R., and Ruoslahti, E. (1989). Multiple domains of the large fibroblast proteoglycan, versican. EMBO J *8*, 2975-2981.